Westinghouse Electric Corporation
Energy Systems

Box 355
Pittsburgh Pennsylvania 15230-0355

NSD-NRC-96-4860
DCP/NRC0638
Docket No.: STN-52-003

October 25, 1996

Document Control Desk
U.S. Nuclear Regulatory Commission
Washington, D.C. 20555

ATTENTION: T. R. QUAY

SUBJECT: AP600 NOTRUMP VERIFICATION AND VALIDATION REPORT, DRAFT SECTION 4

Dear Mr. Quay:

Enclosed is a draft section of the NOTRUMP verification and validation report which is scheduled for completion by December 17, 1996. This draft section is provided in advance of the final V&V report to assist and faciliate the staff review of this document. The enclosed section is in a final form and we anticipate no changes to this document prior to its incorporation into the full report. The enclosed section (Section 4.0, Two-Phase Level Swell Analysis) includes discussion of the following:

- General Electric Small Blowdown Vessel Tests
- ACHILLES Low-Pressure Level Swell Tests
- G2 Tests

The completion of Section 4 of the NOTRUMP V&V report addresses and completes Westinghouse actions toward closure of the following requests for additional information and SDSER open items:

- 440.468, 440.474, 440.515, OI 21.6.2.6-2

Determination of additional separate effects level swell tests necessary for NOTRUMP code qualification is SDSER OI 21.6.2.4-6. Westinghouse has included other level swell tests in addition to the G2 tests (General Electric Blowdown Vessel Tests, and ACHILLES Tests) in this submittal of Section 4. This completes Westinghouse actions toward closure of OI 21.6.2.4-6.

E004

The Westinghouse Electric Corporation copyright notice is attached.

Please contact John C. Butler on (412) 374-5268 if you have any questions concerning this transmittal.

D. B. Sandusky /for

Brian A. McIntyre, Manager
Advanced Plant Safety and Licensing

/nja

Enclosure

cc: T. Kenyon, NRC (w/o Enclosures/Attachments)
W. Huffman, NRC (1E)
R. Landry, NRC (1E)
P. Boehnert, ACRS (1E)
N. J. Liparulo, Westinghouse (w/o Enclosures/Attachments)

COPYRIGHT NOTICE

The reports transmitted herewith each bear a Westinghouse copyright notice. The NRC is permitted to make the number of copies of the information contained in these reports which are necessary for its internal use in connection with generic and plant-specific reviews and approvals as well as the issuance, denial, amendment, transfer, renewal, modification, suspension, revocation, or violation of a license, permit, order, or regulation subject to the requirements of 10 CFR 2.790 regarding restrictions on public disclosure to the extent such information has been identified as proprietary by Westinghouse, copyright protection notwithstanding. With respect to the non-proprietary versions of these reports, the NRC is permitted to make the number of copies beyond those necessary for its internal use which are necessary in order to have one copy available for public viewing in the appropriate docket files in the public document room in Washington, D.C. and in local public document rooms as may be required by NRC regulations if the number of copies submitted is insufficient for this purpose. Copies made by the NRC must include the copyright notice in all instances and the proprietary notice if the original was identified as proprietary.

TABLE OF CONTENTS

LIST OF TABLES

LIST OF FIGURES

LIST OF FIGURES (Continued)

LIST OF FIGURES (Continued)

LIST OF FIGURES (Continued)

4 TWO-PHASE LEVEL SWELL ANALYSIS

4.1 Introduction

The key phenomena for the AP600 small-break loss-of-coolant accident (LOCA) phenomena identification ranking table (PIRT) have been developed, refined, and presented to the NRC (Reference 4-1). The final small-break LOCA PIRT from Reference 4-1 is given as Table 1-1. One of the highly ranked phenomena in the PIRT is the level swell or mixture level in the reactor vessel, downcomer, core, and upper plenum. The prediction of the correct mixture level determines if the core remains covered with a two-phase mixture or if fuel rod heatup could occur. There are several submodels that comprise the prediction that include: the drift flux, which predicts phase fluxes and the void fraction; the logic for determining concurrent and countercurrent flow; and the two-phase/single-phase interface. These submodels act together to produce the mixture height and mass distribution within the reactor vessel, which determine core coolability. This section contains the results of two-phase level swell analyses performed to investigate this important phenomena as calculated by the AP600 NOTRUMP code. Included in the analyses are a set of blowdown tests with varying pressure (General Electric small blowdown vessel tests) and two sets of constant pressure tests with heat addition (ACHILLES and G2). It is important to note that the current AP600 SSAR calculations (Reference 4-2), which use the NOTRUMP code (Reference 4-3) with Appendix K conservatisms, indicate that there is sufficient inventory in the reactor system, due to the ample injection flow from the passive safety-related systems, so that the core does not uncover for small-break LOCAs up to the loss of an 8-in. DVI line or 8-in. CMT cold leg balance line. All smaller cold leg LOCAs also maintain core coverage with no cladding heatup. The results of the SSAR calculations, which show successful performance of the passive safety-related systems, have been supported by the similar results of the SPES-2 (Reference 4-4) and Oregon State University (Reference 4-5) tests.

4.2 General Electric Small Blowdown Vessel Test Simulation

4.2.1 General Electric Small Blowdown Vessel Test Facility

4.2.1.1 Facility Description

The General Electric small blowdown vessel test facility was designed to study basic phenomena such as void fraction distribution and transient liquid-vapor level swell action during blowdown. A description of the tests performed is provided in Reference 4-6.

Blowdown tests were performed in a cylindrical carbon steel vessel. The vessel is a two-piece unit that can be separated at a pair of flanges located near the center of the vessel. The cylindrical portion of the vessel is constructed from Schedule 80 pipe, 12-ft. long with an inside diameter of 0.948 ft. There are elliptical heads welded on to the ends of the pipe to create the vessel. The total vessel volume is 10 ft.^{3}, and the total height is 14 ft. There are five calorimetric heater rods in the bottom of the vessel to heat the water. These rods are 1 in. in diameter and 2-ft. high. The steam exhaust is located at the 13-ft. elevation, with an orifice that is captured in a flange. The orifices used to control the tank blowdown rate are plates with the prescribed hole machined without a chamfer. The orifice is located close to the vessel in a 2-in., Schedule 80 pipe. Figure 4.2-1 is a scaled drawing that shows the vessel, its penetrations, the blowdown line, and a suppression pool where the blowdown effluent was safely discharged.

A 3/4-in. thick perforated plate (containing 109 9/16-in. diameter holes) designed to provide an internal flow restriction is installed between the main vessel flanges at the mid-elevation during some of the tests. The resistance of the plate is varied by plugging a selected number of holes. Orifice plates with different flow areas are used in the blowdown line to limit the blowdown flow rate and vary the vessel depressurization rate (see Figure 4.2-2).

Figure 4.2-2 also shows the instrumentation arrangement used to measure three basic parameters: pressure, pressure differences, and temperature. Vessel pressure and differential pressures are measured using strain-gage pressure transducers, and temperatures are measured using Iron-Constantan thermocouples. The transient void fraction and the mixture level are calculated from differential pressure measurements.

Method of Testing

The vessel was initially filled with demineralized water and boiled at atmospheric pressure for approximately 30 minutes to liberate any dissolved gas in the supply water. A vent at the top of the vessel was then closed, and the water was heated to establish the initial conditions (which were a nominal pressure of 1000 psi and 545°F). Actual initial conditions for each test are given in the test matrix in Table 4.2-1.

With the facility initially heated and pressurized, several top-break blowdown tests were conducted using different-sized orifice plates to vary the blowdown transient. The tests also varied the open area of the resistance plate, which is located at the vessel mid-plane.

The test information available in Reference 4-6 includes calculated void fractions and vessel mixture levels. Reference 4-6 also explains how the void fraction information is calculated from the differential pressure cell data obtained during the test. Therefore, the differential pressure data could be determined from the report, and vessel mass inventory could be calculated. The system pressure behavior is also available as well as the initial conditions in the vessel. There is no information on the break flow rate and the fraction of flow that is liquid; therefore, a mass balance or closure on a mass balance for the vessel could not be obtained with the available data.

4.2.1.2 Test Matrix

Steam blowdown tests conducted in the vessel are summarized in Table 4.2-1. The test initial conditions include the system pressure, initial collapsed head, the flow area of the plate, and the orifice size. Vessel pressure, two-phase mixture level, and void fraction or density distribution are the only data available for each test.

4.2.1.3 Selection and Tests for NOTRUMP Validations

Seven steam blowdown tests are identified in Reference 4-6 and listed in Table 4.2-1. Of these tests, four were selected to be analyzed using the NOTRUMP code: 8-21-1, 8-25-1, 1004-3, and 1004-2. Since the only source of data is the figures from Reference 4-6, the selection of the tests was based on the quality and availability of data for each test. The tests selected cover the range of transient blowdowns both with and without the interior plate.

4.2.2 NOTRUMP Model of the General Electric Small Blowdown Vessel Tests

The General Electric small blowdown vessel tests use a 14-ft. high, vertical vessel with a discharge line at the top. The initial collapsed liquid level does not fill the vessel. The vessel is modeled using a vertical stack of 12 NOTRUMP cells, as seen in Figure 4.2-3. The NOTRUMP cells were chosen so that the cell boundaries correspond with the test location of the differential pressure cells that are used to calculate the void fraction and determine the mixture height. The total volume (10 $ft.^3$) is preserved in NOTRUMP as well as the elevation of the break, as shown in Figure 4.2-1. As Figure 4.2-3 indicates, there are two NOTRUMP fluid nodes that span a differential pressure cell height; therefore, there are two NOTRUMP cell average void fraction values that can be compared to the test data. The flow restrictor plate is located between two NOTRUMP cells at the approximate center of the vessel. The hydraulic resistance of the holes in the plate is modeled in the NOTRUMP code as an equivalent fL/D. It is assumed that the initial mass of water is heated to the saturation temperature of the given pressure. The transient calculation is initialized by assuming that the break opened at time zero with an atmospheric back pressure.

4.2.3 NOTRUMP Comparisons to the General Electric Small Vessel Blowdown Tests

4.2.3.1 Comparisons to Test 8-21-1

Test 8-21-1 is a blowdown from 1015 psia with an initial collapsed liquid level of 8.89 ft. The orifice size used in this test has a diameter of 3/8 in., and the restrictor plate at the vessel center has 109 holes. Figure 4.2-4 shows the predicted and measured vessel pressure. As the figure indicates, agreement is excellent. The discharge coefficient assumed for the orifice for this case is 0.7, which is close to the ideal expected single-phase orifice discharge coefficient of 0.61. Sensitivity studies were performed using discharge coefficients of 0.6 and 0.7, and agreement with the pressure decay is most accurate with the 0.7 discharge coefficient. This value of discharge coefficient is used for the remainder of the tests.

The comparison of the predicted and measured two-phase mixture level for this test is shown in Figure 4.2-5. The test data plot includes an uncertainty band. Since there is no uncertainty band reported for test 8-21-1, the uncertainty band reported for test 8-25-1 (Reference 4-6) is applied to test 8-21-1. NOTRUMP predicts the initial swell with a slight delay relative to the data, but then the code overpredicts the height of the mixture level in the vessel, with the difference increasing as time progresses. The mixture level in the test is determined from the differential pressure cells along the bundle by a linear extrapolation of the calculated two-phase void profile below the level. Differential pressure cells can also sense the presence of the two-phase mixture level within the ΔP span once the mixture level enters the span. The NOTRUMP calculation is within the uncertainty until approximately 10 seconds into the transient and then lies above the data for the remainder of the transient. The trends of the calculation, however, do agree with the data.

Figures 4.2-6 to 4.2-11 show the comparisons of the void fraction calculated from the data using the differential pressure cells to the void fraction calculated, in the same manner, from the NOTRUMP pressure drop results. Also presented are the void fractions calculated directly by NOTRUMP for the two nodes that are contained in the differential cell span. Sozzi (Reference 4-6) calculated a void fraction from the differential pressure measurements, assuming that the elevation head is the only significant term in the momentum equation, as:

$$\overline{\alpha_i} = (\overline{\rho_i} - \rho_f)/(\rho_g - \rho_f) \qquad (4.2\text{-}1)$$

where:

$\overline{\alpha_i}$ = average void fraction in the nodes bounded by the differential pressure cell

$\overline{\rho_i}$ = average mixture density in the nodes bounded by the differential pressure cell

ρ_f, ρ_g = liquid and vapor densities based on the local pressure in the node

A similar calculation was performed using the calculated pressure drops from the NOTRUMP simulation to compare with the data. It would have been preferable to compare directly to the measured pressure drop data; however, only the calculated void fraction, which is based on the pressure drop data, is available. Figures 4.2-6 to 4.2-9 indicate that at the beginning of the test the NOTRUMP-calculated mixture region void fractions correspond with the void fractions calculated using the NOTRUMP-calculated pressure drop in the same manner as Sozzi (Reference 4-6). Both methods of calculating the NOTRUMP void fractions agree well with the test data, as seen by the uncertainty bands on the figures for those times when the NOTRUMP fluid volume remains covered with a two-phase mixture. However, when the mixture level becomes low enough so that it is within the span of the differential pressure cell, the void fraction calculated from the differential pressure cell data increases since less mass is being averaged over the same span of the cell. The span of the differential pressure cells equals two NOTRUMP fluid nodes, as seen in Figure 4.2-3. Once the mixture level enters the differential pressure cell span, the void fraction calculated by NOTRUMP is lower, as indicated on the figures, since the NOTRUMP-calculated void fraction is the average for the region of the fluid node below the mixture level and not the full span of the differential pressure drop measurement. This effect is seen in Figures 4.2-9 to 4.2-11. When the calculated NOTRUMP mixture void fraction rapidly approaches zero, this indicates that the mixture region within the fluid node has disappeared when the mixture level falls below the node bottom elevation. The lower NOTRUMP fluid volume void fraction approaching zero corresponds to the emptying of the differential pressure cell of mixture and to the cell void fraction approaching unity. This corresponds to the void fraction calculated using the NOTRUMP pressure drop data, which also indicates unity when the two-phase mixture drops out of the differential pressure cell span.

In Figure 4.2-10, the data-inferred void fraction and the void fraction calculated from the NOTRUMP differential pressure indicate that the void was initially unity then decreased to 40 percent. This behavior is due to the low initial level for this test, which was below the differential pressure measurement span. This span was initially filled with saturated steam and the void fraction was unity. Once the test began, the flashing of the mixture caused the mixture to swell up into the differential pressure measurement span so that the void fraction dropped to a much lower value. Afterwards, the mixture level again dropped out of the measurement span as the vessel lost mass and depressurized. This same behavior is seen in Figure 4.2-11, except that the mixture did not swell up as high in this differential pressure drop span, and the mixture level quickly dropped out of the span as the vessel depressurized.

As the figures indicate, the NOTRUMP prediction generally lies below the test-calculated void fraction at most of the elevations, which indicates that NOTRUMP is slightly overpredicting the mass in the vessel. At higher elevations, as the two-phase mixture interface approaches the location of the differential pressure cell, the data move upward to a void of unity before the NOTRUMP calculation. This again supports the higher mixture level calculated by NOTRUMP in Figure 4.2-5, and that the code is overpredicting the vessel inventory. The trend of the prediction agrees well with the data but is displaced in time due to the higher calculated vessel mass.

The NOTRUMP calculation captures the trends of this test, and the calculations are within the data uncertainty for significant periods of the transient.

4.2.3.2 Comparisons to Test 8-25-1

Test 8-25-1 is a vessel blowdown test from 1020 psia with an initial level of 8.82 ft. in the vessel. The break orifice used in the test has a bore size of 1/2-in., and the restriction plate has 109 holes. The total transient time for this test is shorter than for test 8-21-1 due to the larger break size used. Figure 4.2-12 shows the measured vessel pressure transient and the NOTRUMP pressure prediction. A discharge coefficient of 0.7 is used in the prediction, and good agreement is obtained. The NOTRUMP calculation crosses over the data in the same manner as for test 8-21-1; however, the differences are small, and the calculation follows the data trends.

Figure 4.2-13 shows the measured and predicted vessel mixture level for test 8-25-1. As the figure indicates, the NOTRUMP mixture level lies above the mixture level estimated from the test void fractions. The NOTRUMP calculation is within the uncertainty bands on the test level for only a short period of the transient and then lies above the test mixture level, indicating that the code is overpredicting the vessel mass.

Comparisons of void fractions calculated from the test differential pressure drop measurements and the NOTRUMP differential pressure drops are shown in Figures 4.2-14 to 4.2-19. Also shown are NOTRUMP void fractions in the mixture level within the fluid volume. The void fractions calculated from either the NOTRUMP pressure drops or from the mixture in the NOTRUMP fluid volume agree within the data uncertainty for the first period of the test. However, as time progresses, the NOTRUMP calculations indicate a lower void fraction as compared to the test data, which indicates that additional mass is being stored in the NOTRUMP calculation. This trend is consistent with the NOTRUMP-predicted vessel mixture level, as seen in Figure 4.2-13. The NOTRUMP-calculated void fraction from the differential pressure drop data is identical to the void fraction calculated from the NOTRUMP mixture within the fluid node until the mixture level enters the node. Once the actual mixture level is within the differential pressure cell span, the test void fraction from the differential pressure is higher since the reduced mass within the cell is averaged over the full span height. The same situation occurs for the void fraction, as calculated from the NOTRUMP pressure drop measurements. The NOTRUMP calculations indicate a delay as the mixture level approaches the span of the differential cell since NOTRUMP is overestimating the mass within the vessel. This behavior is seen in Figures 4.2-16 and 4.2-17.

In Figures 4.2-18 and 4.2-19, the NOTRUMP-calculated mixture void fraction is for two NOTRUMP cells within the same span as the differential pressure cells in the test. As the mixture level drops from the top of the fluid cell within the span to the lower computational cell, the void profile indicates a vertical drop, as seen at 55 seconds in Figure 4.2-18 and 30 seconds in Figure 4.2-19. The calculated mixture void goes to zero when the void calculated from the pressure drop reaches unity, as

seen in Figures 4.2-18 and 4.2-19. When the calculated mixture void is zero, this implies that there is no longer any mixture within the cell.

Figures 4.2-18 and 4.2-19 indicate that the initial void fraction is unity at the beginning of the test. Again, this is due to the initial level being below these elevations. When the break is initiated, the saturated liquid flashes and swells up into the top two differential pressure cell spans. As the mixture level falls, these top spans void first, as indicated in the figures.

4.2.3.3 Comparisons to Test 1004-3

Test 1004-3 is a vessel blowdown test from 1011 psia with an initial level of 10.4 ft. The break orifice used has a 3/8-in. bore, and a discharge coefficient of 0.7 is used. The vessel pressure comparison is given in Figure 4.2-20, and the comparison is similar to the other tests, except that there is more of an overprediction of the vessel pressure for the first 50 seconds.

The comparisons of the test mixture level and predicted level (see Figure 4.2-21) show that the NOTRUMP calculations lie outside the uncertainty of the data for the entire test. NOTRUMP calculations overestimate the vessel mixture level by a large amount for the first 50 seconds, after which the code calculation approaches the data uncertainty. Toward the end of the transient, NOTRUMP indicates a slight overprediction of the vessel mass.

Comparisons of the void fractions are shown in Figures 4.2-22 to 4.2-27. The agreement is good between the NOTRUMP calculations and the test data. The calculations are within the uncertainty of the data for much of the transient.

The difference in the void fraction developed from the measured pressure drop data and the void fraction developed from the NOTRUMP pressure drop data (see Figures 4.2-25 to 4.2-27) is caused by the overprediction of the vessel mass, as indicated by NOTRUMP at this time.

4.2.3.4 Comparisons to Test 1004-2

Test 1004-2 is a vessel blowdown test from 1011 psia with an initial level of 10.5 ft. The blowdown orifice has a bore of 7/8-in., and there is no resistance plate inside the vessel. A discharge coefficient of 0.7 is used for this test. Since the break size is large relative to the size of the vessel, the blowdown transient is short, and a significant portion of the initial inventory is lost out the simulated break.

Figure 4.2-28 compares the calculated and measured vessel pressure for the transient. As the figure indicates agreement is reasonable; however, the NOTRUMP-calculated response is significantly higher before 25 seconds. After this time period, agreement is improved, but the vessel is already depressurized to 200 psia.

Figure 4.2-29 compares the measured mixture level with the NOTRUMP prediction. As the figure indicates, the code prediction is above the data at the beginning of the test but agreement between the prediction and the data is within or below the uncertainty of the data for the majority of the transient.

Figures 4.2.30 to 4.2-35 compare the predicted and measured void fraction for the different NOTRUMP fluid nodes that correspond to the measurement locations for the differential pressure cells. The agreement between the test data and the NOTRUMP predictions is not as good for this test as compared to previous tests for all elevations. The calculations either agree with the data or lie above the data for the first portion of the transient where the pressures are above 200 psia. This is also the time period that the NOTRUMP-predicted pressure is higher than the test, and the initial mixture level predicted by NOTRUMP is higher. For the first 25 seconds of the transient, the NOTRUMP predictions are outside of the uncertainty bands on the data in several cases. As time progresses, the NOTRUMP-predicted void fractions lie below the test data, outside of the data uncertainty. The void fractions developed from the NOTRUMP-calculated pressure drop show the same trends as the data void fractions. The NOTRUMP void fractions from the pressure drop also approach unity, with only a slight delay as compared to the test data. This corresponds to the good agreement between the data mixture level and the NOTRUMP-predicted mixture level.

4.2.4 NOTRUMP Comparisons to the General Electric Small Vessel Blowdown Tests Using the Data Mass Inventory

In Subsection 4.2.3, the General Electric small vessel tests are predicted using a fixed orifice discharge coefficient in conjunction with the Henry/Fauske HEM critical flow model to model the break mass flow out of the test vessel. As indicated in Subsection 4.2.3, the discharge coefficient is varied over a probable range, and the overall most accurate coefficient of 0.7 is used for all of the test simulations. However, compared to the tests results, the NOTRUMP code overpredicts the two-phase level. Investigation into the cause of the overprediction reveals that in the NOTRUMP simulation, more mass remains in the vessel in the simulation compared to the mass remaining in the vessel for the test. This is confirmed by plotting the vessel mass calculated from the axial pressure drop data obtained with the cells along the height of the vessel and comparing the test transient mass to the vessel mass predicted by the NOTRUMP code. Results of this comparison are shown for test 8-21-1 in Figure 4.2-36. Assuming that the reported vessel geometry and the initial conditions are correct, it appears that NOTRUMP underpredicts the mass flow out of the break so that more mass remains within the vessel, resulting in an overprediction of the mixture level. Since the break mass flow and its components are not measured in the test, it is difficult to determine the cause for the overprediction.

Given that a mass discrepancy exists between the test data and the NOTRUMP simulation, a different approach is taken to more accurately examine the NOTRUMP level swell model.

Since the transient vessel mass can be determined from the axial pressure cells along the vessel, it was decided to perform the NOTRUMP simulation maintaining the vessel mass consistent with the test information in addition to matching the vessel pressure history. By matching the vessel mass,

NOTRUMP would have the correct inventory relative to the test during the transient. By matching the vessel pressure history, NOTRUMP should calculate the flashing effects of the mixture as the vessel depressurizes. With this approach, it can be seen that if given the correct vessel mass and depressurization behavior, NOTRUMP can correctly calculate the vessel mixture level.

Two of the tests that are analyzed in Subsection 4.2.3 are reanalyzed as described above in which the test vessel mass and pressure are used as imposed boundary conditions on the NOTRUMP calculation, and the comparisons are made to the mixture level.

4.2.4.1 Comparison to Test 8-21-1 with Fixed Vessel Mass

The NOTRUMP model was revised to include a drain flowlink at the bottom of the vessel that allows the simulation mass inventory to match the test mass inventory. Also the vessel depressurization is matched by calculating the steam flow given the vessel pressure history. The calculated steam flow and liquid drain flow rates are used as boundary conditions in NOTRUMP. Figure 4.2-37 shows the transient pressure comparison for this test by matching the mass flow in the vessel as well as the steam flow out of the vessel. The pressure comparison is improved, as can be seen by comparing Figure 4.2-4 to Figure 4.2-37. The comparison of the transient vessel mass is shown in Figure 4.2-38 and indicates that NOTRUMP is matching the test transient mass. Figure 4.2-39 shows the liquid flow that is removed from the bottom of the vessel in the NOTRUMP calculation to match the transient vessel mass inventory. As this figure shows, the majority of the mass is removed early in time, which implies that in addition to the flashing of the liquid, there is liquid entrainment out the break that depletes the vessel inventory. The NOTRUMP integrated mass flow from the break at the bottom of the vessel and the steam from the break at the orifice is shown in Figure 4.2-40. Note that the mass removed through the drain line in NOTRUMP is only approximately 24 lbm, out of an initial inventory of approximately 280 lbm, or 8.5 percent, which is quite small.

By adjusting the NOTRUMP simulation to match the vessel mass and vessel depressurization behavior, the key parameter calculated by the code is the two-phase mixture level. Figure 4.2-41 shows the mixture level using the above procedure and indicates that the NOTRUMP-calculated level is within the data uncertainty. Matching the vessel mass inventory in the NOTRUMP simulation decreases the predicted mixture level by 9 to 12 in. as can be seen by comparing Figure 4.2-41 to 4.2-5. This difference is consistent with the amount of liquid removed through the drain link. For example, at 100 seconds the system pressure is 300 psia and the void fraction at the top of the froth level is 40 percent. Under these conditions, the liquid content of the 12-in. difference is approximately 25 lbm, which is nearly the amount removed in the NOTRUMP calculation (24 lbm) to match the transient vessel mass.

The comparisons of the predicted and measured void fractions are shown in Figure 4.2-42 to 4.2-47. Comparing these predictions to the void fraction predictions obtained modeling the break in Figures 4.2-6 to 4.2-11 indicates, as expected, that the void fractions obtained by matching the

transient vessel mass agree better with the data as compared to the void fractions obtained using the break discharge coefficient of 0.7.

The conclusion from this test comparison is that the two-phase level swell models in NOTRUMP predict the correct mixture height in the vessel for the correct vessel inventory.

4.2.4.2 Comparison to Test 8-25-1 with Fixed Vessel Mass

The same NOTRUMP modeling for test 8-21-1 is applied to test 8-25-1 so that the transient vessel mass is matched in addition to the vessel depressurization behavior. Figure 4.2-48 shows the calculated and measured vessel pressure transient and indicates excellent agreement using the steam flow that is calculated to match the pressure behavior. The vessel transient mass comparison is shown in Figure 4.2-49, and the agreement is not as good as seen for test 8-21-1. The resulting liquid that is removed by the break at the bottom of the NOTRUMP-simulated vessel is shown in Figure 4.2-50, which indicates that the majority of the mass had to be removed at the beginning of the test to match the vessel mass inventory. Again, this indicates that these tests are not pure steam blowdowns, but rather, the break flow is a two-phase mixture. Figure 4.2-51 shows the integrated liquid flow out of the bottom of the NOTRUMP calculation as well as the integrated vapor flow out the discharge orifice. More liquid flow has to be taken out of the vessel to match the vessel transient inventory for this case compared to test 8-21-1. This is expected for this test since the break area is larger then test 8-21-1, and a more rapid depressurization occurs. Since additional mass is required to be removed to match the transient vessel mass, this supports the hypothesis that the blowdowns are not pure steam but two-phase.

The mixture level for test 8-25-1 is shown in Figure 4.2-52. The NOTRUMP prediction is within or below the data mixture level. Comparing Figures 4.2-52 to 4.2-13 indicates that using the correct vessel mass decreases the NOTRUMP-predicted mixture level by 12 to 15 in., depending on which time is being examined.

The void fraction comparisons are shown in Figures 4.2-53 to 4.2-58. Comparing these figures to Figures 4.2-14 to 4.2-19 indicates that NOTRUMP is predicting the same void as seen in Figures 4.2-14 to 4.2-19 or slightly lower. The NOTRUMP void fraction plots based on pressure drop in Figures 4.2-55 to 4.2-58 show an earlier rise to a void fraction of unity. This is consistent with the lower mixture level that NOTRUMP is now predicting for the same mass in the vessel.

The conclusion from this test comparison, which is the same as for test 8-21-1, is that NOTRUMP does predict the correct mixture height in the vessel for the correct vessel mass.

4.2.4.3 General Electric TRAC Simulations of Test 8-21-1

General Electric also modeled GE small vessel blowdown test 8-21-1 using their version of the TRAC Code (Reference 4-8). Figure 4.2-59 shows the measured and predicted vessel pressure transient with

the TRAC calculations lying below the data for the GE critical flow model, which uses a discharge coefficient of 0.8. GE attributes the lower pressure in the TRAC prediction to entrainment that they believe occurred in the test. Figure 4.2-60 shows the comparison of the predicted to measured depressurization rate for the test. The more rapid measured depressurization rate over the first 40 seconds is believed to be due to the entrainment of liquid out the break, which is not modeled in the TRAC calculation. The effect of the entrainment on the predicted and measured vessel mass is shown in Figure 4.2-61, which shows that there is approximately 20 lbm of liquid difference between the TRAC code prediction and the measured vessel mass in the test. This difference is approximately the same for the NOTRUMP prediction. This is also approximately the amount of mass that is leaked out of the bottom of the NOTRUMP simulation so that the NOTRUMP vessel mass and the test would agree.

Figure 4.2-62 shows the TRAC-predicted mixture level with the test data. While the agreement looks good, there are compensating errors in the calculation since, as shown in Figure 4.2-63, the TRAC-calculated vessel mass is larger than the data. If the TRAC calculation was adjusted to match the vessel mass as in the NOTRUMP simulations, the TRAC mixture level calculation would lie below or show improved agreement with the data since the vessel masses would have agreed. The TRAC assessment confirms the NOTRUMP observations that there is liquid entrainment out the break, which is not accounted for in the calculations, and results in a larger vessel mass and higher two-phase level swell relative to the data. Therefore, by matching the vessel inventory, a more accurate assessment of the level swell model can be obtained.

4.2.5 Noding Sensitivity Study

To investigate the effect of the number of nodes used for the GE simulations on the level swell behavior, a noding sensitivity study is performed with a preliminary version of the input deck. The study includes simulations of test 8-21-1 with 6, 12, 24, and 48 nodes. For this study, the break flow is calculated with the Henry/Fauske HEM break flow model assuming a discharge coefficient of 0.7 for all cases. The main objective of this study is to determine an appropriate number of nodes to use in the NOTRUMP simulations so that the level swell behavior is not significantly affected by the choice.

The system pressure behavior for each of the cases performed is shown along with the test data in Figure 4.2-63. Figure 4.2-63 shows that there is no significant difference between the system pressure response over the range of number of nodes modeled. This is expected since the amount of mass out of the break is the most significant factor in determining system pressure, and the number of nodes used would not be expected to affect the break flow calculation to any significant extent since the vessel mixture level remains below the break orifice by approximately 1 ft. or more for all cases.

The vessel mixture level behavior for each of the cases and the reported test mixture level are shown in Figure 4.2-64. Figure 4.2-64 shows that the only significant change in level occurs in increasing the number of nodes from 5 to 12. Further increases in the number of nodes do not change the

calculated level swell significantly. This study shows that given too much mass remaining in the simulation (as discussed in Subsection 4.2.4), increasing the number of nodes above 12 will not bring the calculated level significantly closer to the test information.

4.2.6 Conclusions

NOTRUMP comparisons to the four General Electric small blowdown vessel tests are performed using the same discharge coefficient for the break (0.7 discharge coefficient). The data comparisons indicate that the NOTRUMP code closely predicts the data trends observed in the tests. NOTRUMP predictions are improved for the tests without the resistance plate located within the vessel and are within the uncertainty of the data for many of the transients. However, it is believed that the plate has little or no effect on the results. Mixture level predictions for the two tests with the resistance plate indicate that NOTRUMP closely follows the trends of the data but generally lies above the data uncertainty. For these cases, NOTRUMP is predicting more mass stored in the vessel or a higher mixture level as compared to the test. The mixture level predictions for the two tests without the plate generally agree with the uncertainty of the test data, but at times are above the test data uncertainty.

Void fractions along the test vessel are calculated in two different ways in the NOTRUMP calculations. The NOTRUMP-calculated pressure drop is converted to a void fraction in the same manner as the data. The second approach is to compare the cell average void fraction as calculated by NOTRUMP. While the two different NOTRUMP calculations are outside the data uncertainty for portions of the transients, the trends of the data are generally predicted by the code.

The NOTRUMP calculations in which the mass in the vessel is matched show improvement in the two-phase mixture level predictions. Matching the vessel mass and depressurization rate removes the uncertainties of the break flow calculation and the amount of entrainment from the vessel two-phase mixture out the break. Therefore, by matching the vessel mass, a more accurate assessment of the NOTRUMP two-phase level swell models can be made. With the break flow and liquid entrainment uncertainties removed, the NOTRUMP level swell models either predict the test data within the data uncertainties or the prediction lies below the data mixture level and is conservative.

In conclusion, the NOTRUMP calculations closely follow the data trends observed in the vessel blowdown tests. In many cases, predictions for the mixture level and void fraction are within the uncertainty of the data. Mixture levels predicted by NOTRUMP tend to be higher than the data using the break model with a discharge coefficient of 0.7, which indicates that the code is calculating that more mass is stored in the vessel. If the vessel mass is matched in the NOTRUMP calculations, the code agrees with the test data within its uncertainty or lies below the data, which is conservative. These comparisons support the application of the NOTRUMP mixture level swell models for the AP600 small-break LOCA analysis.

TABLE 4.2-1
SUMMARY OF TEST PARAMETERS FOR
SMALL BLOWDOWN VESSEL STEAM BLOWDOWN TESTS

Test No.	Orifice Size (in.)	Restriction Plate (9/16-in. diameter holes)	Initial Conditions	
			Pressure (psia)	Level (ft.)
8-21-1	3/8	109 holes	1015	8.89
8-25-1	1/2	109 holes	1020	8.82
8-28-1	1	109 holes	1015	8.76
9-1-1	3/8	77 holes	1014	8.75
9-15-1	3/8	55 holes	1015	8.74
1004-3	3/8	No plate	1011	10.4
1004-2	7/8	No plate	1011	10.5

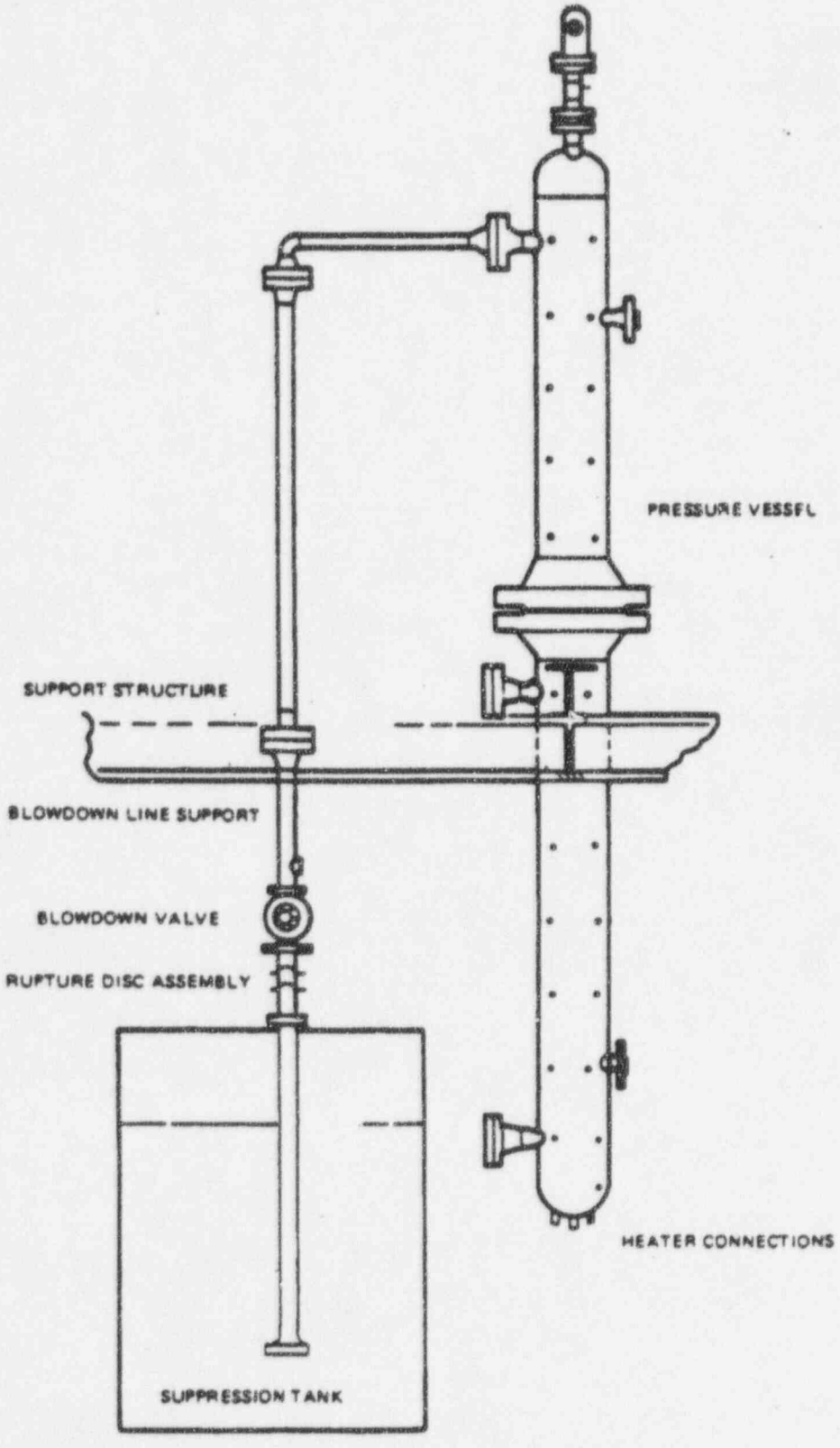

Figure 4.2-1 GE Small Blowdown Vessel

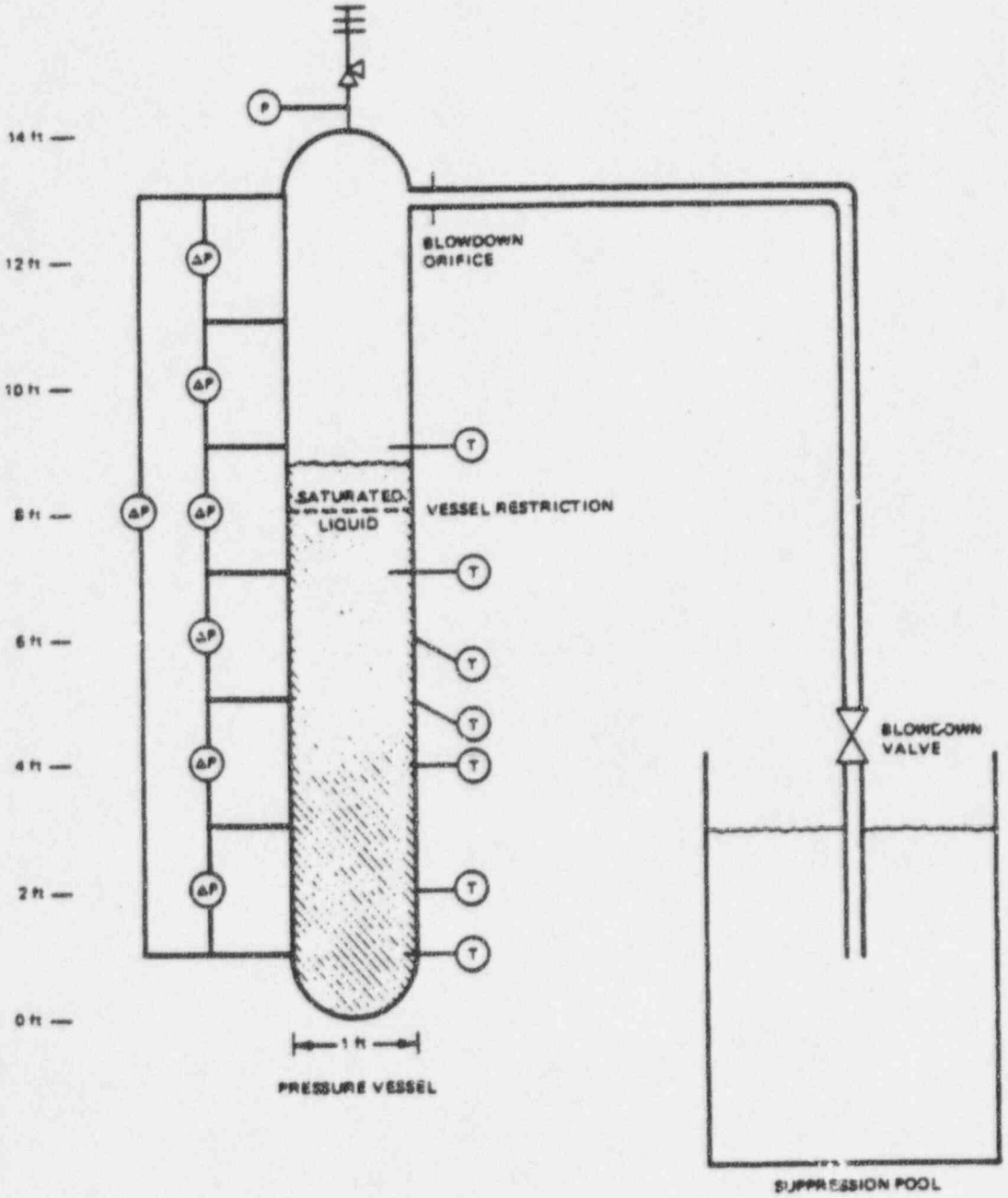

Figure 4.2-2 GE Small Blowdown Vessel Instrumentation

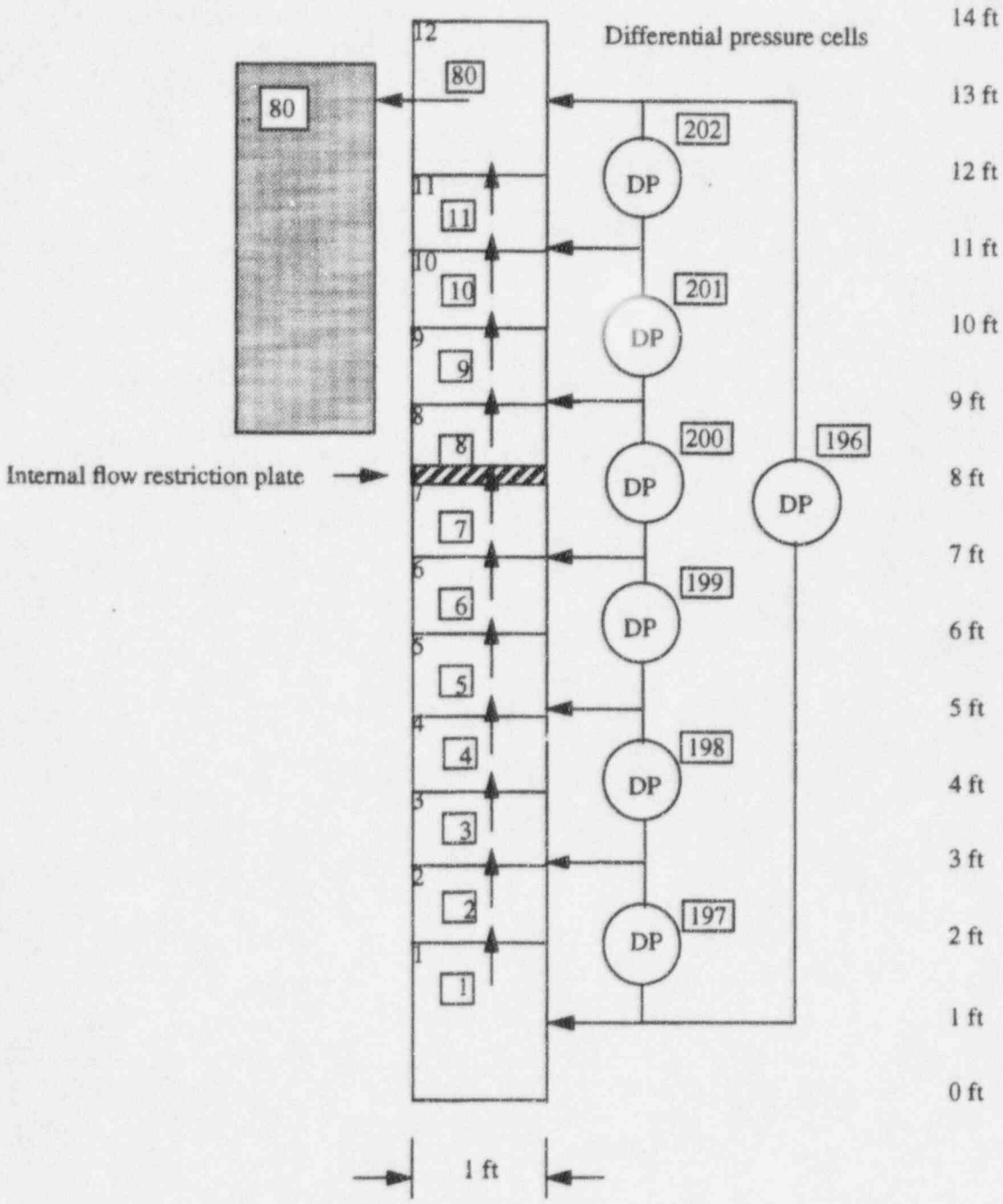

Figure 4.2-3 NOTRUMP Model for GE Small Blowdown Vessel Test Simulation

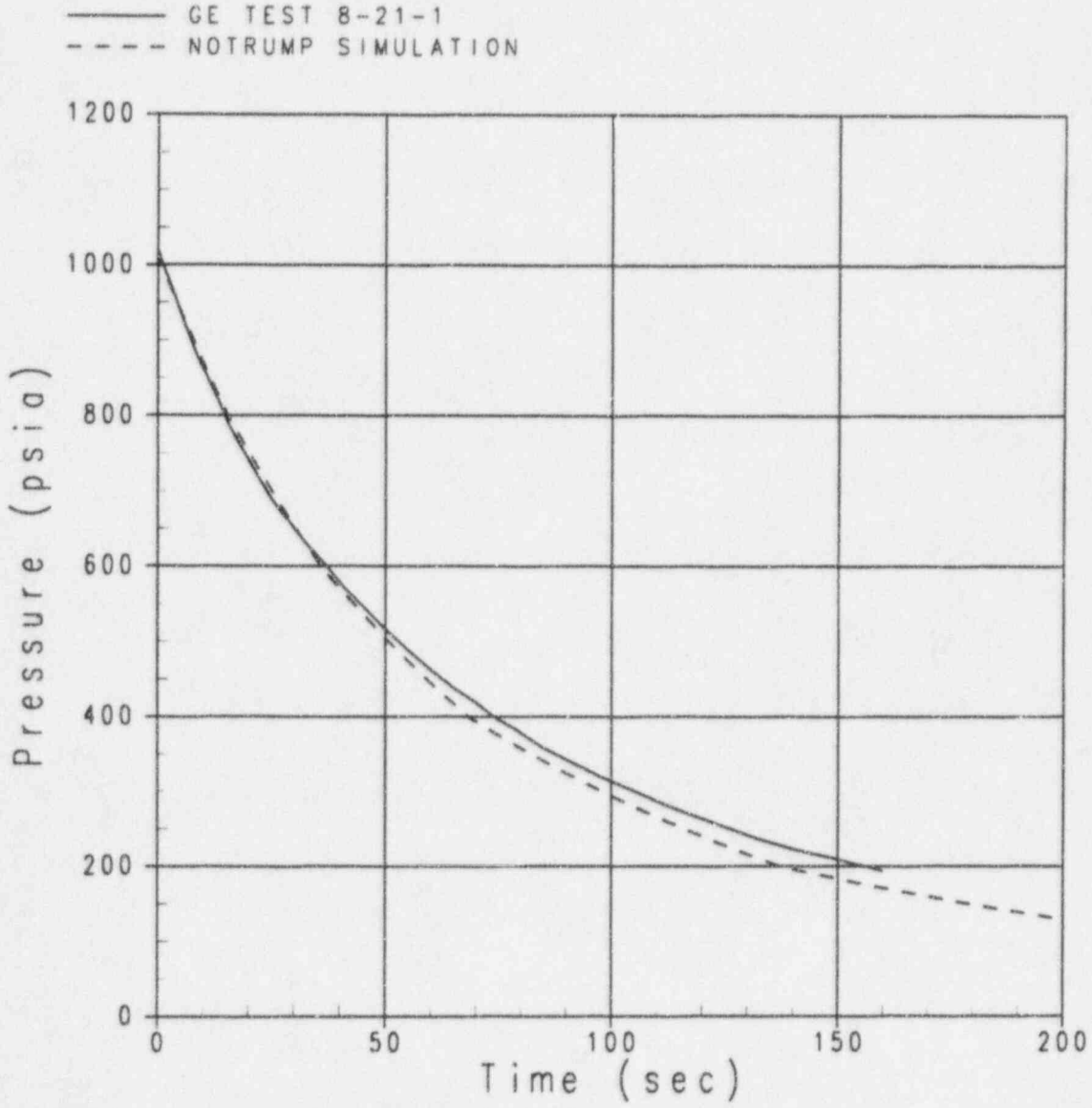

Figure 4.2-4 Vessel Pressure for GE Test 8-21-1 with 3/8-in. Break

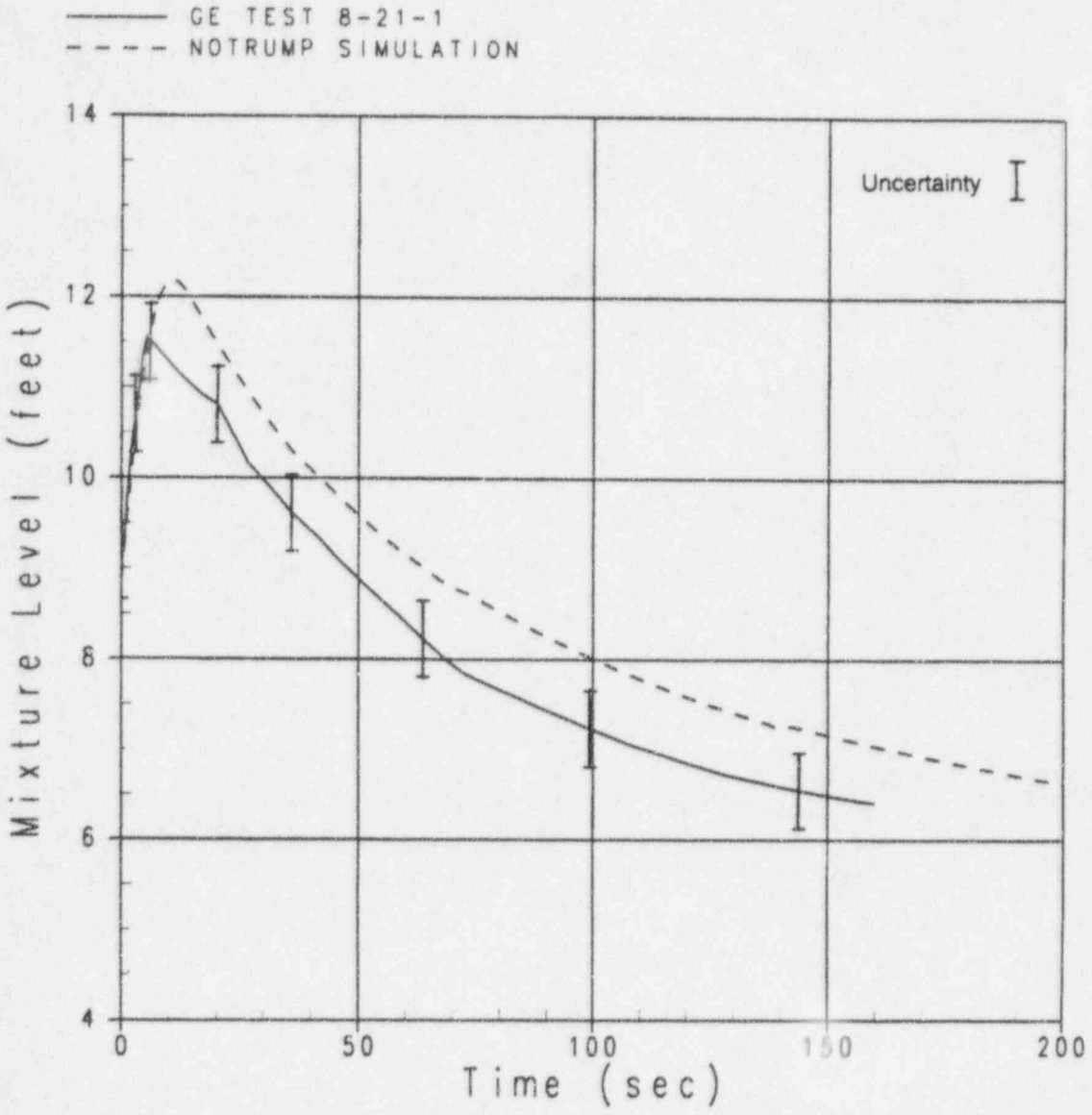

Figure 4.2-5 Vessel Mixture Level for GE Test 8-21-1, 3/8-in. Break

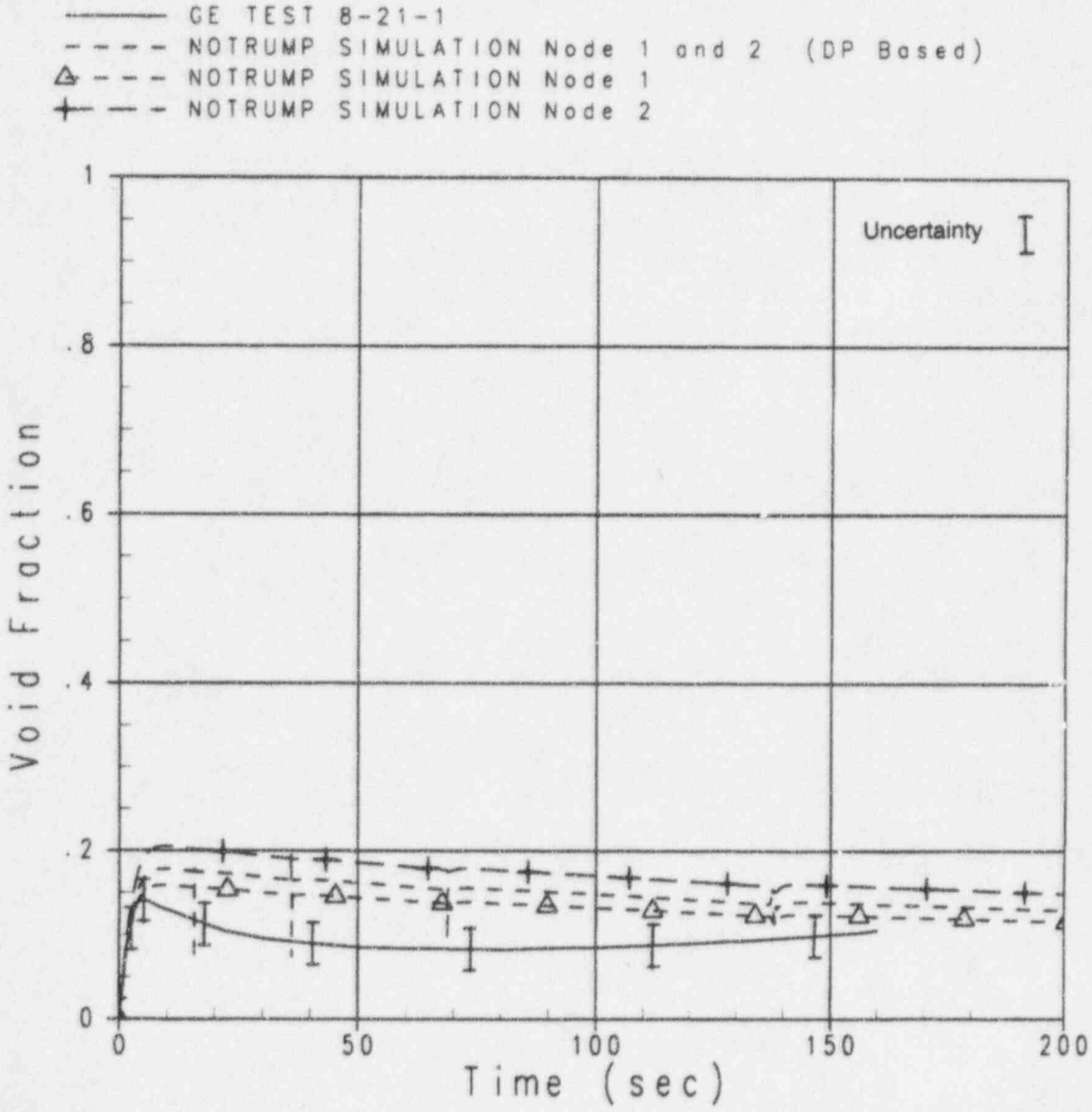

Figure 4.2-6 Void Fraction for GE Test 8-21-1, Nodes 1 and 2

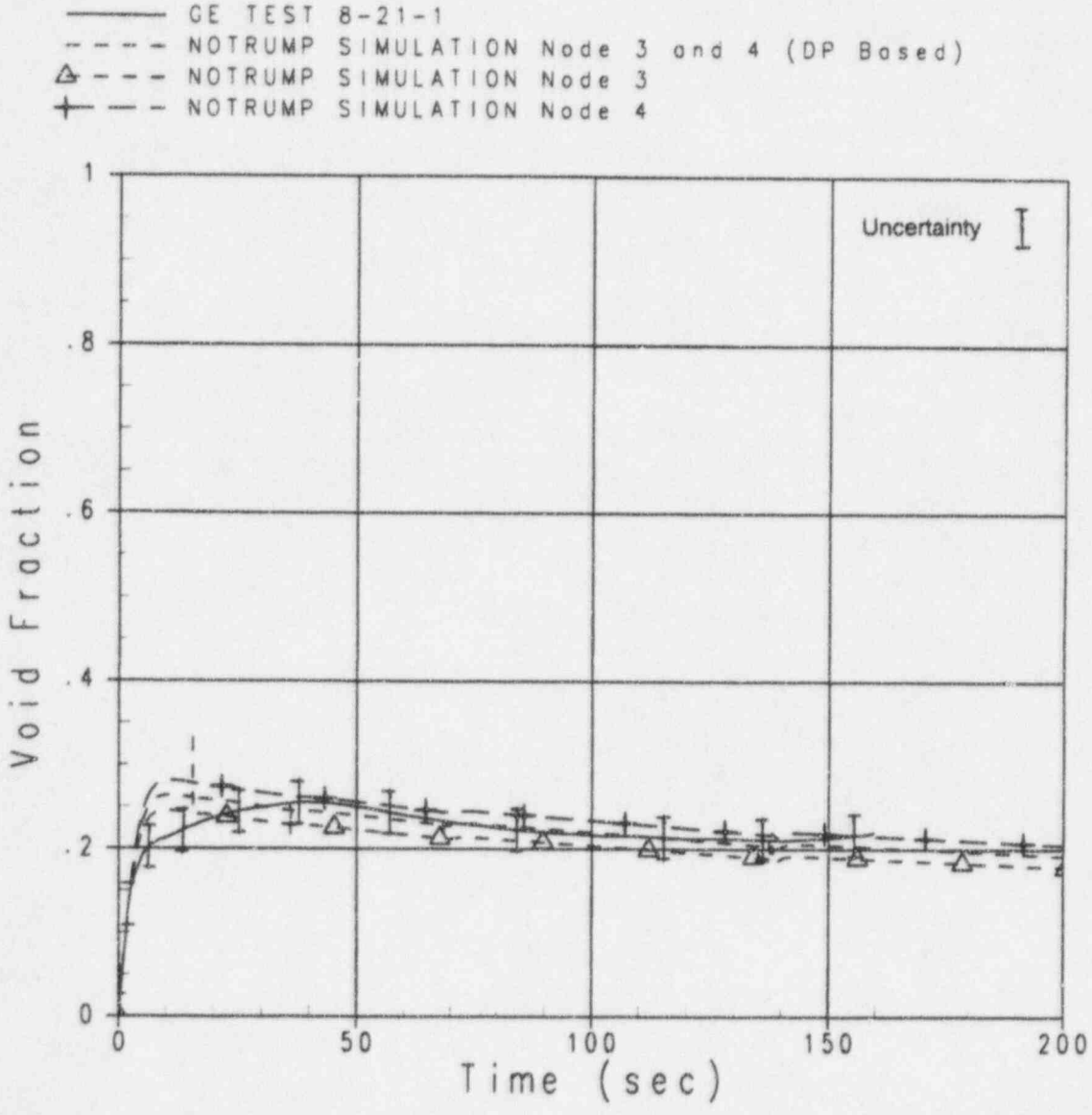

Figure 4.2-7 Void Fraction for GE Test 8-21-1, Nodes 3 and 4

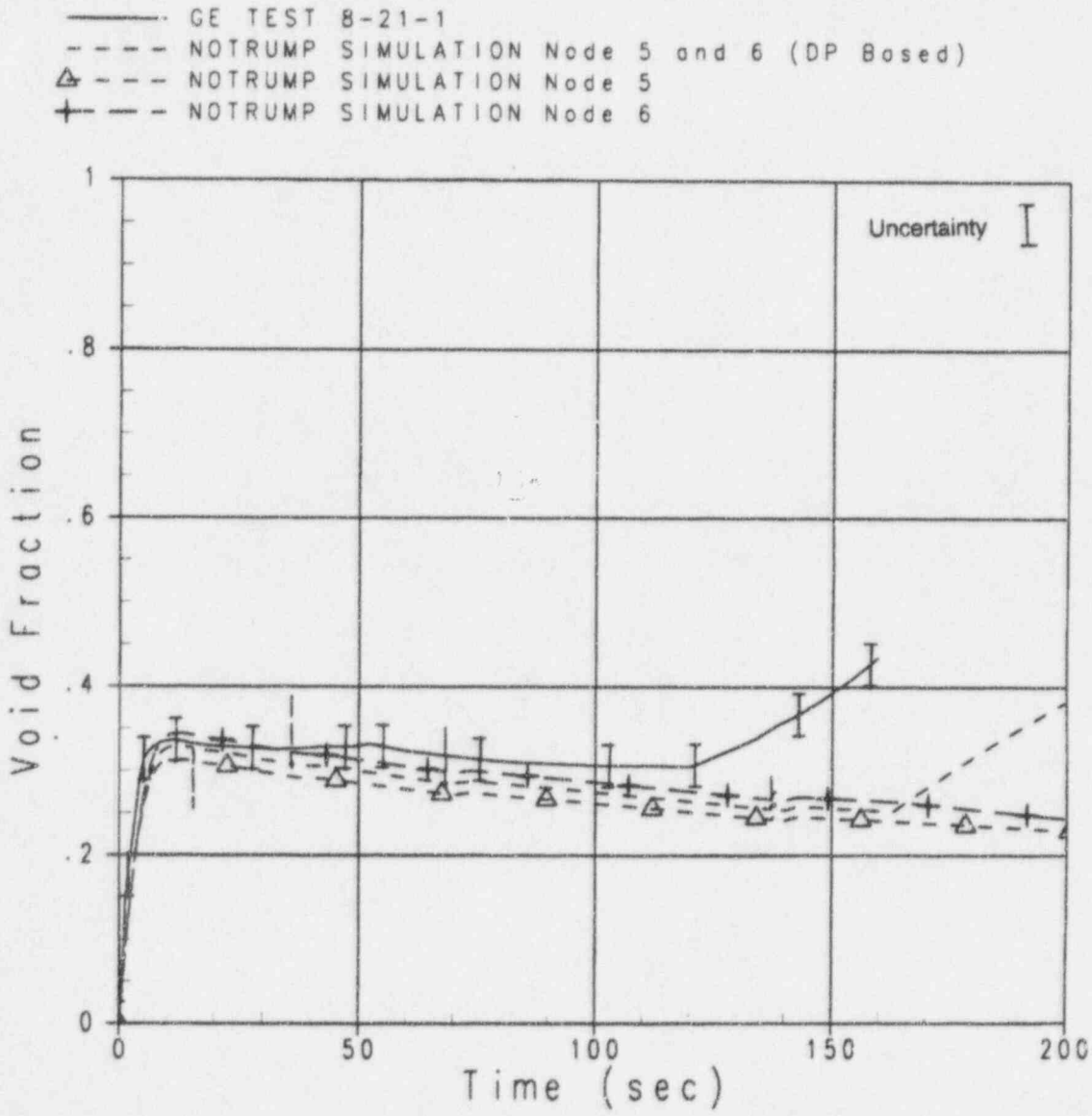

Figure 4.2-8 Void Fraction for GE Test 8-21-1, Nodes 5 and 6

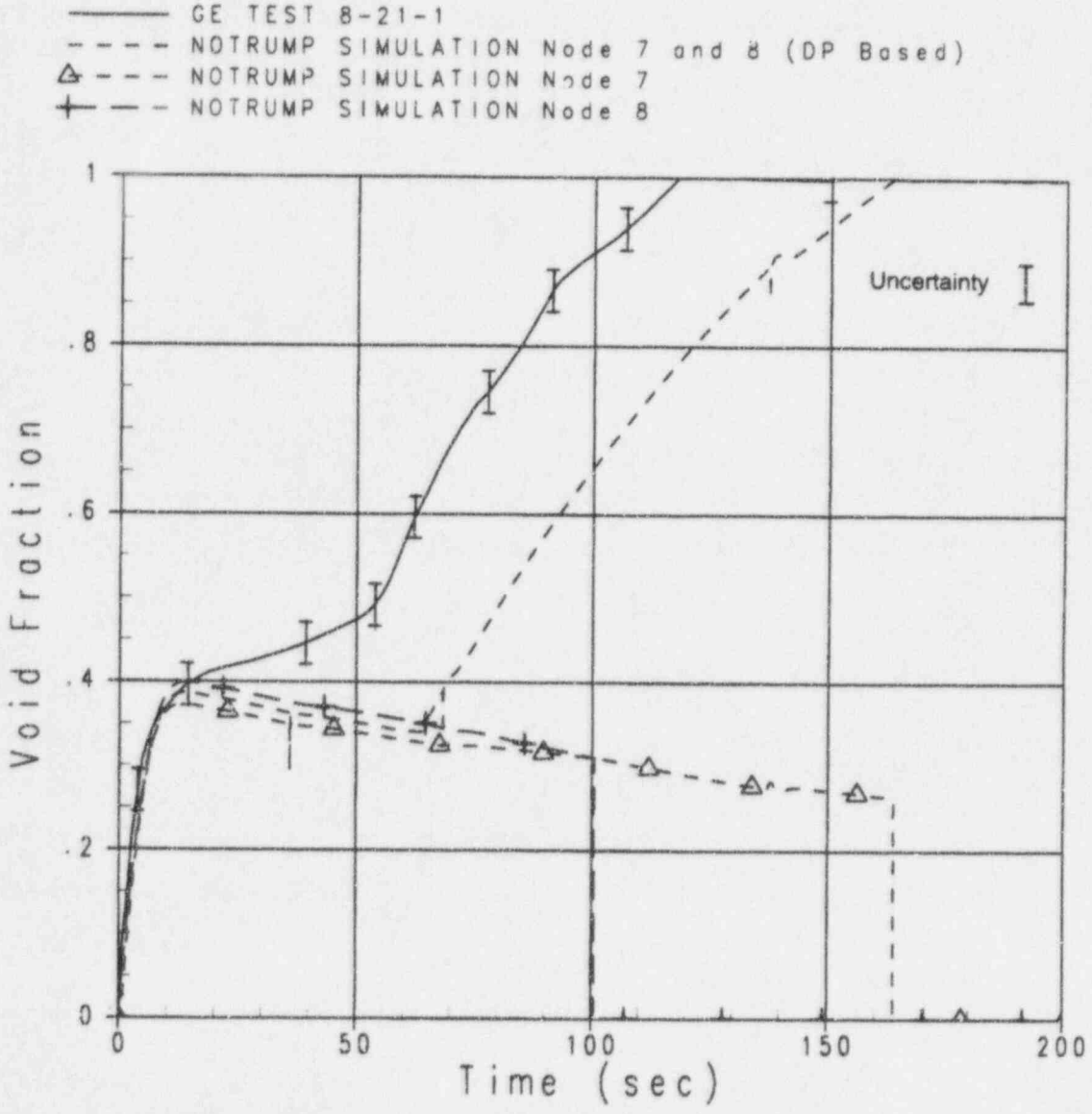

Figure 4.2-9 Void Fraction for GE Test 8-21-1, Nodes 7 and 8

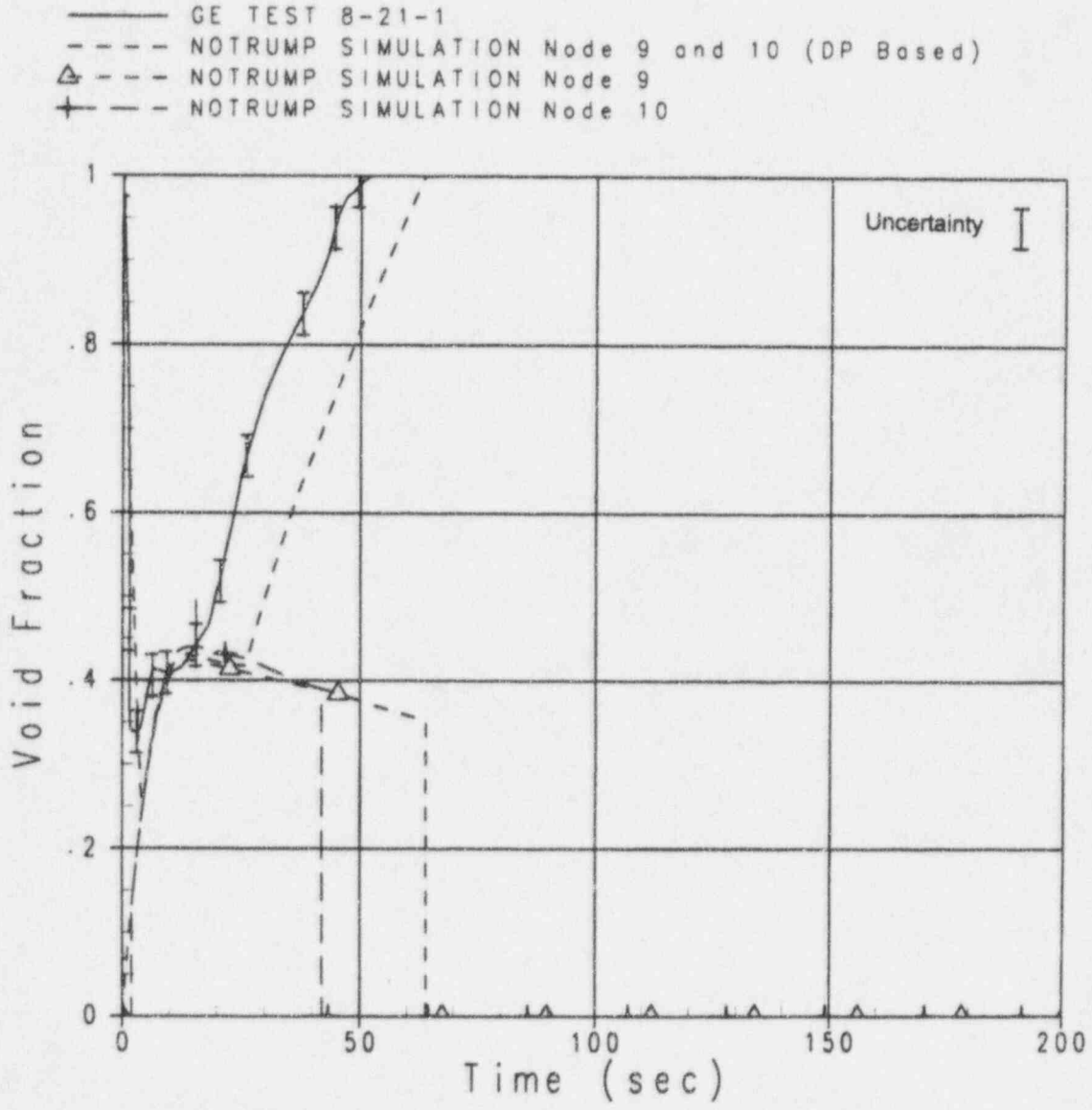

Figure 4.2-10 Void Fraction for GE Test 8-21-1, Nodes 9 and 10

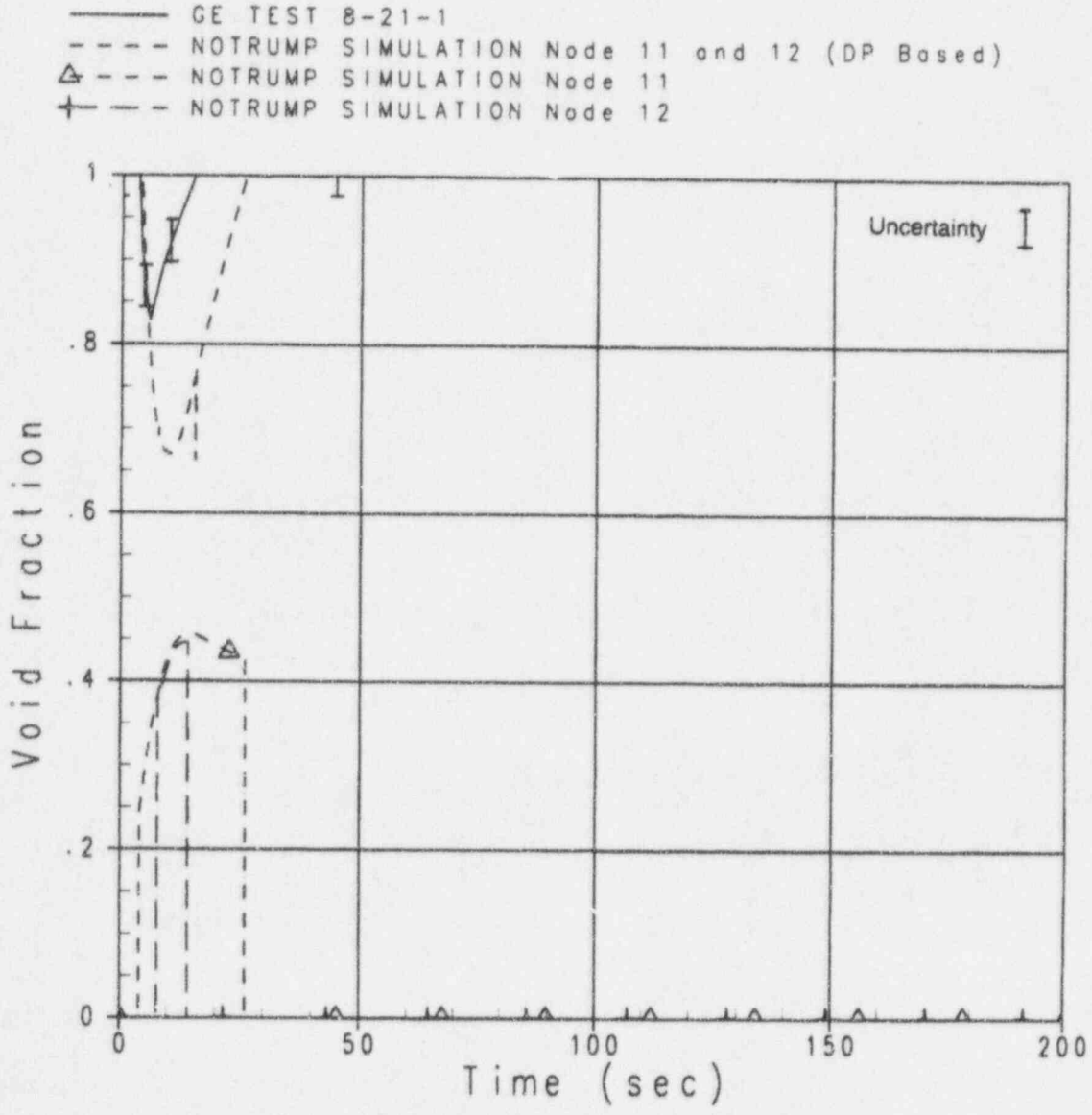

Figure 4.2-11 Void Fraction for GE Test 8-21-1, Nodes 11 and 12

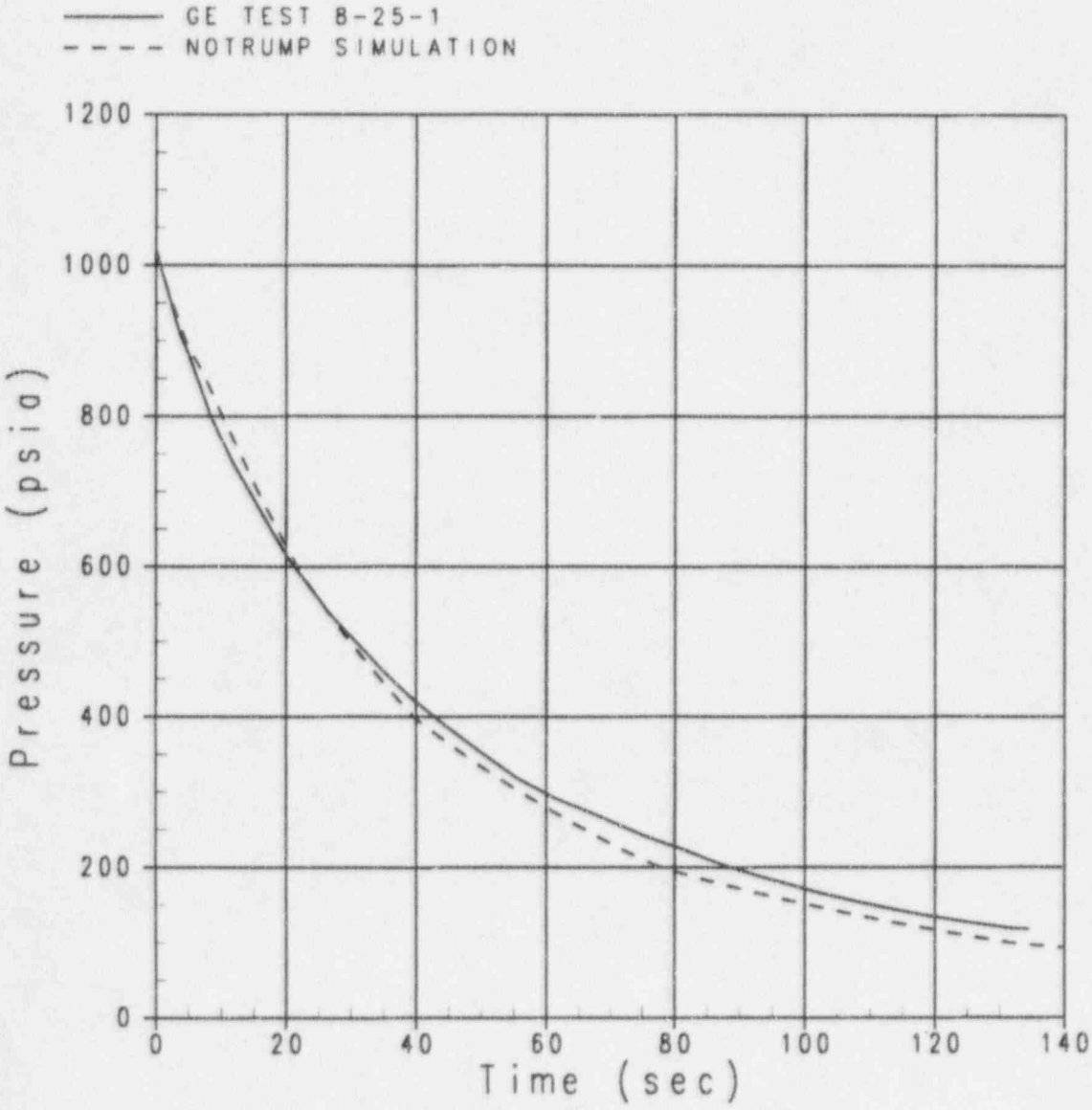

Figure 4.2-12 Vessel Pressure for GE Test 8-25-1, 1/2-in. Break

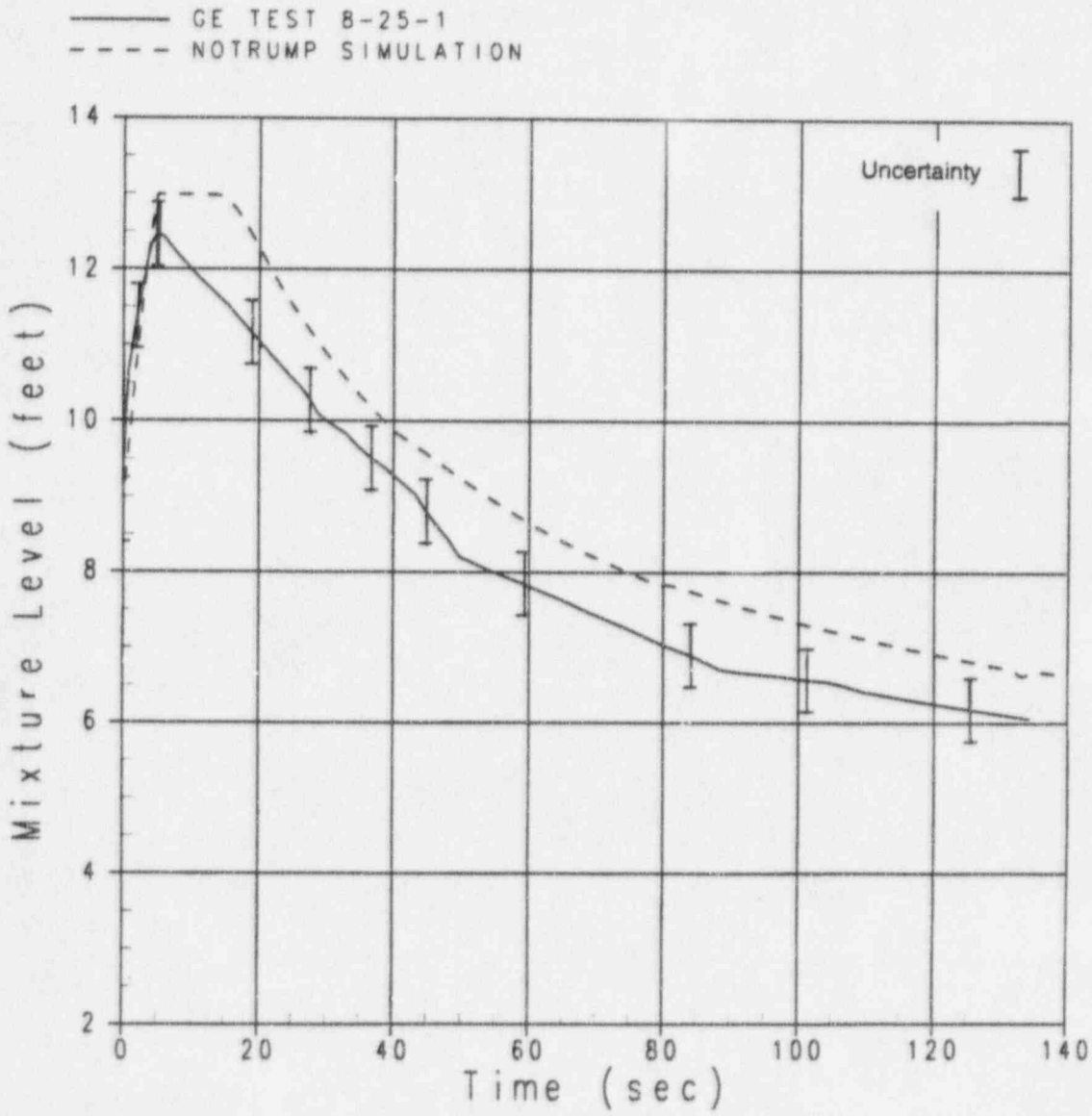

Figure 4.2-13 Vessel Mixture Level for Test 8-25-1, 1/2-in. Break

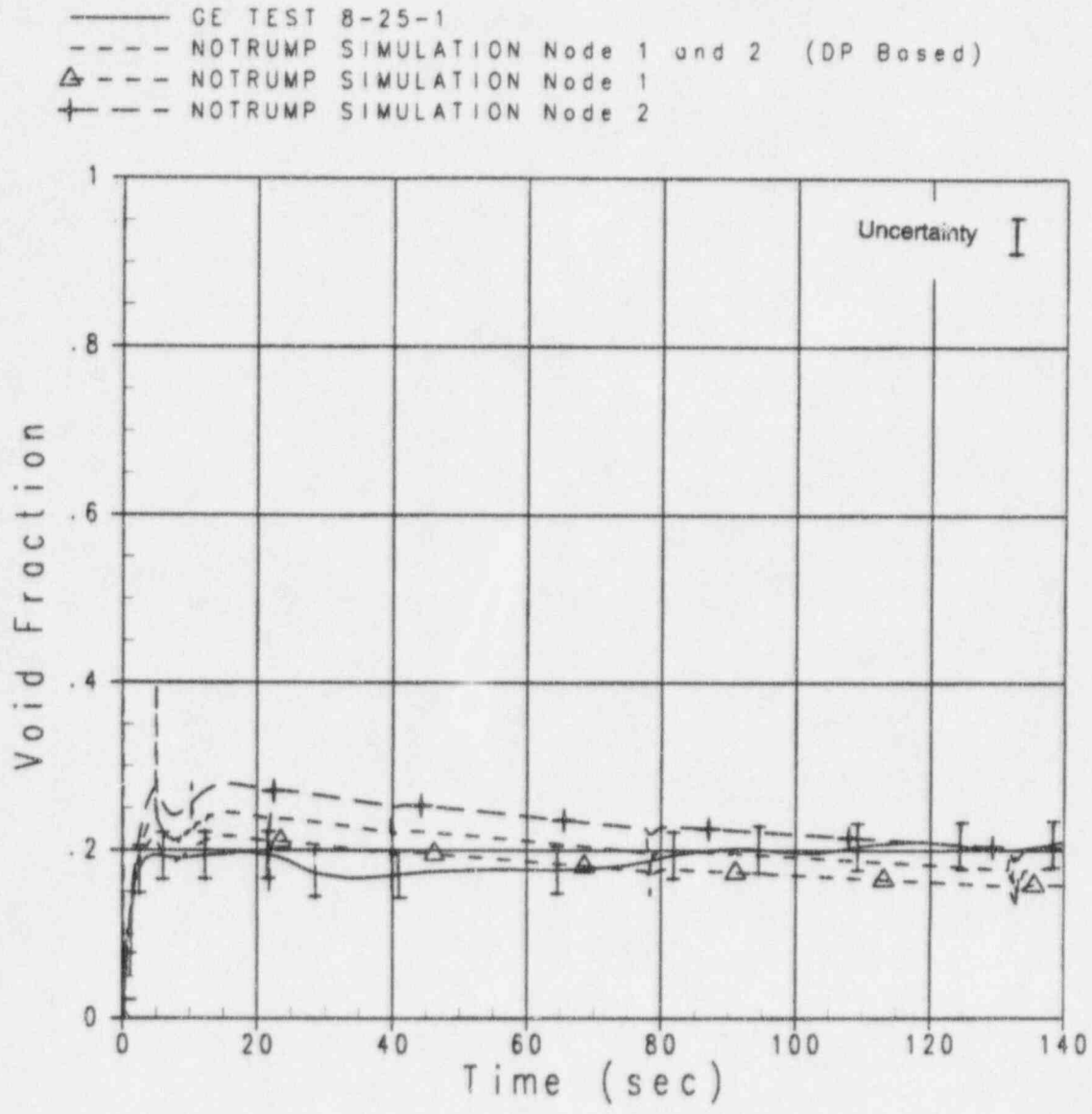

Figure 4.2-14 Void Fraction for GE Test 8-25-1, Nodes 1 and 2

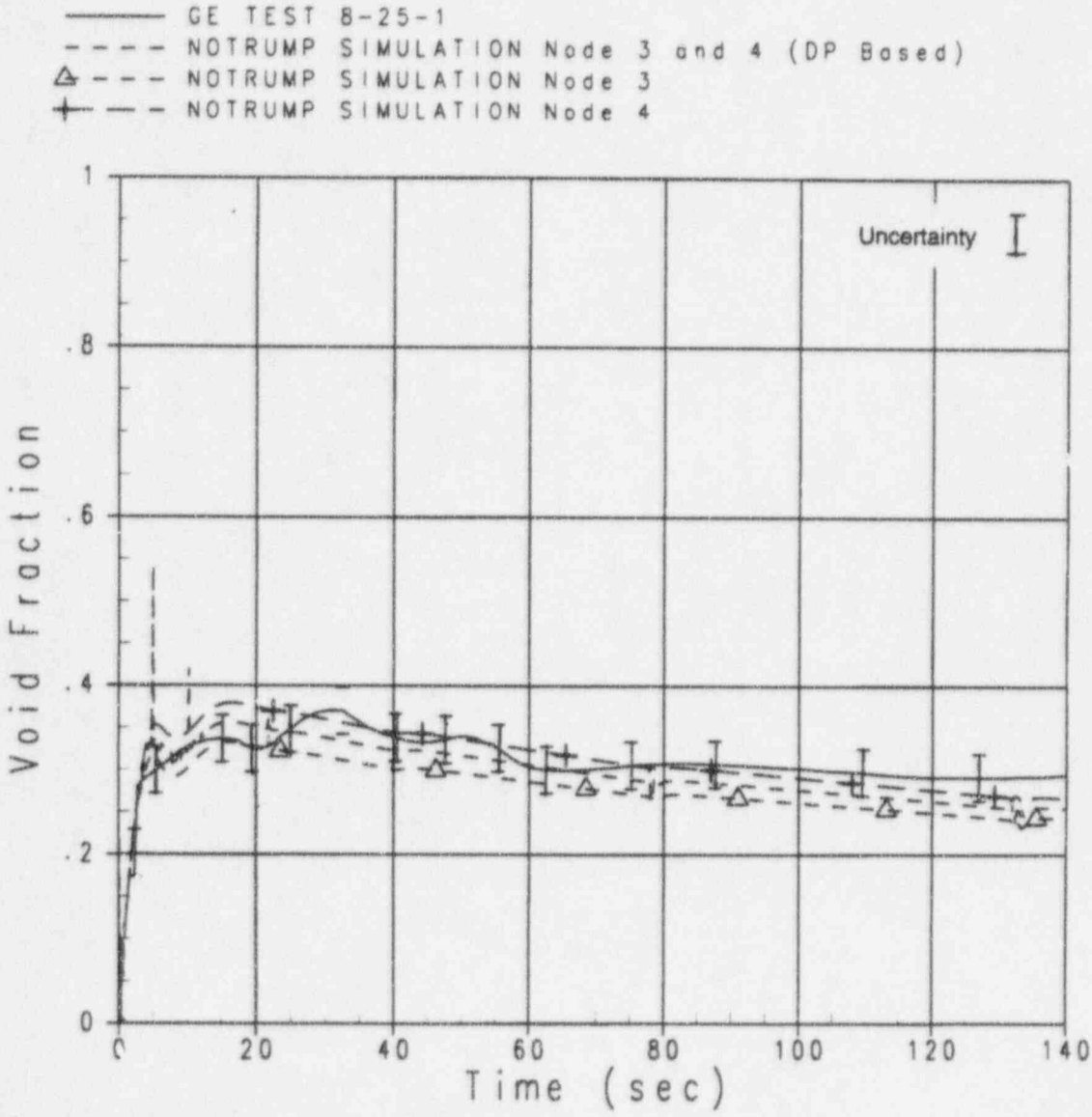

Figure 4.2-15 Void Fraction for GE Test 8-25-1, Nodes 3 and 4

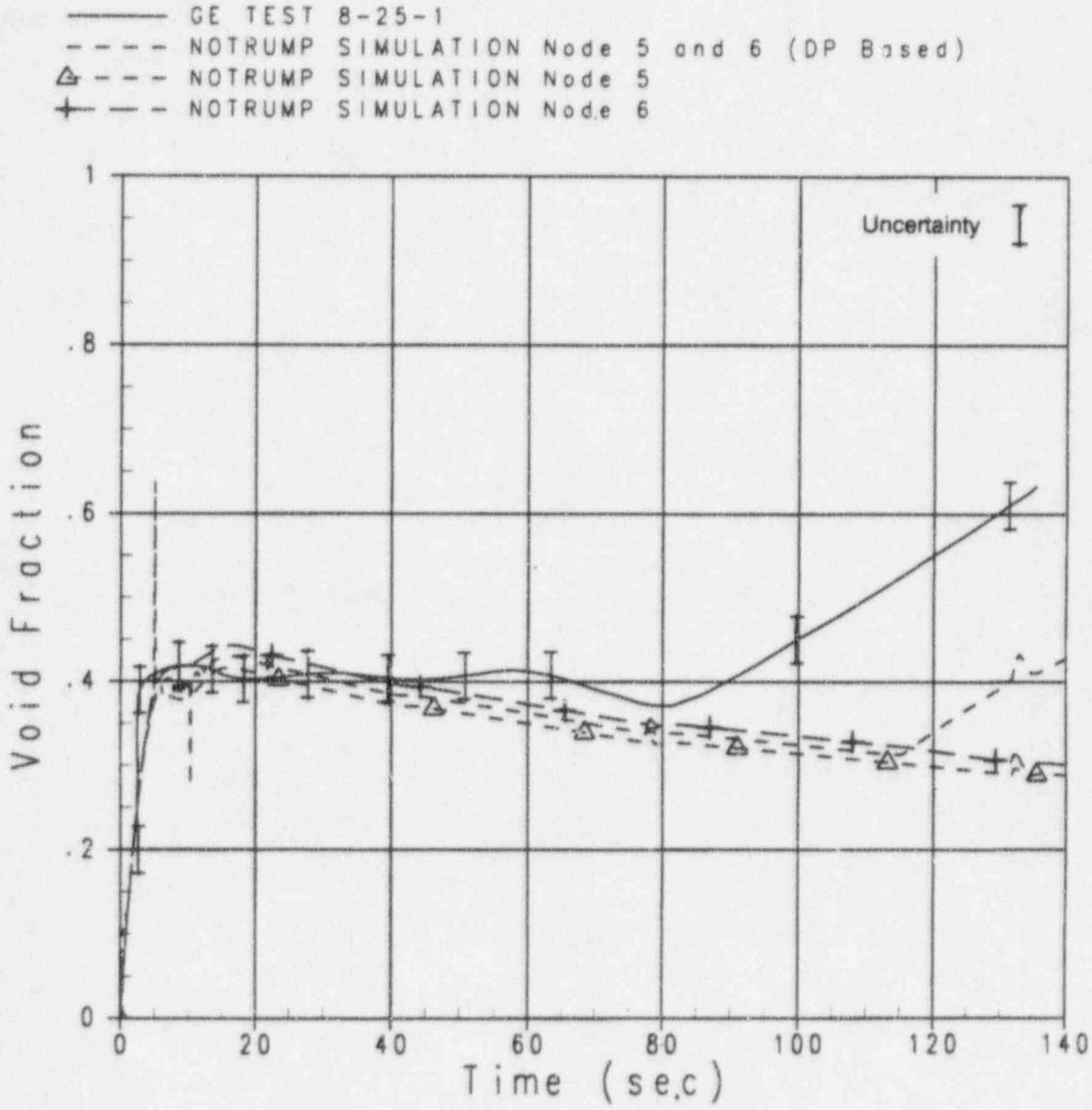

Figure 4.2-16 Void Fraction for GE Test 8-25-1, Nodes 5 and 6

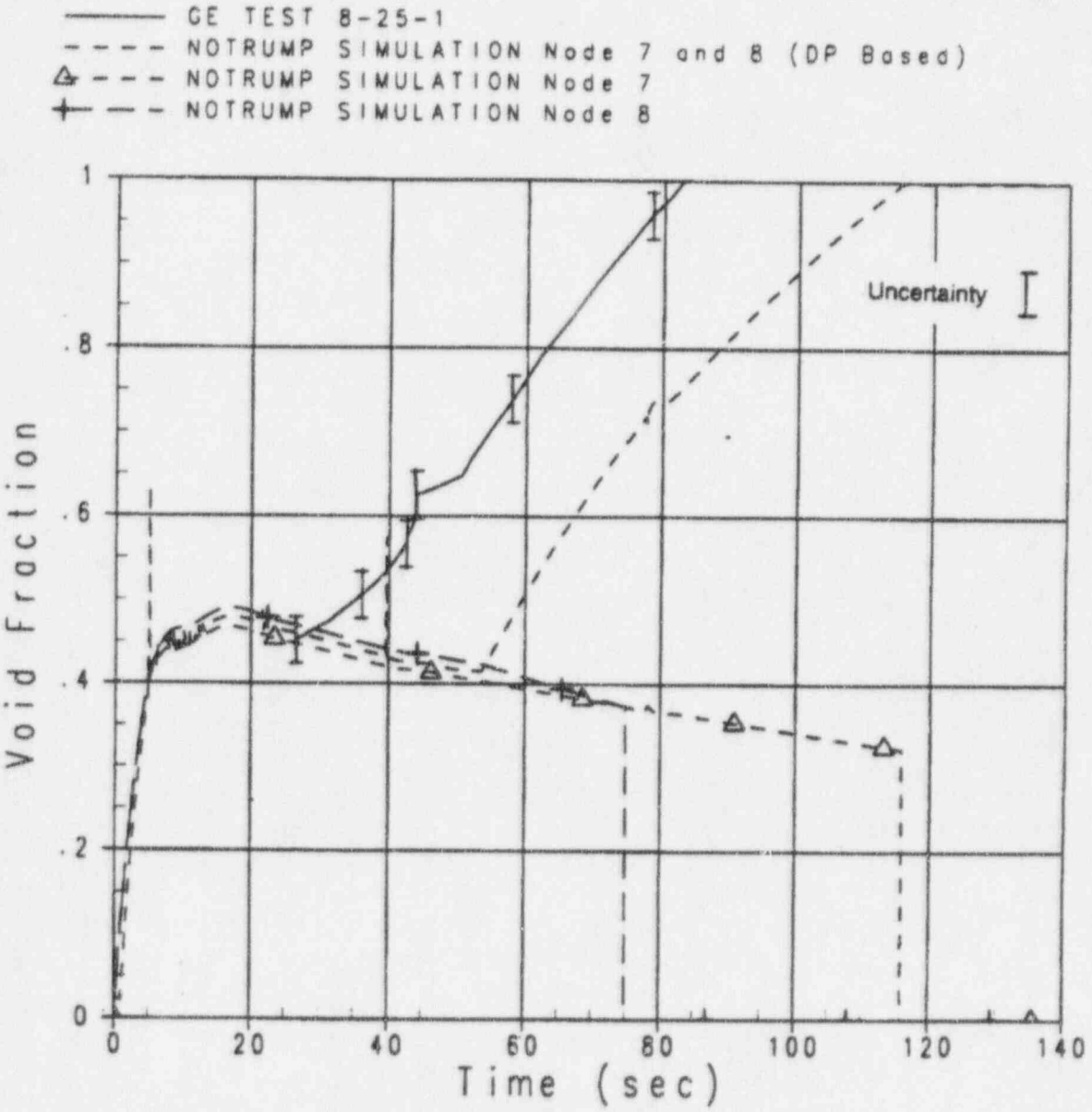

Figure 4.2-17 Void Fraction for GE Test 8-25-1, Nodes 7 and 8

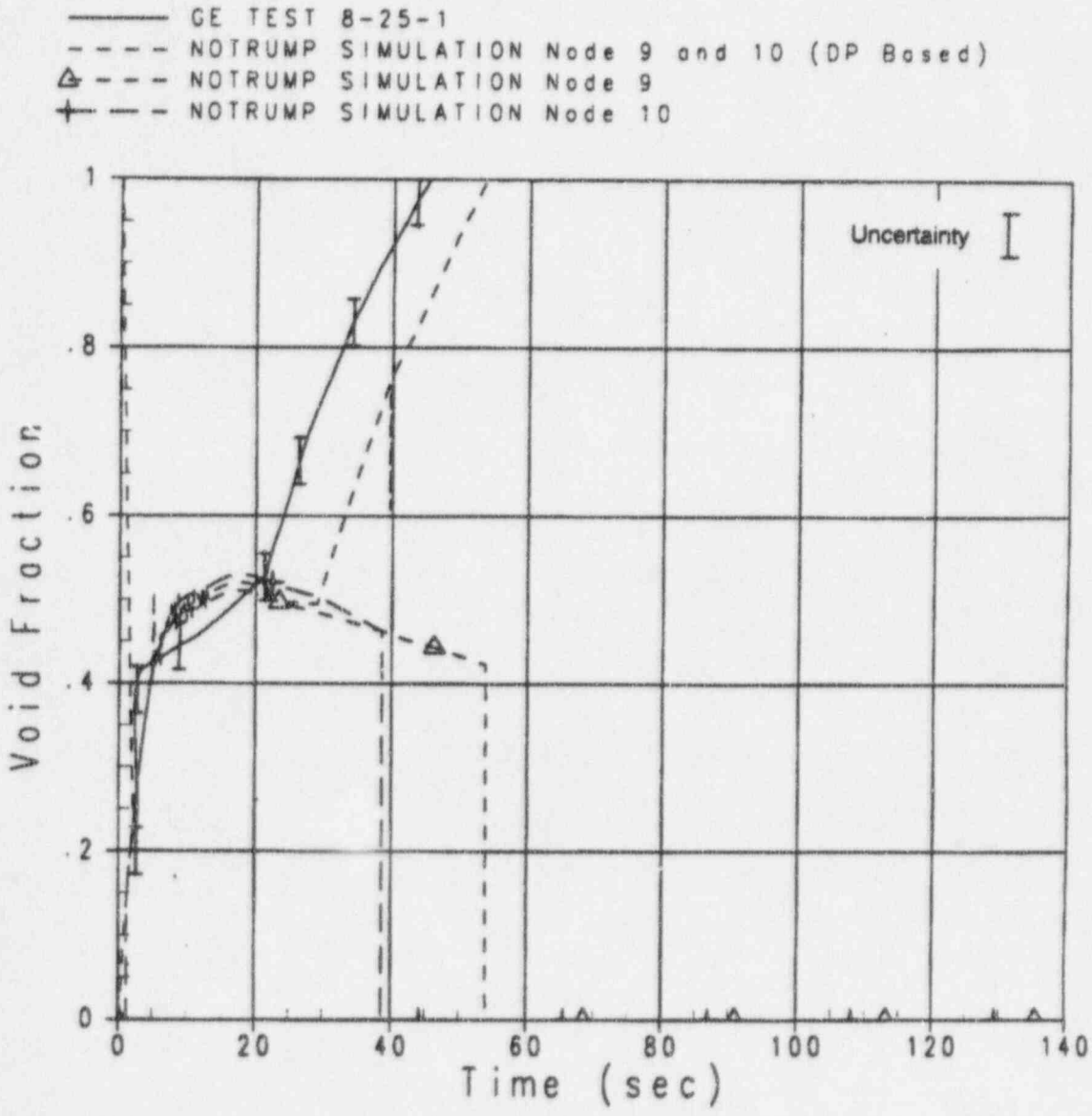

Figure 4.2-18 Void Fraction for GE Test 8-25-1, Nodes 9 and 10

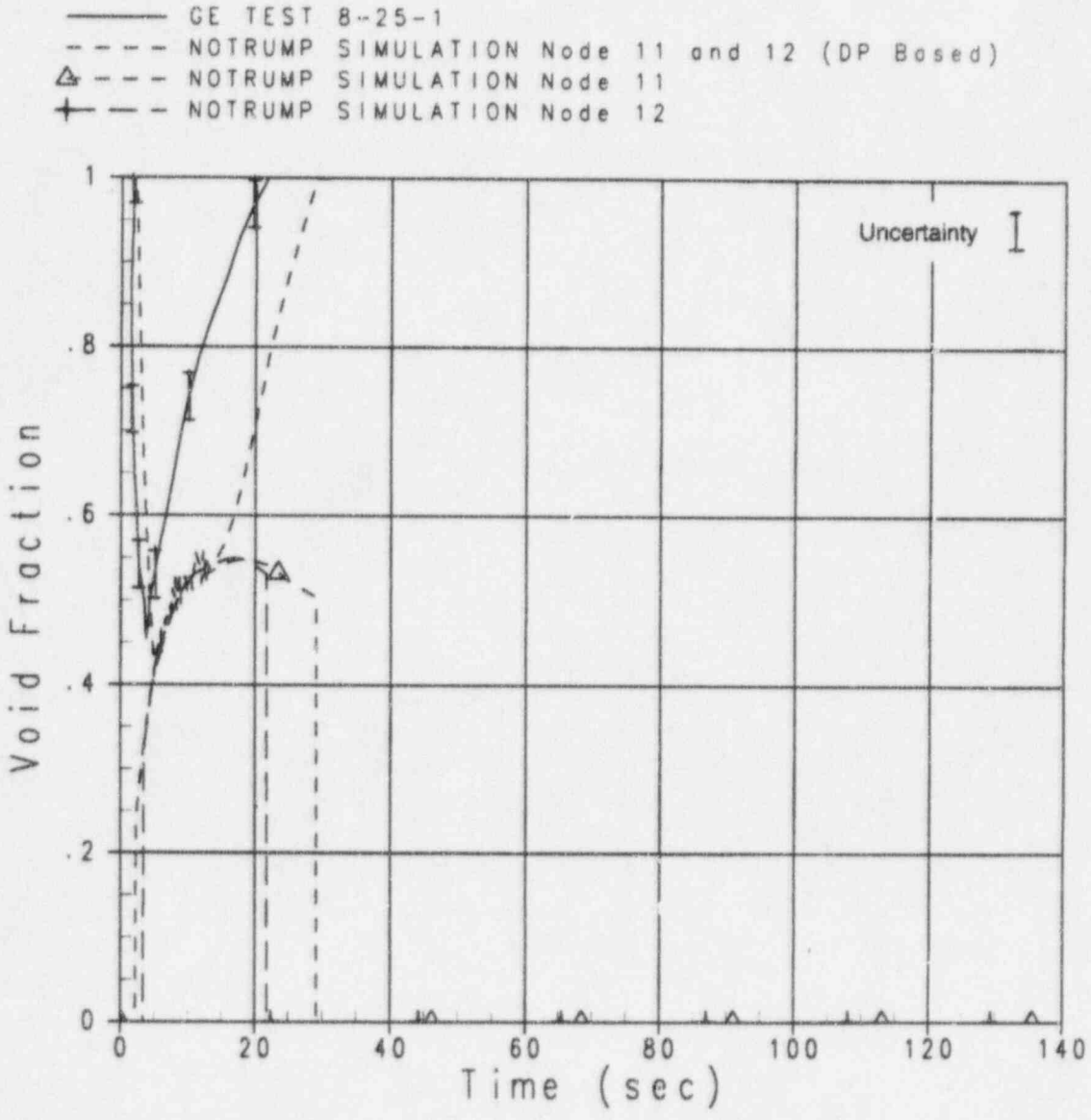

Figure 4.2-19 Void Fraction for GE Test 8-25-1, Nodes 11 and 12

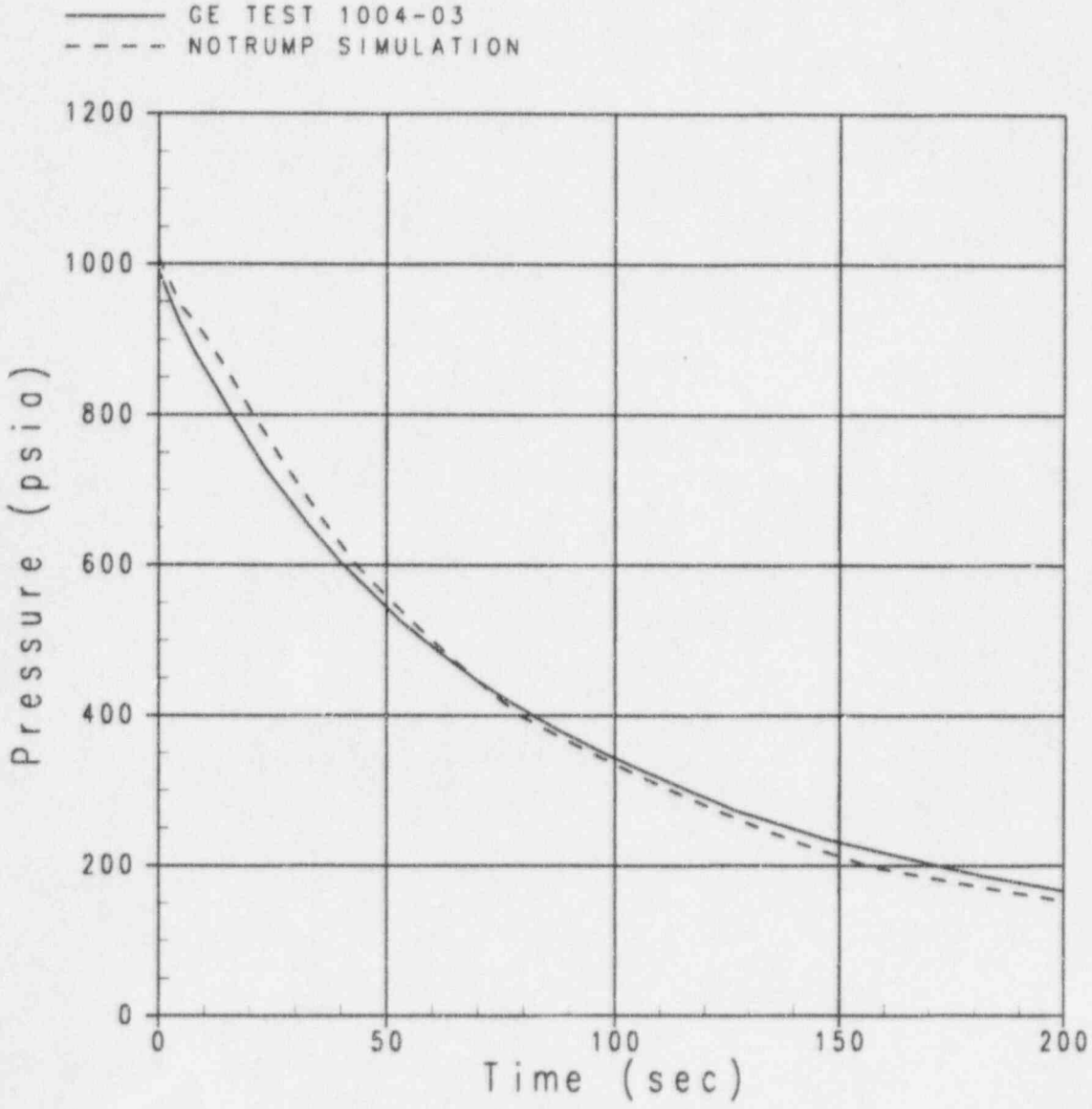

Figure 4.2-20 Vessel Pressure for GE Test 1004-3 with 3/8-in. Break

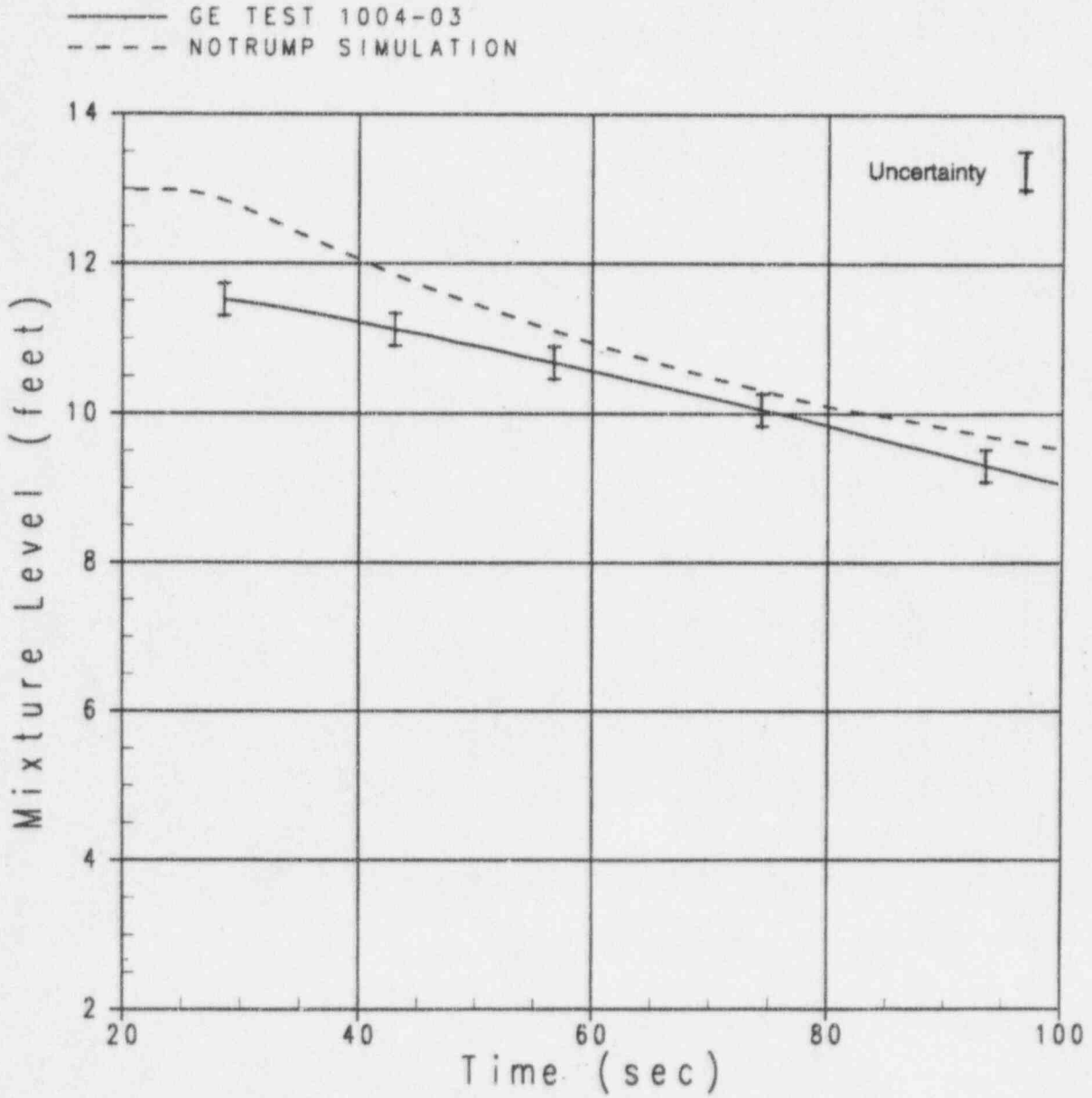

Figure 4.2-21 Vessel Mixture Level for Test 1004-3, 3/8-in. Break

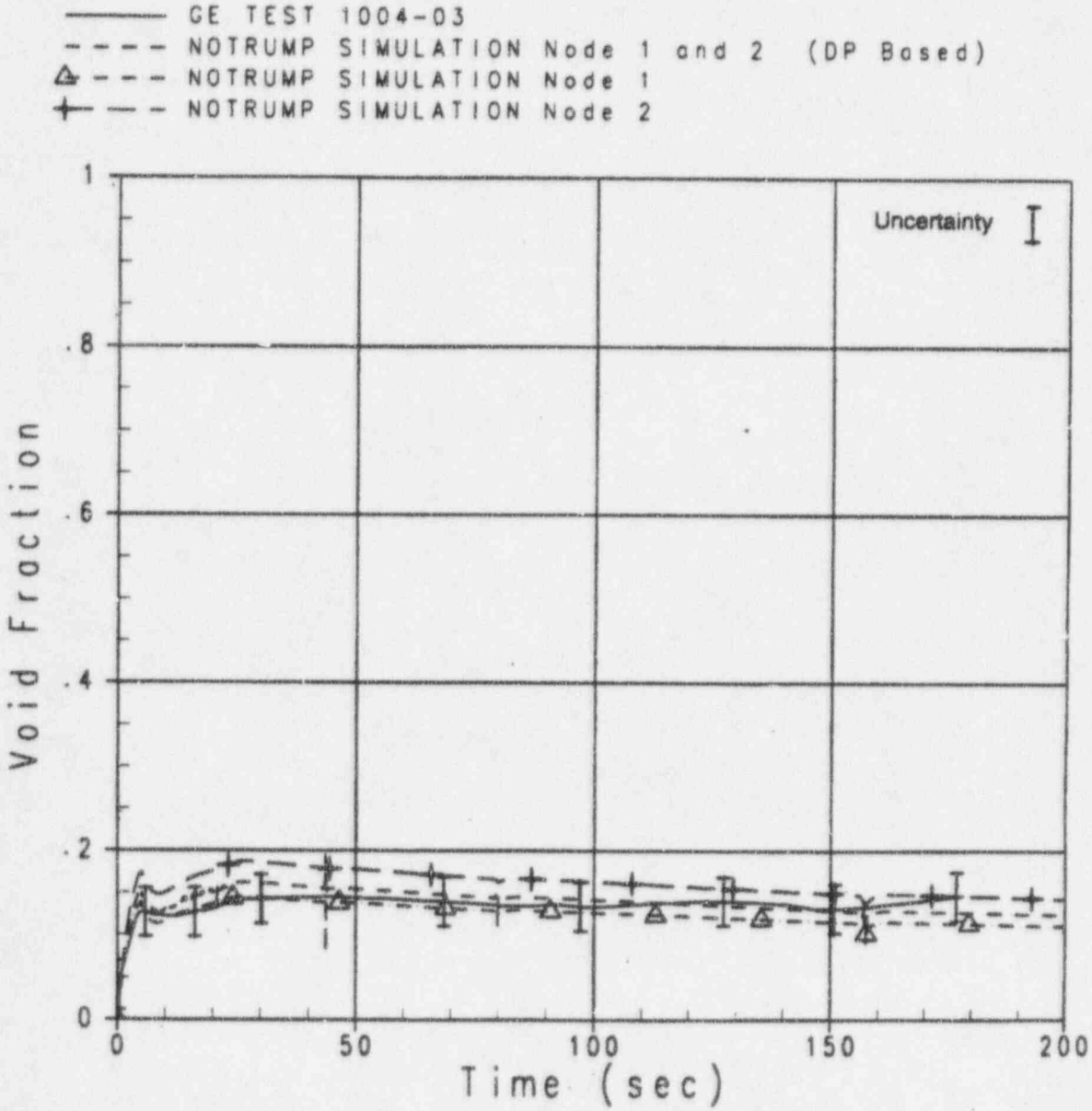

Figure 4.2-22 Void Fraction for GE Test 1004-3, Nodes 1 and 2

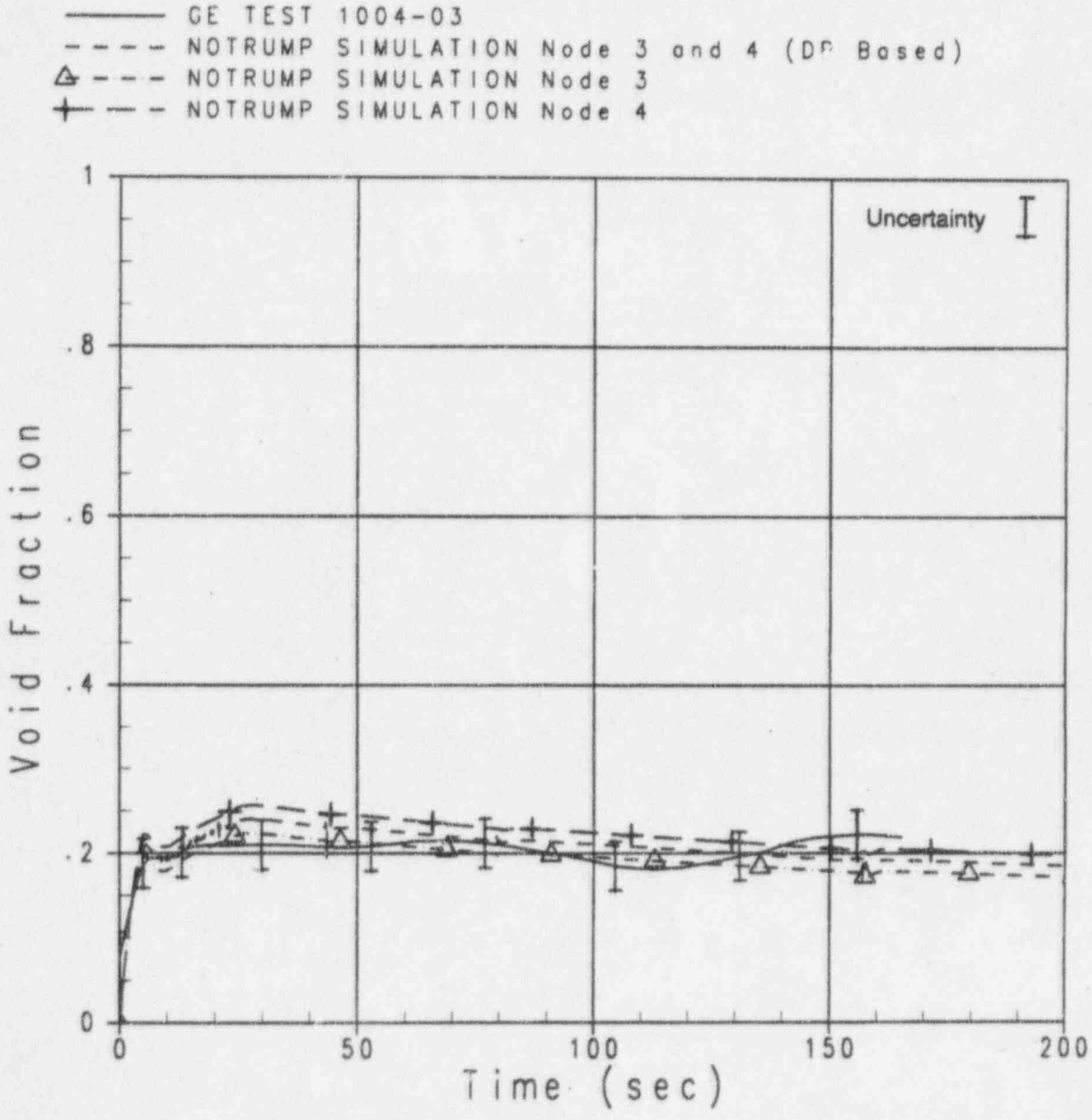

Figure 4.2-23 Void Fraction for GE Test 1004-3, Nodes 3 and 4

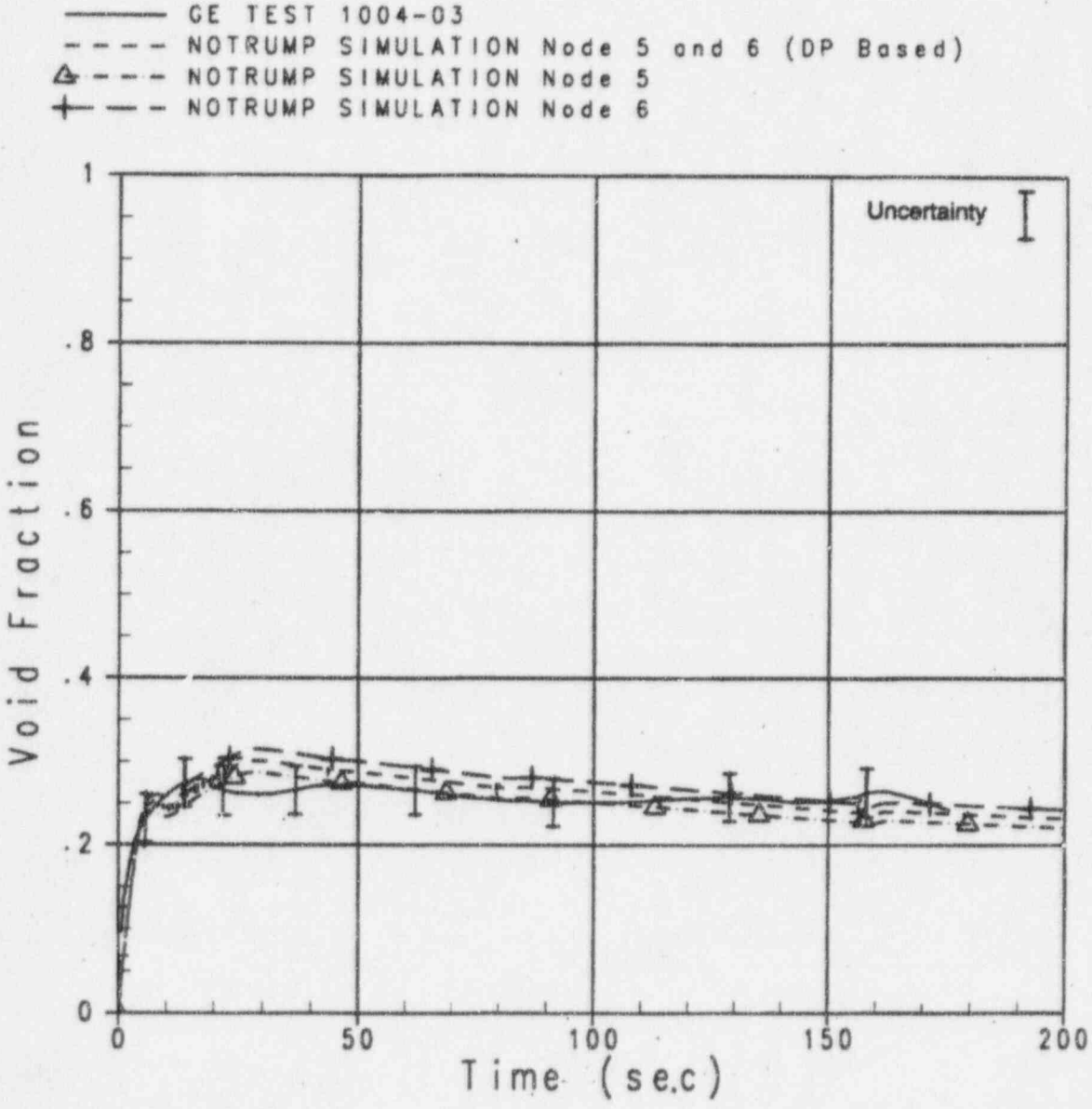

Figure 4.2-24 Void Fraction for GE Test 1004-3, Nodes 5 and 6

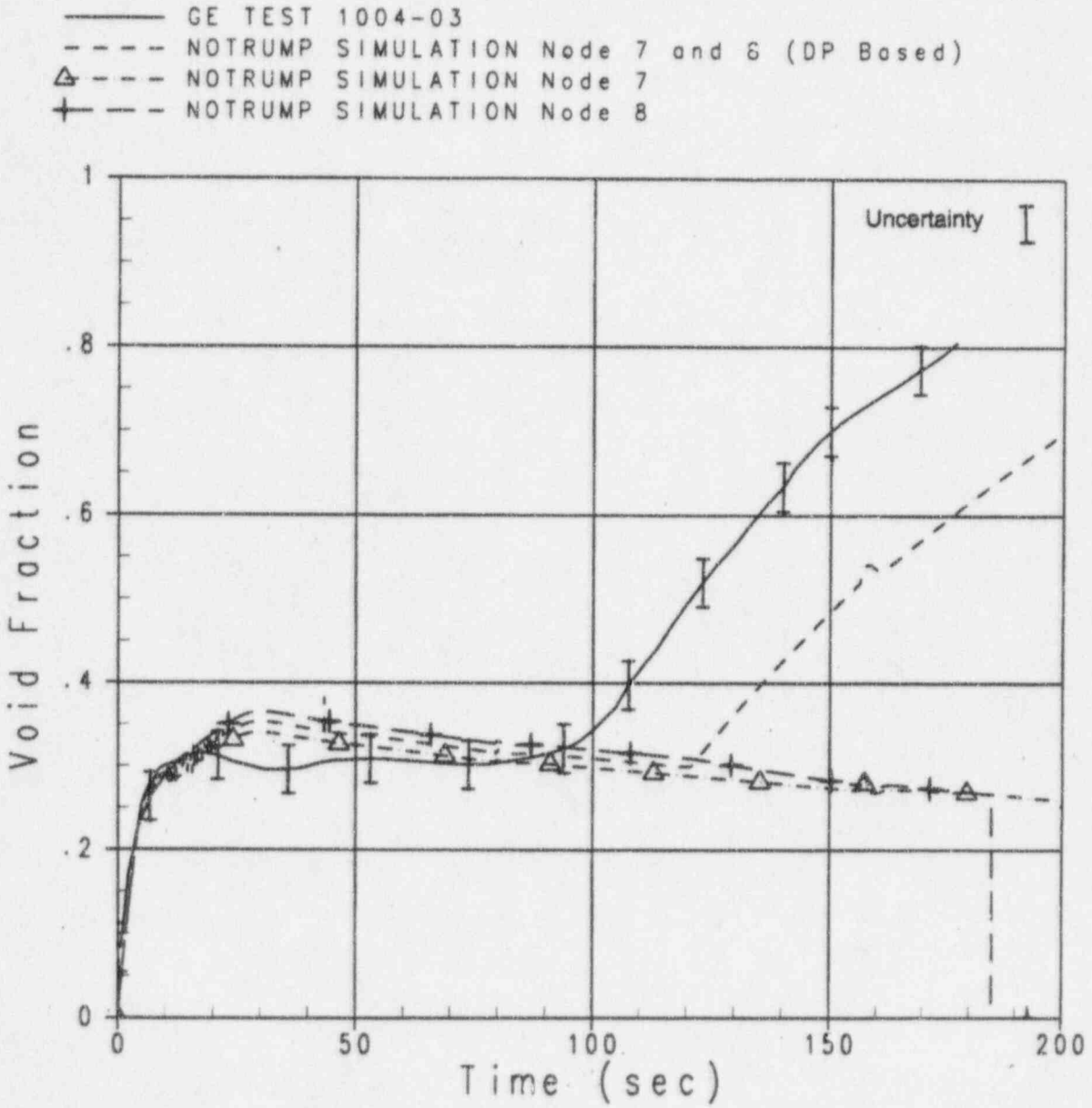

Figure 4.2-25 Void Fraction for GE Test 1004-3, Nodes 7 and 8

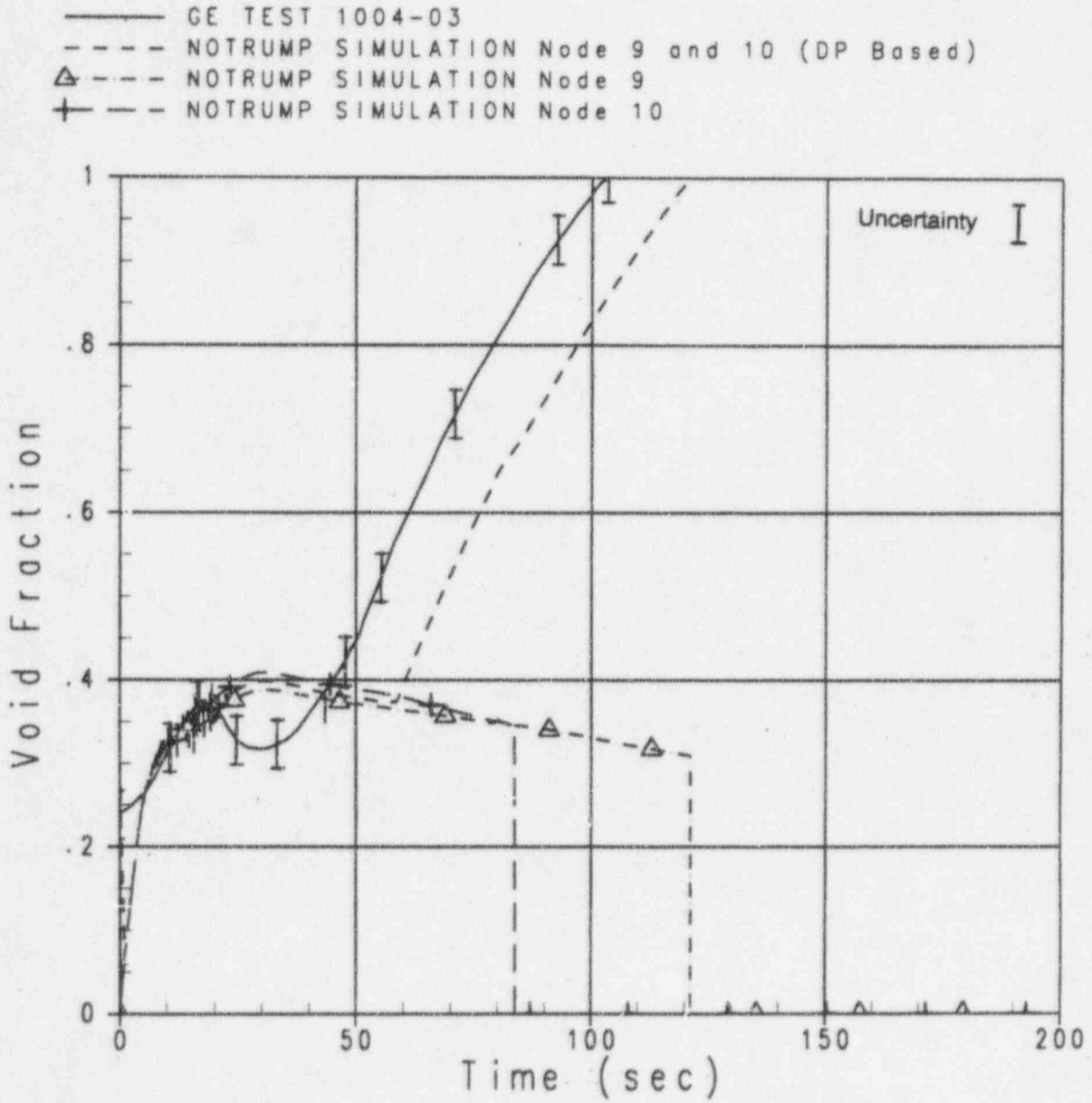

Figure 4.2-26 Void Fraction for GE Test 1004-3, Nodes 9 and 10

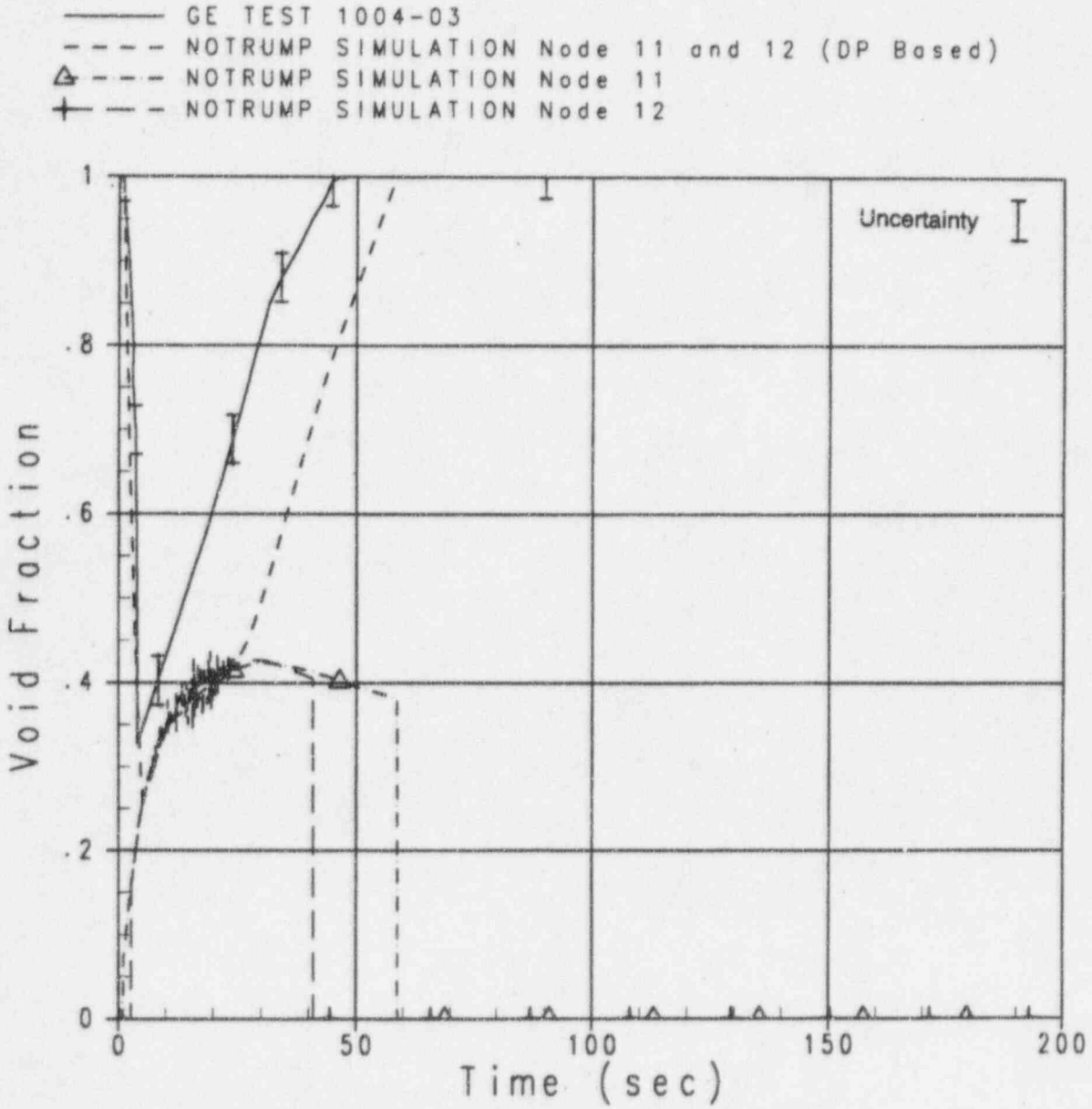

Figure 4.2-27 Void Fraction for GE Test 1004-3, Nodes 11 and 12

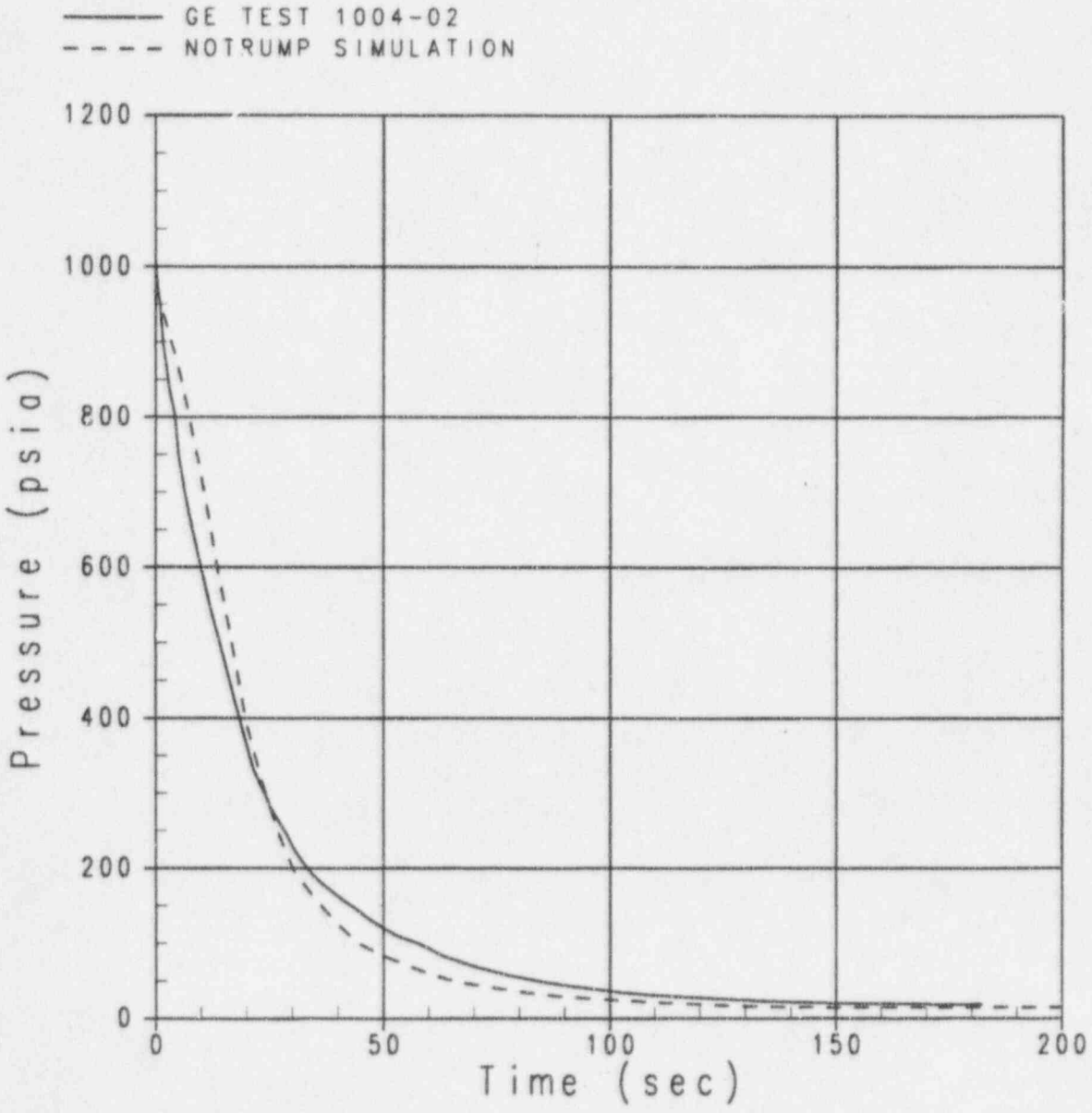

Figure 4.2-28 Vessel Pressure for GE Test 1004-2 with 7/8-in Break

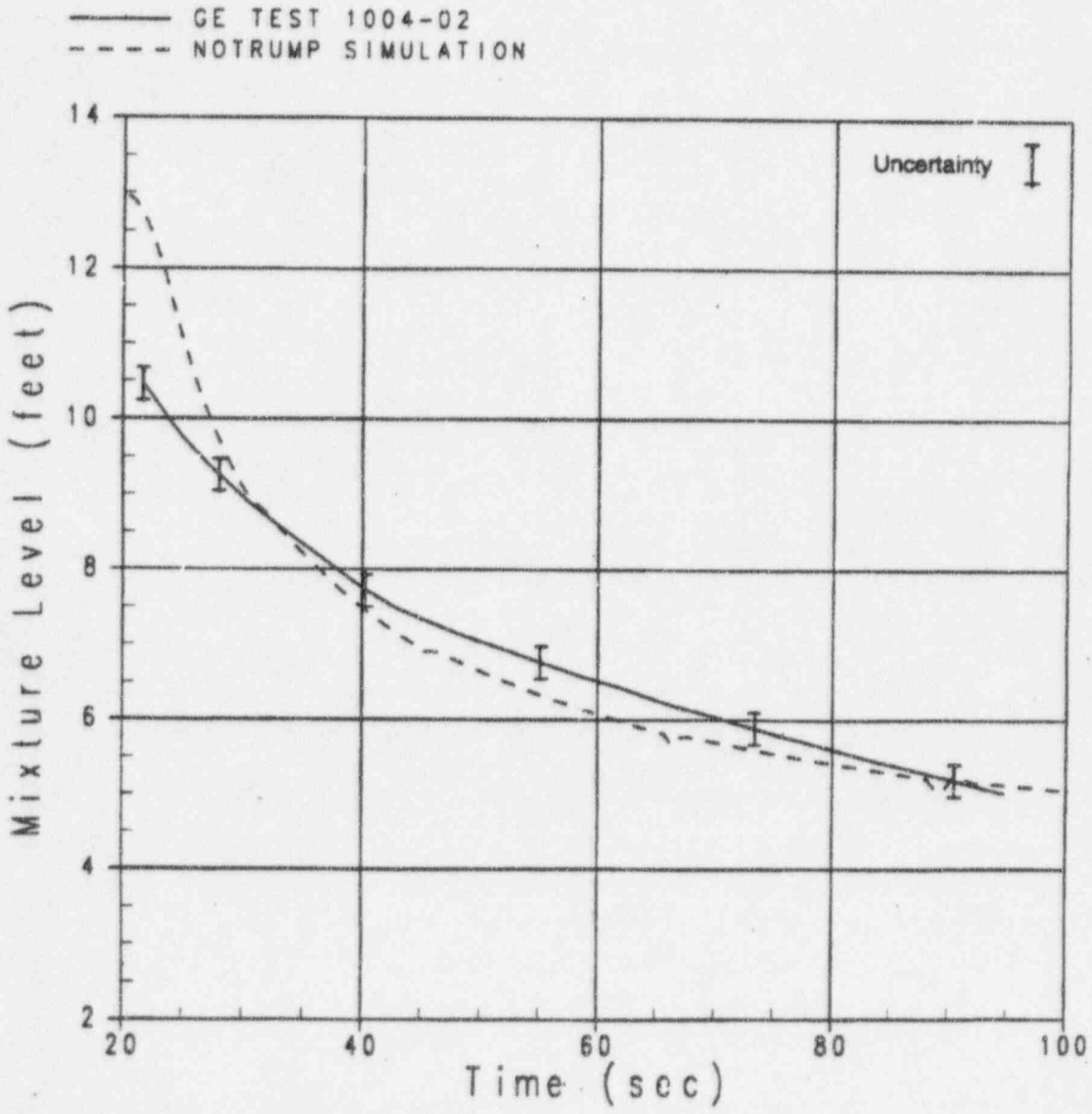

Figure 4.2-29 Vessel Mixture Level for Test 1004-2, 7/8-in. Break

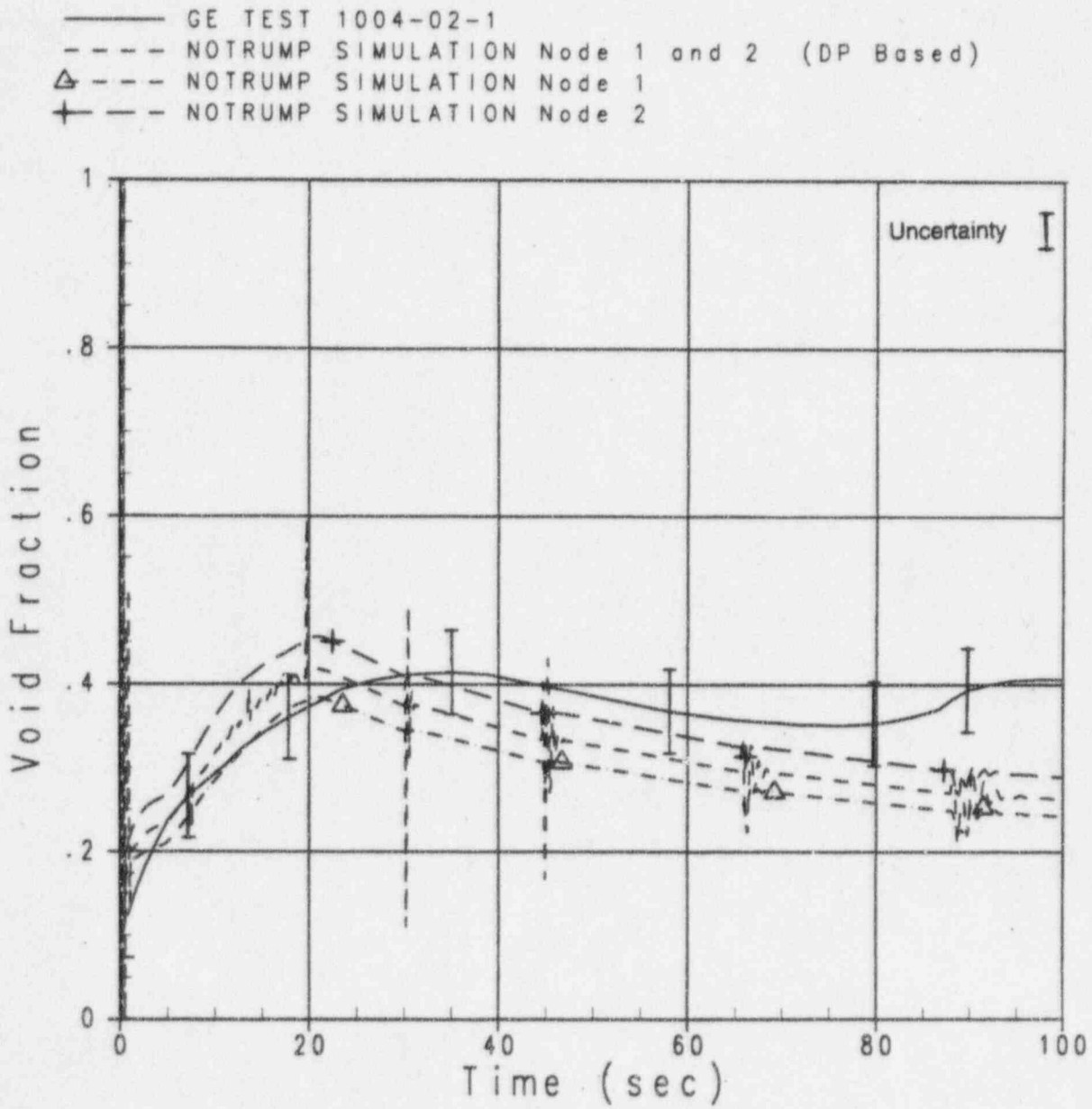

Figure 4.2-30 Void Fraction for GE Test 1004-2, Nodes 1 and 2

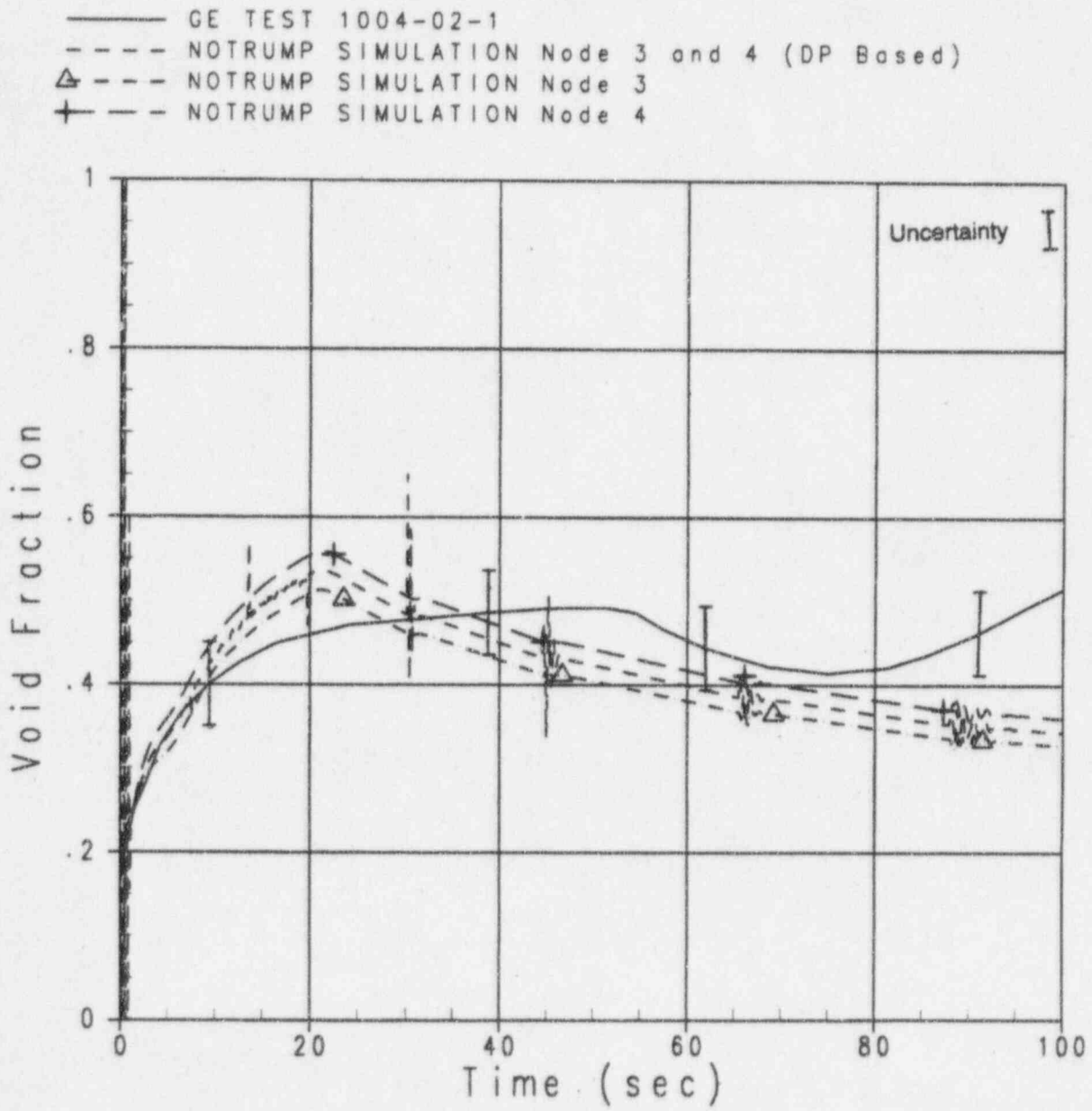

Figure 4.2-31 Void Fraction for GE Test 1004-2, Nodes 3 and 4

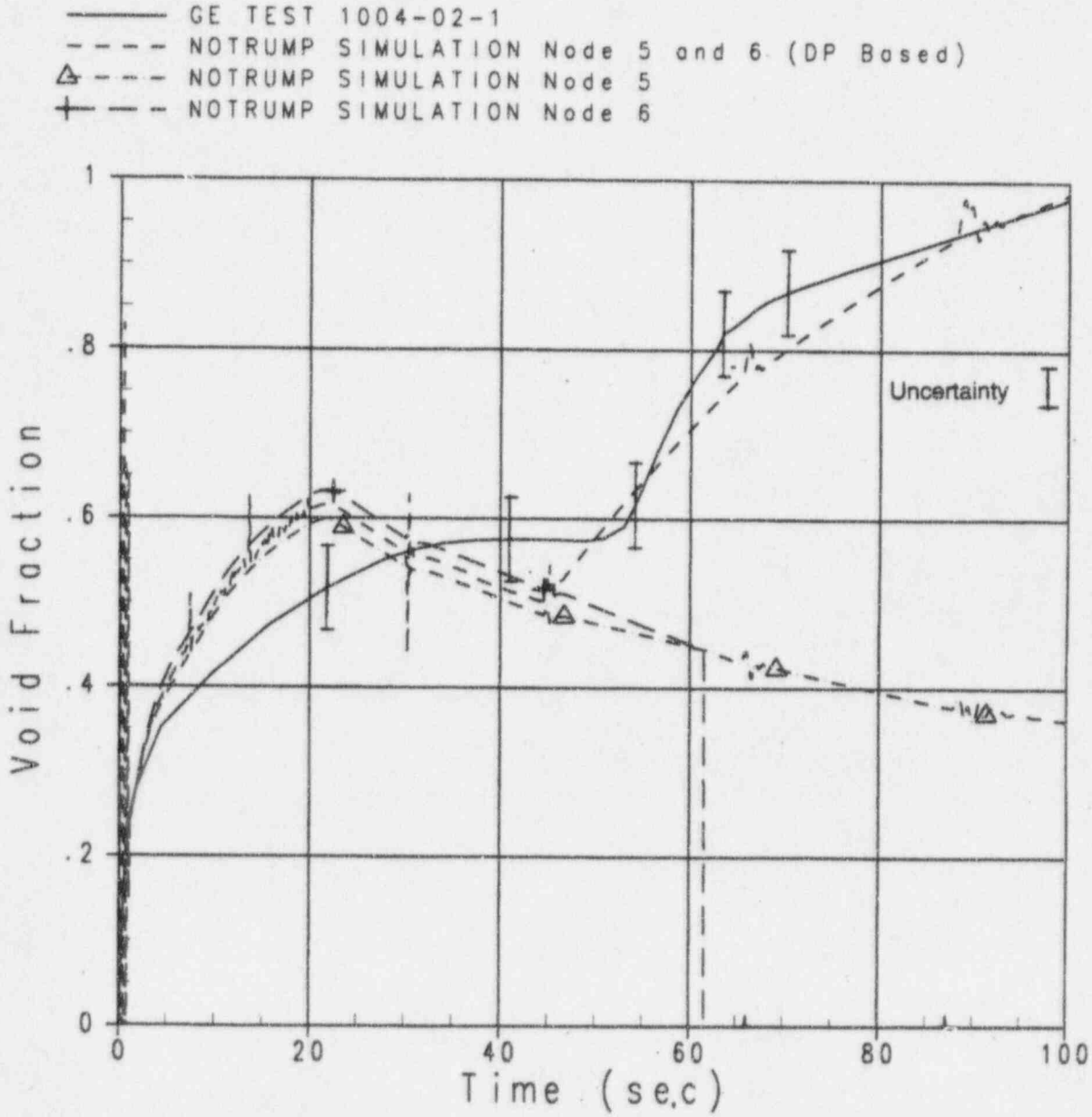

Figure 4.2-32 Void Fraction for GE Test 1004-2, Nodes 5 and 6

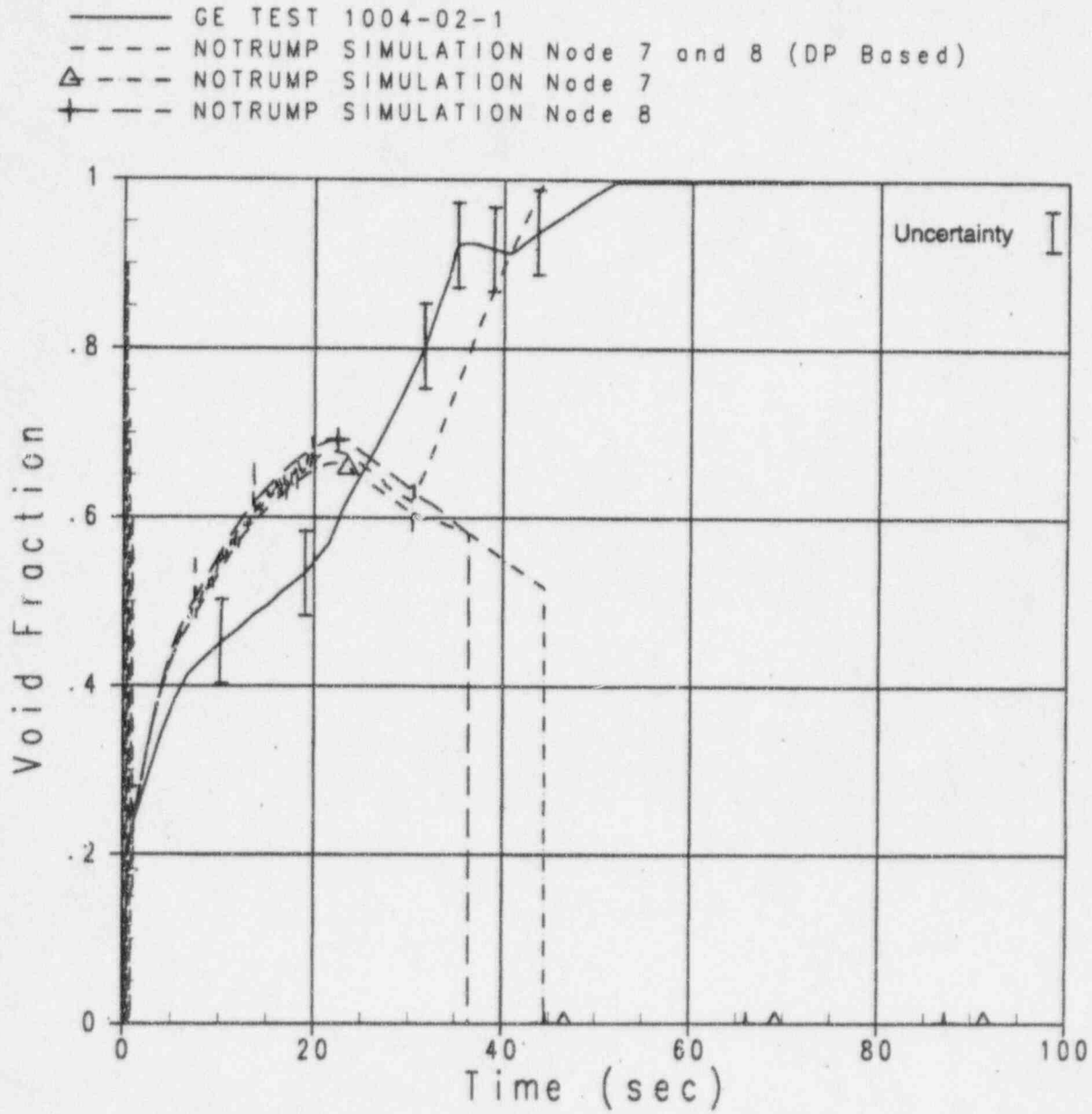

Figure 4.2-33 Void Fraction for GE Test 1004-2, Nodes 7 and 8

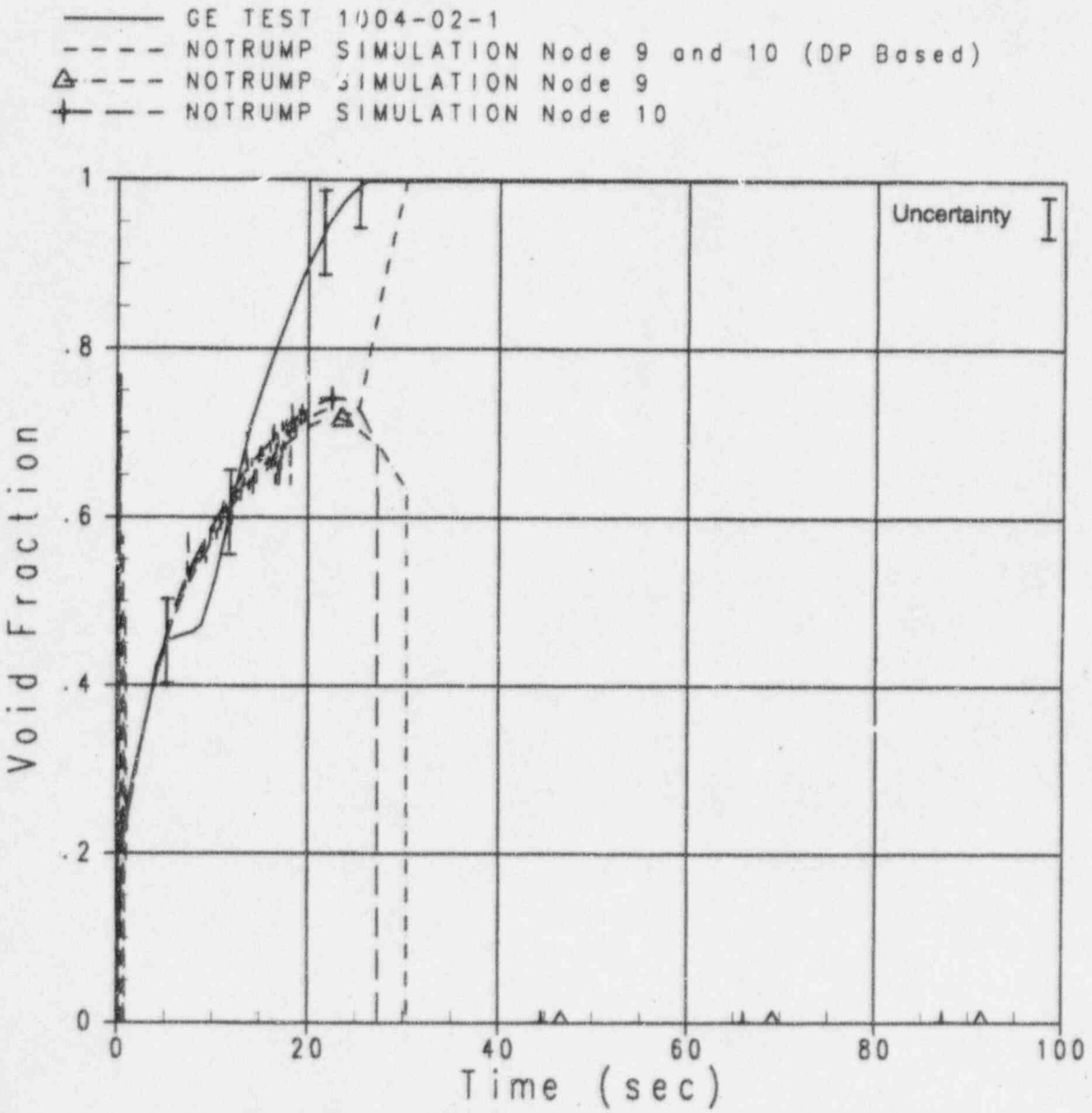

Figure 4.2-34 Void Fraction for GE Test 1004-2, Nodes 9 and 10

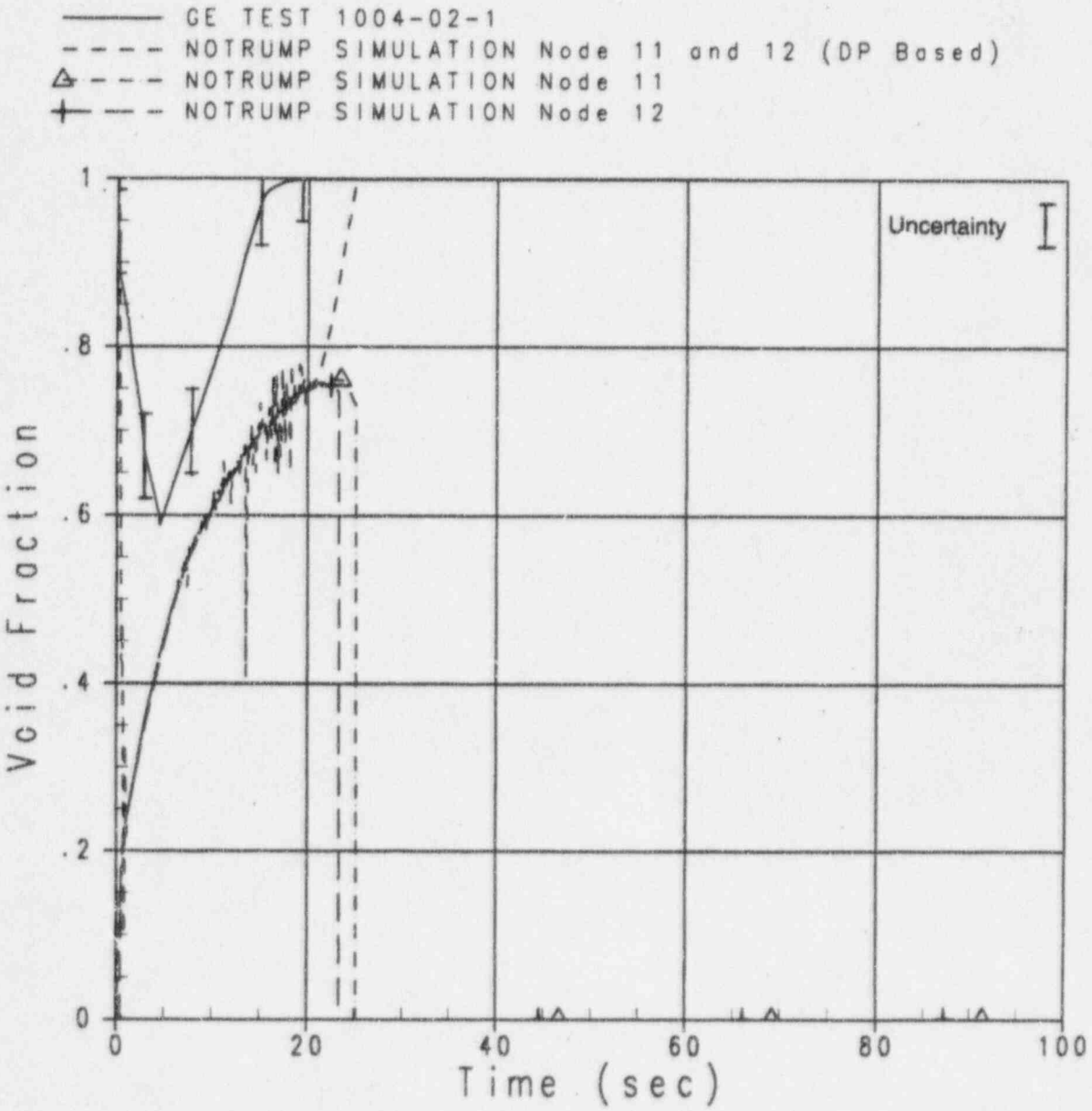

Figure 4.2-35 Void Fraction for GE Test 1004-2, Nodes 11 and 12

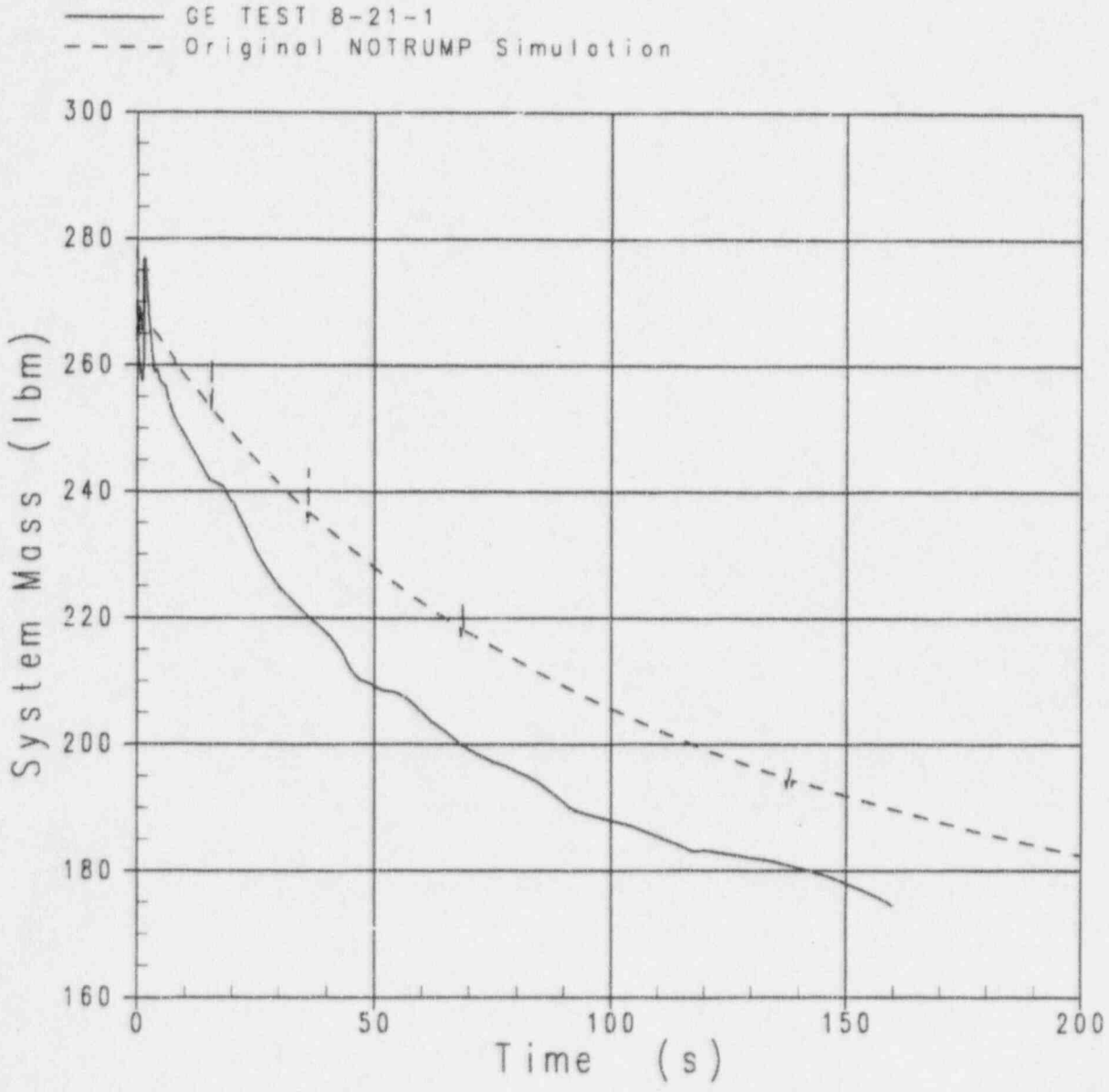

Figure 4.2-36 Vessel Mass for Test 8-21-1 and Original NOTRUMP Simulation with Critical Break Flowlink

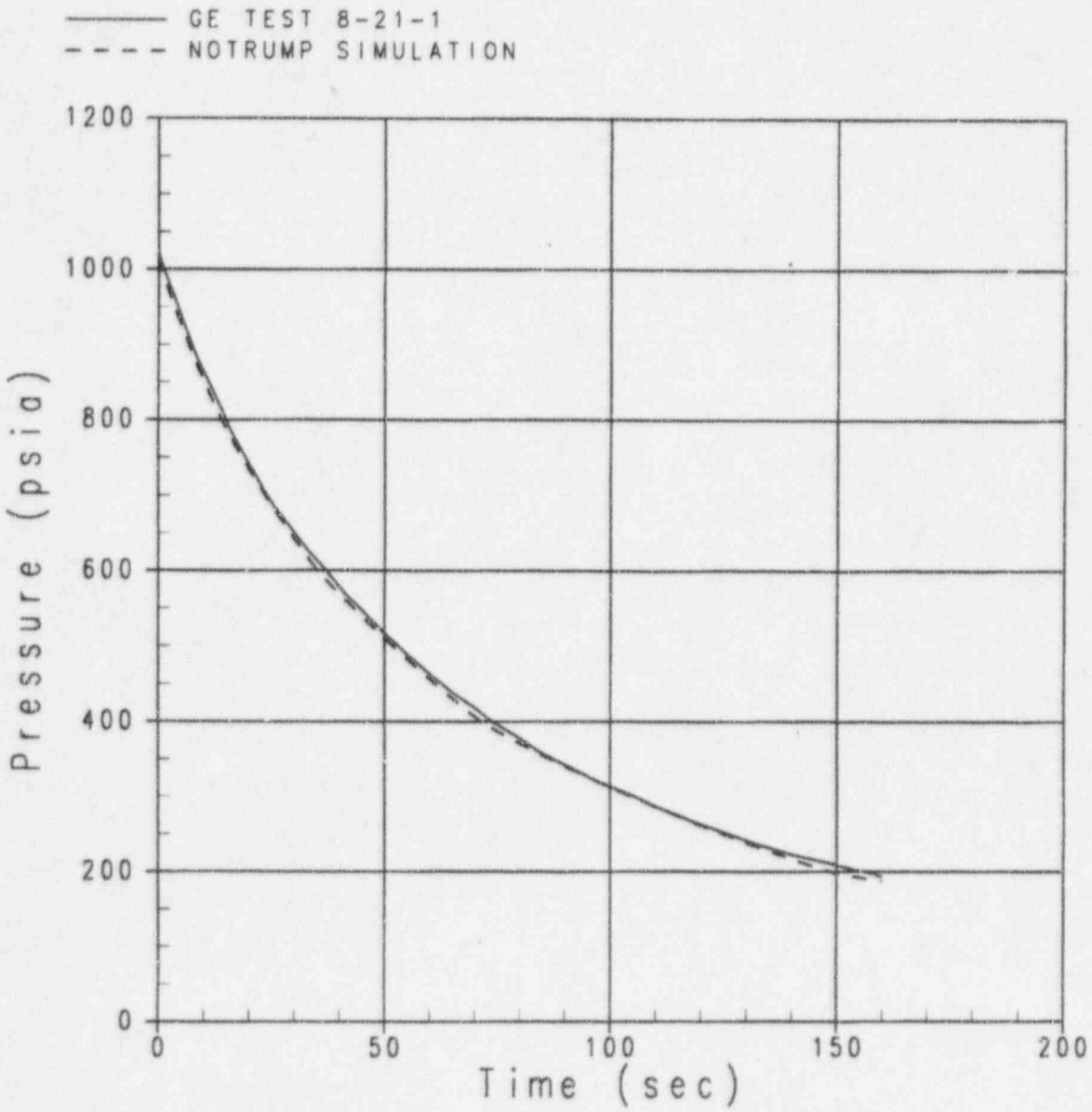

Figure 4.2-37 Vessel Pressure for Test 8-21-1 and NOTRUMP Simulation Matching Mass and Pressure

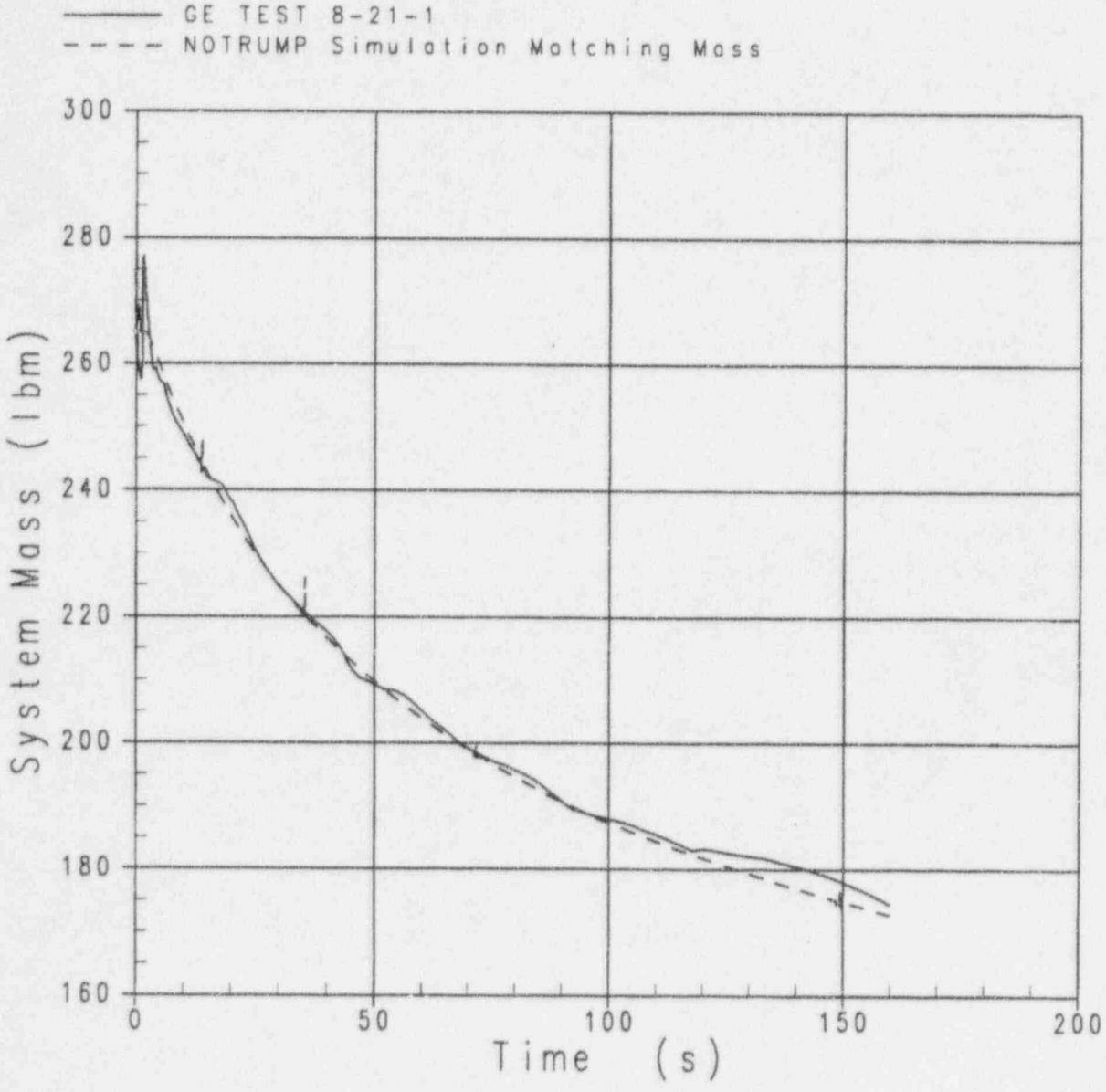

Figure 4.2-38 Vessel Mass for Test 8-21-1 and NOTRUMP Simulation Matching Mass and Pressure

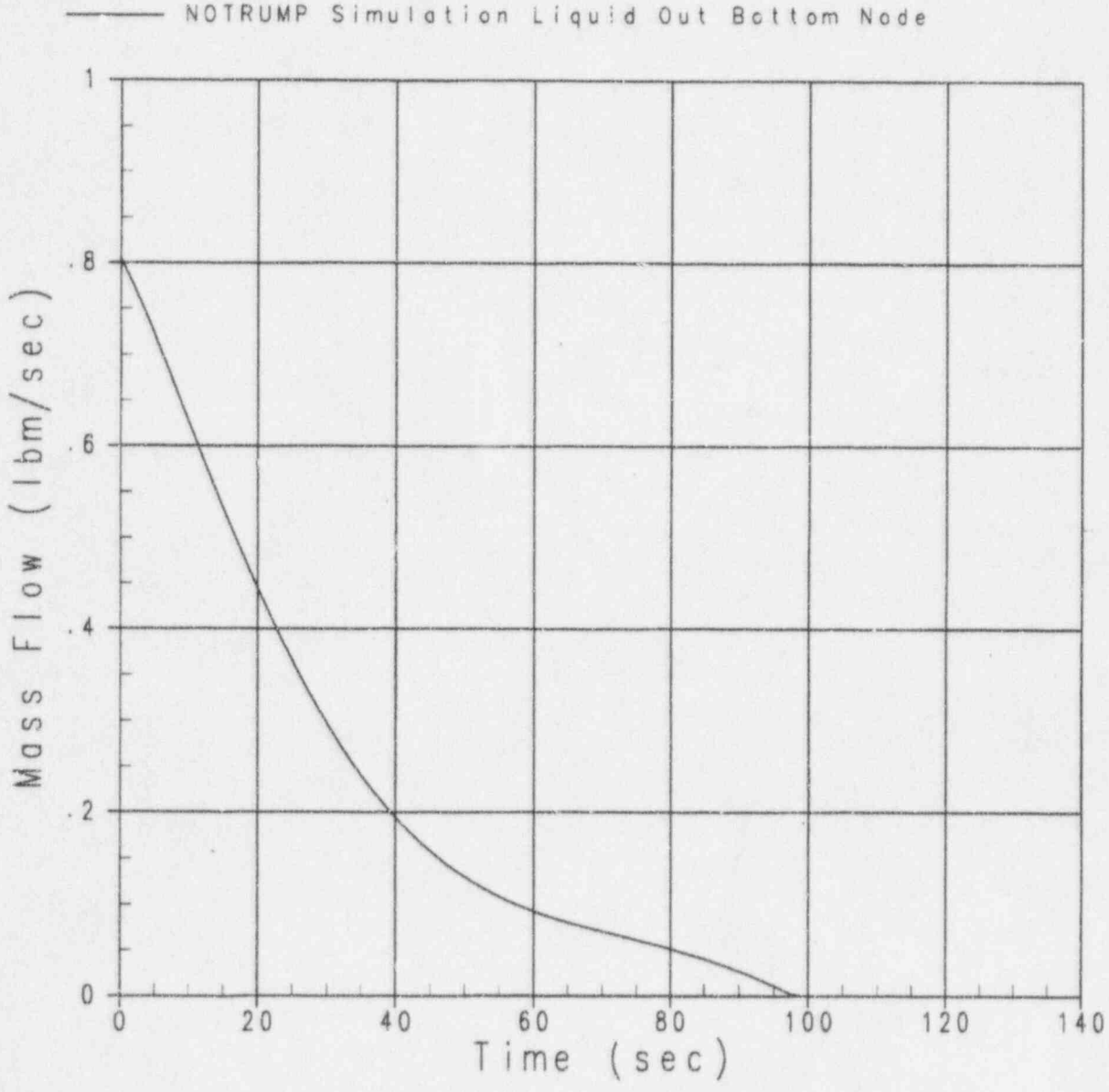

Figure 4.2-39 Liquid Mass Removed from Bottom Node for NOTRUMP Simulation of Test 8-21-1 Matching Mass and Pressure

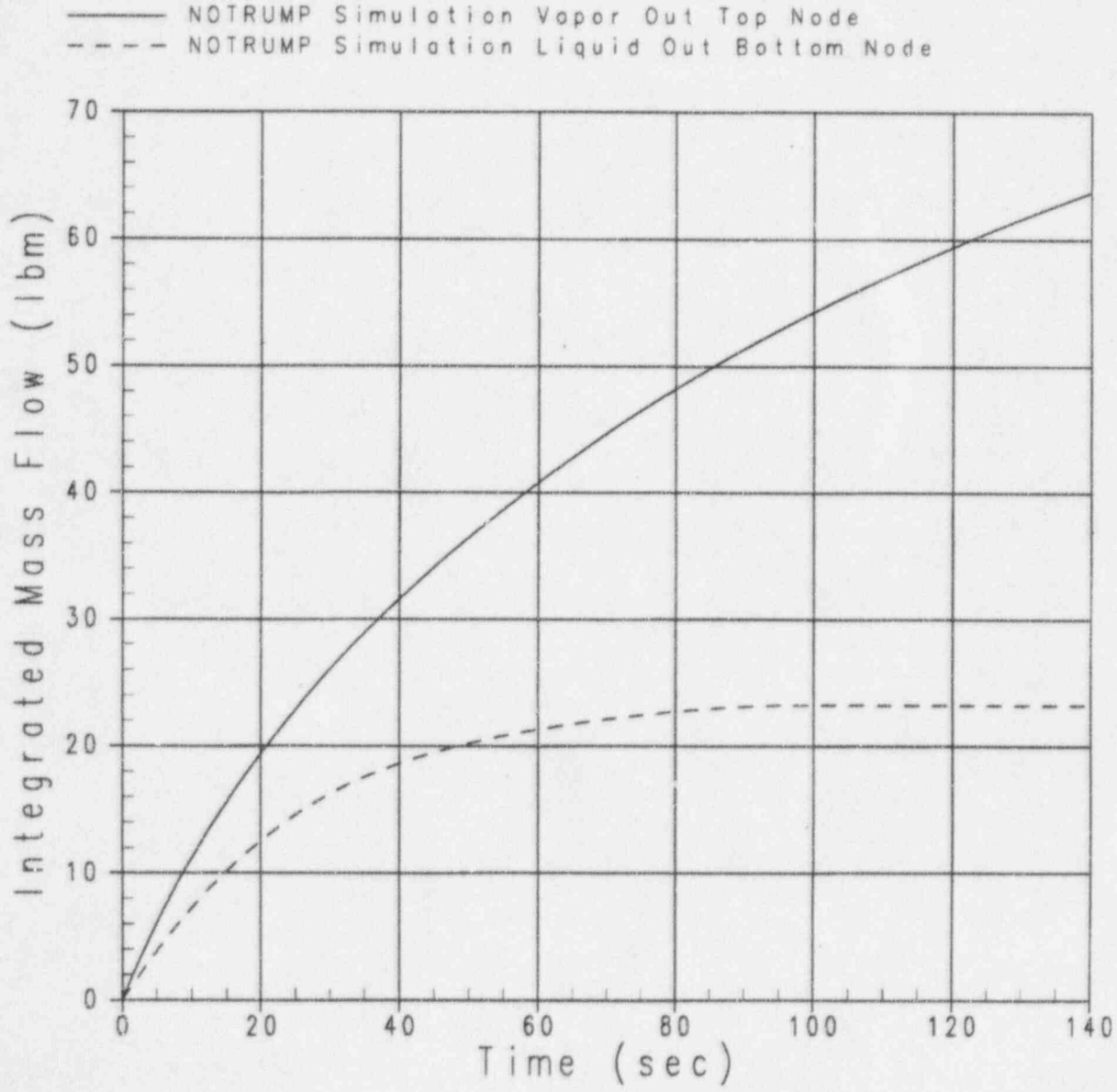

Figure 4.2-40 Integrated Mass Exiting Vessel for NOTRUMP Simulation of Test 8-21-1 Matching Mass and Pressure

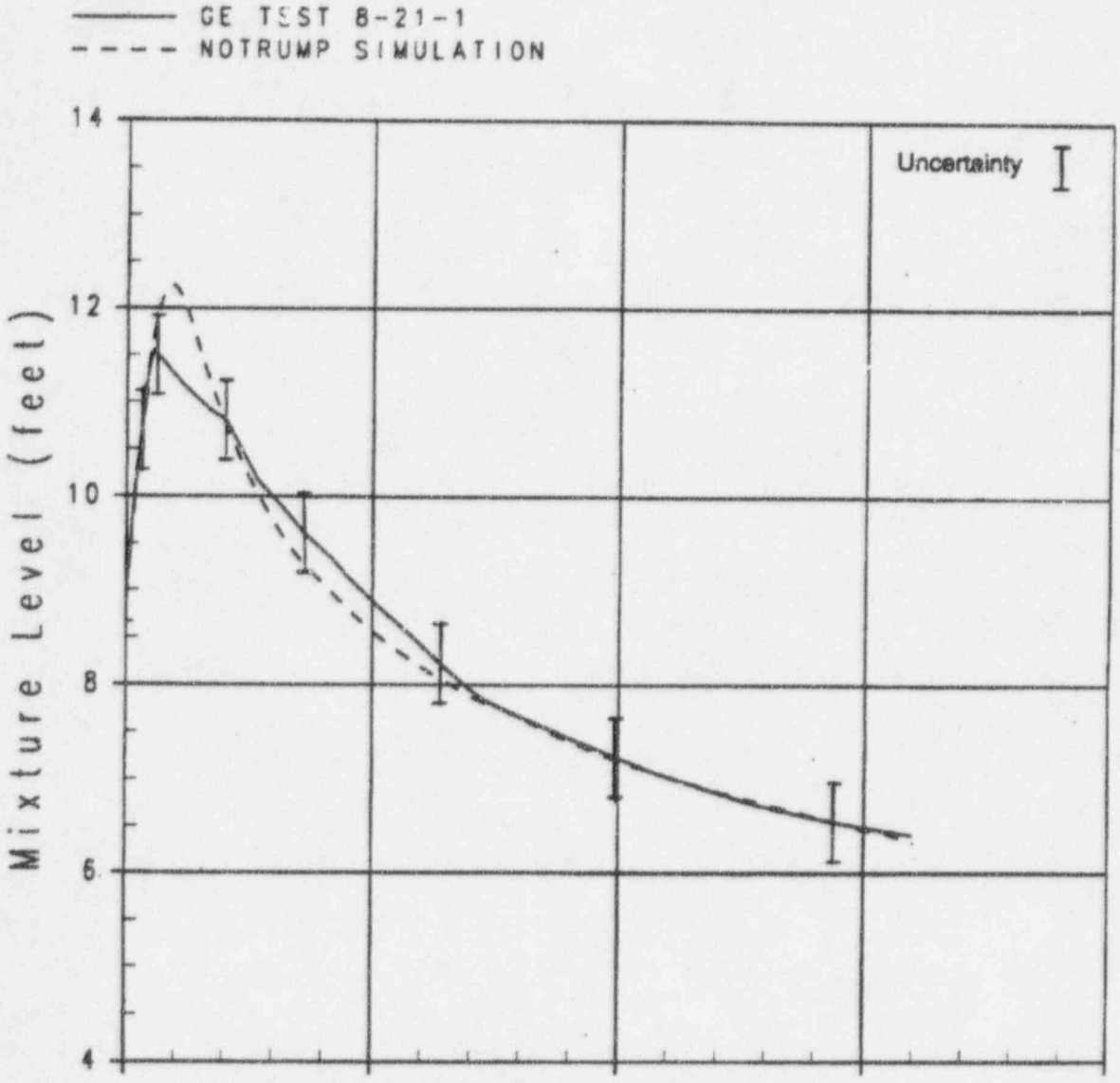

Figure 4.2-41 Vessel Mixture Level for Test 8-21-1 and NOTRUMP Simulation Matching Mass and Pressure

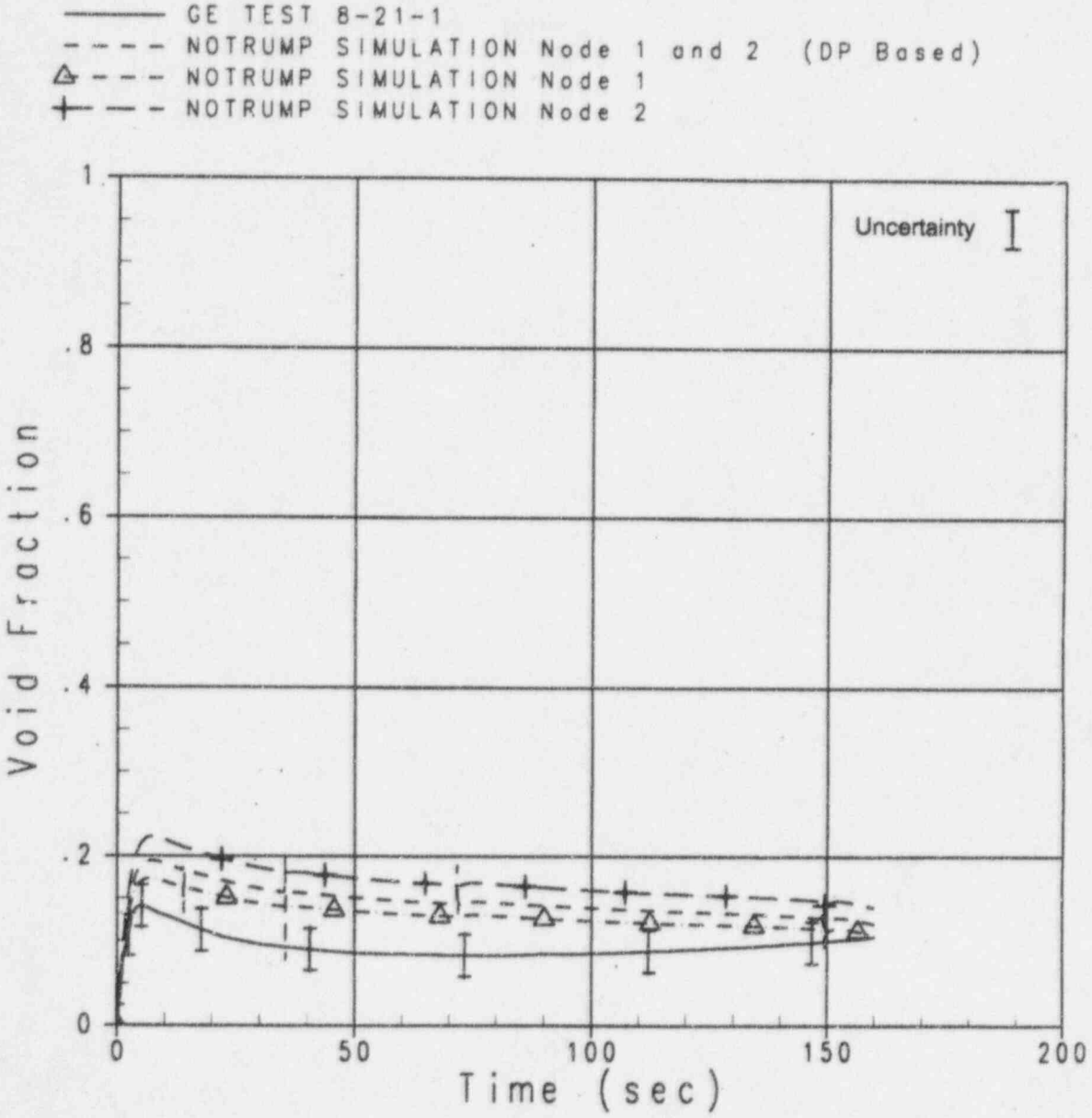

Figure 4.2-42 Void Fraction for Test 8-21-1 and NOTRUMP Simulation Matching Mass and Pressure, Nodes 1 and 2

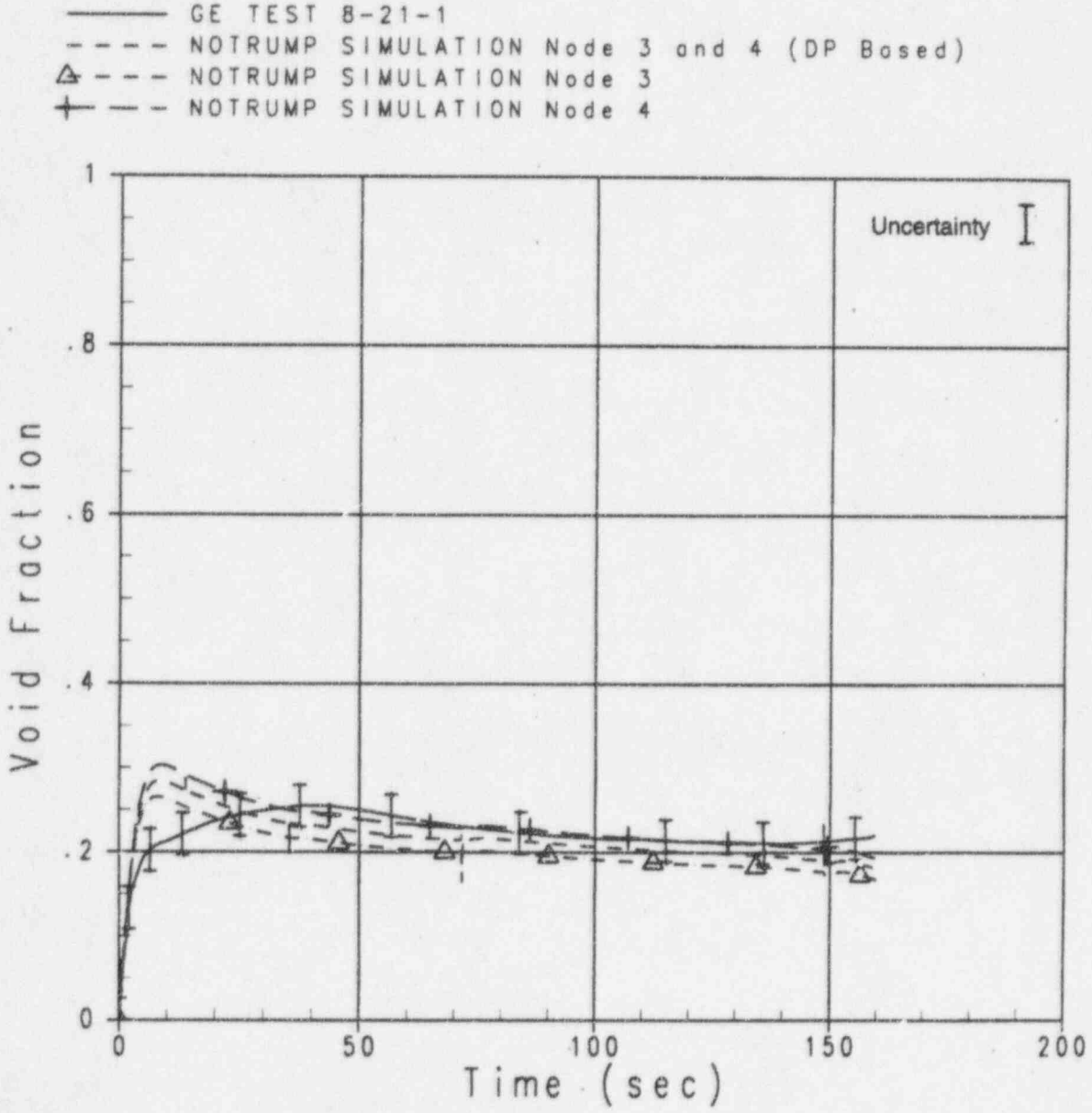

Figure 4.2-43 Void Fraction for Test 8-21-1 and NOTRUMP Simulation Matching Mass and Pressure, Nodes 3 and 4

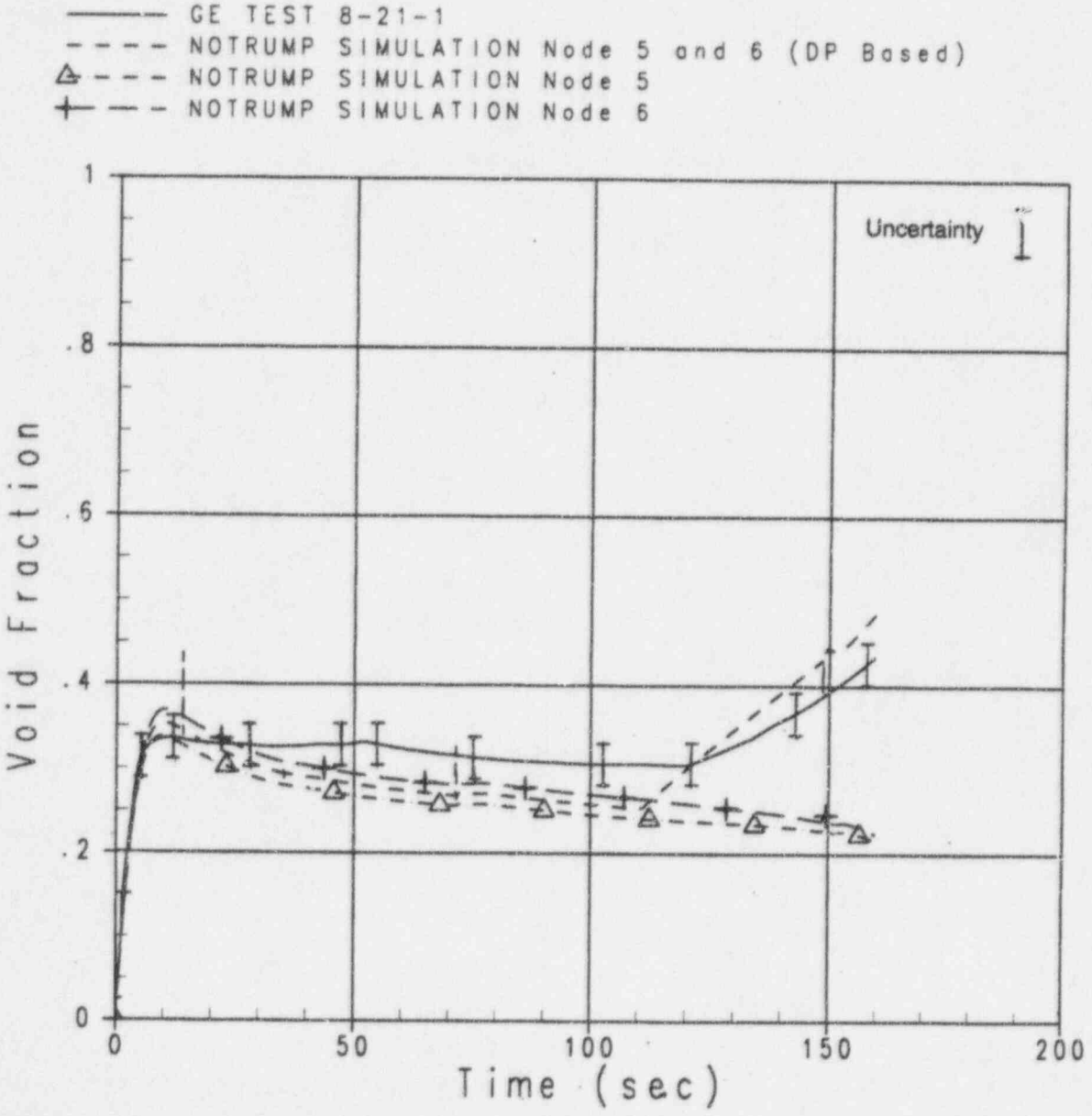

Figure 4.2-44 Void Fraction for Test 8-21-1 and NOTRUMP Simulation Matching Mass and Pressure, Nodes 5 and 6

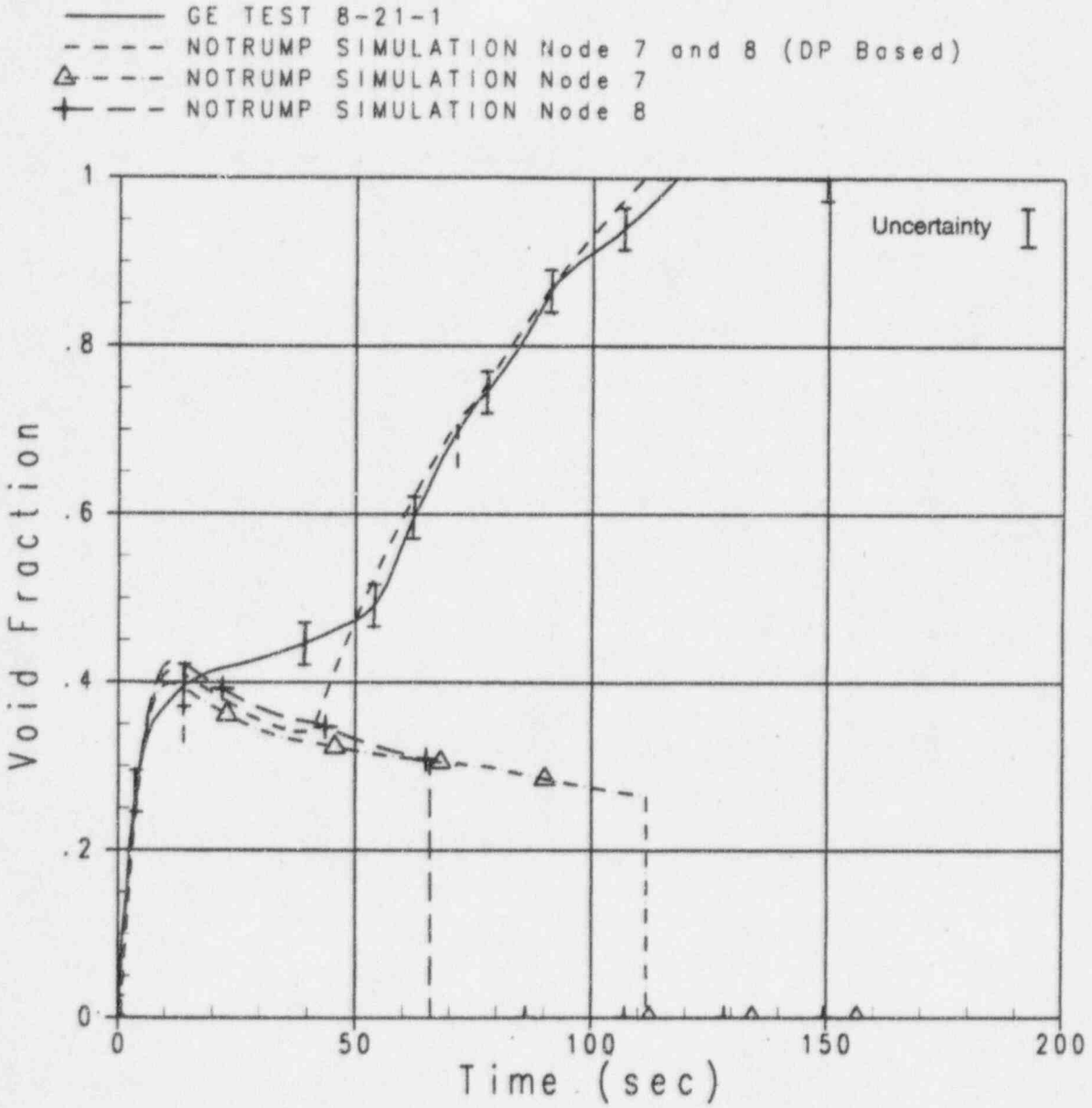

Figure 4.2-45 Void Fraction for Test 8-21-1 and NOTRUMP Simulation Matching Mass and Pressure, Nodes 7 and 8

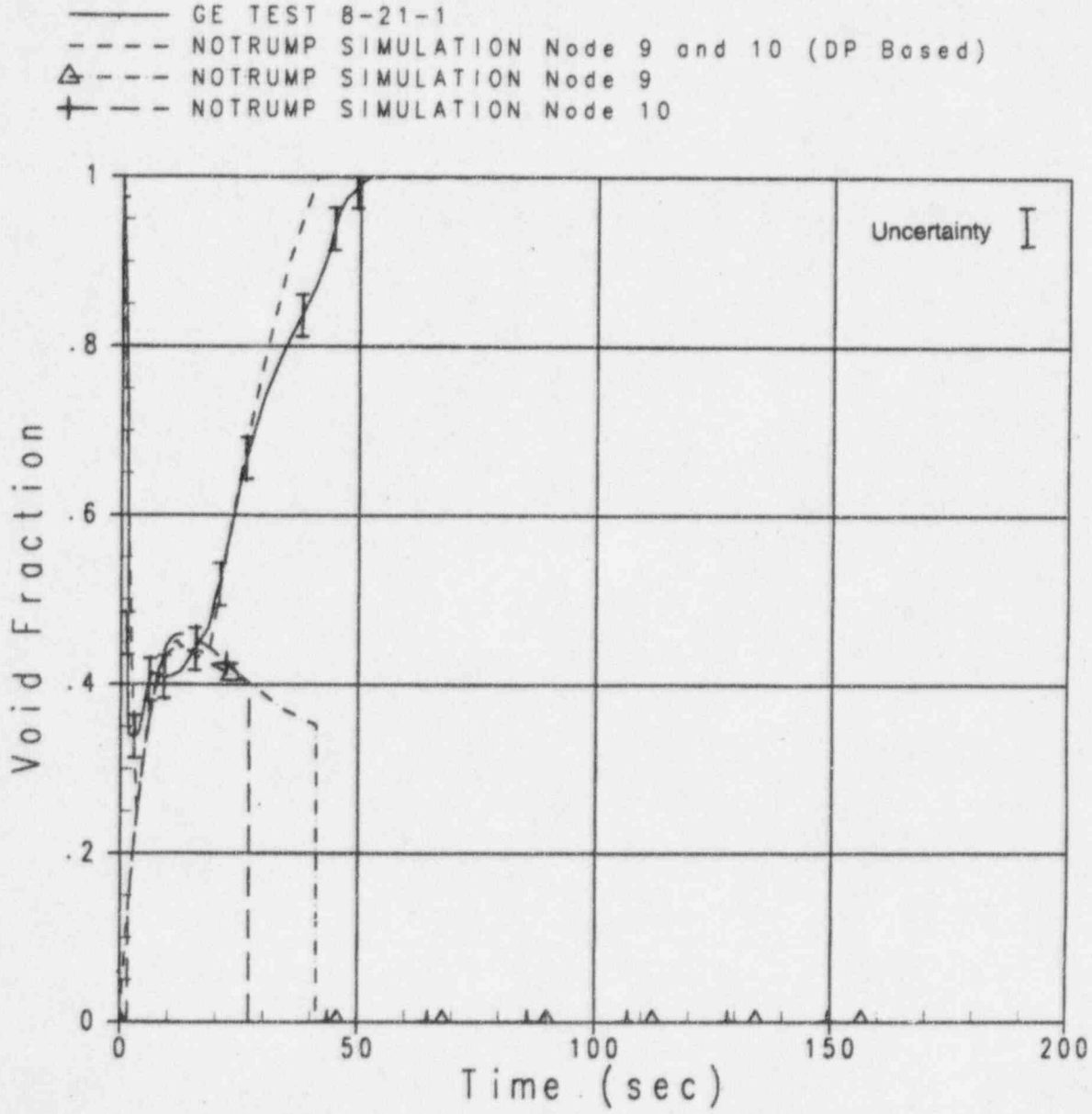

Figure 4.2-46 Void Fraction for Test 8-21-1 and NOTRUMP Simulation Matching Mass and Pressure, Nodes 9 and 10

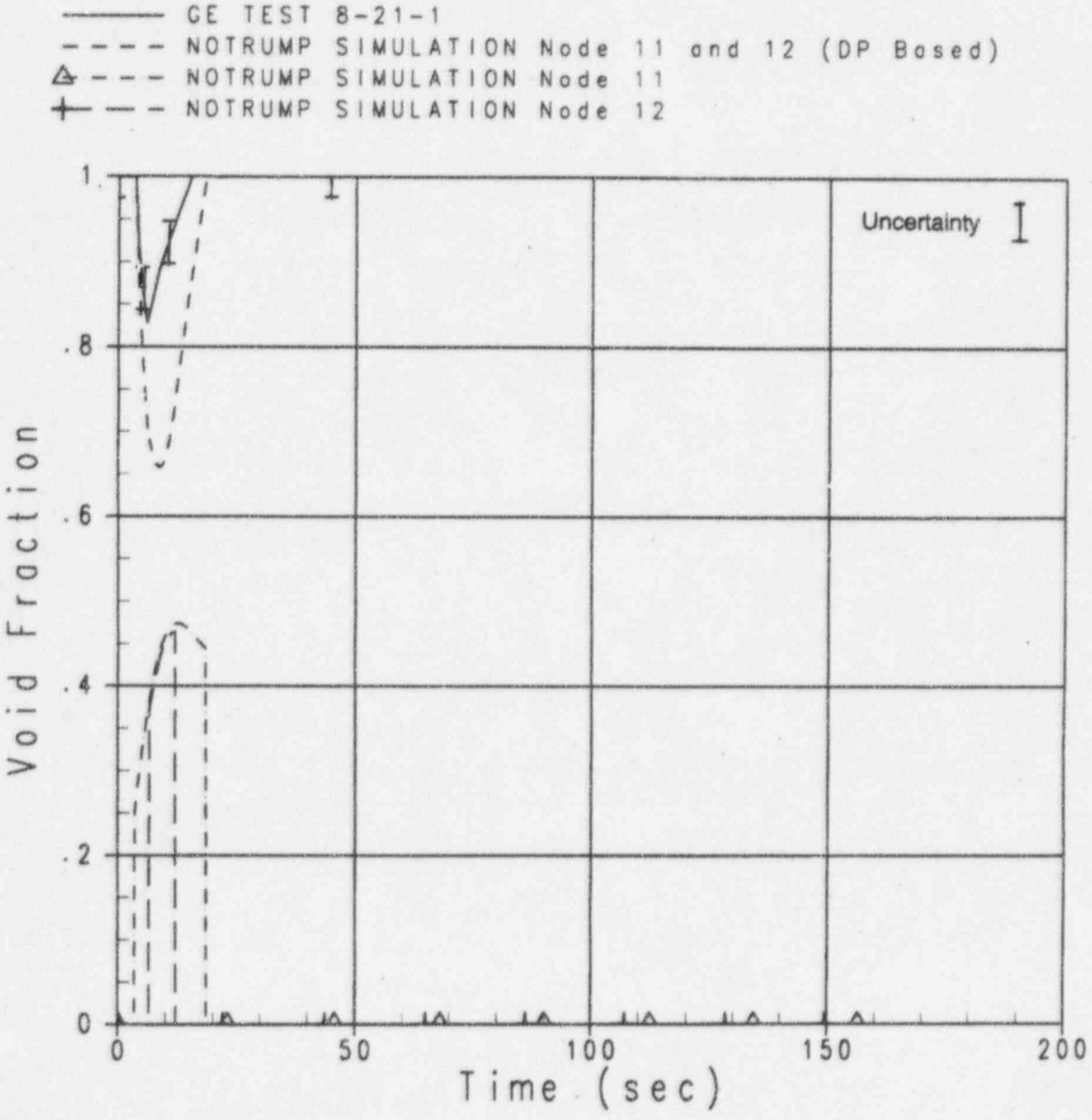

Figure 4.2-47 Void Fraction for Test 8-21-1 and NOTRUMP Simulation Matching Mass and Pressure, Nodes 11 and 12

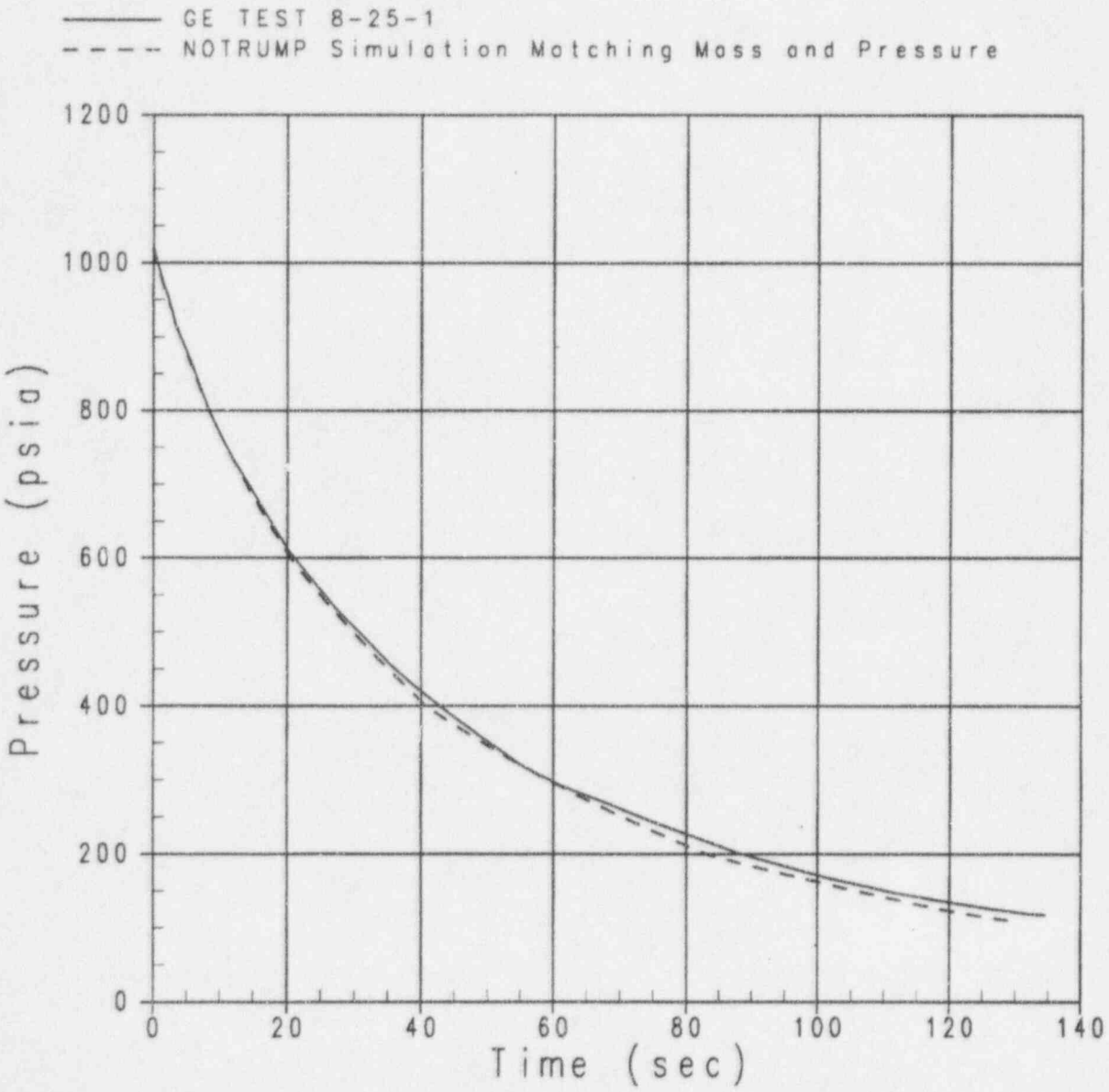

Figure 4.2-48 Vessel Pressure for Test 8-25-1 and NOTRUMP Simulation Matching Mass and Pressure

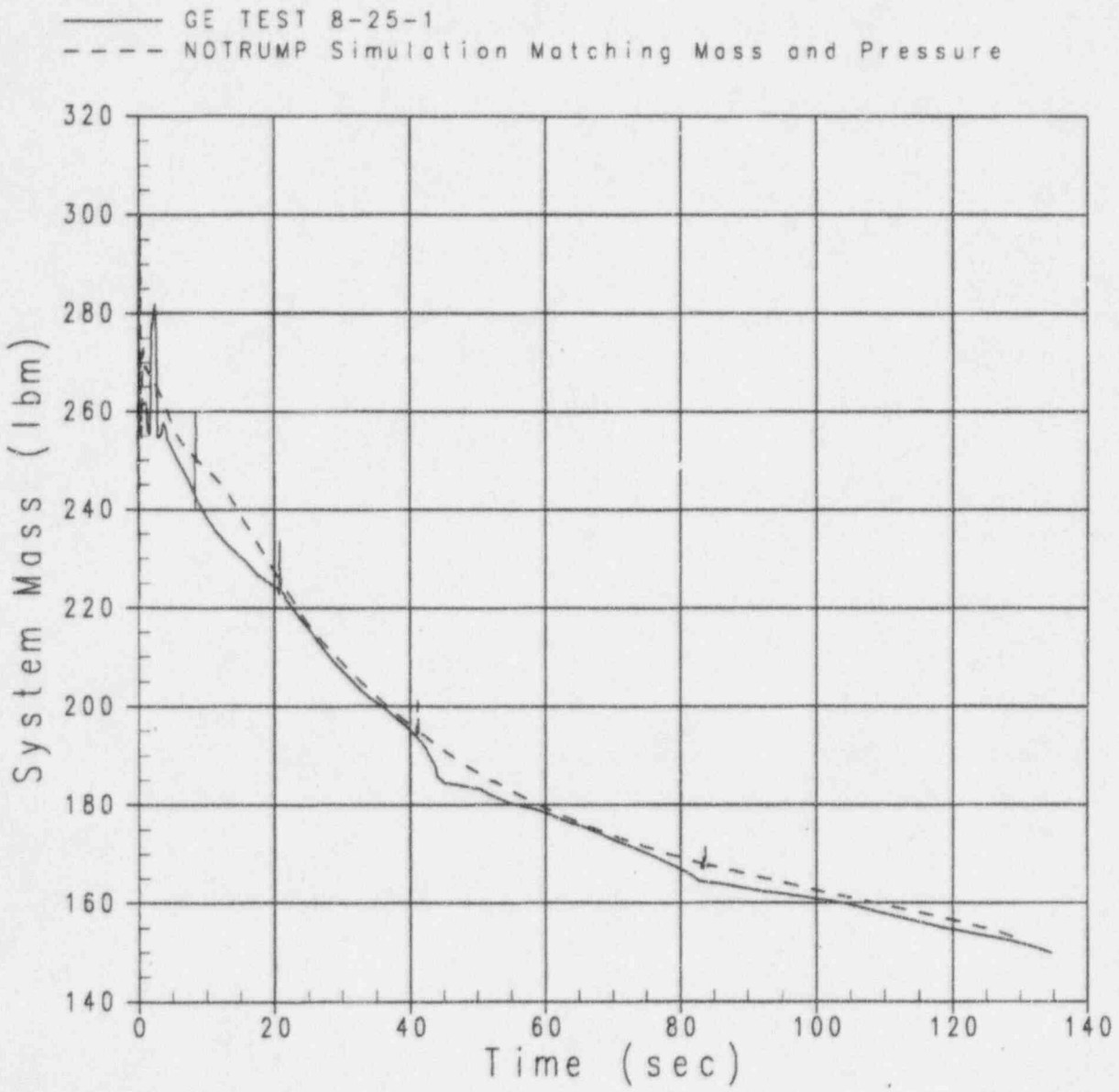

Figure 4.2-49 Vessel Mass for Test 8-25-1 and NOTRUMP Simulation Matching Mass and Pressure

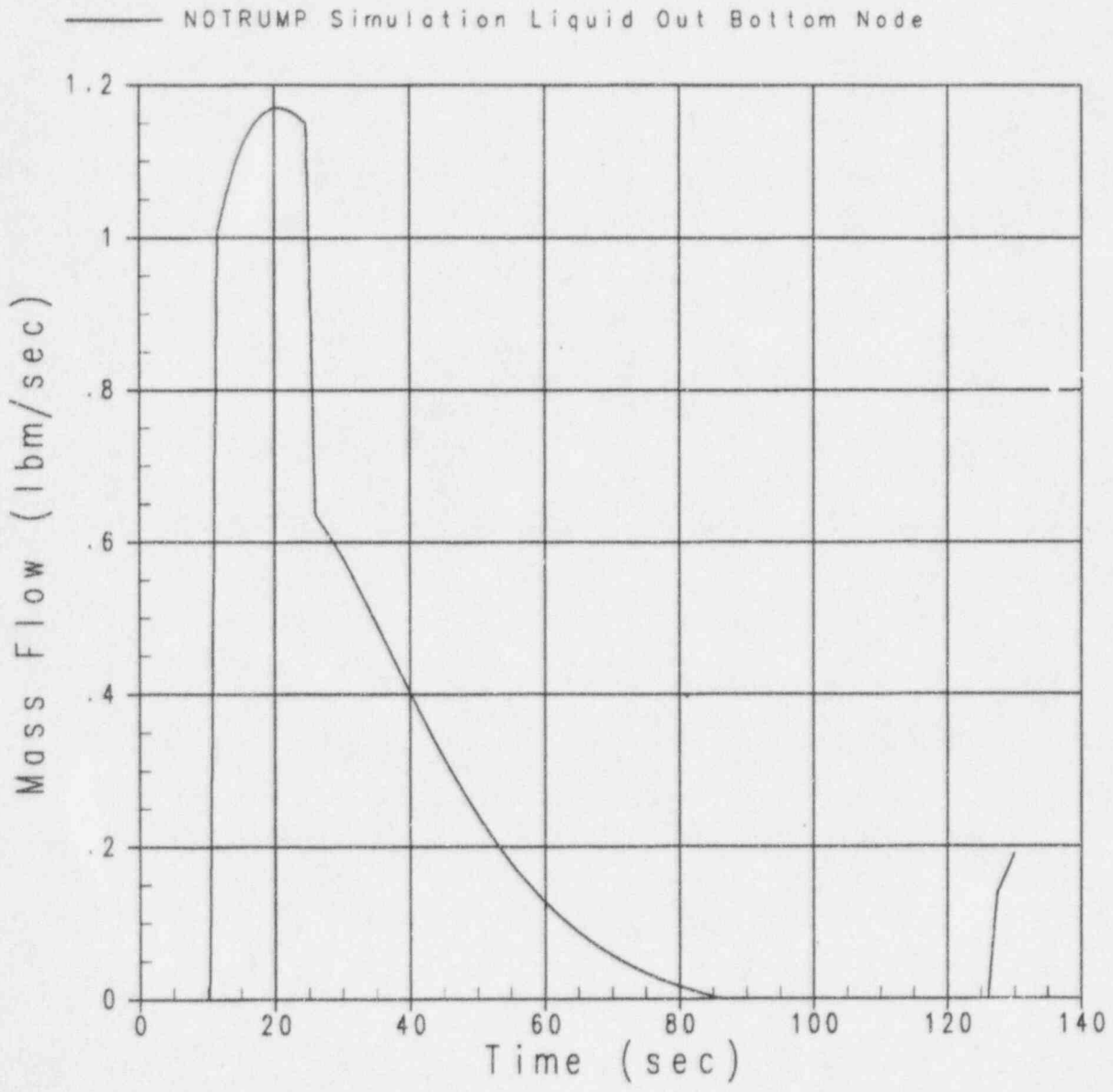

Figure 4.2-50 Liquid Mass Removed from Bottom Node for NOTRUMP Simulation of Test 8-25-1 Matching Mass and Pressure

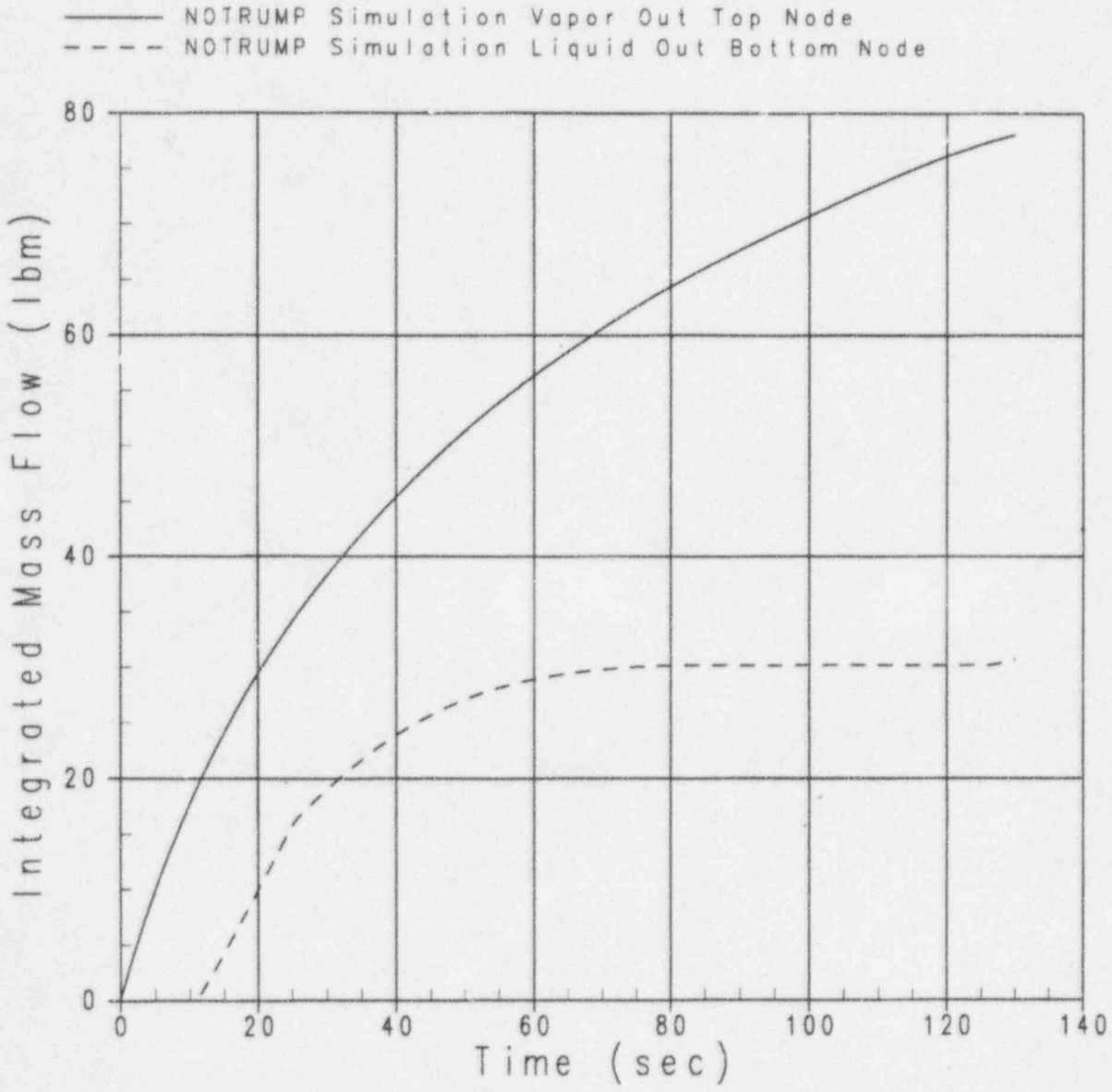

Figure 4.2-51 Integrated Mass Exiting Vessel for NOTRUMP Simulation of Test 8-25-1 Matching Mass and Pressure

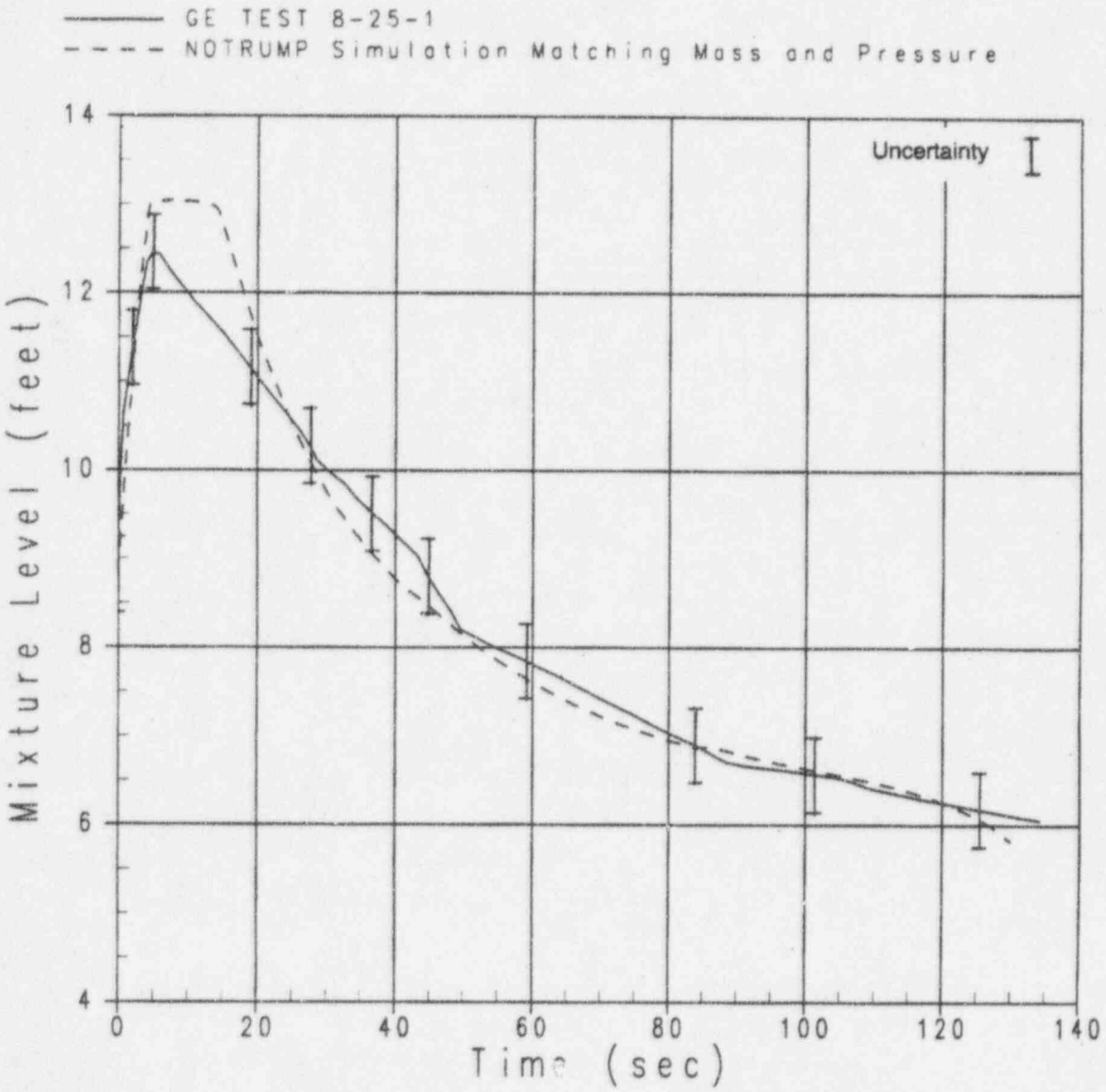

Figure 4.2-52 Vessel Mixture Level for Test 8-25-1 and NOTRUMP Simulation Matching Mass and Pressure

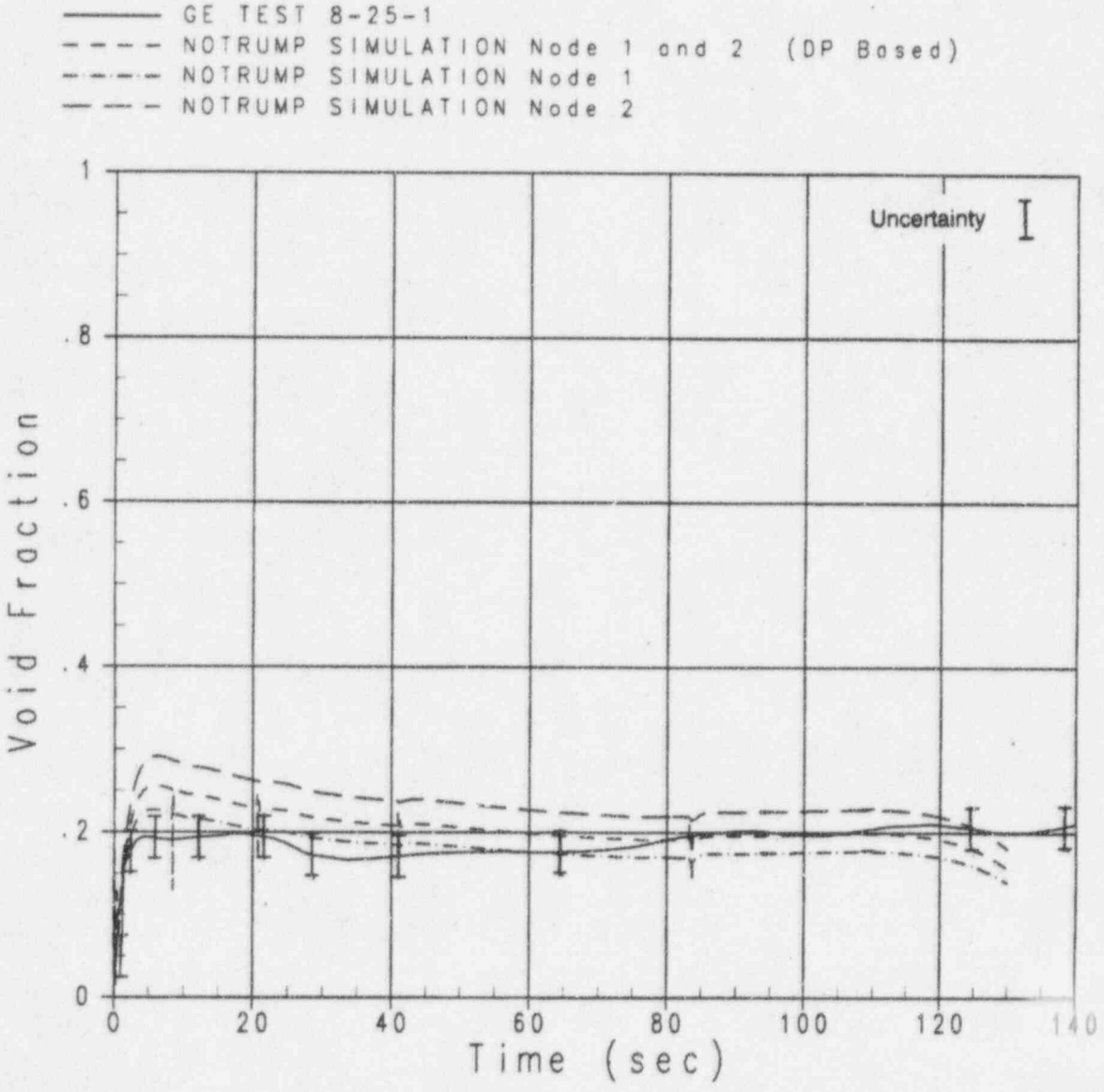

Figure 4.2-53 Void Fraction for Test 8-25-1 and NOTRUMP Simulation Matching Mass and Pressure, Nodes 1 and 2

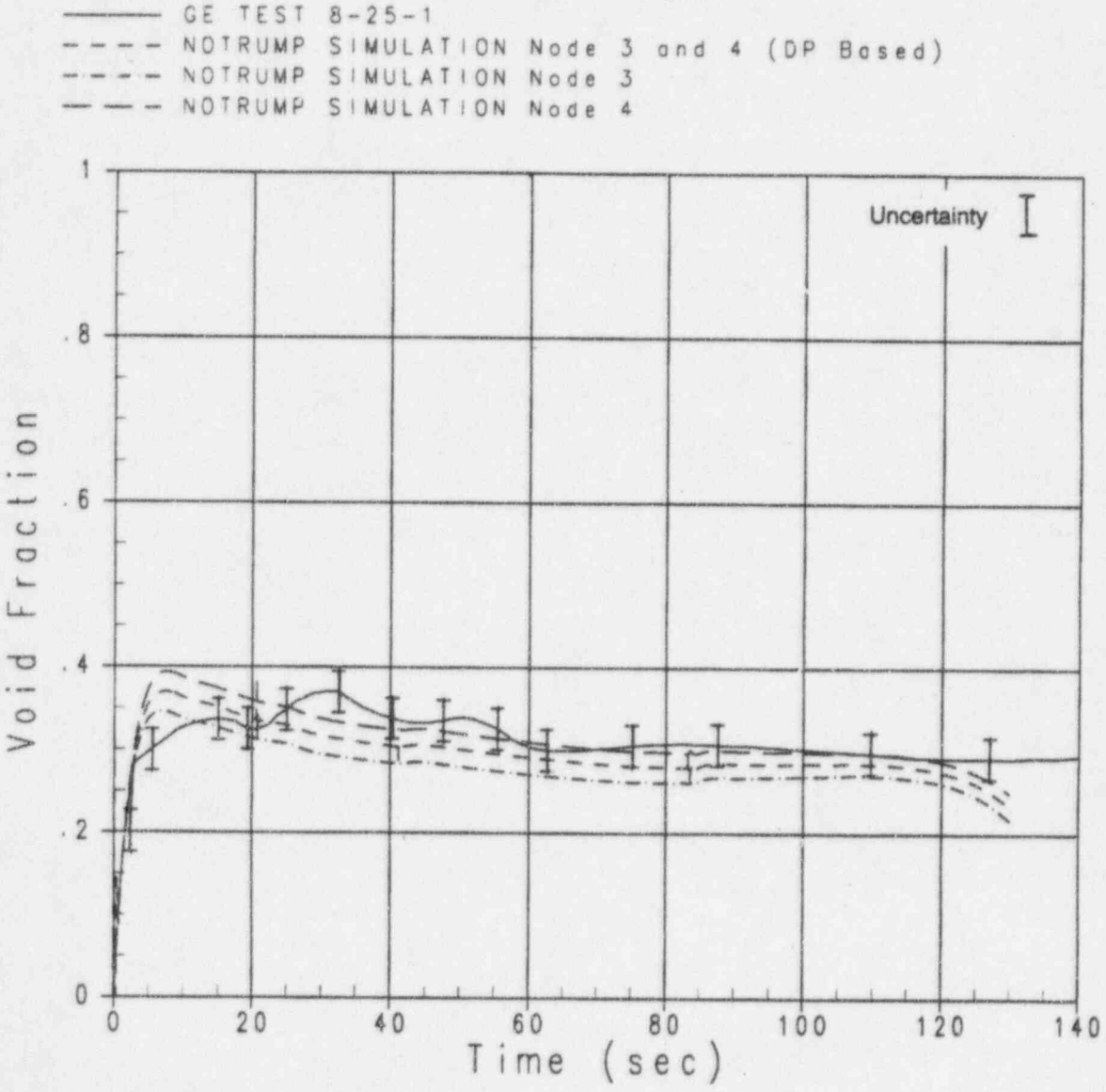

Figure 4.2-54 Void Fraction for Test 8-25-1 and NOTRUMP Simulation Matching Mass and Pressure, Nodes 3 and 4

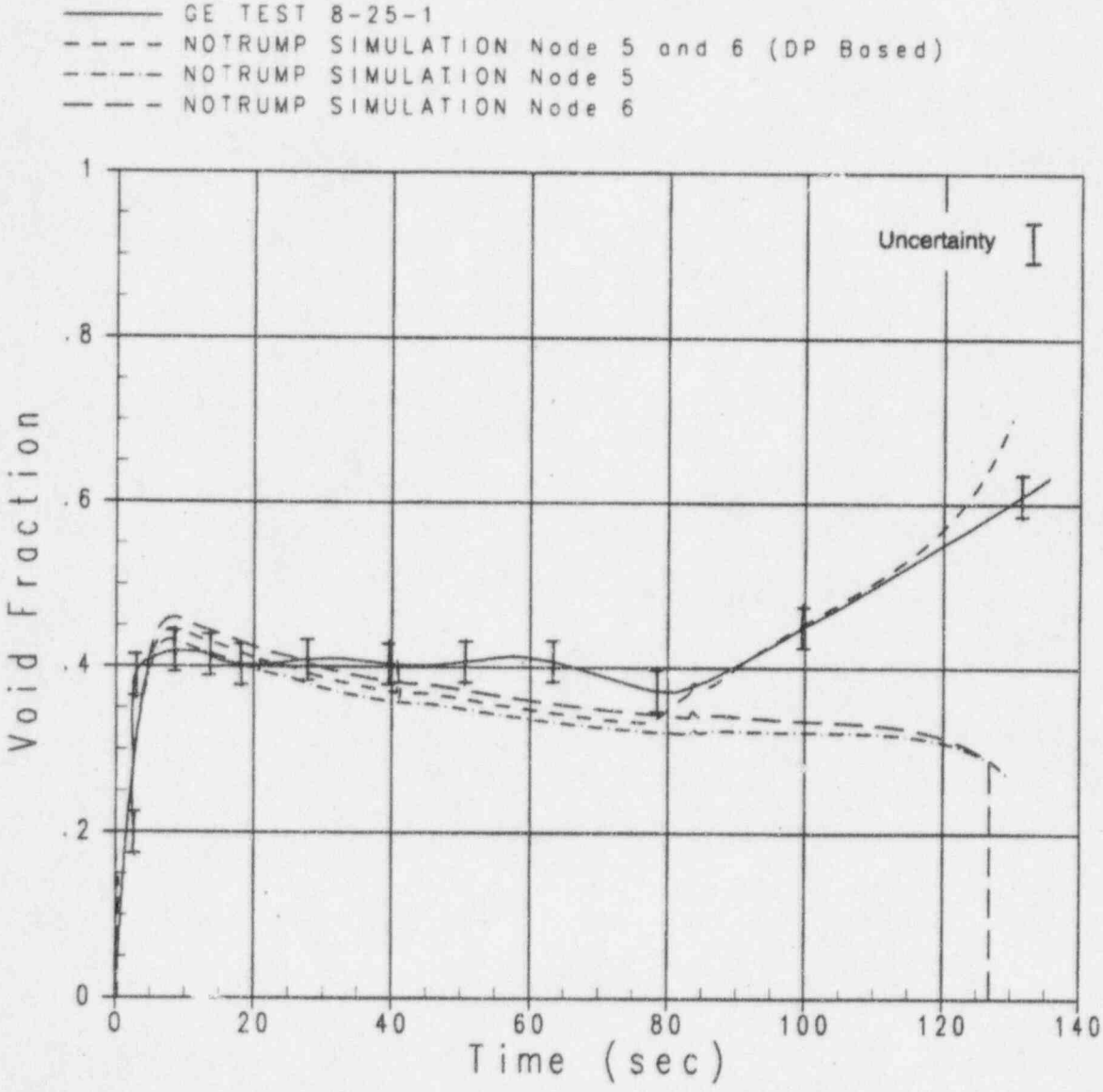

Figure 4.2-55 Void Fraction for Test 8-25-1 and NOTRUMP Simulation Matching Mass and Pressure, Nodes 5 and 6

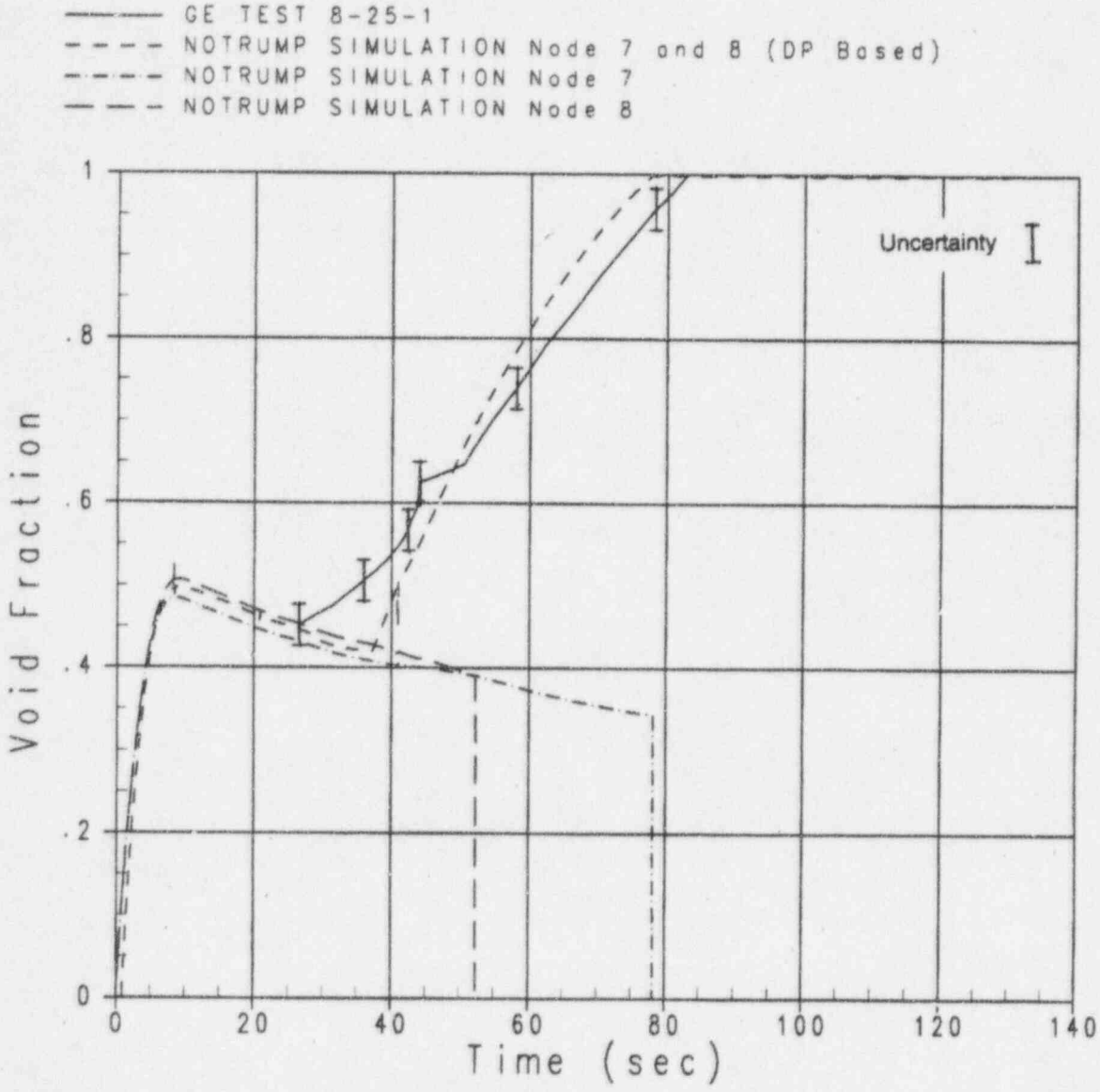

Figure 4.2-56 Void Fraction for Test 8-25-1 and NOTRUMP Simulation Matching Mass and Pressure, Nodes 7 and 8

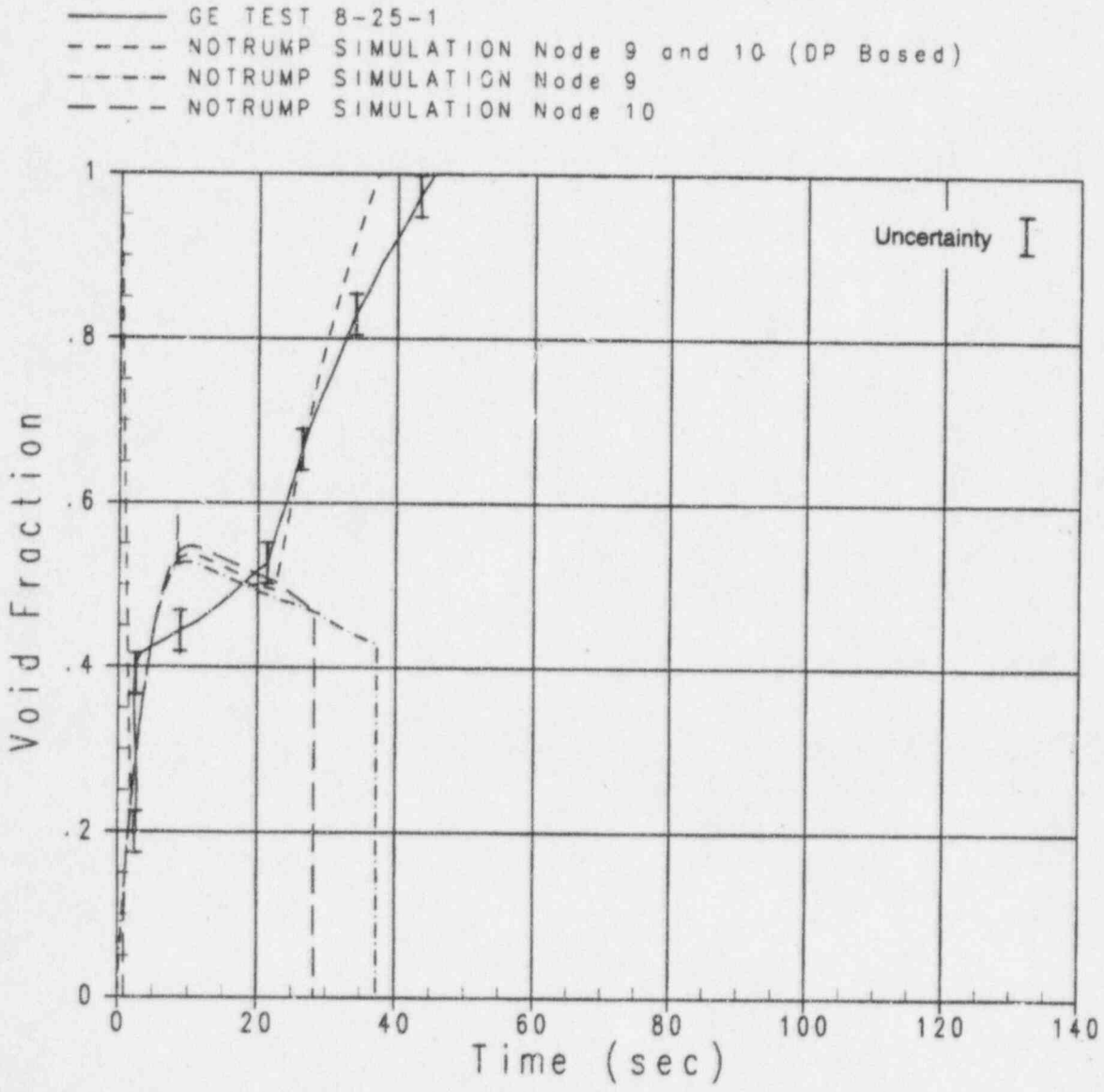

Figure 4.2-57 Void Fraction for Test 8-25-1 and NOTRUMP Simulation Matching Mass and Pressure, Nodes 9 and 10

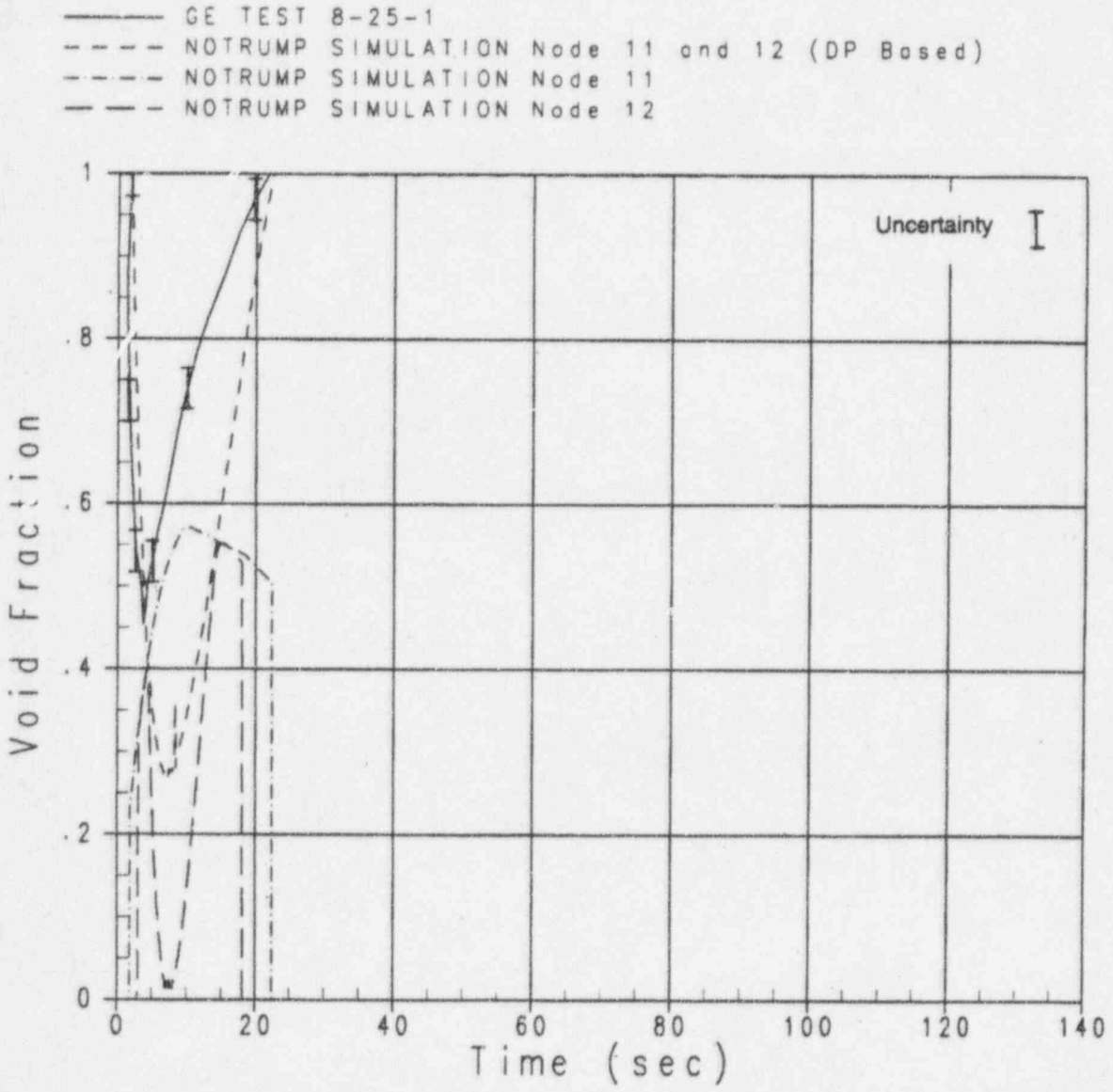

Figure 4.2-58 Void Fraction for Test 8-25-1 and NOTRUMP Simulation Matching Mass and Pressure, Nodes 11 and 12

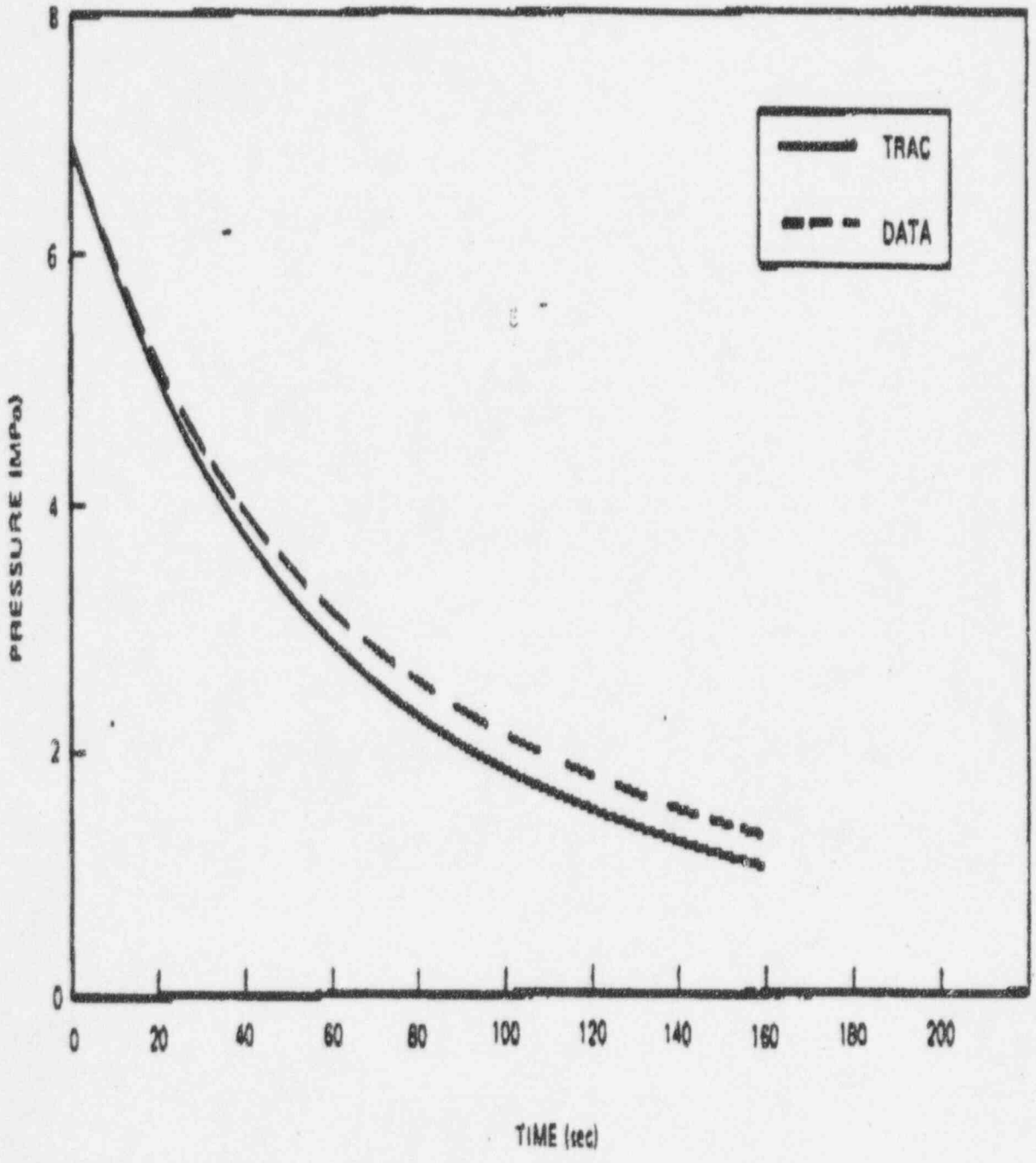

Figure 4.2-59 Comparison of System Pressure (NV 8-21-1)

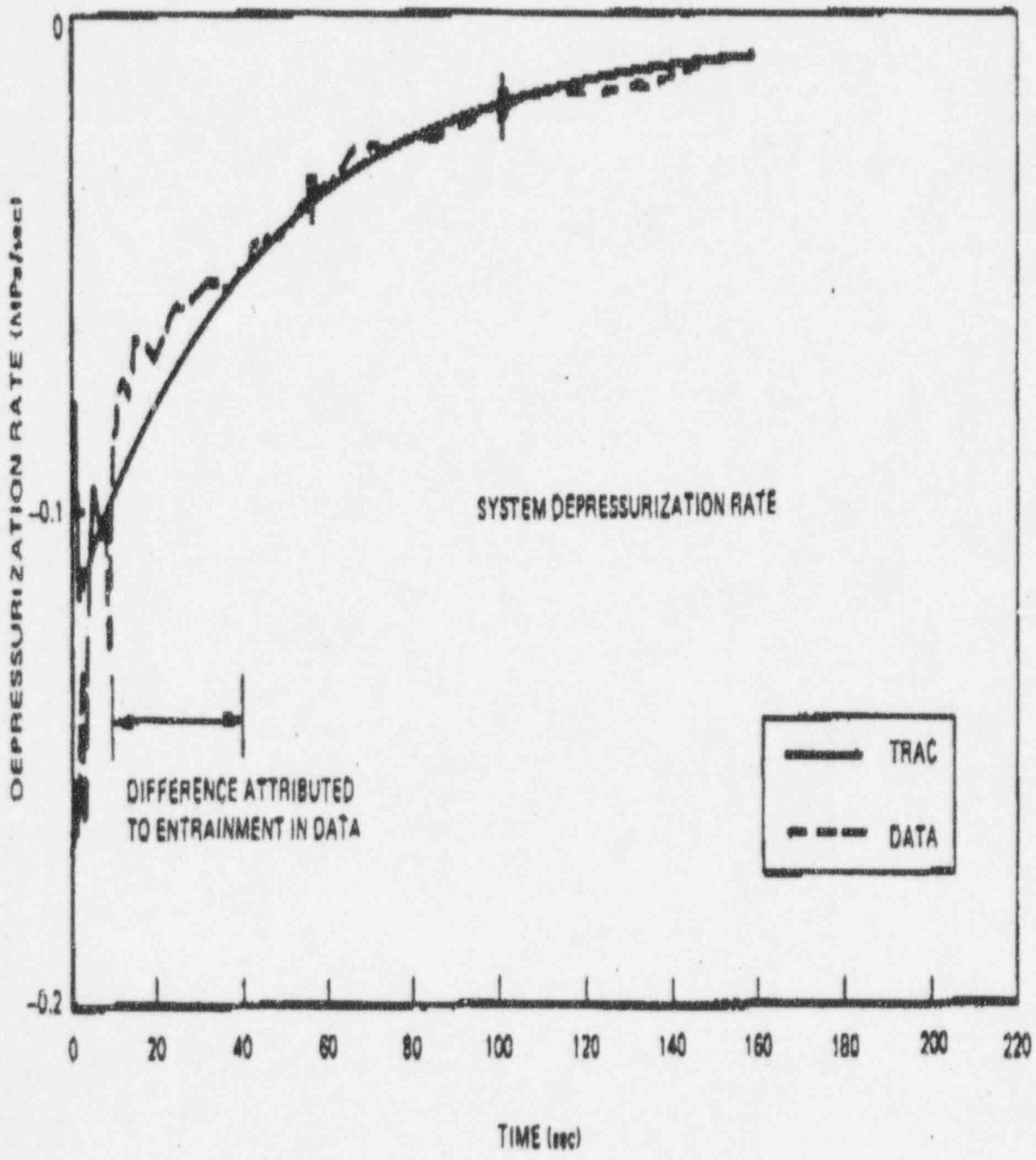

Figure 4.2-60 Comparison of System Depressurization Rate (NV 8-21-1)

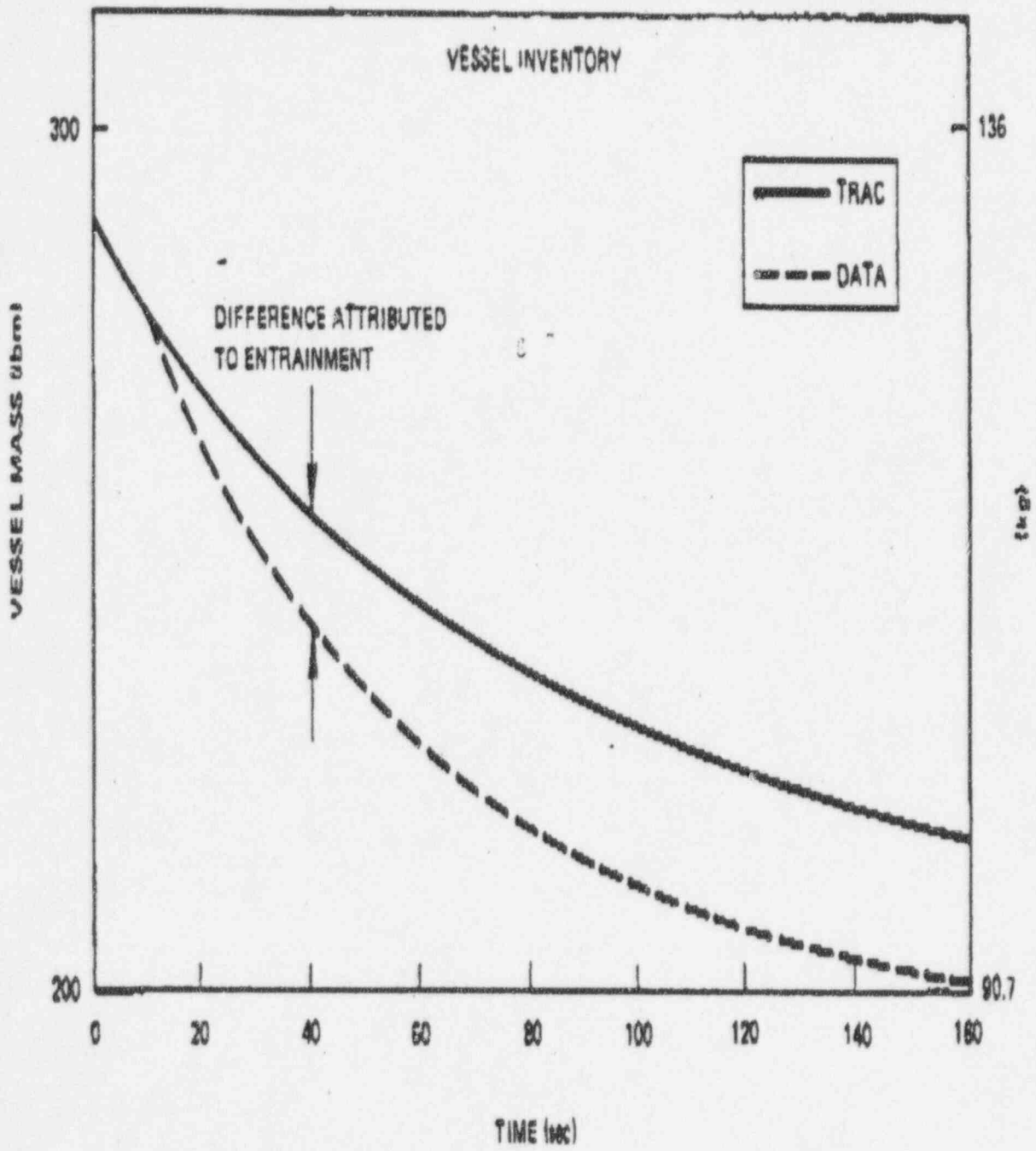

Figure 4.2-61 Comparison of Vessel Fluid Mass (NV 8-21-1)

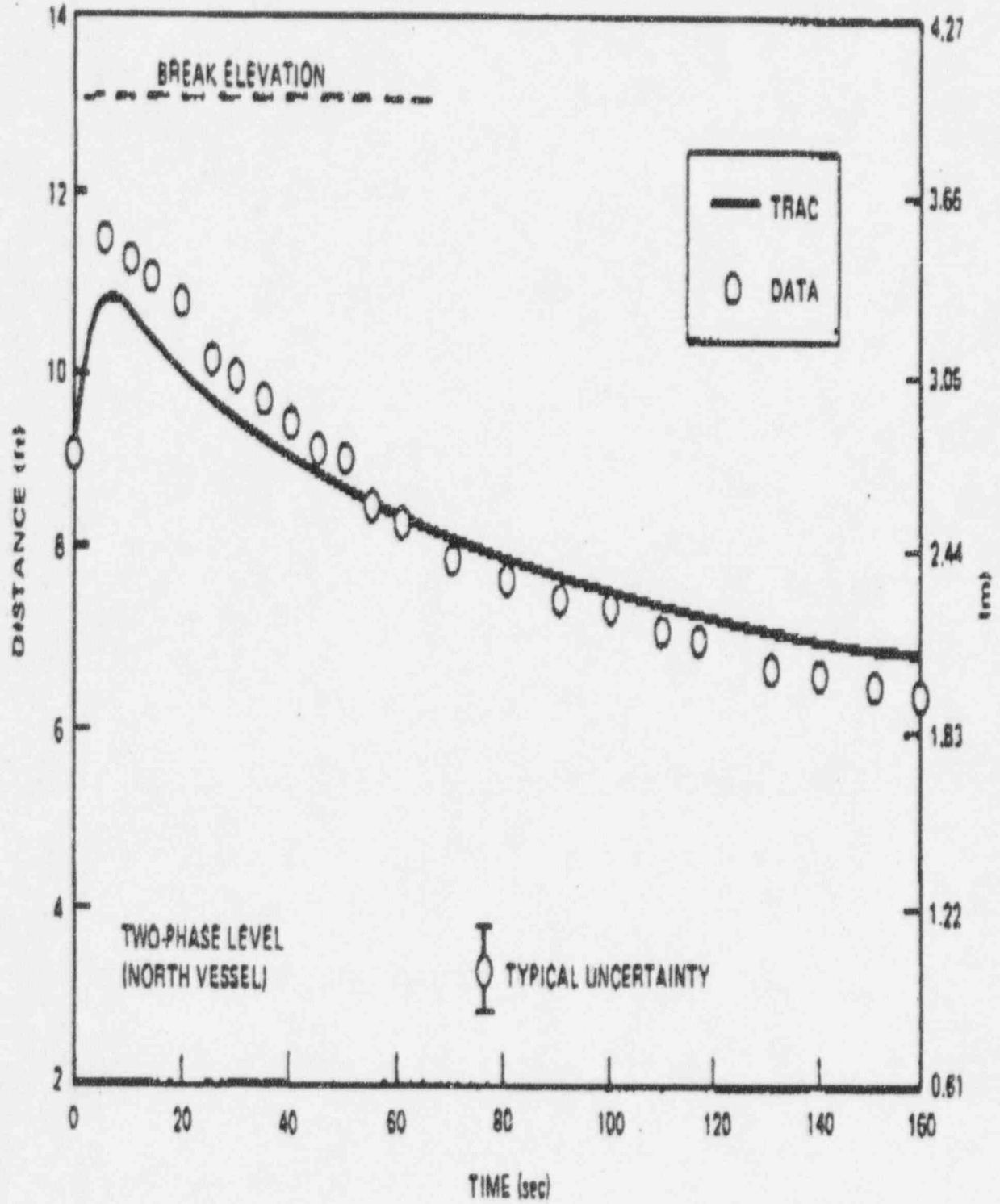

Figure 4.2-62 Comparison of Two-Phase Level (NV 8-21-1)

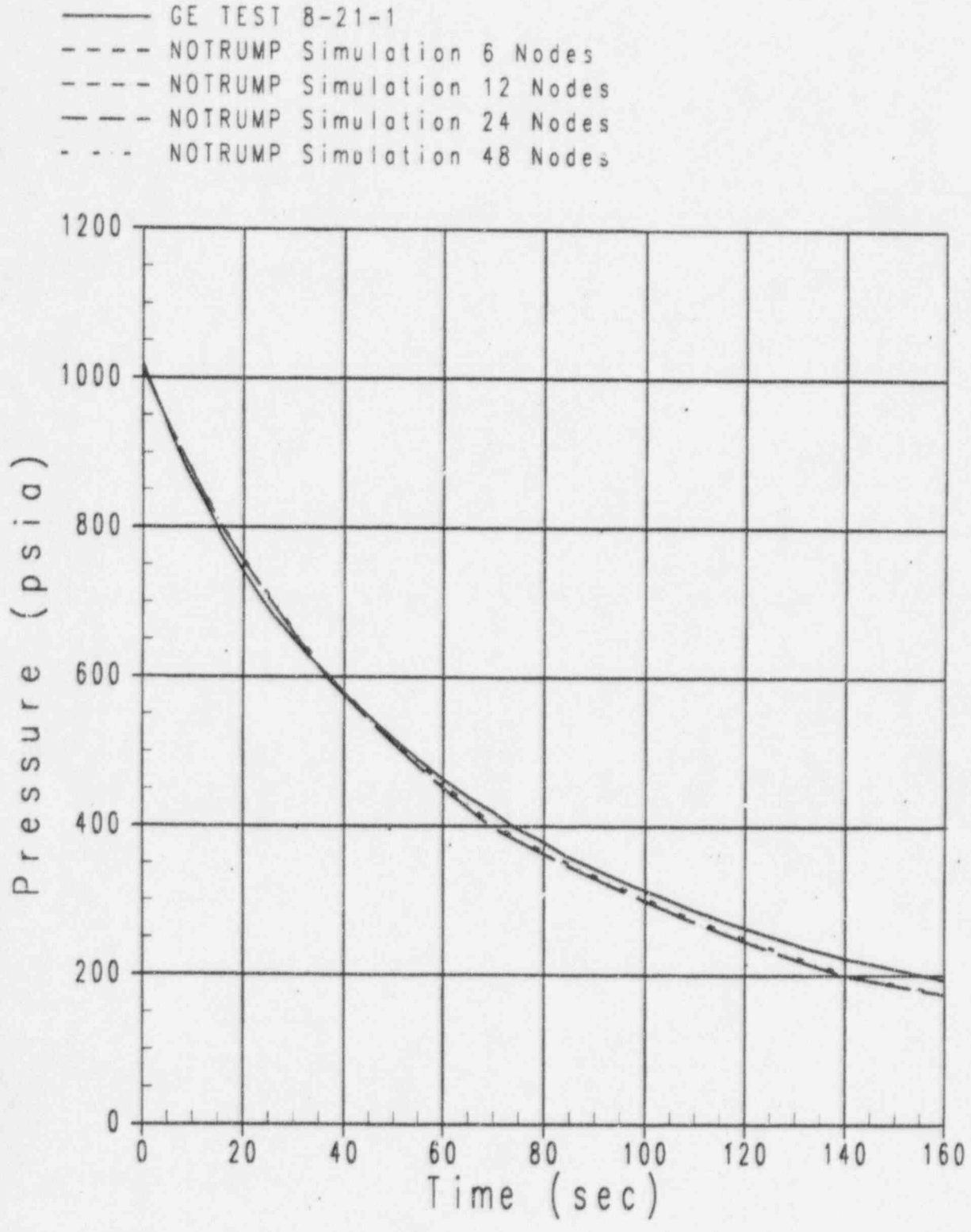

Figure 4.2-63 GE Vessel Pressure Results from Noding Sensitivity Study

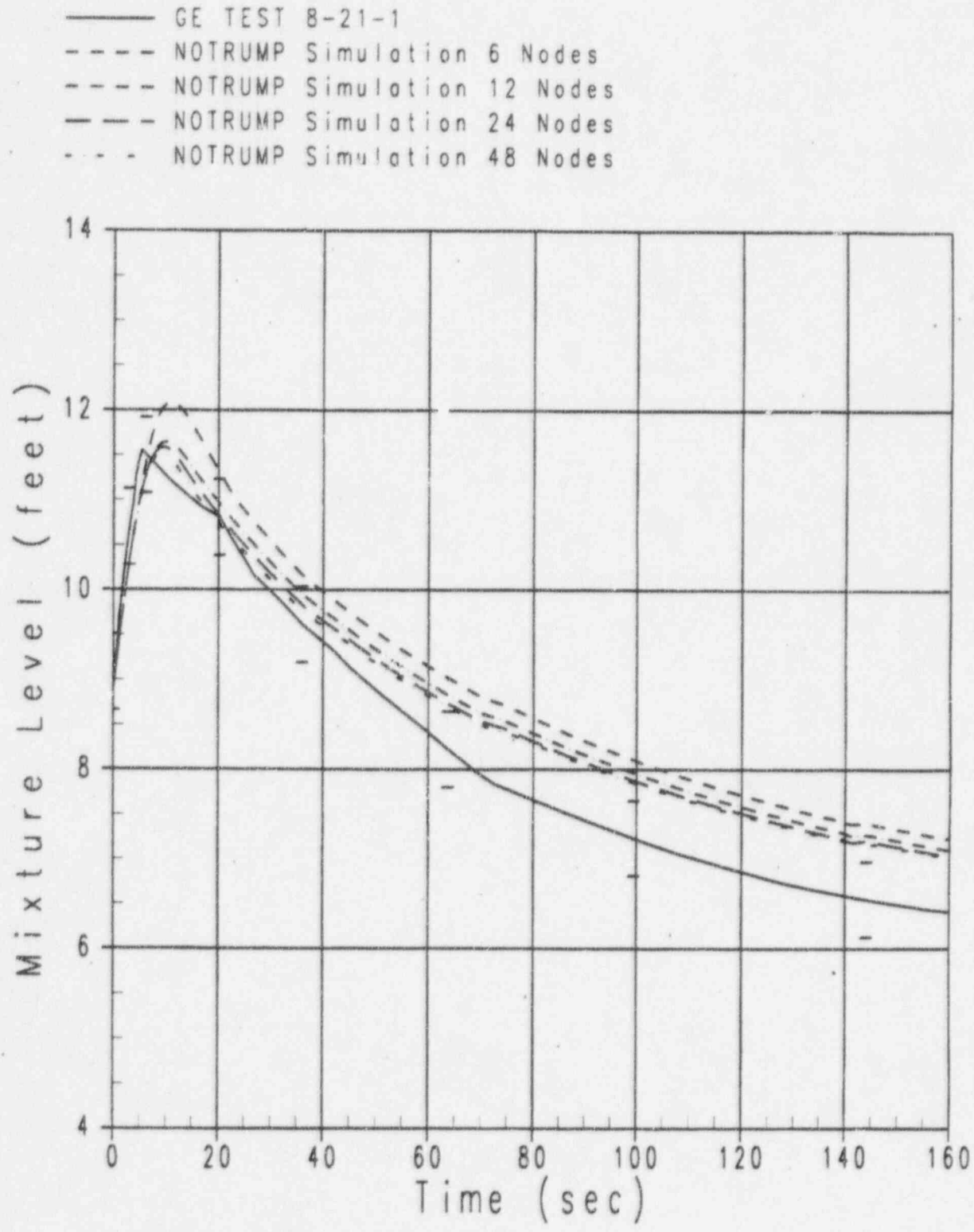

Figure 4.2-64 GE Vessel Mixture Level Results from Noding Sensitivity Study

4.3 ACHILLES Low-Pressure Level Swell Tests

As part of the validation of the NOTRUMP level swell, void fraction, and drift flux models, the ACHILLES low-pressure level swell tests were simulated. The ACHILLES tests were funded by Central Electricity Generating Board (CEGB) and performed by the U.K. Atomic Energy Authority (UKAEA) at Winfrith (Reference 4-9) as part of a general program to examine core heat transfer behavior under postulated loss-of-coolant accident (LOCA) conditions.

Since these tests simulate the two-phase level swell behavior at low pressures, they are particularly useful for the validation of the NOTRUMP level swell and drift flux models that are used to predict the core void distribution and mass inventory for the AP600 design. The activation of the automatic depressurization system (ADS) depressurizes the primary system to near containment pressures, at which time the mass inventory in the reactor vessel is at a minimum, just before the injection from the in-containment refueling water storage tank (IRWST). Calculation of the vessel mass and the two-phase mixture level within the core is important at this time period since the height of the mixture level determines if the core remains covered. Comparisons of NOTRUMP predictions with the ACHILLES mixture level data helps confirm the NOTRUMP code's ability to predict the two-phase level swell in the AP600 plant.

4.3.1 ACHILLES Test Description

4.3.1.1 Facility Description

The layout of the ACHILLES rig circuit is shown in Figure 4.3-1. The most important features are the shroud vessel, which contains the test section, and the downcomer. These represent the core barrel and the annular downcomer in the reactor pressure vessel. The shroud vessel and downcomer are connected at the bottom for the level swell tests. Water can be supplied to the interconnecting pipework from a heated tank at up to 240°F. The flow rate is obtained by a heat and mass balance. Steam separators are installed at the exits from both the shroud vessel and the downcomer to measure the flows of the separated phases. The flow rate of separated steam is measured by a vortex flowmeter. This operates at the bottom of its range in the level swell tests but is adequate at the highest powers employed at the beginning of the test when the steam flows are highest. The steam raiser is used to purge the rig with steam before a test and to preheat the pipework. It continues to operate during a test so that its steam, plus that generated within the test section, flows out to the atmosphere through the pressure control valve. This valve responds to the pressure in the capacity vessel, a large volume on a dead leg whose function is to damp out pressure fluctuations.

The ACHILLES test section is shown in cross section in Figure 4.3-2. It is a cluster of 69 rods in a square array within the circular shroud vessel. The figure shows the letters and numbers used to define rod locations. The rod diameter and pitch (0.374 and 0.496 in.) are typical of PWR dimensions. The internal diameter of the shroud vessel is 5.039-in. Each rod is electrically heated

over a length of 12 ft., which is typical of the nuclear heated length in a PWR fuel rod, and each contains six internal thermocouples.

Figure 4.3-3 shows the axial disposition of the heater rod thermocouple locations. The thermocouples are concentrated in different axial zones and give a detailed axial coverage. However, their exact locations have been optimized for the reflood tests, not for level swell. Figure 4.3-3 also shows the axial disposition of a number of other features. The spacer grids are at prototypic PWR locations and are of prototypic design, having been fabricated from reactor strip material. As in the reactor fuel, all except the bottom and top grids have prototypic mixing vanes. Each grid is fitted with two thermocouples on its top edge. Grids 5 and 7 have an additional two thermocouples on their bottom edges. The axial power profile along the rods is an 11-step approximation to a chopped cosine. The steps are formed by varying the pitch of the heater wire coils during manufacture.

The shroud vessel has five heating zones whose power can be varied independently. The shroud heat flux is as uniform as possible within each zone. The shroud vessel has thermocouples disposed axially in line with rod thermocouples. There are two, and in some cases four, of these at each elevation. Their azimuthal locations are shown in Figure 4.3-2. The shroud heating is used in the level swell tests.

There are pressure taps along the shroud vessel that allow the pressure gradient to be measured. Void fraction data are inferred from these measurements. These taps are uniformly spaced, but alternate pairs contain a spacer grid. This allows the grid pressure drop to be isolated. Instream thermocouples project into the subchannels above and below the grids to measure the local coolant temperature. These subchannels are indicated in Figure 4.3-2.

There are 414 heater rod thermocouples, almost all of which functioned normally throughout the entire test program. These are used to determine the swell level, since those below it remain at about saturation temperature while those above it heat up. Because the axial spacing of the thermocouples is not constant, the precision to which the mixture level can be determined varies from 0.13 m (5.12 in.) near spacer grids to 0.06 m (2.36 in.) between grids.

Differential pressure measurements are used to determine the mean void fraction in the axial interval between a pair of pressure taps. For this purpose the differential pressure is assumed to be due only to the difference in density between the two-phase mixture in the test section and the water in the reference leg. Any contribution from friction or acceleration is ignored. An additional transducer provides the differential pressure over the entire test section. This is used to determine the collapsed liquid level. This is an indication of the level of saturated, void free water that would give the same static differential pressure as the test value. Another differential pressure measurement is made over the height of the downcomer to determine its contents.

The heater rod and shroud measured power are used in heat balances to determine the steam flow rate as a function of elevation in the test section. The power profile along all 69 rods is taken from the

nominal values for each step shown in Figure 4.3-3. The actual power profile, determined experimentally, is in good agreement with this nominal profile. The shroud power is assumed to be axially uniform within each of the five heating zones. The small heat losses are determined experimentally for each of the five zones as functions of temperature. The heat balance extends only up to the swell level, and all of the shroud vessel below this level is assumed to be at saturation temperature for the purpose of calculating the heat losses.

The system pressure is measured at the top of the test section. Local pressures at each differential pressure tap are determined from this pressure plus the sum of all the differential pressures down to the level in question. It is important to apply this correction for the head of the two-phase mixture because it has an effect on steam density at the low pressures of the present tests.

Before starting a test, the rig is purged with steam from the steam raiser. Steam passes out of the rig, which is set to control the rig at the desired pressure. This process is continued until the rig pipework is heated to the saturation temperature. The shroud vessel and downcomer are then partially filled with slightly subcooled water. Power is applied to the rod cluster and the shroud vessel. The shroud power is set up So that the axial power profile approximates the axial power shape along the rods (but with only 5 steps, not 11), and with a magnitude so that the power input per unit flow area is the same near the shroud wall as in the center of the cluster. This compensates for the excess flow area around the outside of the cluster, which is evident in Figure 4.3-2.

The data logger then is started. As water boils off in the shroud vessel, the amount of water in both the shroud vessel and the downcomer decreases. Eventually the top thermocouples are uncovered and begin to heat up. As boildown proceeds, thermocouples progressively lower in the cluster are uncovered.

4.3.1.2 Test Matrix

There are a total of six tests run at different bundle powers and pressures, as shown in Table 4.3-1, as part of the ACHILLES program. Of these six tests, only two tests are reported, tests A1L066 and A1L069, which are the higher power tests. As explained in the data analysis report (Reference 4-9), there are inconsistencies observed in the lower power tests and only the 80 kw tests are analyzed.

4.3.1.3 Selection of Test for NOTRUMP Validation

The NOTRUMP code is used to model both of the valid ACHILLES 80 kw tests. The initial conditions for the two valid tests are given in Tables 4.3-2 and 4.3-3 and are used to establish the NOTRUMP initial conditions for the tests. The tests are transients since the mixture level decreases with time as water is boiled off from the heated rod bundle for the given constant power at the preset constant pressure.

4.3.2 NOTRUMP Model of the ACHILLES Facility

The ACHILLES boil-off tests were initiated with a liquid level in the rod bundle and in the simulated downcomer. Therefore, the NOTRUMP model simulates the rod bundle, downcomer, lower plenum, upper plenum, and the resistances from the downcomer and the upper plenum to a pressure boundary node. The NOTRUMP schematic is shown in Figure 4.3-4. In the rod bundle section, 1-ft. axial nodes are used to obtain a more accurate simulation of the two-phase mixture level. There are UO_2 core nodes that simulate the heater rods. The axial power profile shown in Figure 4.3-3 is used to calculate the power input for the different core nodes. The heat input from the shroud is also accounted for in the model.

The NOTRUMP model simulates the heater rod region of the vessel, lower plenum, downcomer, upper plenum, and a volume (cell 41) that simulates the pressure boundary condition for the calculation. The resistances for the flow between the downcomer and the heater rod region are obtained from the test data using the measured steam flow and the initial collapsed levels in the heater rod and downcomer regions. The losses are set to reproduce the initial collapsed levels in the two volumes in the interconnecting piping between the top of the heater rod vessel and the downcomer. The system pressure condition is specified as a boundary condition in node 41 for the tests.

In the heater rod section, the drift correlation from the Yeh (Reference 4-10) two-phase level swell correlation is used. The SIMARC methodology is used in the flowlinks between the fluid nodes in the heater rod section. The implicit bubble rise model is used in the fluid nodes, and the fluid node stacking logic and mixture level over shoot logic is used in the heated region.

4.3.3 NOTRUMP Comparisons to the ACHILLES Data

4.3.3.1 Comparisons to Test A1L066 1.2 Bar (17.64 psia), 96.5 kw Bundle Power

The ACHILLES tests were started with an initial level above the top of the heater rod bundle. The data for this time period were not recorded; therefore, the mass inventory within the heated bundle was examined to determine when the total mass in the NOTRUMP simulation equaled the total mass in the test facility based on the test data. The void distribution in the bundle is measured from differential pressure cells that are placed at frequent intervals along the heated length of the bundle. The test time "zero" curve is measured and presented in the report. The NOTRUMP calculation is run starting with additional mass in the vessel, and the NOTRUMP time zero is set for the comparisons when the mass inventory agrees with the time zero mass in the bundle. This approach is consistent with the approach used for the RELAP 5 modeling of the ACHILLES tests (Reference 4-11).

Figure 4.3-5 shows the determination of the time zero for ACHILLES test A1L066 test when the NOTRUMP calculation equals the test-measured mass in the bundle. The NOTRUMP time zero values are close to those determined for the RELAP 5 calculations.

Figure 4.3-6 compares the collapsed liquid level (or mass in the heated bundle) and the two-phase mixture level in the bundle to the NOTRUMP predictions for test A1L066. The collapsed liquid level is test-determined from the differential pressure cells along the bundle height by interpreting the differential pressure reading to be due to only the gravitational head and ignoring friction and form losses (single- and two-phase) along the heater rods and across the spacer grids. Hand calculations confirm that the frictional and form pressure drops are negligibly small compared to the gravitational head for the level swell tests. NOTRUMP overpredicts the mass inventory or collapsed level in the bundle as compared to the data. The comparisons are initially within the uncertainty of the data but as time progresses, the NOTRUMP calculation lies above the test data. NOTRUMP does correctly predict the data trend throughout the test.

Figure 4.3-6 also shows the two-phase mixture level in the bundle as determined by the uncovery and heat-up of the heater rod thermocouples in the rods. NOTRUMP lies conservatively below the measured two-phase level swell height for the majority of the time in the test. Towards the end of the test, the NOTRUMP calculation crosses over the data. The NOTRUMP calculation is conservatively low and below the uncertainty of the data as determined from the vertical spread in the thermocouple measurements given in the figure. As time progresses, the NOTRUMP calculation comes within the estimated uncertainty of the level swell height. The NOTRUMP calculation does follow the trend of the data and for some time periods, is within the measured level swell uncertainty.

Figure 4.3-7 shows the comparison of the steam flow rate at the test section exit from the NOTRUMP prediction and estimated steam flow from bundle mass balances, energy balances, and the steam flowmeter in the exit pipe. The steam flowmeter reading is only valid in the beginning of the test when the bundle was covered and the steaming rates were high. As the bundle uncovered, the steaming rate decreased, and the meter was no longer within its range. The heat balance and mass balance calculation indicate a higher steam flow than is predicted by the NOTRUMP calculation. As time progresses, however, the steaming rate calculated by NOTRUMP agrees with the estimated steaming rates from the mass and energy balances.

Comparing Figures 4.3-6 and 4.3-7 indicates that the NOTRUMP calculations are self-consistent within themselves. The more conservative NOTRUMP prediction of the two-phase mixture level results in a lower steam generation rate since it is the covered portion of the heater rods that generate the steam flow. The reduced two-phase mixture level also results in a higher collapsed liquid level since less liquid is evaporated. All the sources of energy, rod power, and shroud power were accounted for in the analysis so that the steaming rate should be close to the data. Since all energy sources are accounted for, and the calculation used saturated liquid in the bundle, the difference between the data and calculation is due to the conservative level swell model used in NOTRUMP.

Figure 4.3-8 shows the cross plot of the mixture swell level with the collapsed liquid level for the test data and the NOTRUMP prediction for test A1L066. The figure indicates that for a given mass inventory in the bundle, NOTRUMP always predicts a lower two-phase mixture level as compared to

the test data. The prediction trends are consistent with the data, however, the NOTRUMP level swell height is conservative.

4.3.3.2 Comparisons to Test A1L069, 2.0 Bar (29A psia), 96.3 kw Bundle Power

Test A1L069 is similar to test A1L066, except that the system pressure is at 2.0 bars. Figure 4.3-9 shows the NOTRUMP prediction of the collapsed level (bundle mass) in the bundle and the determination of the zero time for the comparisons. The time is similar, but longer than the time determined in test A1L066.

Figure 4.3-10 shows the comparisons of the collapsed level (bundle mass) and the two-phase level swell. As with test A1L066, NOTRUMP overpredicts the collapsed liquid level and underpredicts the two-phase mixture level in the bundle. Figure 4.3-11 shows the NOTRUMP-predicted steam flow and the calculated steam flow from the data mass balance and energy balances and the test flowmeter values. Again, the trends for this test are consistent with test A1L066 in which NOTRUMP underpredicts the steam flow in the bundle. The NOTRUMP calculations are self-consistent in that the underprediction of the steam flow results in an overprediction of the mass storage in the bundle and an underprediction of the two-phase level swell.

Figure 4.3-12 shows the data values for the two-phase mixture level as a function of the collapsed liquid level in the bundle. The NOTRUMP-predicted values of the two-phase level swell height and the collapsed liquid level are also shown and indicate that for the same mass or collapsed liquid level in the bundle, NOTRUMP always predicts a lower two-phase mixture level in the bundle and therefore is conservative.

4.3.4 Noding Sensitivity Studies on the NOTRUMP ACHILLES Model

The noding chosen as the basis for the axial resolution in the ACHILLES NOTRUMP model as well as the other level swell simulations is 1-ft. axial nodes. This noding was chosen to investigate if the 1-ft. axial nodes would yield a sufficiently converged solution for the level swell calculation for the ACHILLES tests. Similar axial noding studies were performed on the General Electric small vessel blowdown tests, and the results were found to be only slightly sensitive to the number of axial nodes, and only at the beginning of the test when the depressurization rates were the highest and the vapor generation was the largest. These results are shown in Figure 4.2-64.

A similar axial noding sensitivity study was performed using the ACHILLES test A1L066, a 1.2-bar (17.64 psia), 96.5-kw bundle power test. The same procedures as used in Subsection 4.3.3 were used for this study. Figure 4.3-13 shows the results of the noding study for different numbers of axial nodes along with the test data and the estimated uncertainty bands. As the figure indicates, fewer than 12 nodes increase the predicted two-phase mixture level, which agrees better with the data early in the transient. However, as time progresses the four-node model overestimates the two-phase level and yields a nonconservative result. For finer axial-noded cases such as the 24- and 48-node calculations,

the predicted two-phase mixture level is more conservative than the 12-node case. The trends of all the calculations are similar, and they converge as the mixture level decreases and the steaming rates become smaller. While the 12-node case (1-ft. axial nodes) is not fully converged, use of this number of nodes (12) yields a better, yet conservative, estimate of the test data two-phase mixture level. Therefore, the 1-ft. axial noding will be retained for future NOTRUMP simulations of heated bundles or cores.

TABLE 4.3-1
ACHILLES LEVEL SWELL TEST MATRIX

Run Number	Pressure (bar absolute)	Cluster Power (kw)
A1L066	1.2 (17.64 psia)	80*
A1L067	1.2 (17.64 psia)	40
A1L068	1.2 (17.64 psia)	20
A1L069	2.0 (29.4 psia)	80*
A1L070	2.0 (29.4 psia)	40
A1L071	2.0 (29.4 psia)	20

*Simulated with NOTRUMP

TABLE 4.3-2
DATA FOR RUN A1L066 AT ZERO TIME

Cluster Power	80.3 kw
Shroud Zone 5 (top)	2.3 kw
Shroud Zone 4	3.9 kw
Shroud Zone 3	4.4 kw
Shroud Zone 2	3.8 kw
Shroud Zone 1 (bottom)	2.3 kw
Heat Losses	0.5 kw
Exit Steam Flow	41 g/s
Flow from Downcomer	16 g/s
Inlet Temperature	81°C
Collapsed Liquid Level	1.39 m
Downcomer Level	1.51 m

Elevation (m)	Pressure (bar)	Vs (m/s)	Voidage
3.888			
Grid	1.23	7.27	0.981
3.090			
Grid	1.23	6.96	0.960
3.128			
	1.24	6.55	0.988
2.867			
Grid	1.24	6.01	0.858
2.605			
	1.24	5.38	0.862
2.344			
Grid	1.25	4.68	0.763
2.082			
	1.25	3.94	0.745
1.821			
Grid	1.26	3.19	0.605
1.559			
	1.27	2.46	0.632
1.298			
Grid	1.28	1.78	0.500
1.036			
	1.29	1.17	0.460
0.775			
Grid	1.31	0.65	0.329
0.513			
	1.33	0.26	0.079
0.252			

TABLE 4.3-3
DATA FOR RUN A1L069 AT ZERO TIME

Cluster Power	80.1 kw
Shroud Zone 5 (top)	2.3 kw
Shroud Zone 4	3.9 kw
Shroud Zone 3	4.4 kw
Shroud Zone 2	3.8 kw
Shroud Zone 1 (bottom)	2.3 kw
Heat Losses	0.5 kw
Exit Steam Flow	42 g/s
Flow from Downcomer	15 g/s
Inlet Temperature	102 °C
Collapsed Liquid Level	1.51 m
Downcomer Level	1.57 m

Elevation (m)	Pressure (bar)	Vs (m/s)	Voidage
3.888			
Grid	2.06	4.57	0.999
3.090			
Grid	2.06	4.40	0.977
3.128			
	2.06	4.14	0.936
2.867			
Grid	2.07	3.80	0.816
2.605			
	2.07	3.40	0.803
2.344			
Grid	2.08	2.97	0.679
2.082			
	2.09	2.50	0.674
1.821			
Grid	2.10	2.03	0.496
1.559			
	2.11	1.58	0.574
1.298			
Grid	2.12	1.15	0.428
1.036			
	2.13	0.76	0.412
0.775			
Grid	2.15	0.44	0.307
0.513			
	2.17	0.19	0.169
0.252			

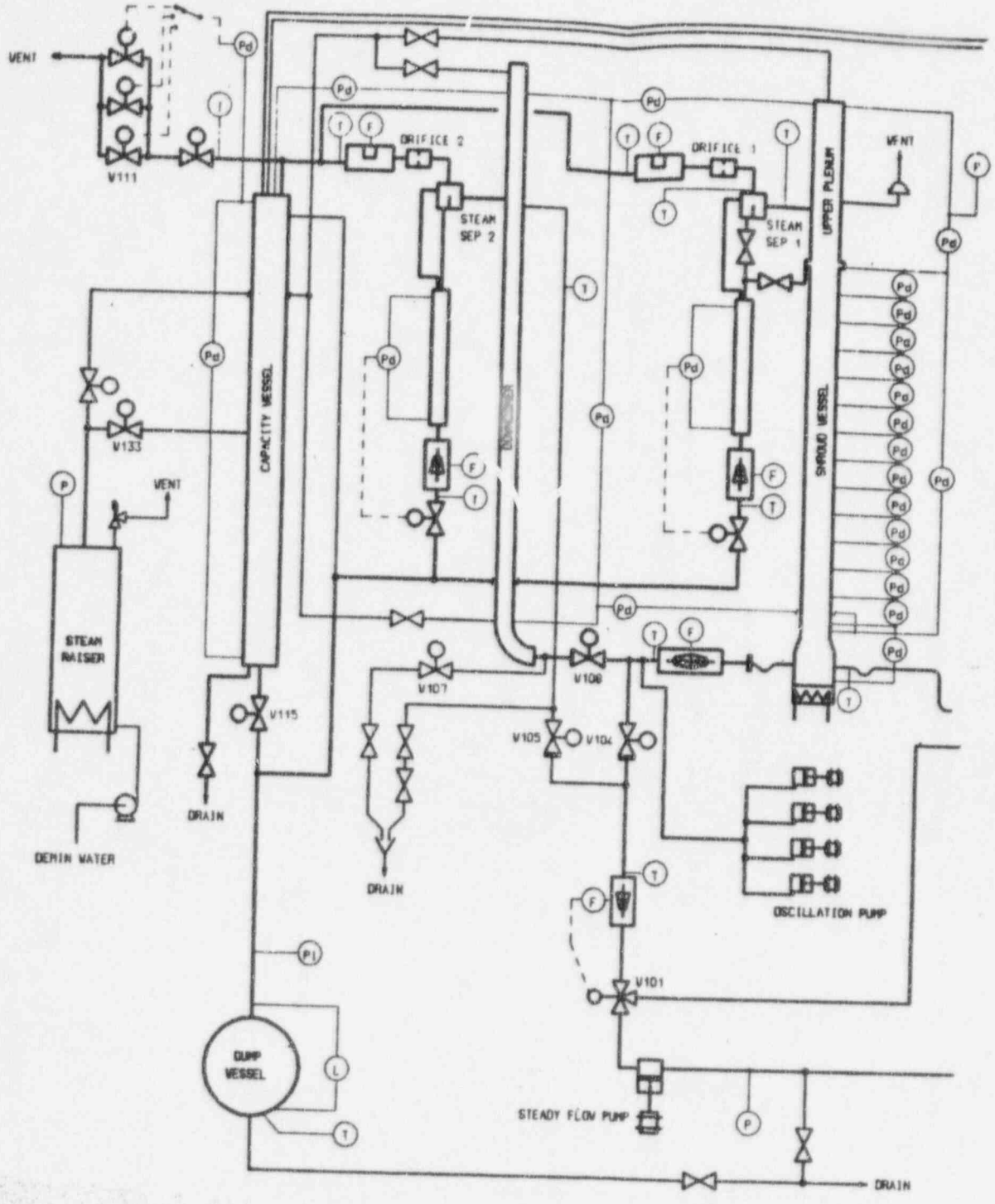

Figure 4.3-1 ACHILLES Flow Schematic

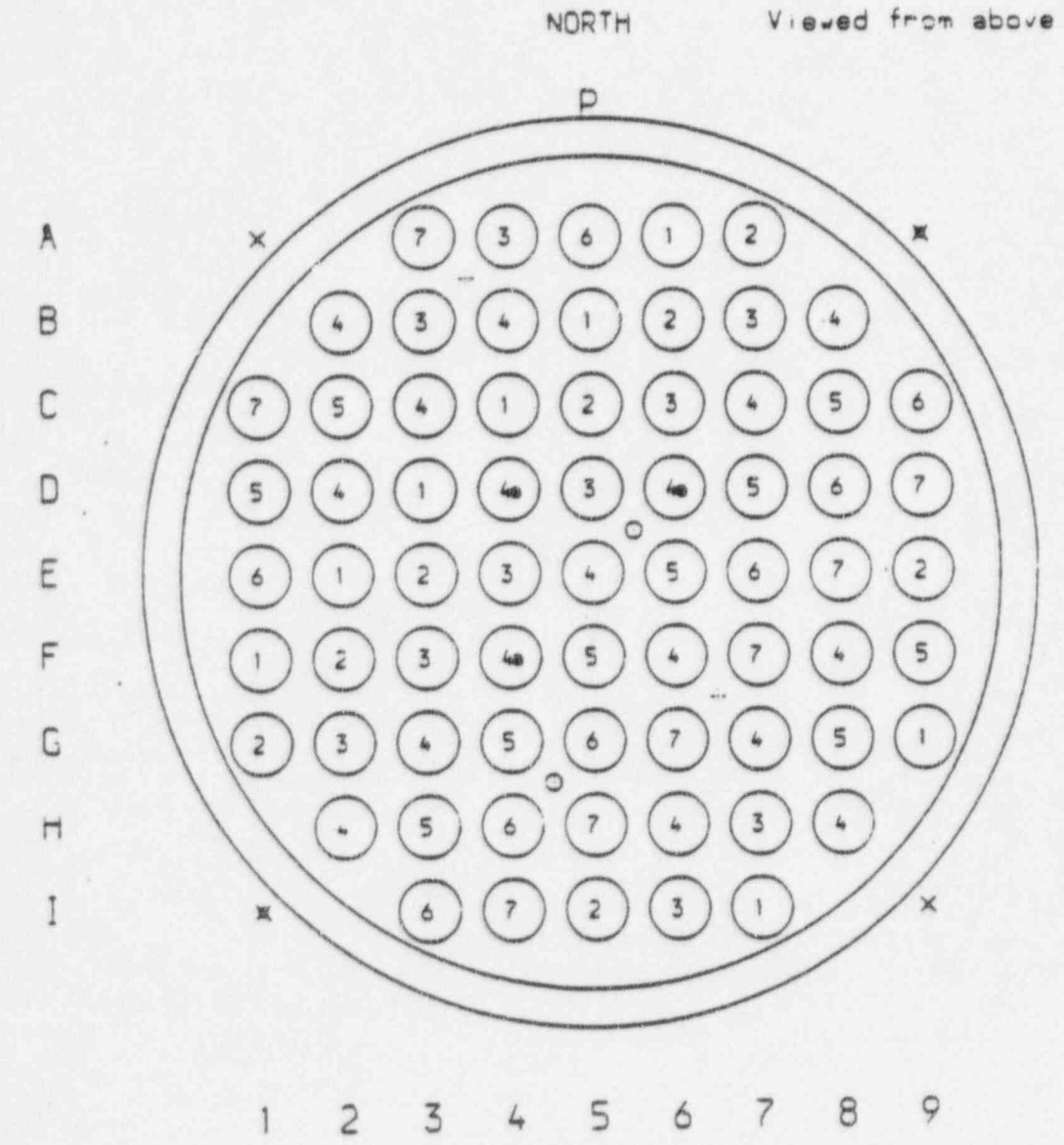

Figure 4.3-2 Cross-Section Through Test Section

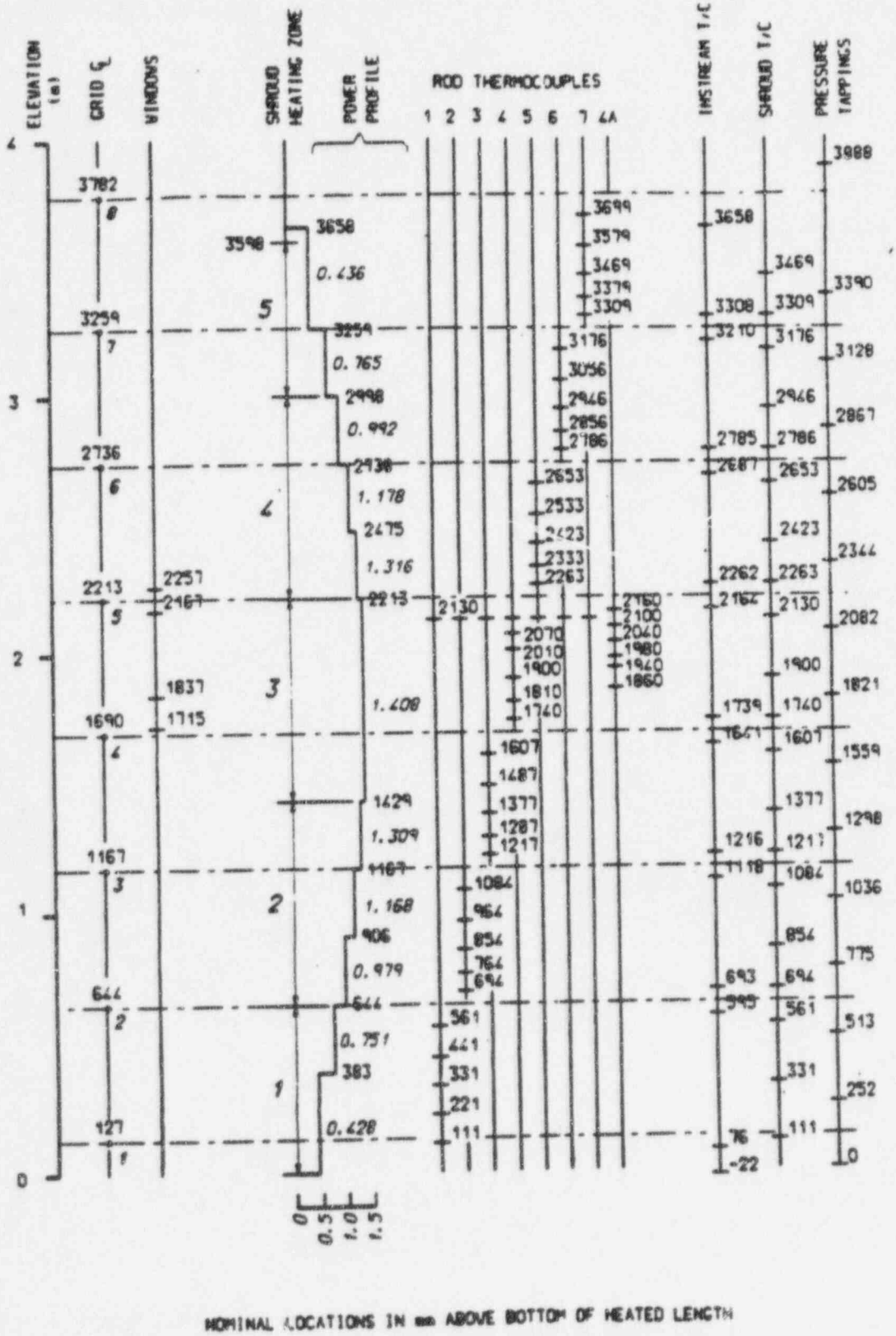

Figure 4.3-3 Axial Locations in Test Section

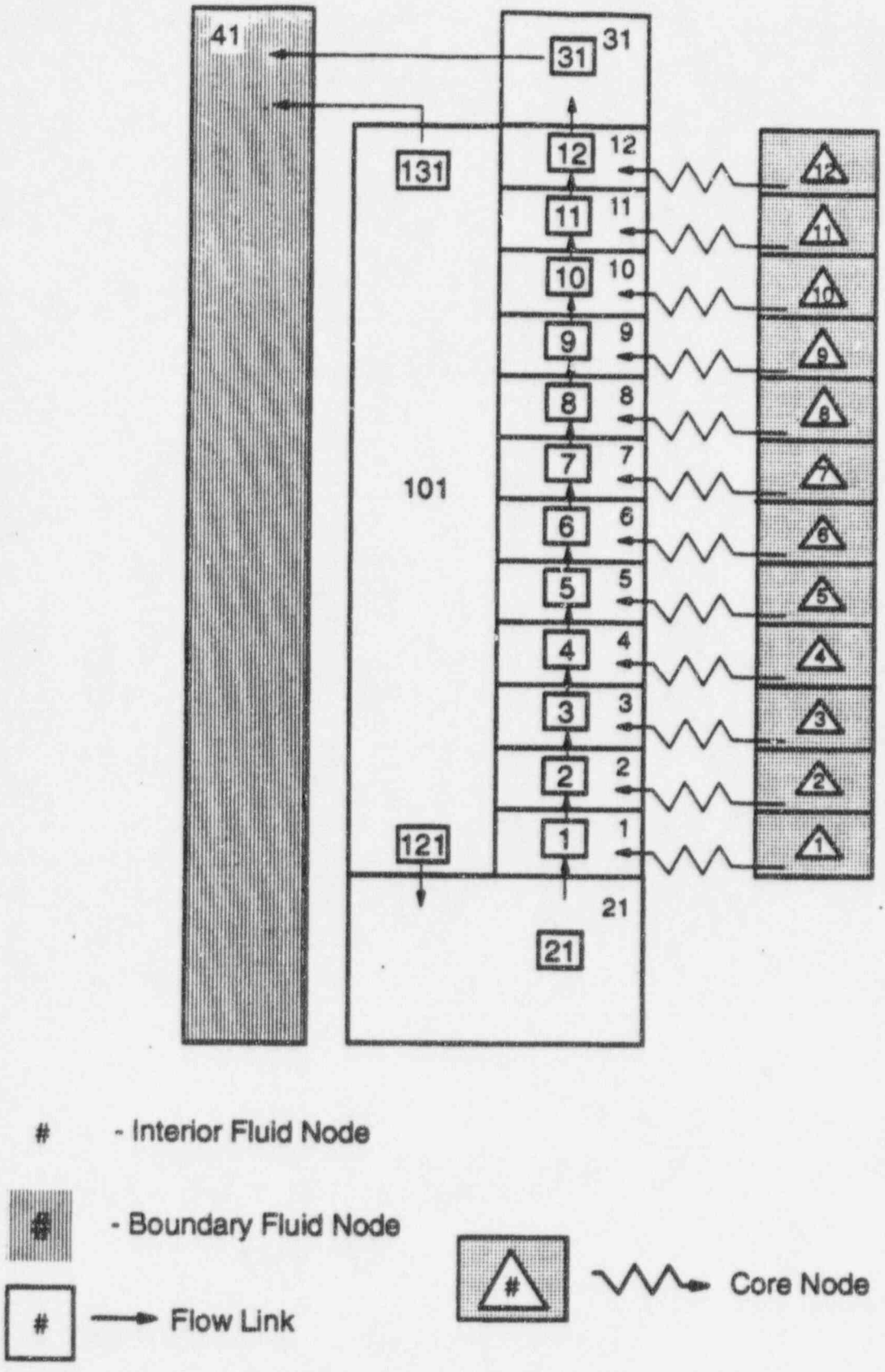

Figure 4.3-4 NOTRUMP Model of ACHILLES

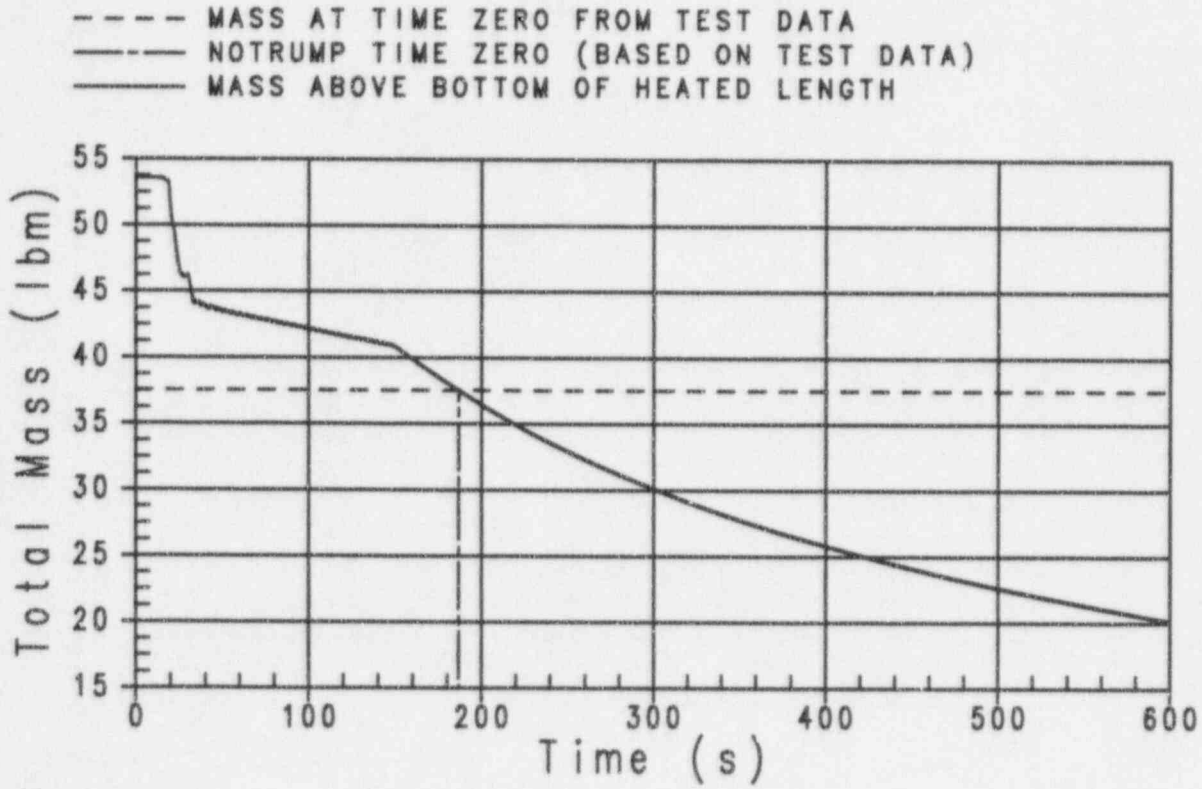

Figure 4.3-5 ACHILLES Mass and Determination of NOTRUMP Time Zero for Test A1L066

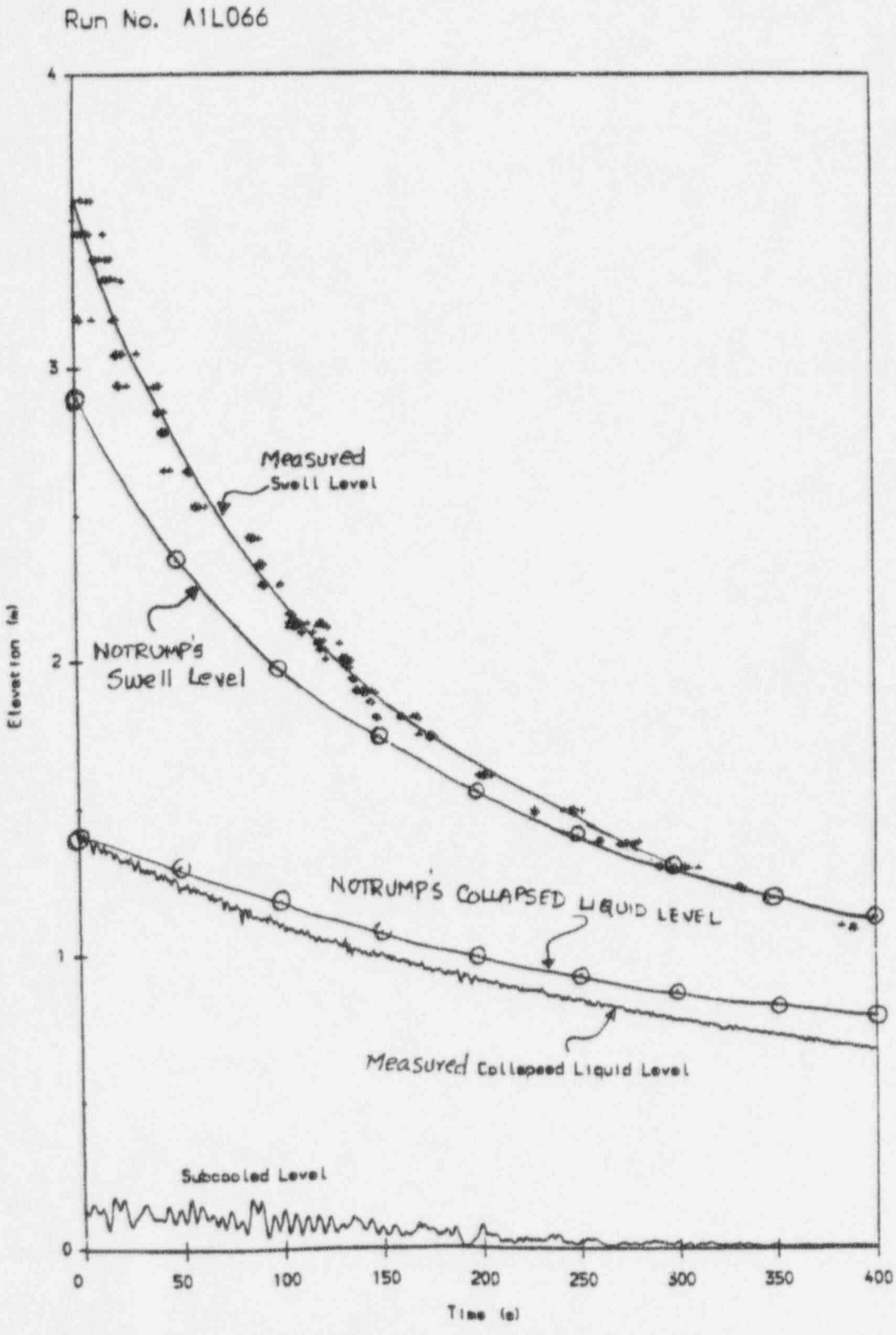

Figure 4.3-6 NOTRUMP Comparisons of Level Swell and Collapsed Level for Boildown Transient at 1.2 bar and 80 kw for Test A1L066

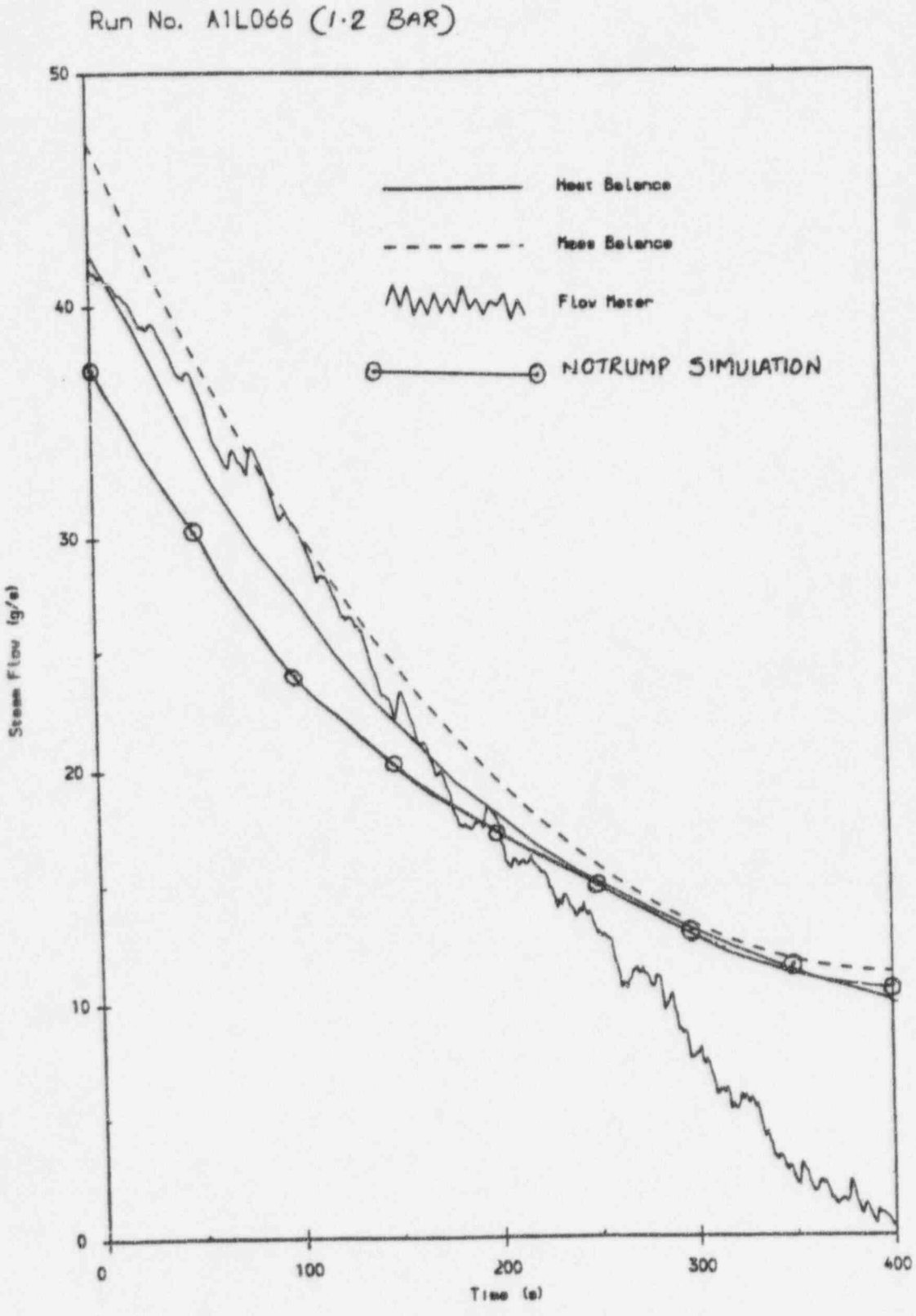

Figure 4.3-7 NOTRUMP Comparisons to Measured Steam Flow Rate at Test Section Exit for Test A1L066

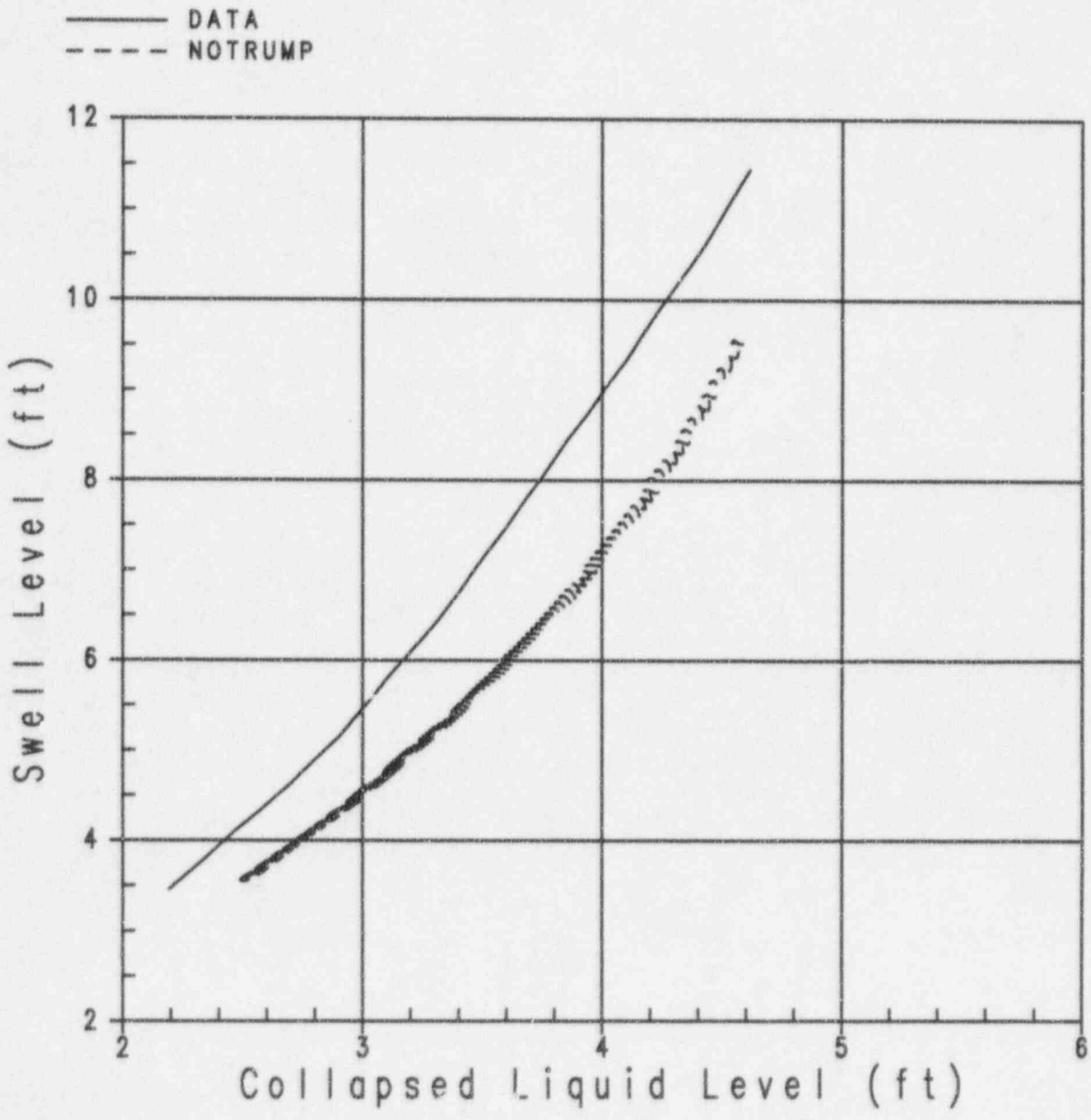

Figure 4.3-8 Comparisons of NOTRUMP and Test Data Level Swell and Collapsed Levels for Test A1L066

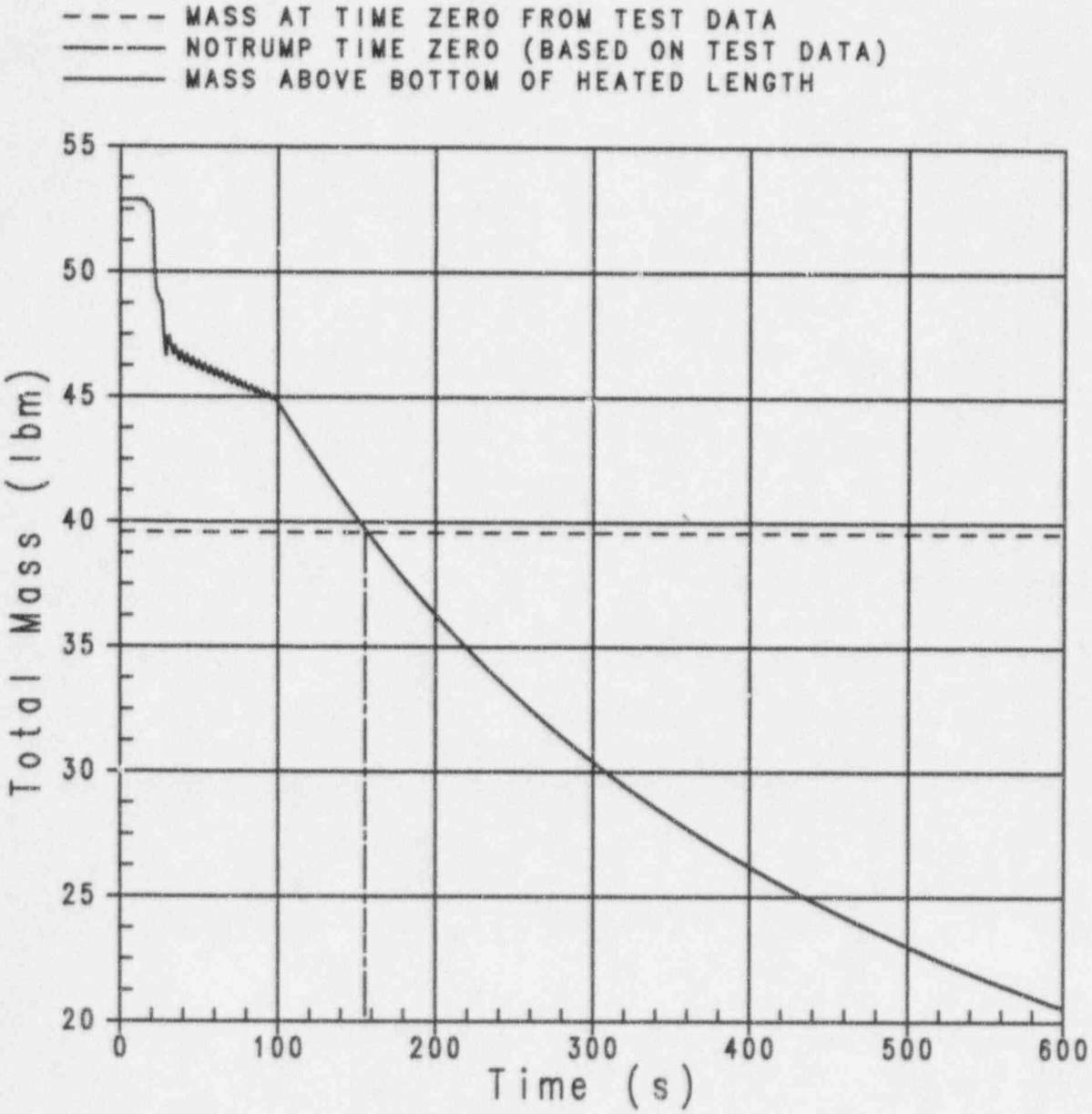

Figure 4.3-9 ACHILLES Mass and Determination of NOTRUMP Time Zero for Test A1L066

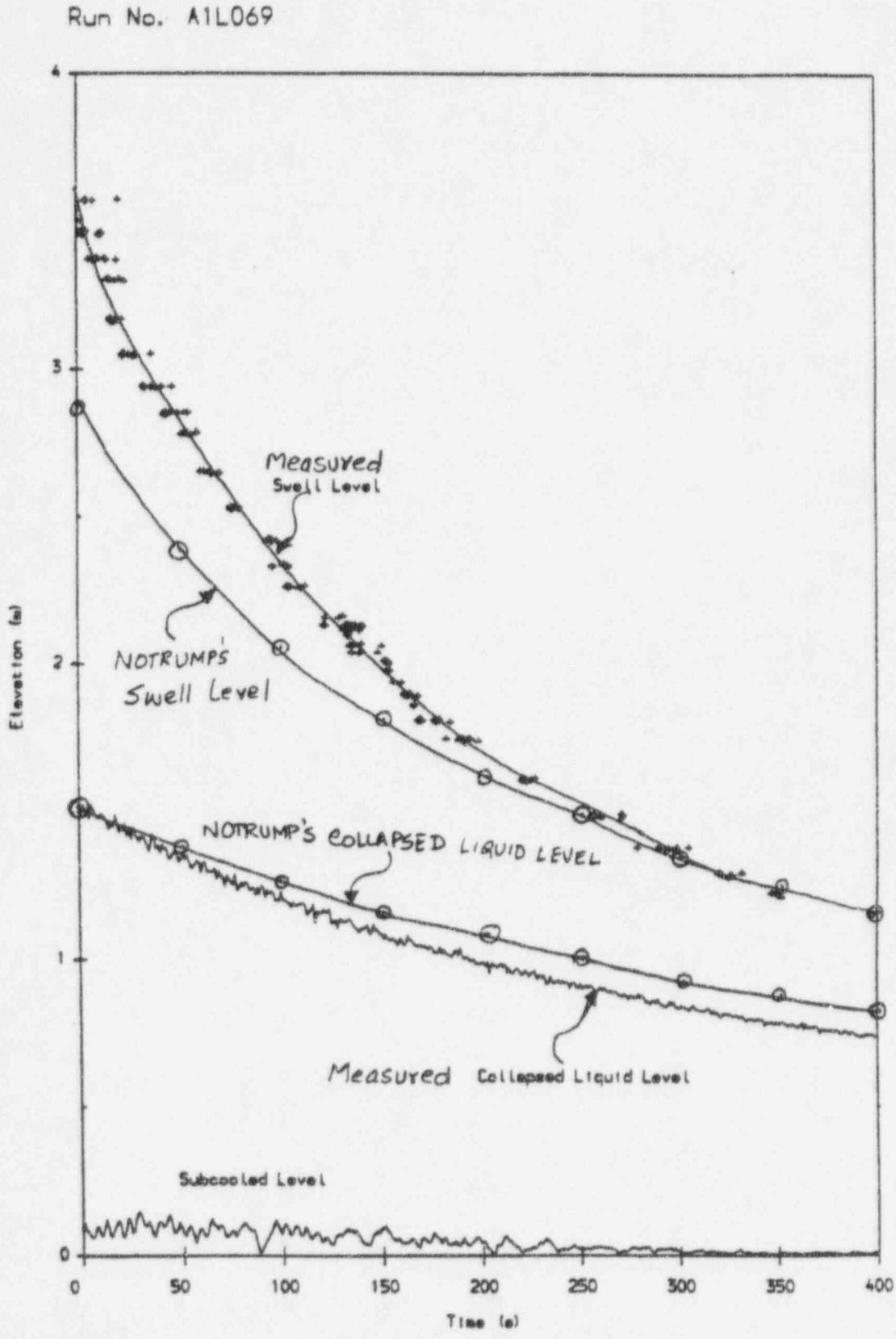

Figure 4.3-10 NOTRUMP Comparisons of Level Swell and Collapsed Level for Boildown Transient at 2.0 bar and 80 kw for Test A1L069

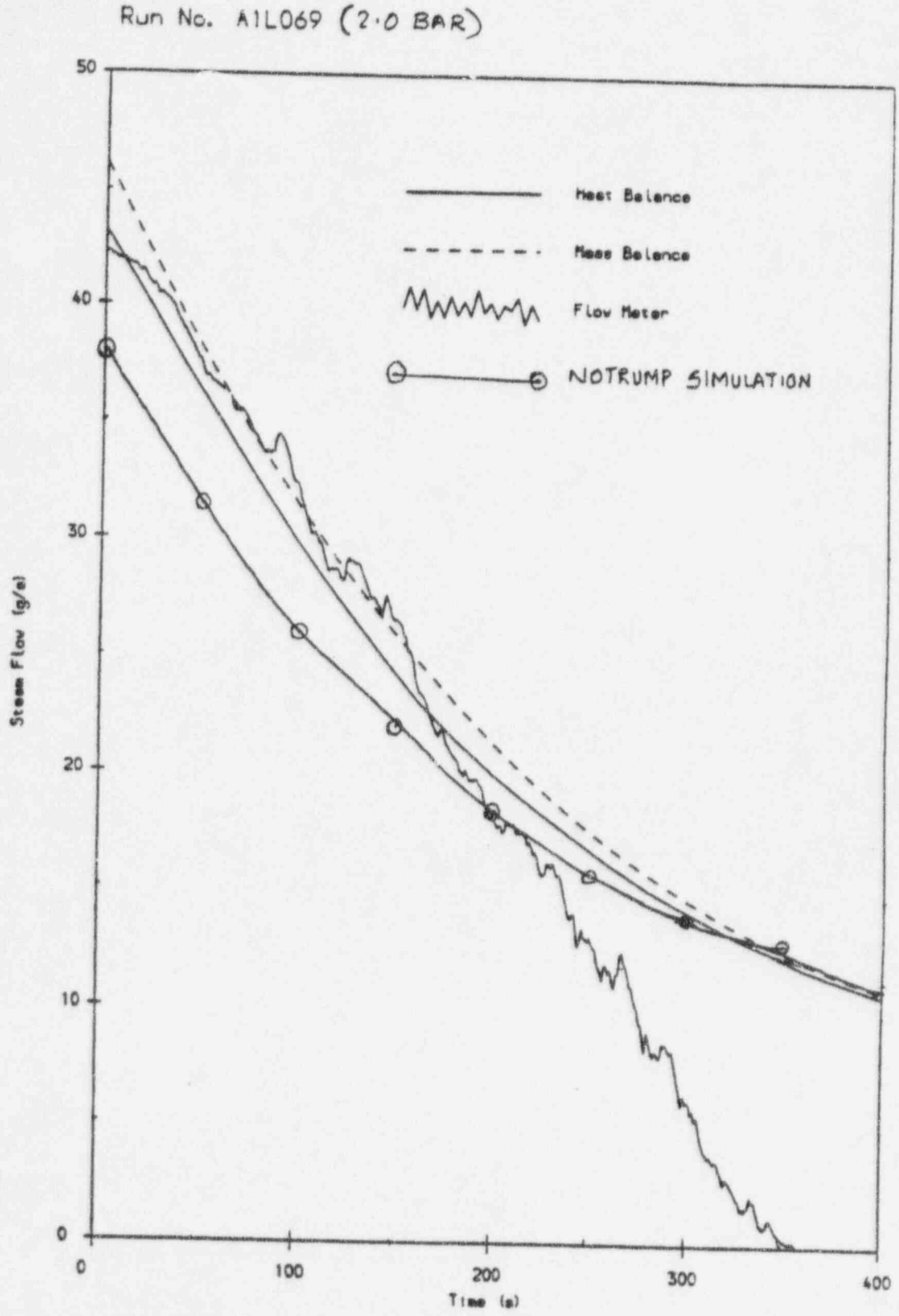

Figure 4.3-11 NOTRUMP Comparison to Measured Steam Flow Rate at Test Section Exit for Test A1L069

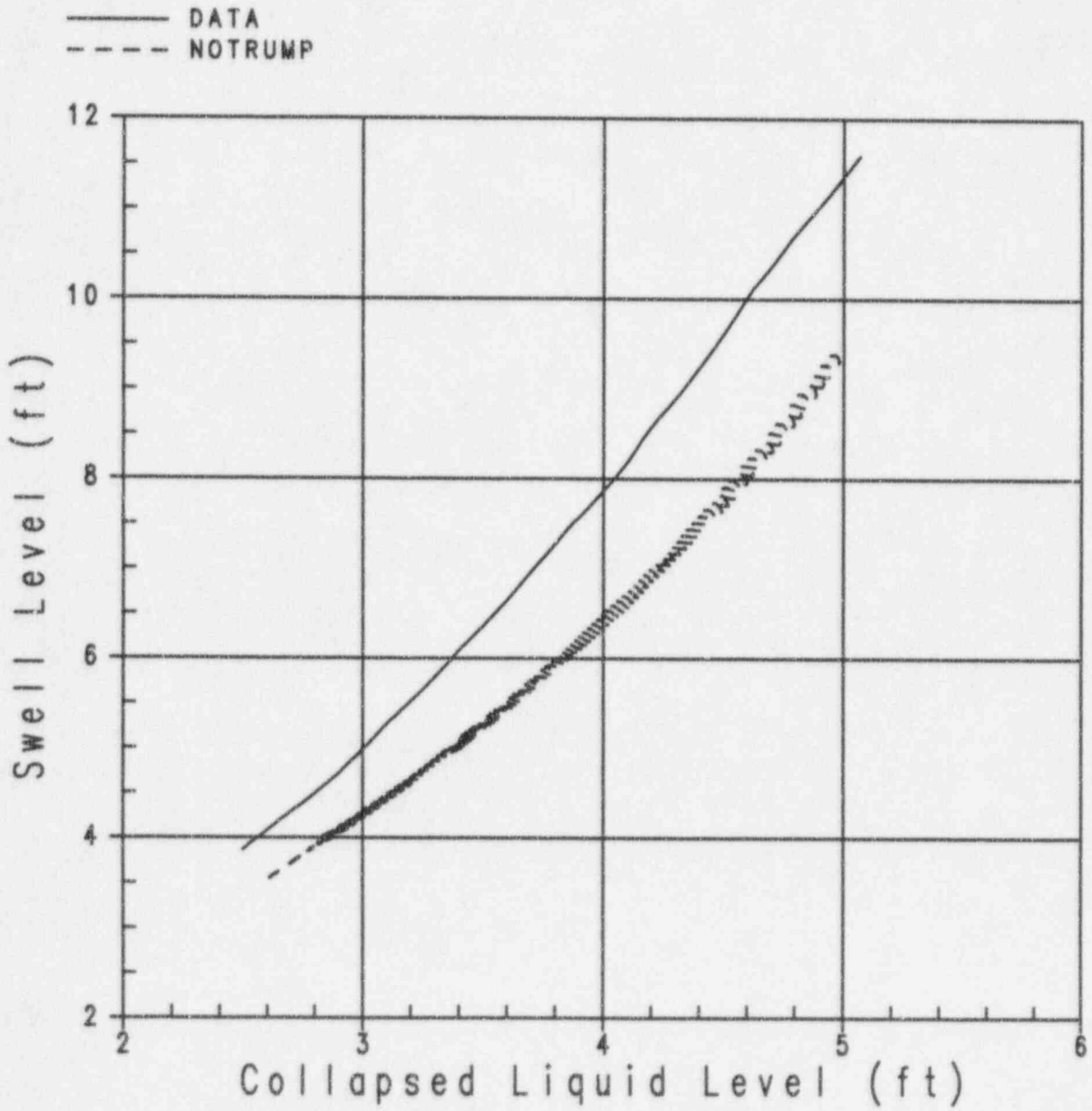

Figure 4.3-12 Comparisons of NOTRUMP and Test Data Level Swell and Collapsed Levels for Test A1L069

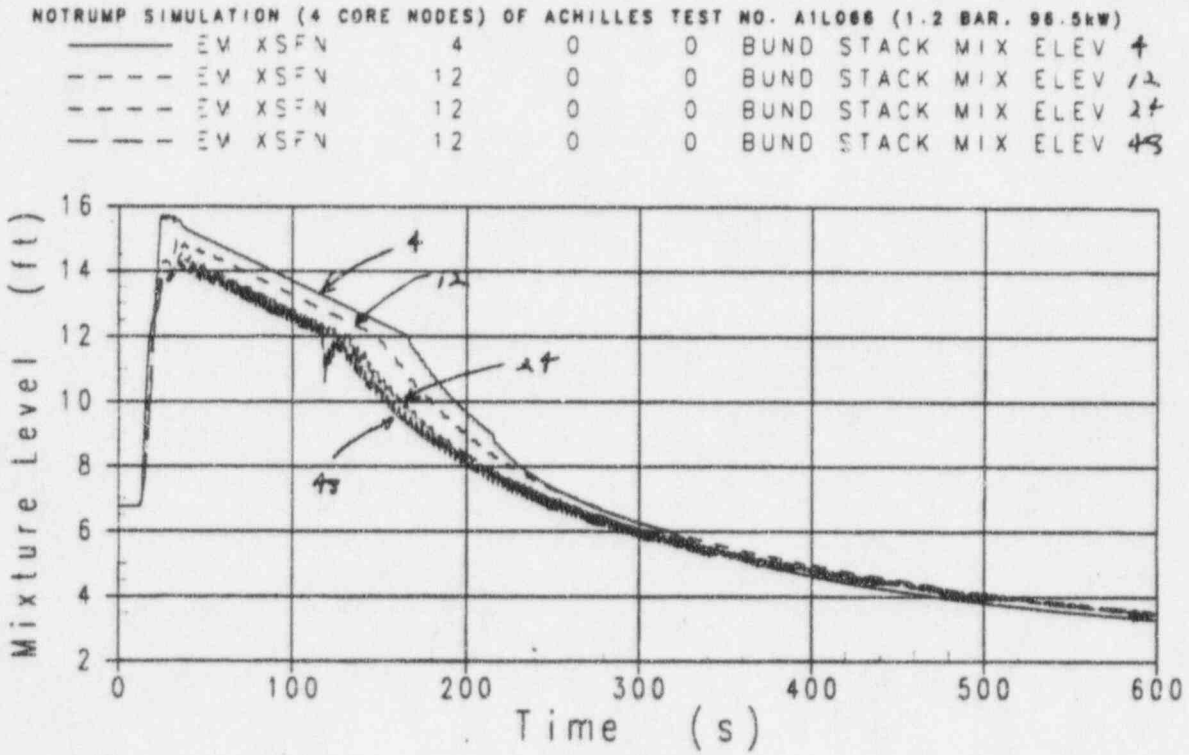

Figure 4.3-13 NOTRUMP Noding Sensitivity Studies for ACHILLES Test A1L066

4.4 G2 Test Simulation

4.4.1 Introduction

Another set of separate effects tests that are analyzed with NOTRUMP are the G2 level swell tests. More specifically, several core uncovery tests that were performed in the Westinghouse G2 test facility (Reference 4-12), are analyzed with NOTRUMP to assess the predictions of two-phase mixture level, void fraction, and heater-rod heatup above the mixture level.

The G2 tests are quasi-steady-state separate effects core uncovery tests performed at constant pressure and constant bundle power. The transient parameter in the tests was the two-phase mixture level, which decreases with time as the mass inventory is boiled-off in the heater bundle.

The G2 tests, along with other tests, are analyzed with NOTRUMP, provide the basis for the NOTRUMP validation for AP600 small-break loss-of-coolant accident (LOCA) analysis.

4.4.2 G2 Test Facility Description

The G2 test facility is designed to provide data for downflow film boiling, reflood heat transfer, and core uncovery over a range of power, flow, temperature, and pressure conditions that simulate pressurized water reactor (PWR) large-break and small-break LOCAs. Reference 4-12 provides details and data from the G2 core uncovery tests.

The G2 facility loop schematic is given in Figure 4.4-1 and shows: the test vessel, which contains the heater rod bundle; separator 1, which is used for facility heatup and pressurization; and separator 2, which is used to collect any liquid carryover out of the test vessel. The test facility design pressure is 2252 psia at a design temperature of 650°F.

The primary loop is a closed piping system that simulates thermal and hydraulic conditions representative of the environment in the core of a PWR after a hypothetical LOCA, based on safety analysis design calculations. For the core uncovery tests, the test loop is initially heated and pressurized with saturated steam generated in steam-water separator 1 to obtain the desired initial test conditions for a given test run. The test vessel, which houses the test section (see Figure 4.4-2), consists primarily of the vessel shell, a spool piece, and two end closures.

Specific details concerning the test vessel and separators can be found in Reference 4-12.

The flow from the test vessel hot legs is directed into separator 2, in which the flow that enters the vessel impinges on a deflector plate. This plate imparts a circular motion to the flow, which helps separate the steam and water phases. The water is allowed to fall to the bottom, while the steam is discharged from the vessel through a 6-in., Schedule 160 Grayloc nozzle welded to the top of the elliptical head. In this fashion, the steam flow measurement at FM-2 is free of any entrained liquid

(Reference 4-12) flow and is a valid single-phase flow measurement. The steam is then directed to the exhaust valves, V-2 and V-16, through a run of 6-in., Schedule 160 pipe.

All interconnecting primary loop piping is 6-in., Schedule 160 carbon steel pipe, except for the pipe connecting the test vessel baffle annulus region to the hot leg discharge from the test vessel, which is 4-in., Schedule 160 carbon steel. Flange tap orifice installations are used in the primary system for flow measurement for FM-2 (see Figure 4.4-1) to measure the exit steam flow from separator 2. Blank orifice plates are used to direct flow paths for a desired test or to isolate piping sections. The orifice plate at FM-2A is used for flow measurement.

For core uncovery testing, it is only necessary to scale the portion of the facility that is within the flow boundary in the test section, that is, the rod bundle. In addition, the ground plate and the upper plenum (see Figure 4.4-2) are designed to give hydraulic resistance and/or flow velocities that are representative of the reactor.

The instrumentation used on the G2 loop test facility consists of thermocouples, absolute pressure transducers, bidirectional differential pressure transducers, and differential pressure transducers in vessels and piping. Differential pressure transducers measure pressure drops throughout the system and across orifices for flow measurement, level transmitters determine vessel water levels, and thermocouples measure fluid or wall surface temperatures. The facility has sufficient instrumentation for making a mass balance check on the system.

The test section, consisting of a bundle of electrical resistance heater rods surrounded by a flow guide baffle, is contained within the test vessel, which has a 19.87-in. inside diameter and a 249.5-in. inside length. Saturated coolant is introduced at one of the 6-in. nozzles in the lower plenum of the vessel until the desired initial water level for start of test is achieved. The steam or steam-water mixture generated in the bundle flows past the heater rods, up through the ground plate into the upper plenum, and exits radially through 6-in. nozzle. The cross section of the test section is illustrated in Figure 4.4-3.

The rod bundle contains 336 heater rods. The overall length of the heater rods is 226 in. (5.74 m), with a heater length of 164 in. A schematic diagram of a typical heater rod is shown in Figure 4.4-4, and the normalized axial power distribution produced by the rods is shown in Figure 4.4-5. Nine grids are located along the length of the bundle (seven mixing vane grids and two end grids), as in an actual 17 x 17-XL PWR fuel assembly (see Figure 4.4-2). These are made from standard Westinghouse PWR 17 x 17 grids and spotwelded to eight support thimbles.

The diameters of the test bundle heater rods, thimbles, and instrumentation tube, and the square pitch arrangement of the rods are the same or nearly the same as those in a 17 x 17 or 17 x 17-XL PWR assembly, as shown in Table 4.4-1. Although in the 17 x 17 PWR assembly, all thimbles and the instrumentation tube have the same diameter, two different thimble diameters are used in the test bundle. The reactor-to-test-bundle flow area ratio is 153. The mixing vane grid and end grid designs

used are prototypical. The axial locations of the grids are the same as in the preliminary 17 x 17-XL PWR design at the time of the G2 loop facility design, except that the sixth grid is at 106.6 in. rather than at 107.6 in. from the beginning of the heated length. (The 107.6-in. location can interfere with pressure taps in the vessel.)

The G2 loop test section contains 82 instrumented heater rods, each with 6 thermocouples. Half of the instrumented rods (41 rods) have thermocouple junctions at the 12.3-in., 36.9-in., 54.7-in., 82.0-in., 110.7-in., and 135.4-in. elevations, and the other half have junctions at the 28.7-in., 45.1-in., 69.7-in., 94.3-in., 118.9-in., and 147.6-in. elevations from the bottom of the heated length. The thermocouples are contained within the boron nitride h[illegible]r element insulation, with the junction located 0.020 in. from the inside wall of the heater rod tubing (clad). The thermocouples are ungrounded chromel-alumel (type K), premium grade, 0.006-in. diameter wire with a 0.040-in. diameter 304 stainless steel sheath. The junction is insulated from the sheath by high-purity magnesium oxide insulation with a resistance of 100 megohms at ±50 volts dc for each specified length. The entire length of each thermocouple is annealed to maintain a premium grade accuracy of ±6°F during heater rod manufacturing. All test section heater rod thermocouples use a 150°F reference junction for computer readout.

The flow holes in the ground plate are sized to give approximately the same hydraulic resistance to upward flow as would be provided in the PWR by the upper fuel nozzle and the upper core plate during reflood. The reactor core inlet loss coefficient of 2.82 for the 17 x 17 fuel assembly is matched in the test bundle ground plate by the use of 324, 0.315-in. diameter holes with a 0.02-in. (+0.01, -0.00) radius at the inlet (bottom) side and 72, 0.225-in. diameter holes without radius at the bottom edge.

The cross-sectional flow area in the upper plenum is scaled to model the PWR axial velocity above the ground plate. To attain this, the PWR ratio (1.65) of upper plenum cross-sectional flow area just above the ground plate to reactor core cross-sectional flow area is maintained in the G2 loop test vessel.

Four plates bolted along their edges form the baffle, which provides a flow boundary around the rod bundle. The enclosed cross-sectional flow area for the rod bundle is 49.5 $in.^2$ The vessel side of the baffle plates has a honeycomb design obtained by electromechanical machining to provide a low-mass baffle. The cross-sectional area of the cavity between the baffle and the test vessel is approximately 190 $in.^2$ A summary of the flow areas associated with the test bundle, the spacer grids, and the flow baffle/test vessel annulus is given in Table 4.4-2.

After initial blowdown testing in the facility and prior to running the core uncovery tests, baffle seal leakage checks were made and forced flooding tests were run to check out the facility. These tests indicated that the rate at which coolant could leak from the rod bundle into the cavity behind the baffle was substantially greater than expected. Therefore, a number of tests were performed to determine the magnitude of the leakage and its variation along the axial length of the baffle flange

leakage tests (including tests run after the reflood test series was completed) indicate consistently low leakage below the 70-in. level. Since a leakage path in the upper half of the baffle would result in an accumulation of entrainment in the baffle/vessel cavity behind the more leaktight lower portion of the baffle, the core uncovery tests were run with the baffle/vessel cavity prefilled with water to the same height as the water in the test section.

4.4.3 Method of Testing

The test facility is initially heated and pressurized using the electrical heaters in separator 1. The desired test pressure is maintained for at least 1 hour before a test run to ensure complete heating of the facility. Any noncondensible gases are vented from the facility at the high points, and the condensate found during heating is drained from the test vessel lower plenum so that it remains empty. After the test vessel and lower plenum approach the saturation temperature of the desired system pressure, saturated water is pumped into the test section and baffle regions through the lower plenum. When the test vessel and baffle region are filled to the desired level, the inlet flow is terminated. Differential pressure transducer 550 is used to set the initial heater rod bundle level.

Initial water levels are calculated to cover the axial length of the bundle when power is first applied to the bundle. The calculations are made using the Yeh (Reference 4-10) void fraction correlation to compute the void fraction distribution in the bundle at given pressures and powers, and hence the net liquid height (that is, the collapsed liquid level), when the froth level is at the top of the bundle heated length. A small height of water, amounting to several inches, is added to each of the calculated heights to ensure that the bundle is initially covered by the froth level.

With the facility heated, pressurized, and filled, the test is initiated by starting the data acquisition system (DAS). The rod bundle power is then applied to the bundle 10 to 12 seconds after the DAS starts. The rod bundle power is stepped from zero to the desired level and then held constant for the duration of the test. The vessel pressure is also maintained consistent during the test. The test is terminated by either: the test run duration is reached and maximum allowable heater rod temperature is exceeded, or the test operator scrams the test.

4.4.4 Test Matrix

The matrix of tests that were performed in the G2 core uncovery test program are shown in Table 4.4-3.

The test independent parameters are the bundle power, system pressure, and initial collapsed water level. A total of 22 tests were performed.

4.4.5 Selection and Tests for NOTRUMP Validations

A total of 22 core uncovery tests were preformed in the G2 test facility. Of these tests, a total of 10 tests were selected to be analyzed using the NOTRUMP code. The selected tests are numbers 715, 716, 719, 720, 724, 725, 728, 729, 732, and 733. These tests were selected to cover the full pressure range expected for the AP600 as well as to cover the expected power levels for the AP600 small-break transients. The power level of 0.6 MW corresponds to the maximum power that the Appendix K plant calculation reaches at 100 psia.

Since the AP600 calculated minimum vessel inventory usually occurs just before IRWST injection (Reference 4-2), the modeling of all the 50- and 15-psia tests is believed to be most important. The unique application of the NOTRUMP code for the AP600 occurs at the lower pressure typical of IRWST injection.

The selection of the G2 tests for NOTRUMP validation covers the primary variables of interest and provides an ample database to validate the level swell models and phenomena that are ranked as a high item in the AP600 small-break LOCA PIRT.

4.4.6 NOTRUMP Modeling of G2 Test Facility

To produce an accurate simulation of the G2 mixture level swell, a model must accurately predict the steam flow through the bundle. Although all of the heat generated in the rod bundle is expected to be carried out of the vessel through steam flow, analysis of the G2 test data indicates that a significant fraction of the heat generated in the heater rods does not exit the test vessel as steam.

Figure 4.4-6 presents a comparison of the measured test vessel steam flow to the expected steam flow for the first few hundred seconds of G2 test number 732 based on the bundle power. The expected steam flow is calculated from the heater rod bundle power and the latent heat of vaporization at the test vessel pressure. The first few hundred seconds of test number 732 are chosen for this comparison for three reasons:

- The measured temperatures within the test vessel are stable during this time period of this test, so the "missing" energy is not going into sensible heat.

- There is no evidence of superheating anywhere within the test vessel during this time period of this test, so the exhaust steam cannot be significantly superheated.

- The decrease in vessel liquid mass agrees well with the measured steam flow throughout this test, so the steam flow measurement is reliable and there is no significant liquid entrainment out of the vessel.

Therefore, Figure 4.4-6 shows that about 20 percent of the heat generated within the bundle during the first few hundred seconds of test 732 leaves the vessel through a mechanism other than steam flow through the exhaust line. Similar analyses of the remainder of test 732 and other G2 tests also show the exhaust steam does not account for all the heat generated in the rod bundle.

Investigation of this issue led to the identification of another significant heat loss mechanism within the G2 test vessel. This mechanism is composed of two parts: subcooling of the liquid within the lower plenum and leakage of coolant through the flow baffle surrounding the heater rod bundle. Throughout the G2 tests, heat is continuously lost from the liquid in the lower plenum while the leakage of coolant through the flow baffle surrounding the rod bundle sets up a recirculation flow of liquid through the test vessel. Although, by itself, the degree of rod bundle inlet subcooling resulting from heat transfer from the lower plenum is insufficient to account for the lost steam flow by the observed amount, the effect of inlet subcooling on the rod bundle steam generation rate is amplified by the recirculation flow. The following paragraphs describe both the recirculation flow and lower plenum heat transfer in more detail.

Throughout the G2 tests, the heater rod bundle and baffle/vessel annulus regions are connected at both their top and bottom. At their bottom, they interact through the open flow path from the bottom of the baffle/vessel annulus region to the bottom of the bundle lower plenum. Toward their top, they interact through the axially distributed leakage paths through the baffle.

After power is applied to the rod bundle, the fluid in the bundle froths up to some quasi-equilibrium position while fluid in the baffle/vessel annulus region remains collapsed. Above the bundle froth level, pressures in the bundle and baffle/vessel annulus region remain roughly in equilibrium due to leakage of steam through the baffle. This is shown in Figure 4.4-7, which presents the measured differential pressure across the baffle at the top of the heated length of the rod bundle for test number 732. In the axial region below the bundle froth level and above the baffle/vessel annulus liquid level, the higher density of the two-phase mixture in the bundle leads to higher pressures on the bundle side of the baffle. This pressure difference across the baffle reaches its maximum just above the liquid level in the baffle/vessel annulus region. At elevations successively further below this level, the higher density of single-phase water in the baffle/vessel annulus region leads to a reduction of the pressure difference across the baffle. The pressure difference across the baffle once again equals zero somewhere near the bottom of the heated length of the bundle, and it probably even changes direction toward the bottom of the heated length, tending to drive flow from the baffle/vessel annulus region into the heater rod bundle. However, the axial distribution of the pressure difference across the baffle drives flow predominantly from the bundle into the baffle/vessel annulus region. Due to this pressure difference across the baffle, liquid flows from the bundle into the baffle/vessel annulus region, increasing the liquid level in the baffle/vessel annulus.

The resulting flow of liquid from the bottom of the baffle/vessel annulus region into the bundle and then back into the baffle/vessel annulus region through the leaky baffle is analogous to the flow of liquid through a recirculating steam generator. However, unlike the liquid flow through a recirculating

steam generator, the liquid flow through the G2 test vessel decreases as the bundle mixture level decreases since the liquid inventory is not replenished as steam flows out of the vessel.

Recirculation of liquid through the G2 heater rod bundle impacts the two-phase mixture level swell in two significant ways:

- The resulting increase of the liquid level in the baffle/vessel annulus "steals" liquid inventory from the bundle region. This affect is further amplified by two factors, the non-zero void fraction in the bundle and the 4-to-1 ratio of areas between the baffle/vessel annulus and bundle. For every unit increase in baffle/vessel annulus mixture level, the bundle loses four units of collapsed liquid level, which represents significantly more than four units of froth level due to the bundle's non-zero void fraction.

- The recirculation of liquid moves the single-phase/two-phase interface upward within the rod bundle since the coolant flowing into the heated length of the rod bundle is subcooled. This further reduces the two-phase mixture level within the rod bundle.

The subcooling of the liquid within the lower plenum ultimately comes from two sources. The first source of subcooling is the near-ambient temperatures of the outer regions of the test vessel lower flanges and lower spool piece. Flow from the baffle/vessel annulus region into the lower plenum passes directly through radial holes bored through the test vessel lower flange and lower spool piece. This flow path cools the fluid since the outer surfaces of the test vessel lower flange and lower spool piece are near ambient temperatures, as is shown in Figure 4.4-8, which presents the outer surface temperature of the test vessel lower flange for test 732. Therefore, liquid flowing from the baffle/vessel annulus region loses a significant amount of heat as it passes through the bores.

The second source of subcooling is the coolant water circulated through the cavity between the test vessel lower closure and bottom seal flange to cool the heater rod power leads and O-ring seals. Although this coolant water never leaks into the test vessel itself, it maintains the bottom of the lower plenum at a temperature significantly below saturation, as shown in Figure 4.4-9 for test 732. Since the conduit from the baffle/vessel annulus region connects to the bottom of the lower plenum, liquid flowing from the baffle/vessel annulus region is delivered directly into this region of lower temperatures.

Evidence of the impact of recirculation flow and inlet subcooling on G2 test results can be found in Figures 4.4-10 and 4.4-11. Figure 4.4-10 presents the measured fluid temperature in the lower plenum at an elevation of -5.88 in. where 0 in. is the bottom of the heated length on the electrical heater rods. Figure 4.4-11 shows the measured steam flow out of the test vessel. At about 400 seconds, Figure 4.4-10 indicates that the temperature at the inlet to the rod bundle heated length is about 208°F. Figure 4.4-11 indicates that the steam flow out of the test vessel is about 0.2 lbm/sec., and the linear heat generation rate within the bottom 24.6 in. of heater rod heated length is 0.6314 Btu/(sec.-in.). If there was no recirculation of liquid through the baffle, the liquid flow into the heated region of rods

would be roughly equal to the flow of steam out of the bundle. If this happened in the test, the fluid in the bundle would reach saturation within 5 in. of the bottom of the heated length. However, test data indicate that the fluid in the heated section of the rod bundle does not reach significant void fractions below 27.30 in. from the bottom of the heated length. Estimated values of recirculation flow indicate that the recirculation flow can cause the level where saturation is reached to move well above 5 in.

Figure 4.4-12 presents the noding diagram for the NOTRUMP model of the G2 test facility. The individual components are described below.

The fluid nodes in the NOTRUMP model of the G2 test facility can be categorized into the following five groups:

- Interior fluid nodes representing the coolant within the heater rod bundle
- An interior fluid node representing the coolant within the upper plenum
- An interior fluid node representing the coolant within the lower plenum
- An interior fluid node representing the coolant within the baffle/vessel annulus
- A boundary fluid node representing a pressure boundary condition

Interior fluid nodes are mass and energy control volumes for which the NOTRUMP code calculates time-varying fluid properties based on conservation of mass and energy. Boundary fluid nodes are infinite sources or sinks of fluid maintained at a user-specified state.

Fluid nodes 1 through 14 represent the water and steam adjacent to the heated length of the heater rod bundle. Each of these fluid nodes has a height of 1.0 ft. except fluid node 14, which has a height of 0.667 ft.

Fluid node 31 represents the water and steam within the G2 test vessel between the top of the heated length of the rod bundle and the highest differential pressure tap within the test vessel. Since the height of this fluid node is fixed by the elevations of the top of the rod bundle heated length and the highest pressure tap, the volume of the fluid node is set to conserve the flow area through the upper plenum of the test vessel. This modeling choice does not account for all the volume within the G2 test vessel above the top of the rod bundle heated length; however, this does not affect the code prediction of mixture level swell since the pressure in the upper plenum is controlled by the pressure in the boundary fluid node to which it is connected.

Following the modeling methodology applied to the AP600 plant and the OSU and SPES-2 integral test facilities, the fluid nodes in the G2 rod bundle and upper plenum are all stratified fluid nodes grouped into a single stack. This modeling allows only one mixture elevation to exist within this entire group of nodes.

Fluid node 21 represents the water and steam within the G2 test vessel below the bottom of the heated length of the rod bundle. This node's only significant impact on the mixture level swell within the heater rod bundle is that it sets the temperature of the fluid flowing into the heated length.

Fluid node 101 represents the water and steam within the baffle/vessel annulus. This volume contains the majority of the coolant inventory within the G2 test vessel, which is stratified into mixture and vapor regions.

Finally, fluid node 41 represents the pressure boundary condition through which the pressure in the upper plenum is controlled. For each test, the pressure in fluid node 41 is held constant at the nominal test pressure, and the enthalpy is held constant at the saturated vapor enthalpy of the nominal test pressure.

Flowlinks 1 through 14 and 21 represent fluid flow through the heater rod bundle. The modeling of these links is consistent with the modeling of links internal to the core in the AP600 plant and integral test facility models. Each of these links covers 1.0 ft. evenly staggered across the fluid node boundary it spans. The frictional pressure drop computed within these flowlinks accounts for both skin friction within the rod bundle and the form losses resulting from the seven mixing vane grids and two non-mixing vane grids, with the form losses resulting from the grids being distributed evenly throughout the heated length of the rod bundle. Flowlink 14 also includes the form losses associated with the ground plate physically located at the top of the heater rod bundle in the G2 test vessel.

Flowlink 121 represents flow from the baffle/vessel annulus region into the lower plenum. Reference 4-12 does reports that part of this flow path is composed of 0.813-in. diameter holes bored through the test vessel lower flange and the lower spool piece. Reference 4-12 also shows these bore holes on scale drawings and indicates that the piping external to the test vessel that connects these bore holes has a significantly higher flow area than the holes themselves.

The geometrical and frictional characteristics of flowlink 121 are derived from this information. The flow area is set to that of a 0.813-in. diameter circle. The scale drawing shows that the combined length of these 0.813-in. diameter holes in the lower flange and spool piece is about 47 in. Assuming a Darcy friction factor within the holes of 0.02, the flowlink skin friction loss coefficient (fL/d) is about 1. The flowlink form losses are based on an assumption that the flow area through the external piping connecting the holes through the flanges is large compared to the flow area through the holes themselves. With this assumption, the form loss is due to flow through two sudden contractions and two sudden expansions. The first contraction is between the baffle/vessel annulus and the hole through the test vessel lower flange, and the first expansion is between this hole through the lower flange and the external piping. The second contraction is between the external piping and the hole through the spool piece, and the second expansion is between this hole through the spool piece and the test vessel lower plenum. Estimating the form loss is one-half velocity head through each contraction and an entire velocity head through each expansion, the total form loss coefficient is about 3. In

summation, the total irrecoverable loss coefficient through the flowlink is estimated to be about 4. Since this value is a rough estimate, a large uncertainty of +/- 50 percent is associated with the losses.

Flowlink 31 connects the rest of the model to the pressure boundary condition, fluid node 41. The flowlink 31 connection to the upper plenum spans the same elevational range as the hot leg discharge pipe of the G2 test vessel. Since there is no flow path connected to the upper plenum above flowlink 31, the flowlink effectively prevents the two-phase mixture level from swelling above it.

Flowlinks 81 through 94 represent fluid leaking through the flow baffle surrounding the heater rod bundle. Again, little information is available about these flow paths, and the existing model is derived from information in Reference 4-12. Appendix E of Reference 4-12 presents the results of several leakage tests performed with the G2 test vessel. The latest of these tests, performed on January 4, 1975, is used to determine the sizes of the NOTRUMP model baffle leakage flowlinks.

In the leakage test of January 4, 1975, the baffle/vessel annulus was filled with liquid water at approximately 260°F while the bundle region was continually drained and the flow path from the baffle/vessel annulus to the lower plenum was isolated. As fluid in the baffle/vessel annulus drained into the bundle, the baffle level was recorded as a function of time. The leakage rate through the baffle as a function of the baffle/vessel annulus liquid level was then determined from the recorded data. These derived data were used to size the baffle leakage flowlinks, flowlinks 81 through 94.

The flow areas through the baffle leakage links were determined from the test-determined baffle leakage rates by working from the link at the lowest elevation toward the link at the highest elevation. The flow area through flowlink 81 was determined by filling the NOTRUMP model baffle/vessel annulus to the top of fluid node 1 and then varying the flowlink flow area until the test-determined flow rate was achieved. The flow area through successively higher baffle leakage flowlinks was then determined by filling the NOTRUMP model baffle/vessel annulus to the top of the corresponding fluid node and then varying the link flow area until the sum of the flows through the baffle leakage flowlinks equaled the test-determined leakage rate for that baffle/vessel annulus liquid level. Throughout this process, a form loss coefficient of 1.0 was assumed to characterize the pressure drop through each baffle leakage flowlink.

Application of the resulting baffle leakage model involves several assumptions. The first assumption is that the leakage rates from the bundle into the baffle/vessel annulus are the same as the leakage rates in the opposite direction. Although this assumption was not specifically validated in the latest baffle leakage tests, earlier baffle leakage tests run on October 24 and 25, 1994 indicated little or no directional sensitivity in the baffle leakage rates. The second assumption is that the leakage rates are not sensitive to temperature. Although this assumption is not supported by the results of the baffle leakage tests, there is not sufficient information to determine the dependence of baffle leakage on temperature. The third assumption is that the leakage rates do not change during the time period over which the level swell tests were performed. Again, this assumption is not supported by the results of the baffle leakage tests, but there is not sufficient information to determine the change in baffle

leakage that probably occurred as the level swell tests were performed. The final assumption is that two-phase flow through the baffle can be approximated with homogeneous flow. Again, this assumption is due to the lack of a basis to apply any available drift model to the leakage flowlinks. In summary, the modeling of baffle leakage is more reasonable than assuming there is no leakage through the baffle, but the uncertainty in the leakage rates predicted by the model is large. This uncertainty is estimated to be -70 percent to +150 percent of the nominal losses assumed.

Core nodes 1 through 14 represent the G2 heater rod bundle. In this model, the dimensions of the heater rods, the axial power distribution, and the total rod bundle power output are reproduced exactly. However, the properties of the heater rod filler material, boron nitride, is not available in NOTRUMP, so the properties of UO_2 are used instead. Although the resulting property differences should not impact the quasi-steady-state void distribution underneath the two-phase mixture level, they may impact the time required to reach this quasi-steady-state, and the property differences will impact the transient rod heatup above the mixture elevation, which is not an important parameter in the evaluation of level swell.

Boundary metal node 1 represents the heat sinks connected to the lower plenum. This metal node is essentially a temperature boundary condition and is connected to fluid node 21 by a heatlink that has a negligibly small resistance to heat transfer. As a result, the temperature in fluid node 21 is held at the temperature of the metal node.

The addition of boundary metal node 1 to the model was needed to remove heat from the fluid in node 21 to match the temperature at the bottom of the heated length of the heater rod bundle. As discussed in Subsection 4.3.1, heat is lost directly from the fluid in the lower plenum and from the fluid flowing from the baffle/vessel annulus into the lower plenum. Although the resulting degree of subcooling would be insignificant if there was no leakage through the baffle, the baffle is also known to leak. Thus, NOTRUMP calculates the leakage rates through the baffle while the temperature of the lower plenum is held at a value representative of the measured fluid temperature near the bottom of the rod bundle heated length. This allows simulation of the G2 level swell tests to account for time-varying baffle leakage rates and heat loss from the fluid in the lower plenum.

4.4.7 Modeling of Test Boundary and Initial Conditions

There are three boundary conditions in the NOTRUMP model of the G2 test facility: the system pressure, the rod bundle power, and the rod bundle inlet temperature. The system pressure is established through boundary fluid node 41. The pressure of this node is set to the value listed in Table 2-3 of Reference 4-12 for the NOTRUMP simulation of each test. The rod bundle power is also taken from Table 2-3 of Reference 4-12. The rod bundle inlet temperature of each NOTRUMP simulation is established by the temperature of the boundary metal node connected to the lower plenum. This metal node temperature was determined from a plot of lower plenum fluid temperature 5.88 in. below the bottom of the rod bundle heated length. In tests where this thermocouple was

inoperable, the metal node temperature was determined from plots of rod bundle center thimble interior surface temperature at 0.0 and 4.0 in. below the bottom of the rod bundle heated length.

There are two initial conditions that must be set in the NOTRUMP model of each G2 level swell test: the initial axial temperature distribution within the heater rod bundle and the initial liquid levels in the heater rod bundle and baffle/vessel annulus. Although the G2 vessel was nominally heated to saturation for each test, the heater rod thermocouples indicate that some initial temperatures were significantly subcooled, especially near the bottom of the rod bundle heated length. To account for this subcooling, the initial temperatures (time 0.0) of each operable thermocouple at a given elevation were averaged to determine the initial temperature at that elevation. The initial temperature of each core node was then determined from these averaged thermocouple temperatures, assuming a linear temperature distribution between thermocouple elevations. The initial temperature of the liquid in each fluid node below the initial mixture elevation was then set to the temperature of its associated core node. Since there are few fluid thermocouples in the baffle/vessel annulus region, the liquid in the baffle/vessel annulus is assumed to be saturated at the beginning of each test.

Having determined the initial liquid temperature distribution in the bundle and baffle/vessel annulus regions, the initial liquid levels in both regions are determined from the measured axial differential pressures at time zero.

4.4.8 Analysis Results and Comparisons

4.4.8.1 Method of Analysis

At the beginning of each of the NOTRUMP simulations, the NOTRUMP model is initialized to the test pressure in the upper plenum, the enthalpy distribution in the test section, and the initial collapsed water level. Although the test report (Reference 4-12) indicates that the water in the facility was initially at saturation temperature, a review of the temperature data at different locations shows that there is some subcooling in the lower plenum as discussed in Subsection 4.4.6. This subcooling is modeled in the initial enthalpy distribution and by using a measured inlet fluid temperature during the test. Once the NOTRUMP model is initialized, the simulation is run for 10 sec. with no heat input to verify stability in the initial level. At 10 sec., the power is turned on to its full value and held constant for the remainder of the test. The addition of the heat causes an initial swell of the bundle mixture level as the water transitions from single-phase to a two-phase mixture. After the initial level swell, the level decreases as the inventory in the system boils off and exits through the steam line.

The test mixture level is determined from the heater rod thermocouple temperature transients. As long as the heater rod thermocouple is covered and remains in nucleate boiling, its temperature is slightly above the saturation temperature at the upper plenum pressure. Once the mixture level drops below the instrumented location, the heater rod thermocouple drys out and begins a thermal or temperature excursion. The time at which the thermocouple drys out is used to determine the mixture height. The

dryout is uniform across the test bundle with a small variation in the different heater rod temperature responses at a given elevation plane.

4.4.8.2 NOTRUMP Comparisons to the G2 Tests

Comparisons to Test 716

Test 716 is described in detail. The complete set of figures are shown for the remaining tests, and the discussion concentrates on the specific key features and results. Test 716 was performed at 775 psia with a bundle power of 0.252 MW. The initial collapsed water level for this test was approximately 11.5 ft.

The comparison of the predicted and measured two-phase mixture level for this test is shown in Figure 4.4-13. The first indication from the data of uncovery is from the thermocouples on the heater rods at the top-most elevation. The two-phase mixture, which is initially above the top of the heated length, must uncover the rod bundle down to a level of 147.6-in., which is the highest instrumented elevation on the rod bundle before an indication of the mixture level is detected. Once the power is turned on, the bundle mixture level increases to approximately 13 ft. before reaching its peak and then begins a steady descent. At approximately 200 sec. when the first test data are shown, the mixture level data reach the 147.6-in. elevation. The NOTRUMP-calculated mixture level lies below the data at 200 sec., as indicated in Figure 4.4-13. After 200 sec., the difference between the measured mixture level and that predicted by NOTRUMP increases with the NOTRUMP prediction lying below the data.

The two-phase mixture level is influenced significantly by the void fractions in the bundle region. To evaluate the calculated voiding relative to the test data, the measured differential pressure data are compared against the differential pressure data calculated by NOTRUMP. These comparisons are presented for locations starting 5.88 in. below the bundle up to near the top of the heater rods, approximately 223 in. above the bottom. The locations of the taps in inches relative to the bottom of the heated bundle are: -5.88, 27.3, 54.7, 82.0, 109.3, 136.7, 164.0, 190.0, and 222.8 in. The comparisons are provided as Figures 4.4-14 through 4.4-19. These comparisons show that the calculated differential pressures are reasonably close to the test data and are usually within the measurement uncertainties for the pressure cells.

From the bottom of the heated bundle up to 54.7 in., the calculated pressure differential is slightly higher than the data for most of the test (see Figures 4.4-14 and 4.4-15), which indicates the NOTRUMP-calculated void fraction is slightly lower than the test data.

Between 54.7 and 82.0 in., the NOTRUMP-calculated differential pressure agrees well with the test data being slightly lower as seen in Figure 4.4-16. After 1900 seconds, the NOTRUMP differential pressure decreases below the data as a result of the lower NOTRUMP-calculated mixture level, which decreases prior to the actual level in the test. For both the test data and the calculation, the differential

pressure in a region decreases significantly as the mixture level moves through the region as the void fraction above the two-phase level becomes unity.

The comparisons between the NOTRUMP-calculated differential pressure and the test data for the span of 82.0 and 109.3 in. is excellent as seen in Figure 4.4-17. Again, as the two-phase mixture level passes through the span, NOTRUMP calculates an earlier decrease in the differential pressure, indicating that the code is predicting a lower mixture level. This occurs at approximately 950 seconds into the test.

The comparisons of the differential pressure for the span between 109.3 and 136.7 in. are not as good as other elevations with the NOTRUMP-calculated differential pressure drop lying below the test data as shown in Figure 4.4-18. Again, NOTRUMP indicates an earlier indication of the calculated mixture level passing through the cell span as compared to the test data, which is consistent with the lower two-phase mixture level predicted by NOTRUMP.

The upper-most region between 136.7 to 164.0 in. indicates good agreement as the bundle uncovers from time 0 to 350 sec. as shown in Figure 4.4-19. The uncovery behavior of the data and the NOTRUMP calculation agree well at this elevation. This is the top-most elevation within the heated bundle.

The total heated bundle pressure drop can be used to infer the transient mass history in the bundle during the test. Figure 4.4-20 shows the NOTRUMP-predicted transient mass in the bundle as compared to the test data for test 716. As the figure indicates, the agreement is good and the calculation is within the data uncertainty. The baffle pressure drop can be also used to infer the transient mass behind the baffle. Figure 4.4-21 shows the NOTRUMP-predicted baffle mass and indicates that NOTRUMP is predicting the correct mass in the baffle region.

The steam flow is measured in the G2 tests using an orifice that is located downstream of a separator. Figure 4.4-22 shows the comparison of the measured steam flow and the predicted steam flow from the NOTRUMP calculation for test 716. The NOTRUMP calculation initially overpredicts the steam flow out of the bundle. The overprediction of the steam flow is consistent with the NOTRUMP overprediction of the rate of mass decrease in the bundle, as seen in Figure 4.4.20, particularly at early times in the transient.

As indicated in Section 4.3, the baffle surrounding the heater rod bundle leaks, mostly above the vessel mid-plane, and creates a circulation flow pattern within the test vessel. This circulation pattern creates additional mixing in the lower plenum of the vessel so that subcooled liquid can be injected and provides an alternate flow path of the mixture out of the heater rod bundle. The leakage effects are modeled in the NOTRUMP calculation with a loss coefficient estimated from the leakage test results given in Reference 4-12. The uncertainties are also estimated for the leakage flow paths. Additional NOTRUMP calculations are performed using the upper and lower bounds of the uncertainties to determine the effects on the NOTRUMP-predicted mixture level within the bundle.

The objective of the calculations is to investigate whether inclusion of the uncertainties would significantly bias the conclusions drawn from the NOTRUMP comparisons to the mixture level swell data. Figure 4.4-23 shows the predicted NOTRUMP two-phase mixture level as compared to the test data with the additional NOTRUMP calculations using the upper and lower bound uncertainties for the leakage path through the baffle. For this particular test, there is little difference in the calculated response of the mixture level and all calculations lie below the test data, which gives confidence in the NOTRUMP results. The conclusion that NOTRUMP is underpredicting the mixture level for this test remains valid.

NOTRUMP Comparisons to the Remainder of the G2 Tests

Table 4.4-3 indicates which G2 tests are analyzed using NOTRUMP. The results of the other test comparisons are similar to those of test 716, so only the mixture level plots are presented for the remainder of the tests.

Figure 4.4-24 shows the comparisons of the NOTRUMP calculation to test 715, which is a 779-psia test at 0.603 MW bundle power. As the figure indicates, the NOTRUMP two-phase mixture level calculation initially lies above the data for the first 150 sec. and then lies below the data for the remainder of the test. The uncertainty bands are also on Figure 4.4-24 and show that the NOTRUMP calculation with the uncertainty initially overpredicts the mixture level at the beginning of the test then crosses the data and lies below the tests when the level is low. Once the level decreases below the region of high leakage, the uncertainty decreases and the calculation lies below the data.

Figure 4.4-25 shows the NOTRUMP comparisons to the mixture level for test 719, which is a 394-psia test at 0.297 MW power. As the figure indicates, in the region where data exist, the NOTRUMP calculation with the uncertainty lies below the data, resulting in a lower mixture level.

Figure 4.4-26 shows the NOTRUMP-calculated mixture level for test 720, which is a 395-psia test at 0.615 MW power. As shown in the figure, the data are within the uncertainty of the NOTRUMP calculation for approximately half of the test time. The NOTRUMP calculation then lies under the data at later times when the mixture level is lower.

Figure 4.4-27 shows the comparison of the NOTRUMP mixture level prediction to the G2 test data for test 724, which is a 96-psia test at 0.252 MW power. As the figure indicates, the NOTRUMP mixture level calculation with uncertainty lies below the test data for the majority of the test.

The NOTRUMP predictions for test 725 are shown in Figure 4.4-28. This test is a 96-psia test at 0.599 MW bundle power. As with the lower-power test at the same pressure, the NOTRUMP calculation brackets the test data at the beginning of the transient and then lies below the data as the mixture level decreases.

Figure 4.4-29 shows the NOTRUMP predictions to test 728, which is a 50-psia test at a bundle power of 0.596 MW. The mixture level test data lie above the best-estimate NOTRUMP calculation but within the uncertainty of the calculation for the first 300 sec. of the test. Once the mixture level drops below the zone of larger leakage, the uncertainty is reduced and the predictions lie conservatively below the data.

NOTRUMP comparisons to the level swell data for test 729 are shown in Figure 4.4-30. Test 729 is a 50-psia test at 0.25 MW bundle power. The calculations including the uncertainty all lie below the test data for the duration of the test as shown in the figure.

Figure 4.4-31 shows the NOTRUMP predictions for test 732, which is a 15-psia test at 0.254 MW bundle power. The predictions including the uncertainties in the NOTRUMP calculations all lie below the test data over the transient period.

The NOTRUMP predictions for test 733 are shown in Figure 4.4-32. Test 733 is a 15-psia test at a power of 0.600 MW. As the figure indicates, the NOTRUMP calculations including the uncertainties lie well below the G2 test data for these conditions.

4.4.9 Conclusions

NOTRUMP has been compared to several G2 constant-pressure, heated-bundle level swell tests over a range of powers and pressures typical of the AP600 small-break LOCA. There was leakage in the test, which made modeling the tests difficult. Analysis was performed to predict the mixture level accounting for the uncertainties in the leakage. The results indicate that for the majority of conditions, NOTRUMP predicts a mixture level below that indicated in the test data for the level swell transients, even when the uncertainties caused by the leakage are considered. This indicates that the two-phase and drift flux models used in NOTRUMP predict a conservatively low mixture level in heated bundles.

TABLE 4.4-1
COMPARISON OF 17 x 17-XL PWR ROD AND TEST ROD BUNDLE

Item	PWR Rods	Test Rods
Diameter	0.374 in.	0.374 in. (0.950 cm)
Thimble Outside Diameter Support Thimbles (9) Removable Thimbles (16)	 0.4894 in. (0.431 in. dashpot) ---	 0.484 in. (0.431 in. dashpot) 0.465 in. (0.431 in. dashpot)
Instrumentation Tube Outside Diameter	0.484 in. (0.431 in. dashpot)	0.484 in. (0.431 in. dashpot)
Rod Pitch	0.496 in. square pitch	0.496 in. square pitch
Clad Thickness	0.0225 in.	0.020 - 0.024 in.
Clad Material	Zircaloy-4	Type 347 stainless steel
Heated Length	168 in.	164 in.[a]
Filler Material	UO_2	Boron nitride
Flow Grid Characteristics Flow Area[b] K-Factor for Standard (Non-Mixing Vane) Grid[c] Reynolds Number = 10^3 Reynolds Number = 10^4 K-Factor for Mixing Vane Grid[d] Reynolds Number = 10^3 Reynolds Number = 10^4	 29.7258 in.^{2} 1.4 ± 30% 1.2 ± 30% 1.8 ± 20% 1.5 ± 20%	 29.80 in.^{2} 1.4 ± 30% 1.2 ± 30% 1.8 ± 20% 1.5 ± 20%

Notes:

a. The original 17 x 17-XL fuel length was 164 in. at the time the facility heater rods were purchased. Since that time, the PWR fuel length has been increased to 168 in.

b. The flow area given is applicable to both mixing vane and nonmixing vane grids.

c. There are two standard grids in the test bundle: one at the beginning of heated length and one at the end of heated length.

d. There are seven mixing vane grids in the test bundle located between the two standard grids.

TABLE 4.4-2
G2 LOOP CORE UNCOVERY TEST VESSEL FLOW AREAS

Location	Flow Area $in.^2$
Test Bundle	49.30
Spacer Grid	29.80
Flow Baffle/Test Vessel Annulus	194(1)

Note:
1. This is an average cross-sectional area that accounts for volumes of nozzles welded to the vessel. This average area was used to calculate liquid height and mass in that annulus.

TABLE 4.4-3
G2 LOOP CORE UNCOVERY TEST PARAMETERS

Run Number	Pressure psia	Bundle Power (MW)	Initial Bundle Water Level in.	Tests Analyzed with NOTRUMP
715	779	0.603	114	✓
716	775	0.252	138	✓
717	796	0.905	102	
718	799	1.258	90	
719	394	0.267	138	✓
720	395	0.615	114	✓
721	394	0.914	102	
722	395	1.264	84	
723	395	0.614	114	
724	96	0.252	126	✓
725	96	0.599	96	✓
726	96	0.857	84	
727	97	1.247	78	
728	50	0.596	84	✓
729	50	0.250	114	✓
730	50	0.894	66	
731	50	1.244	54	
732	15.1	0.254	102	✓
733	15.8	0.600	72	✓
734	16.1	0.900	60	
735	16.7	1.249	54	
736	15.3	0.253	102	

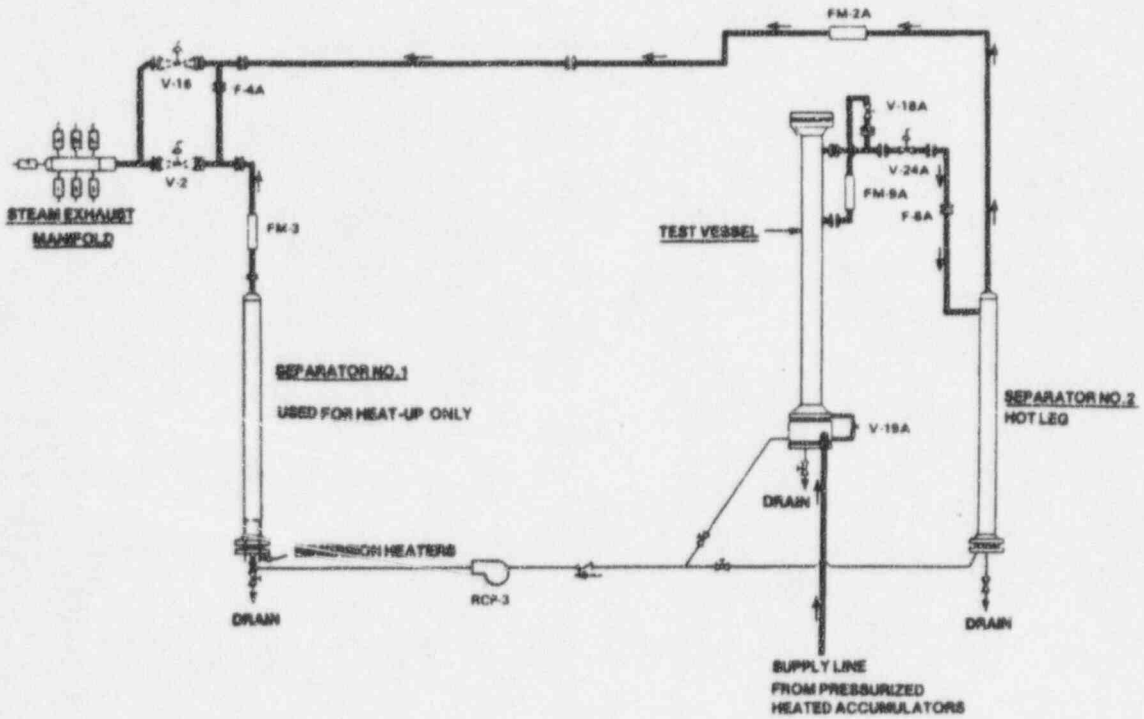

Figure 4.4-1 G2 Loop Test Facility Core Uncovery Flow Diagram

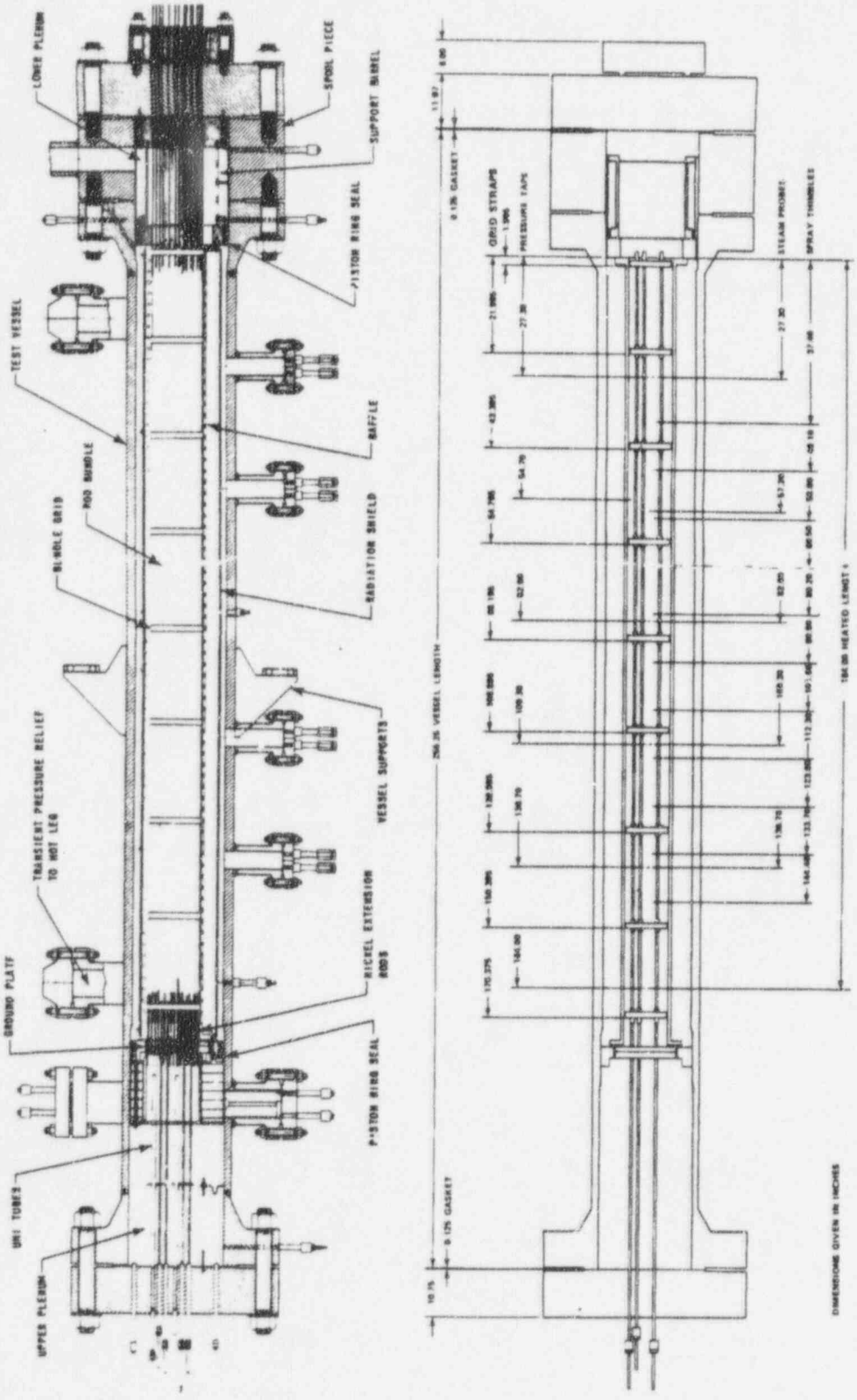

Figure 4.4-2 G2 Test Vessel and Test Section

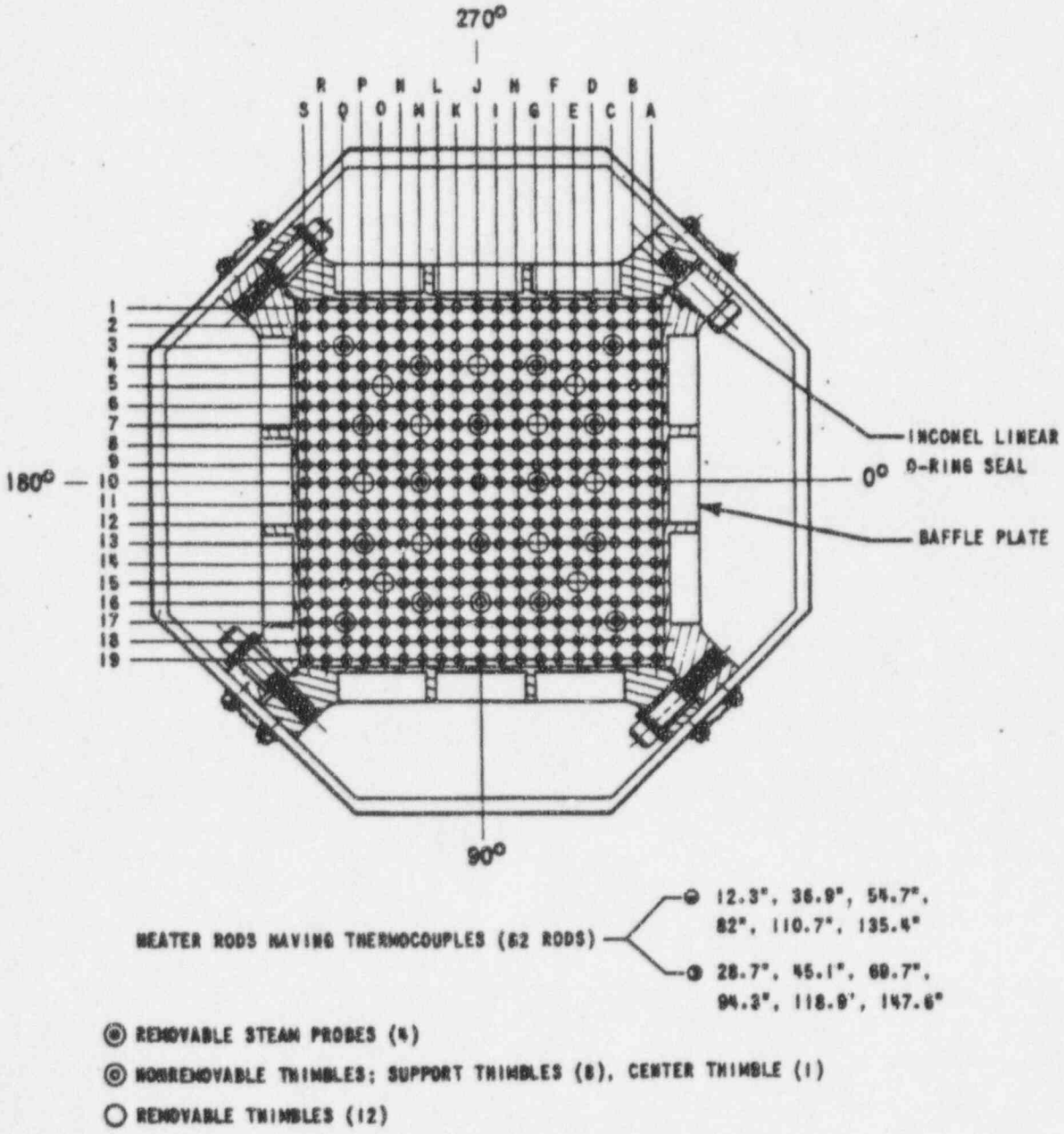

Figure 4.4-3 G2 Loop Rod Bundle, Baffle Cross Section, and Bundle Instrumentation

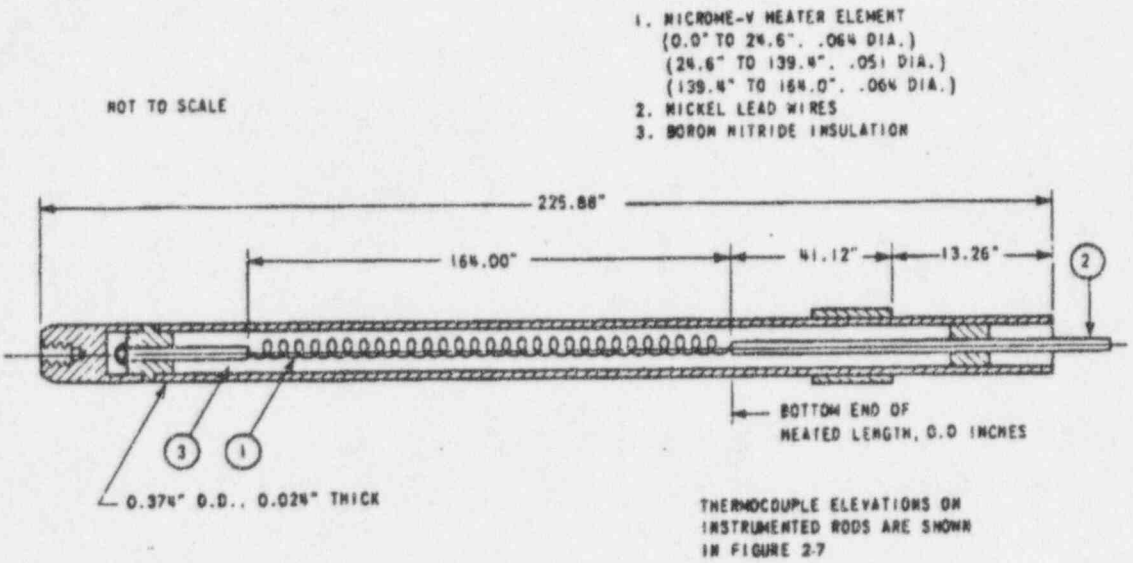

Figure 4.4-4 G2 Loop Heater Rod

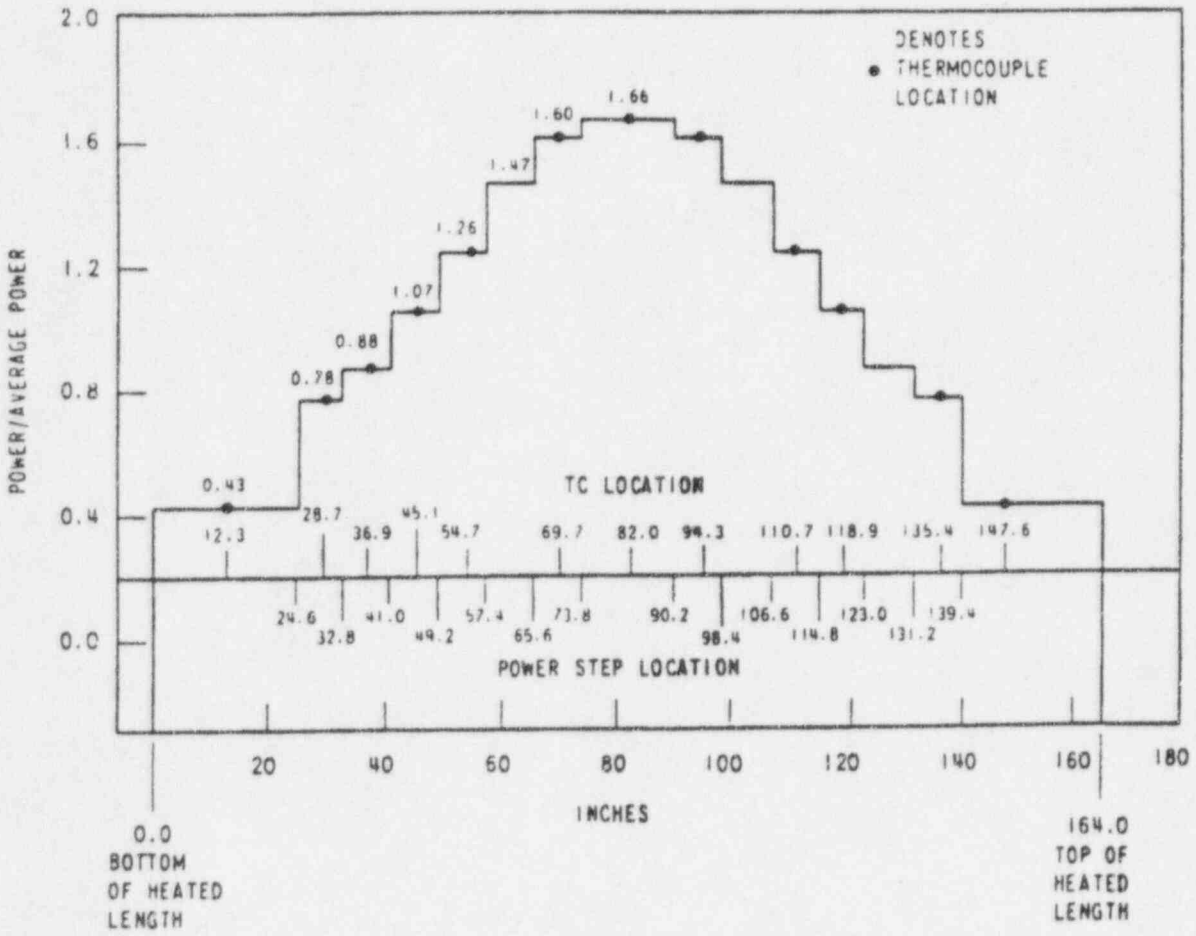

Figure 4.4-5 G2 Loop Heater Rod Axial Power Profile

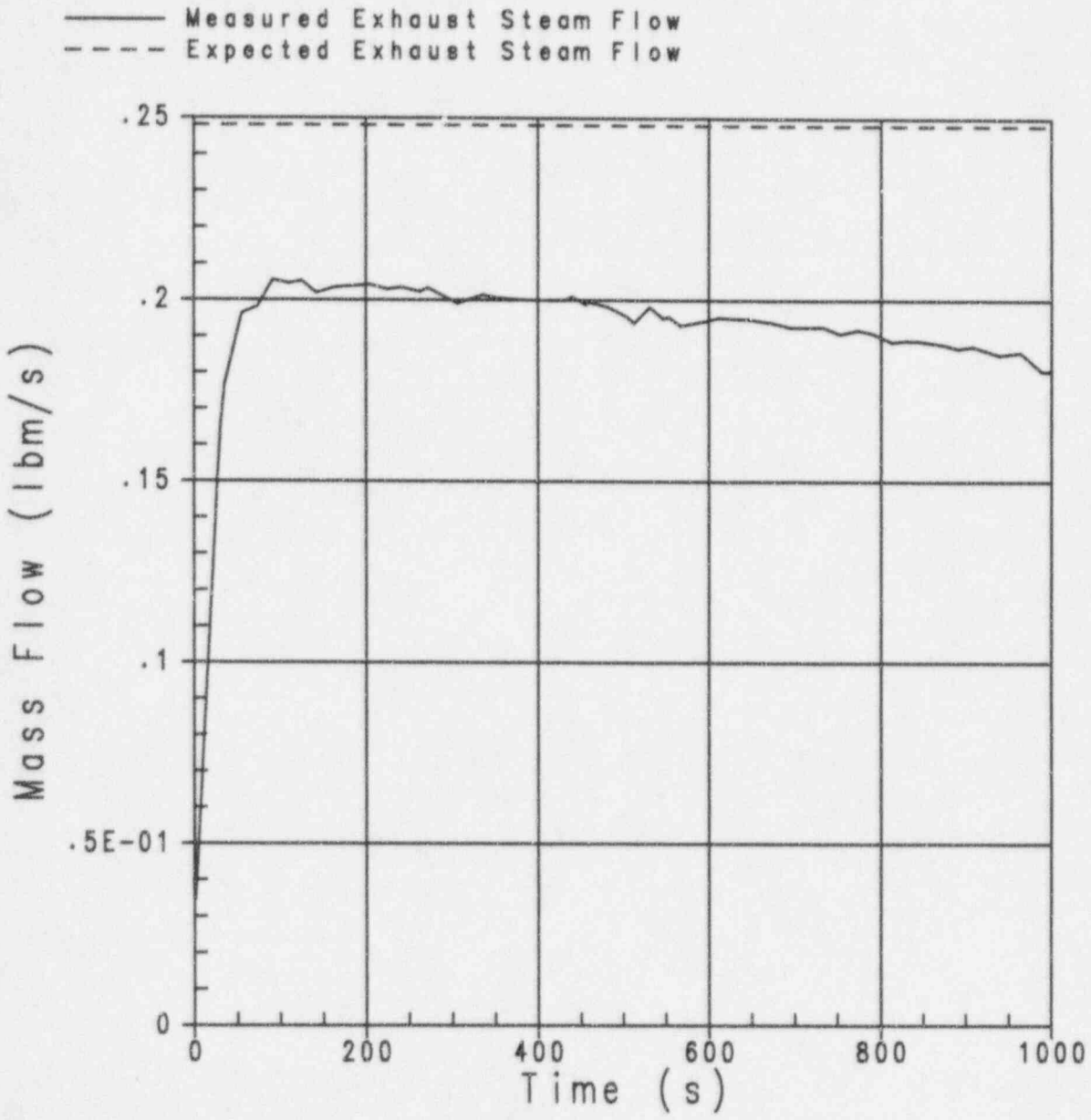

Figure 4.4-6 Comparison of Measured Steam Flow at Test Section Exit to Expected Steam Flow from Power Measurements for Test 732

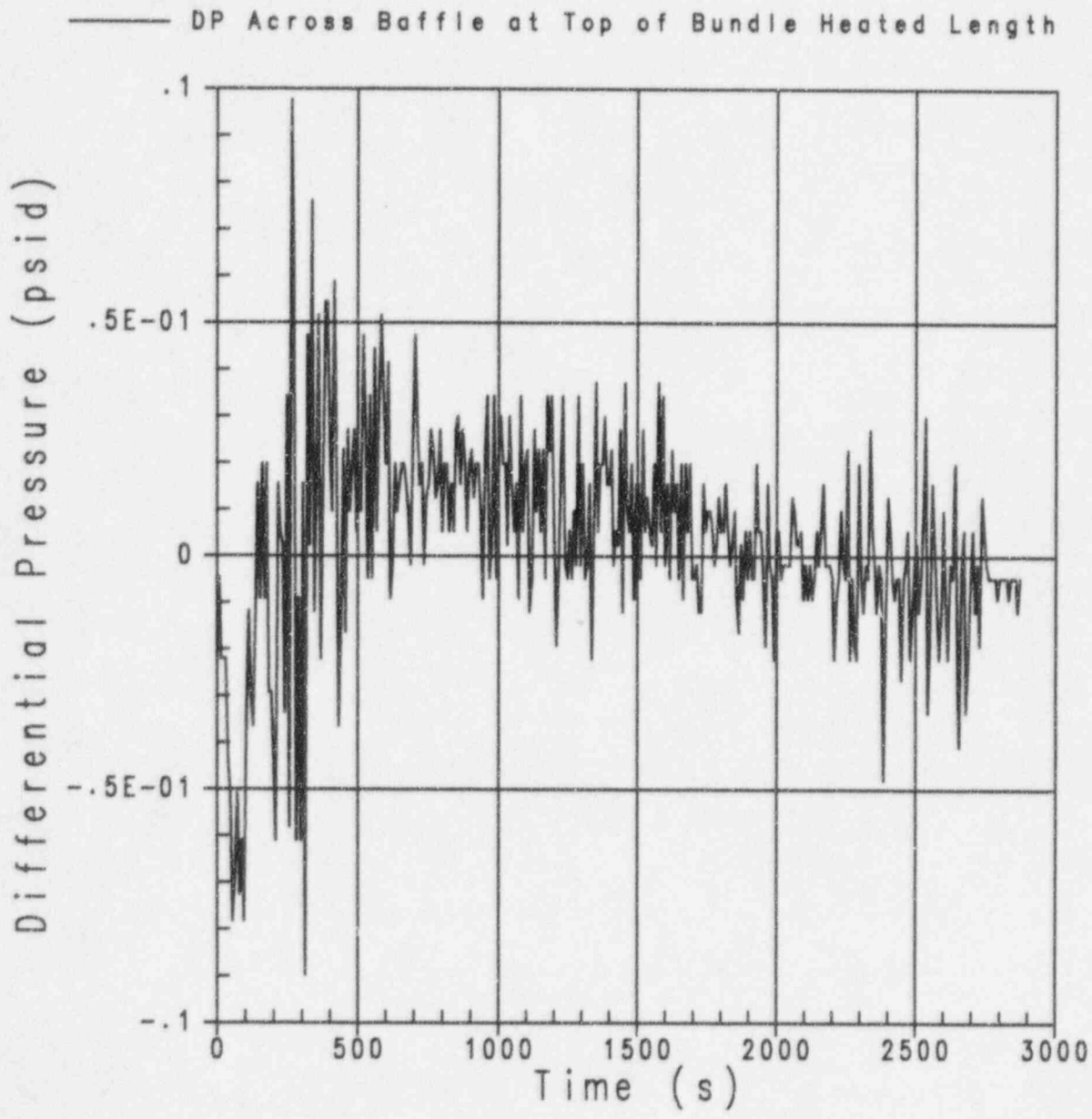

Figure 4.4-7 Measured Differential Pressure Between Heated Bundle and Baffle Region for Test 732

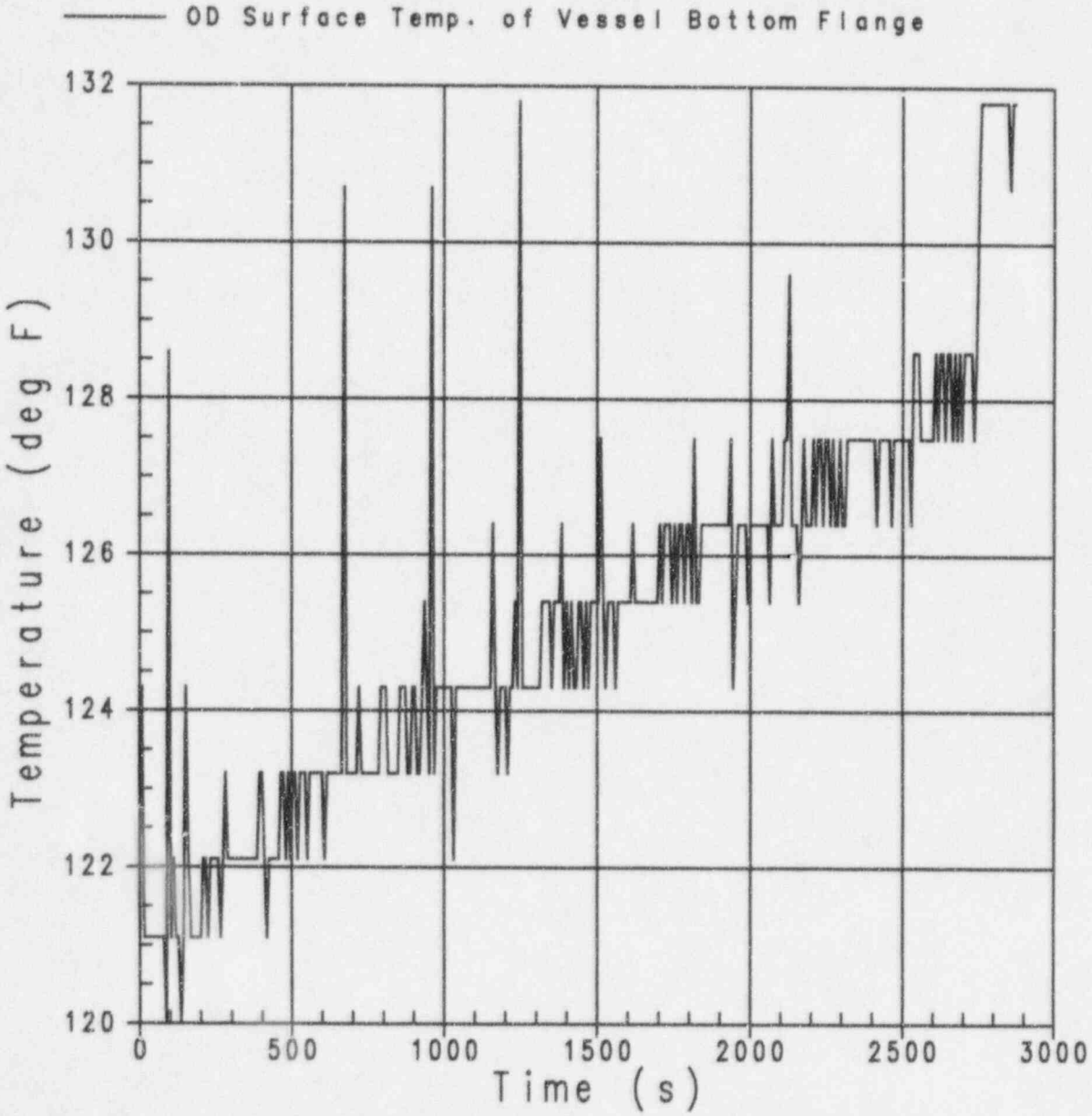

Figure 4.4-8 Measured Test Vessel Lower Flange Outer Temperature for Test 732

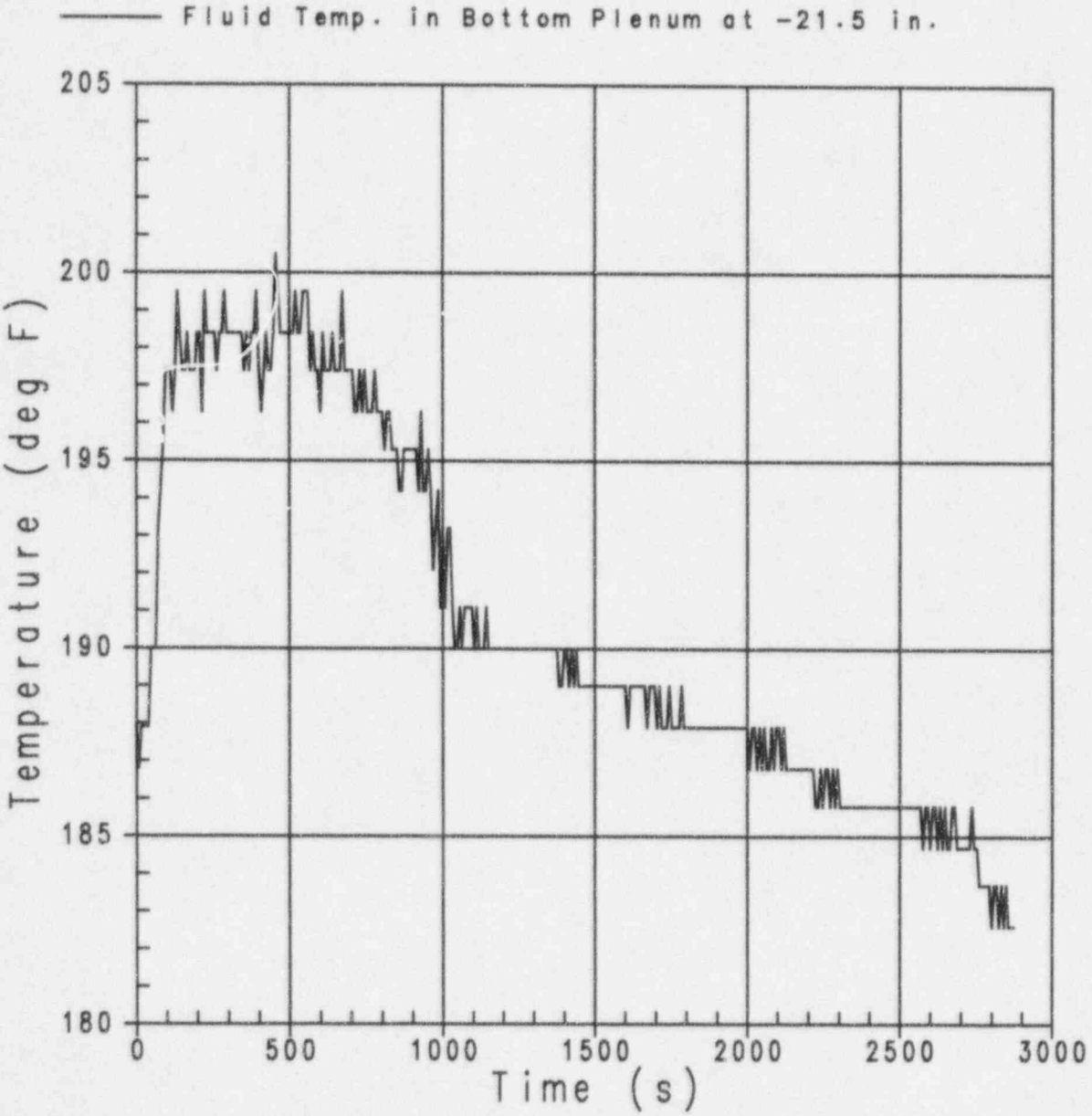

Figure 4.4-9 Measured Lower Plenum Temperature at -21.5-in. Elevation for Test 732

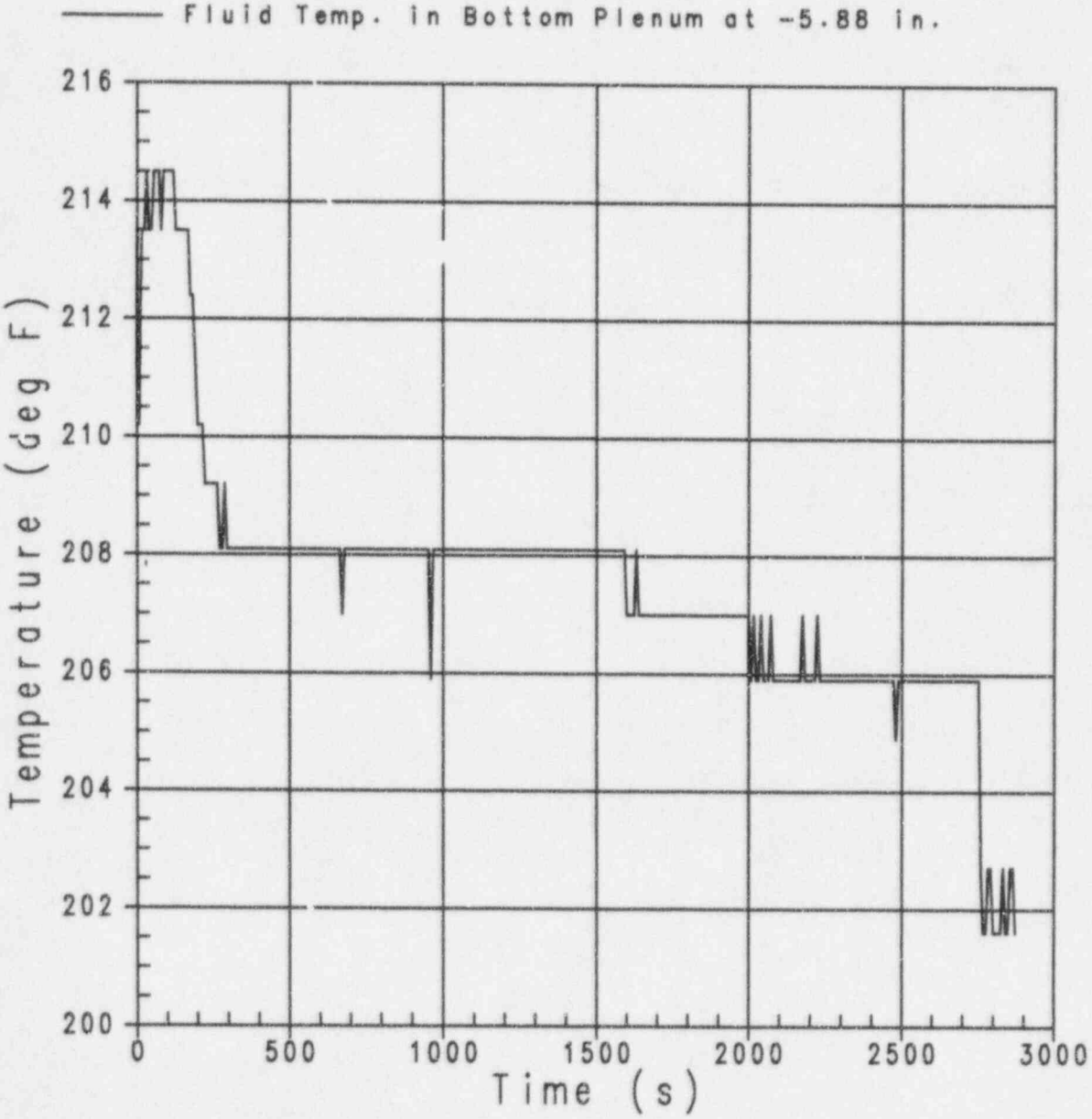

Figure 4.4-10 Measured Lower Plenum Temperature at -5.88-in. for Test 732

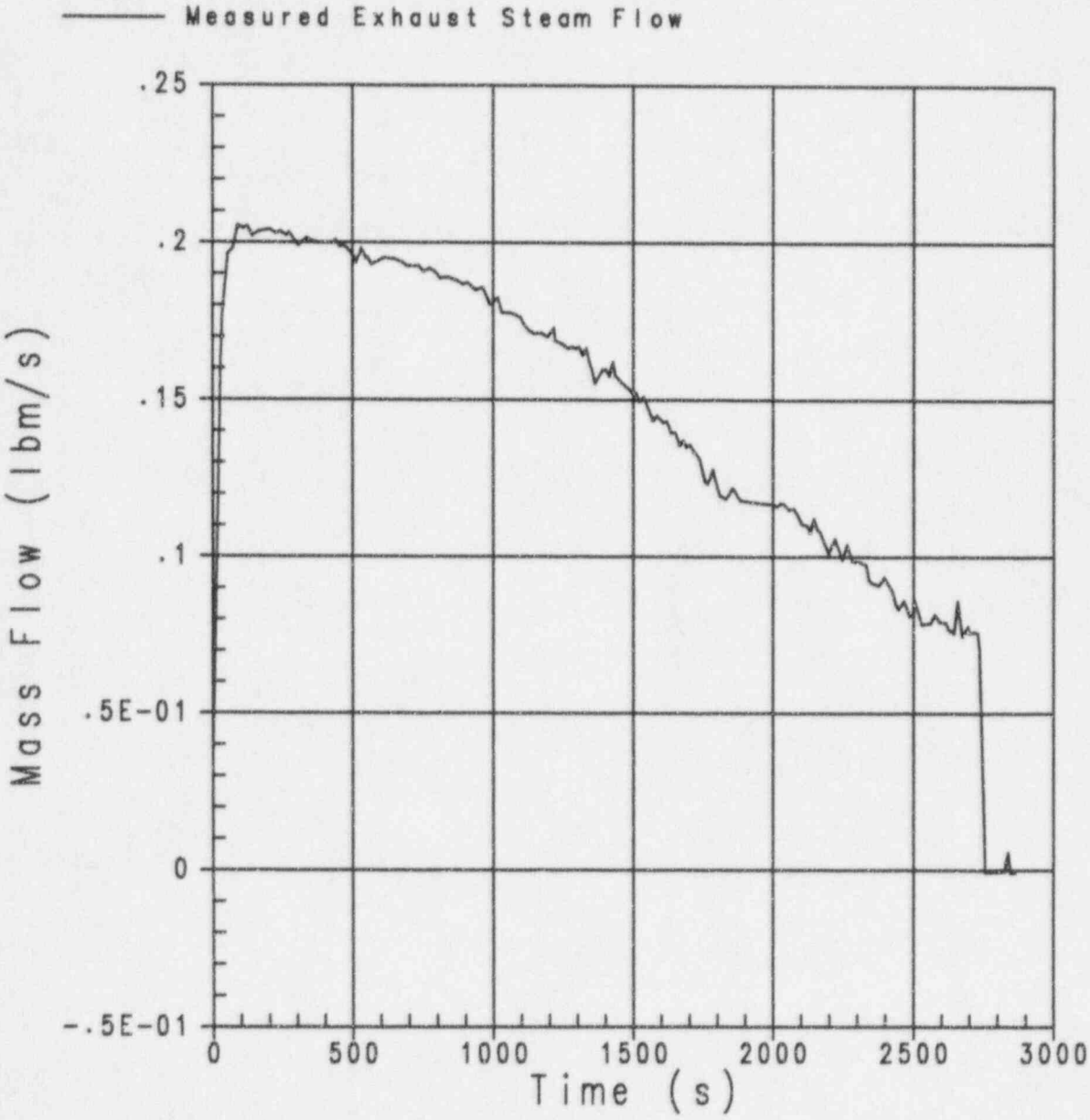

Figure 4.4-11 Measured Test Section Steam Exit Flow for Test 732

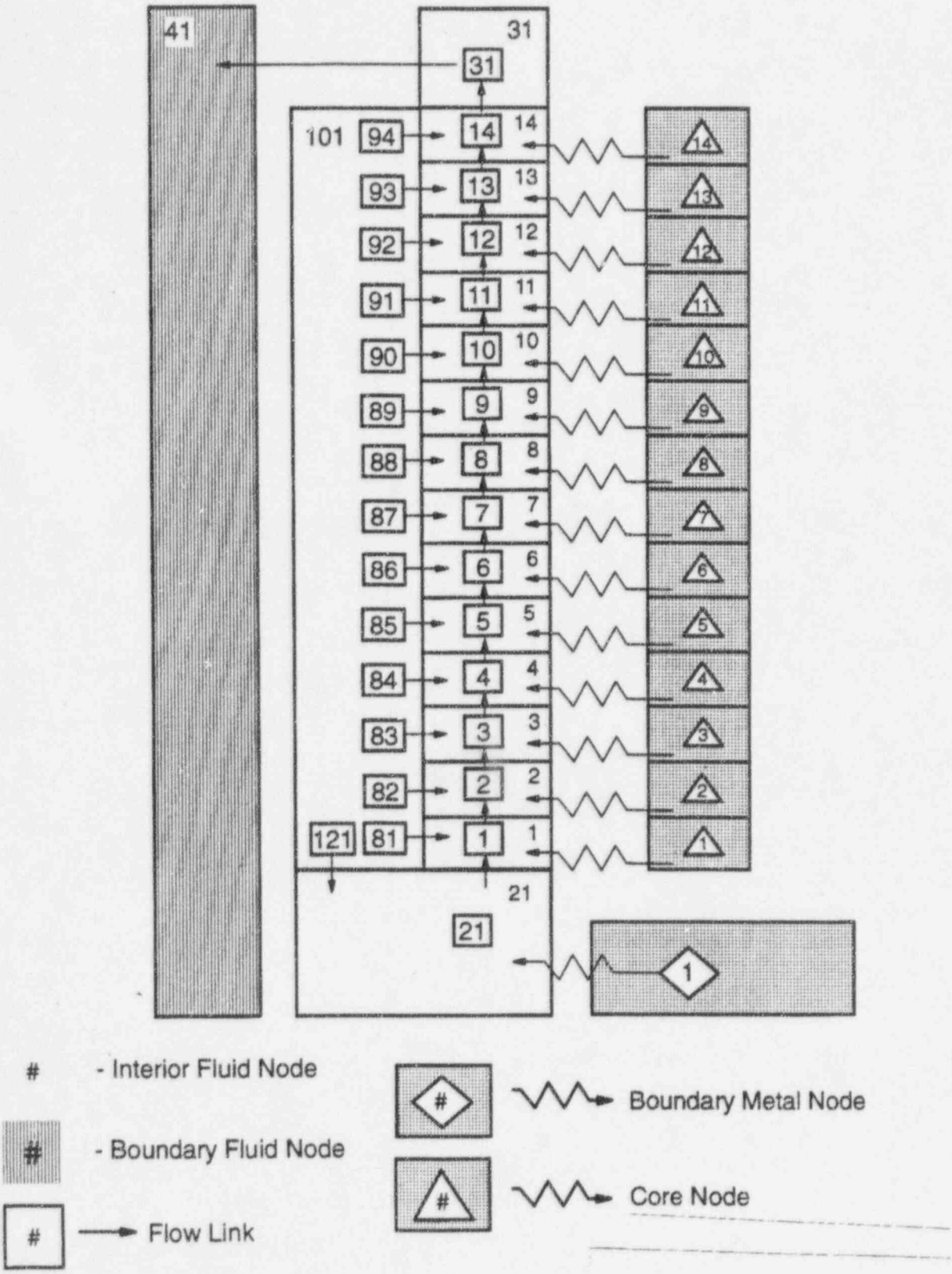

Figure 4.4-12 NOTRUMP Noding Diagram for the G2 Tests

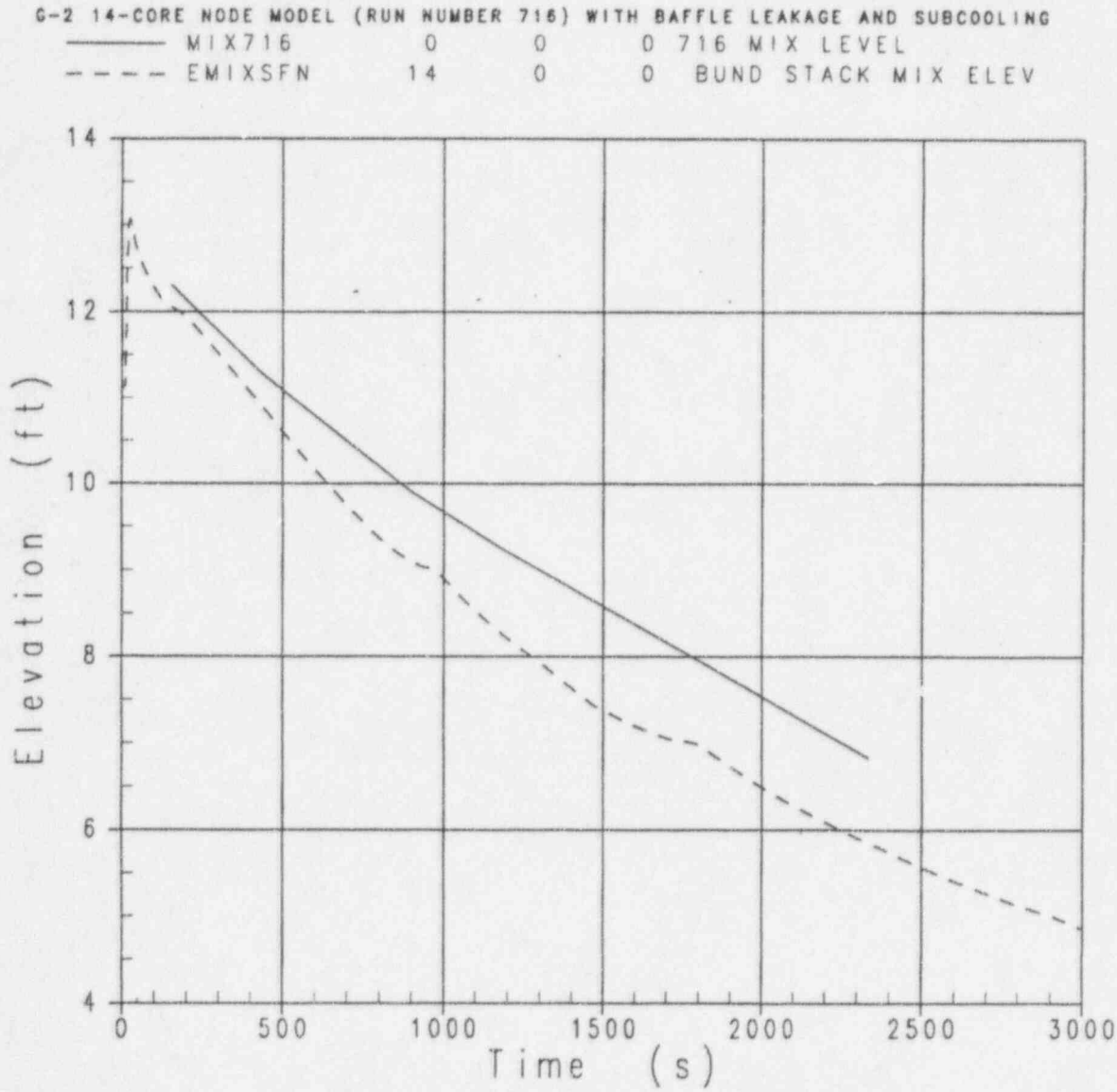

Figure 4.4-13 Comparisons of NOTRUMP Mixture Level to G2 Data for Test 716

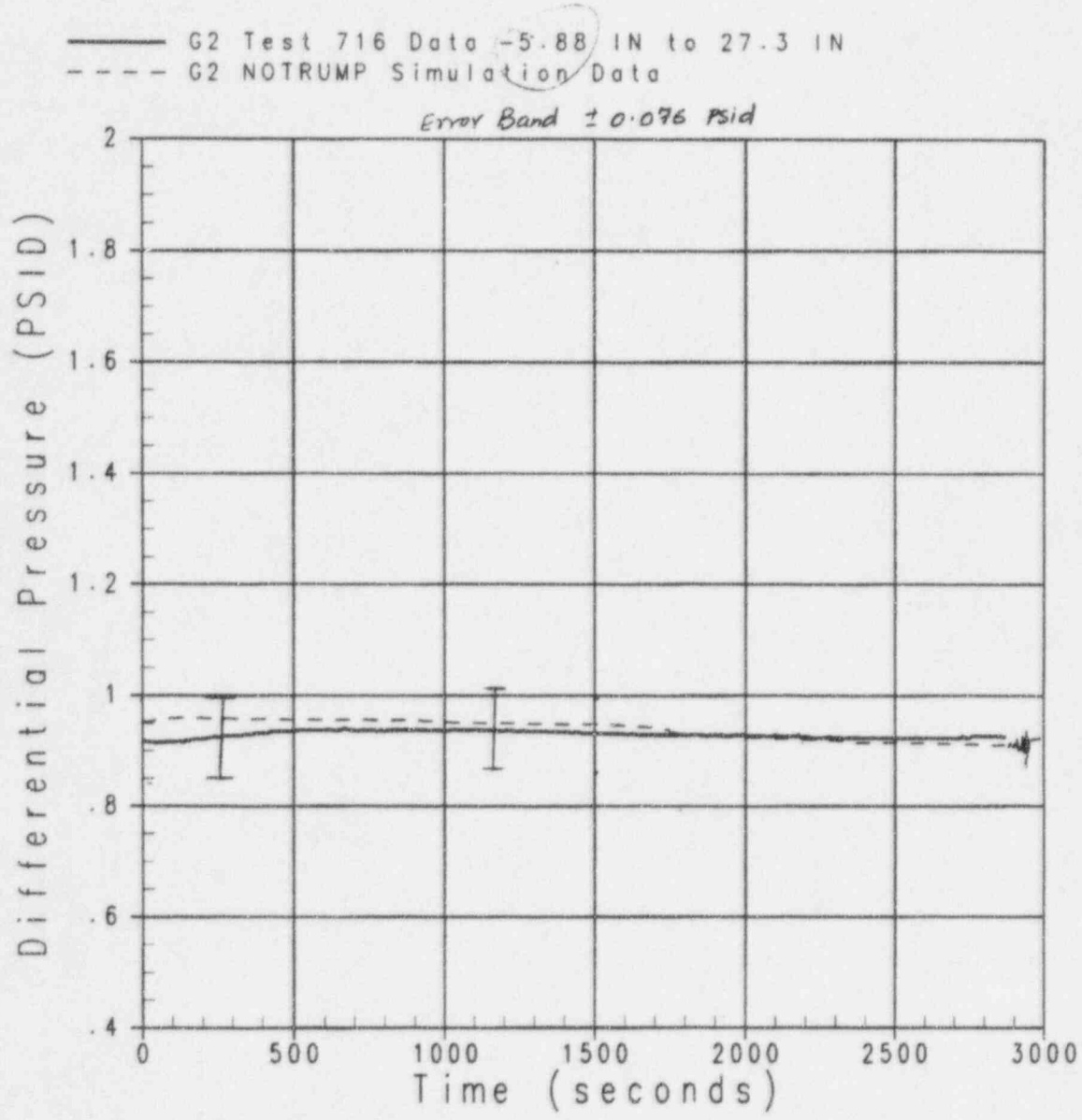

Figure 4.4-14 NOTRUMP Pressure Drop Comparisons to G2 Test 716, -5.88-in. to 27.3-in. in Test Bundle

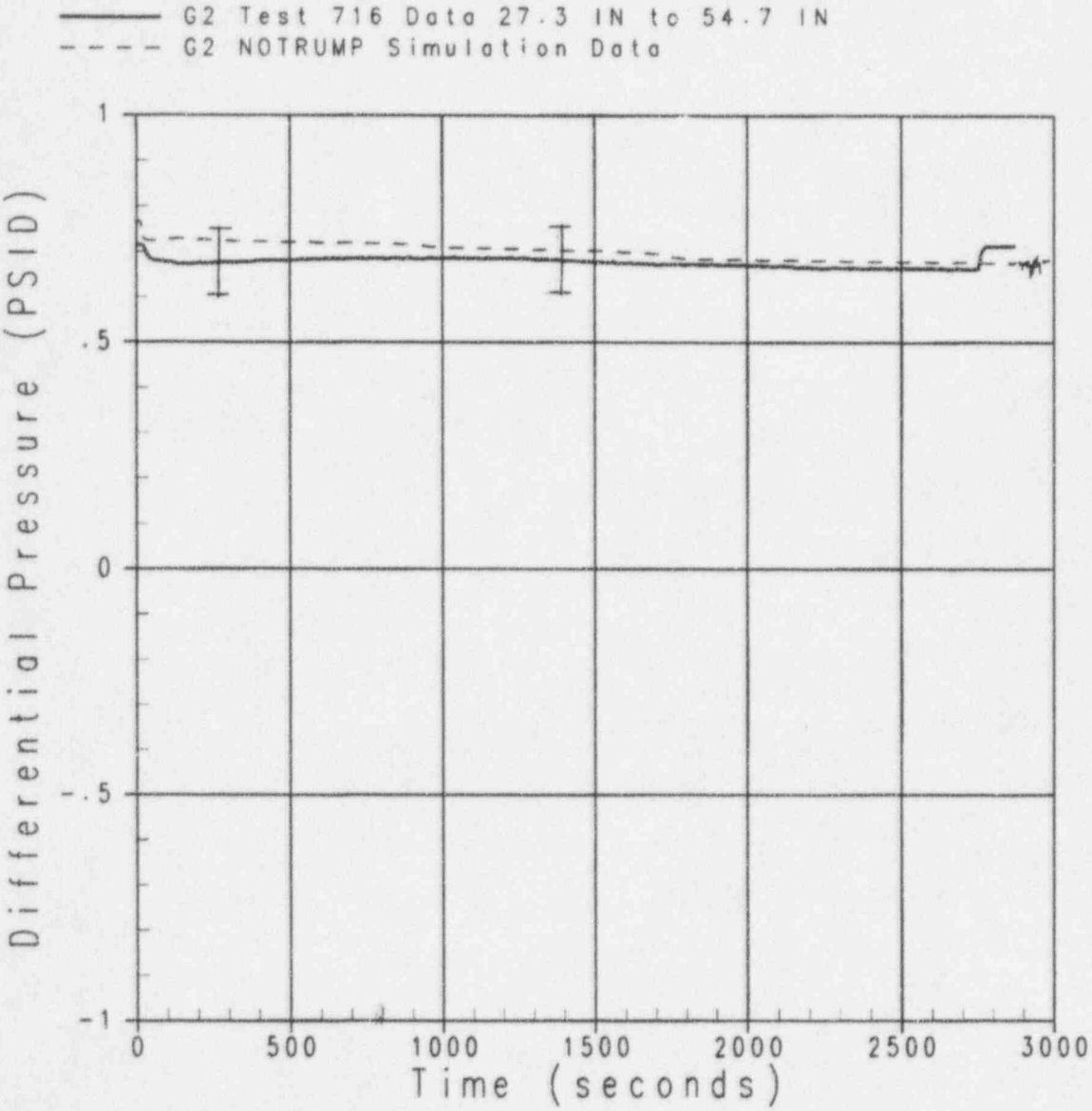

Figure 4.4-15 NOTRUMP Pressure Drop Comparisons to G2 Test 716, 27.3-in. to 54.7-in. in Test Bundle

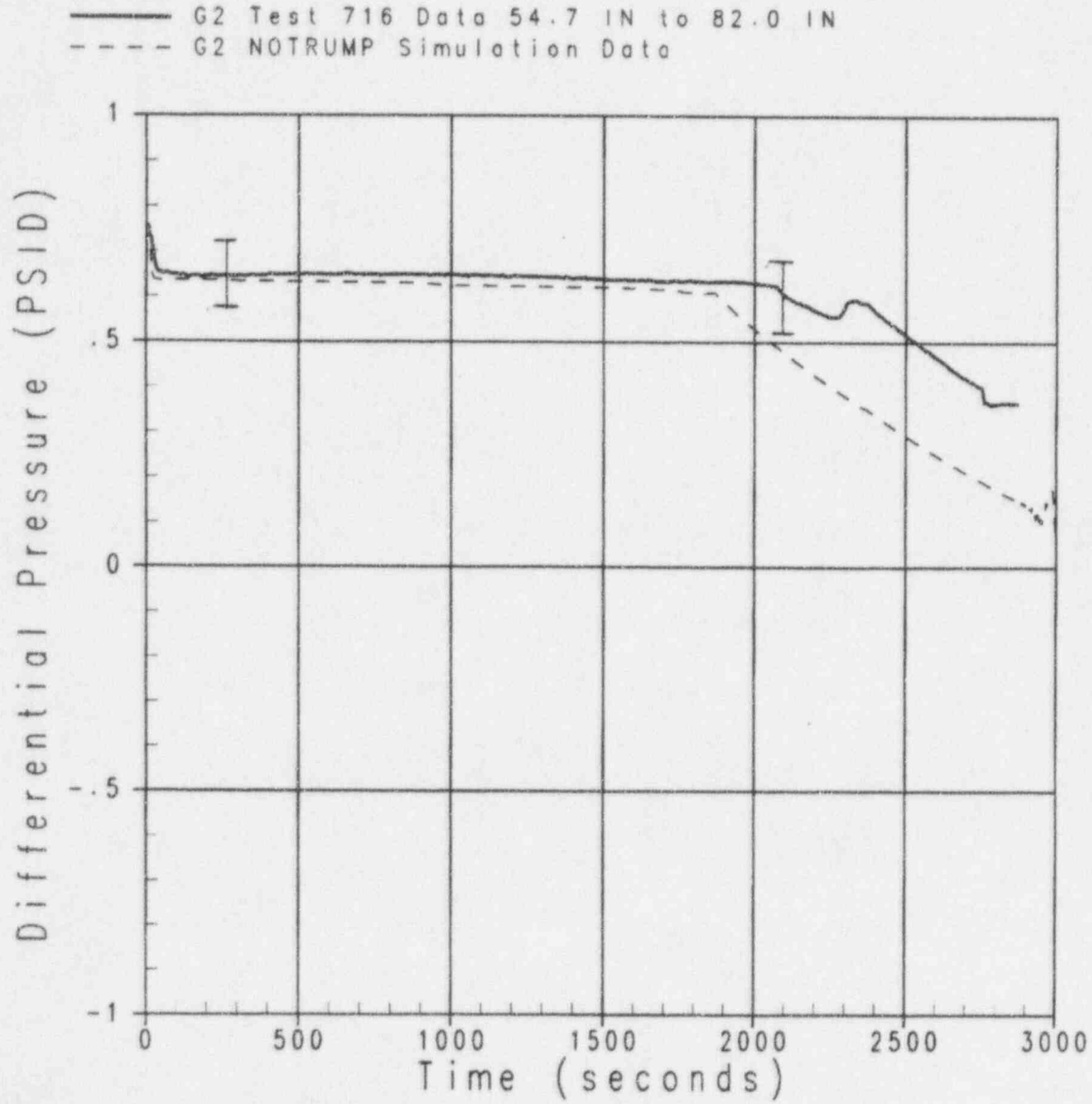

Figure 4.4-16 NOTRUMP Pressure Drop Comparisons to G2 Test 716, 54.7-in. to 82.0-in. in Test Bundle

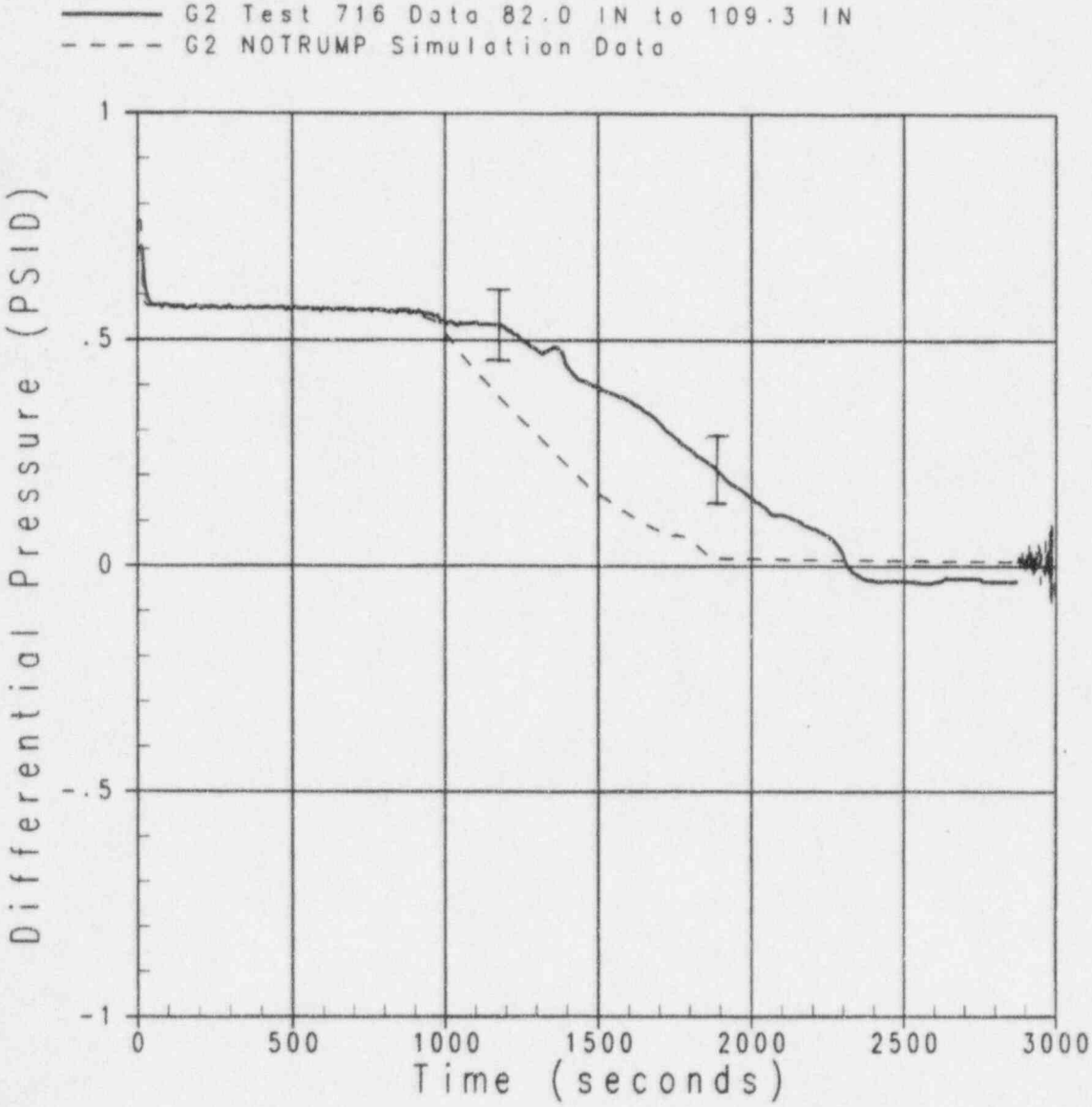

Figure 4.4-17 NOTRUMP Pressure Drop Comparisons to G2 Test 716, 82.0-in. to 109.3-in. in Test Bundle

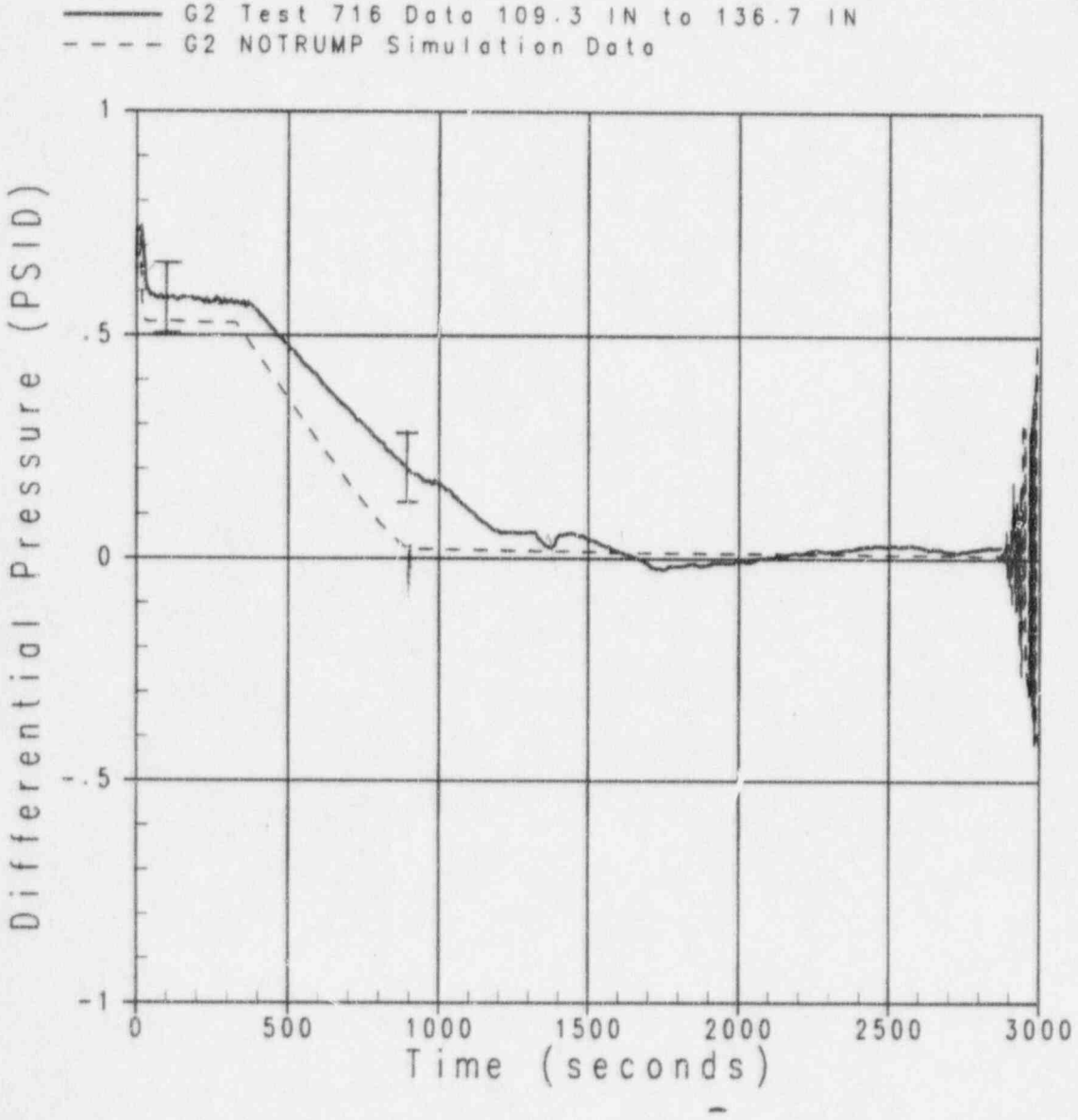

Figure 4.4-18 NOTRUMP Pressure Drop Comparisons to G2 Test 716, 109.3-in. to 136.7-in. in Test Bundle

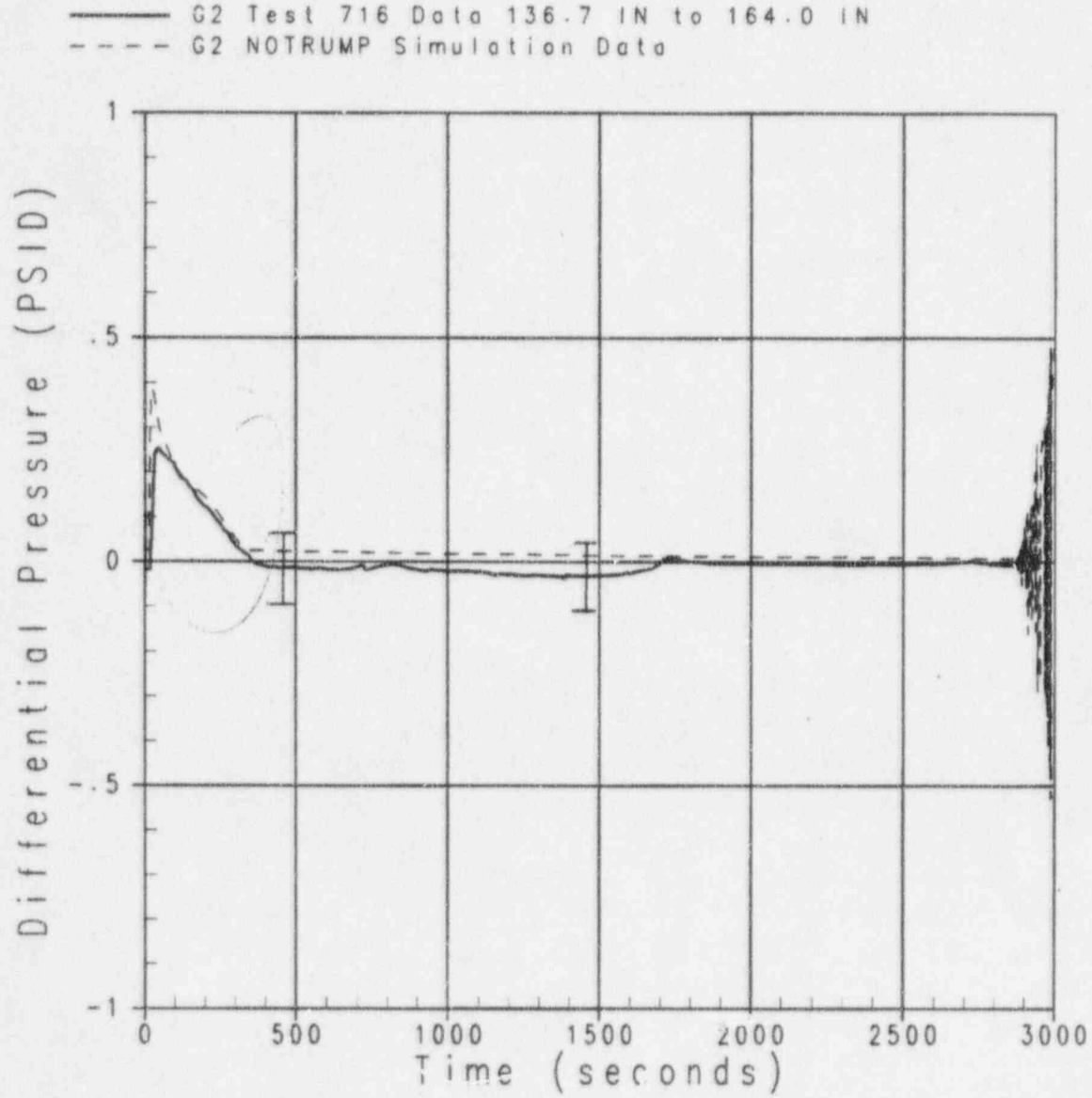

Figure 4.4-19 NOTRUMP Pressure Drop Comparisons to G2 Test 716, 136.7-in. to 164.0-in. in Heated Bundle

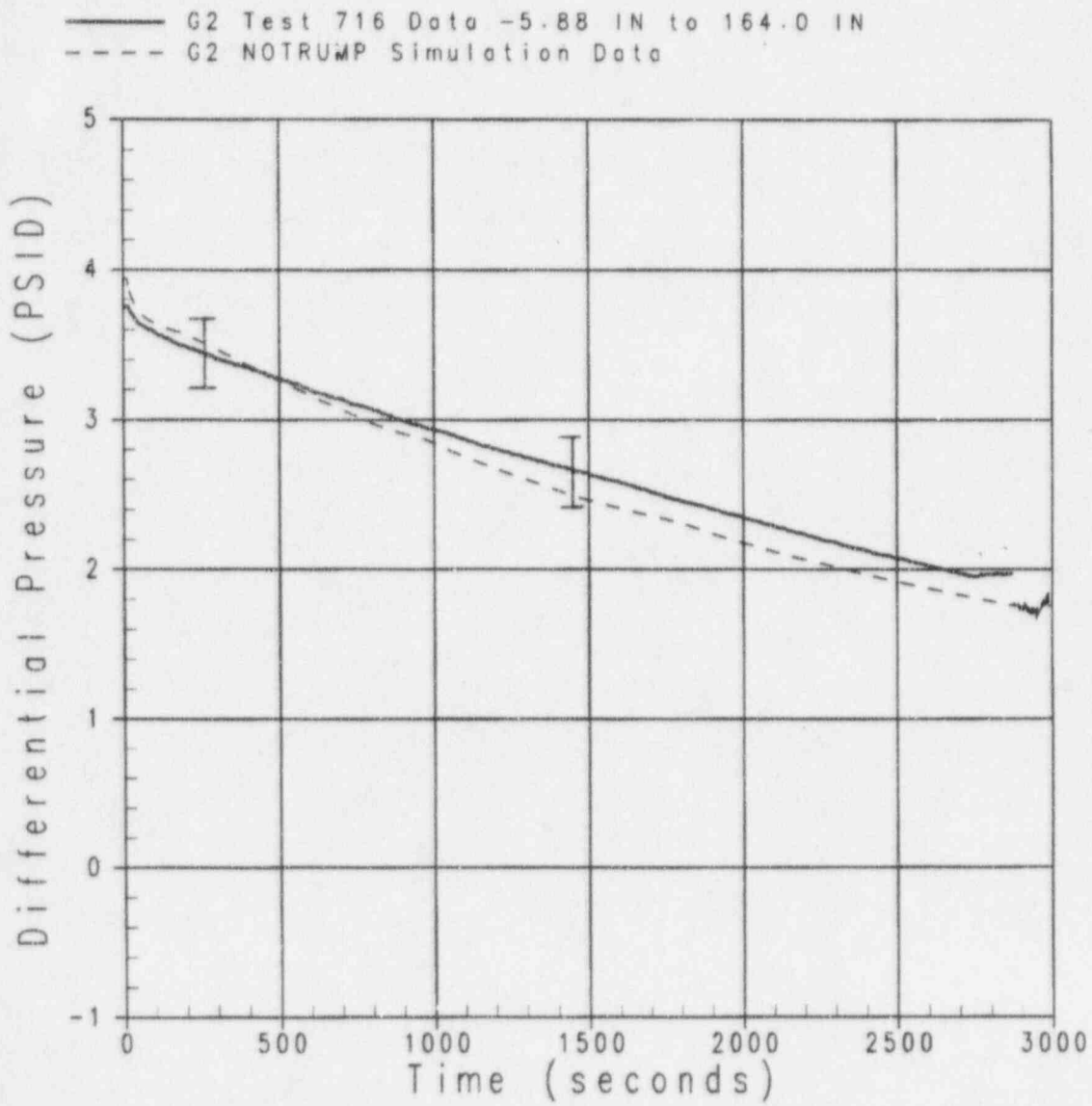

Figure 4.4-20 NOTRUMP Comparisons to Total Rod Bundle Pressure Drop for Test 716

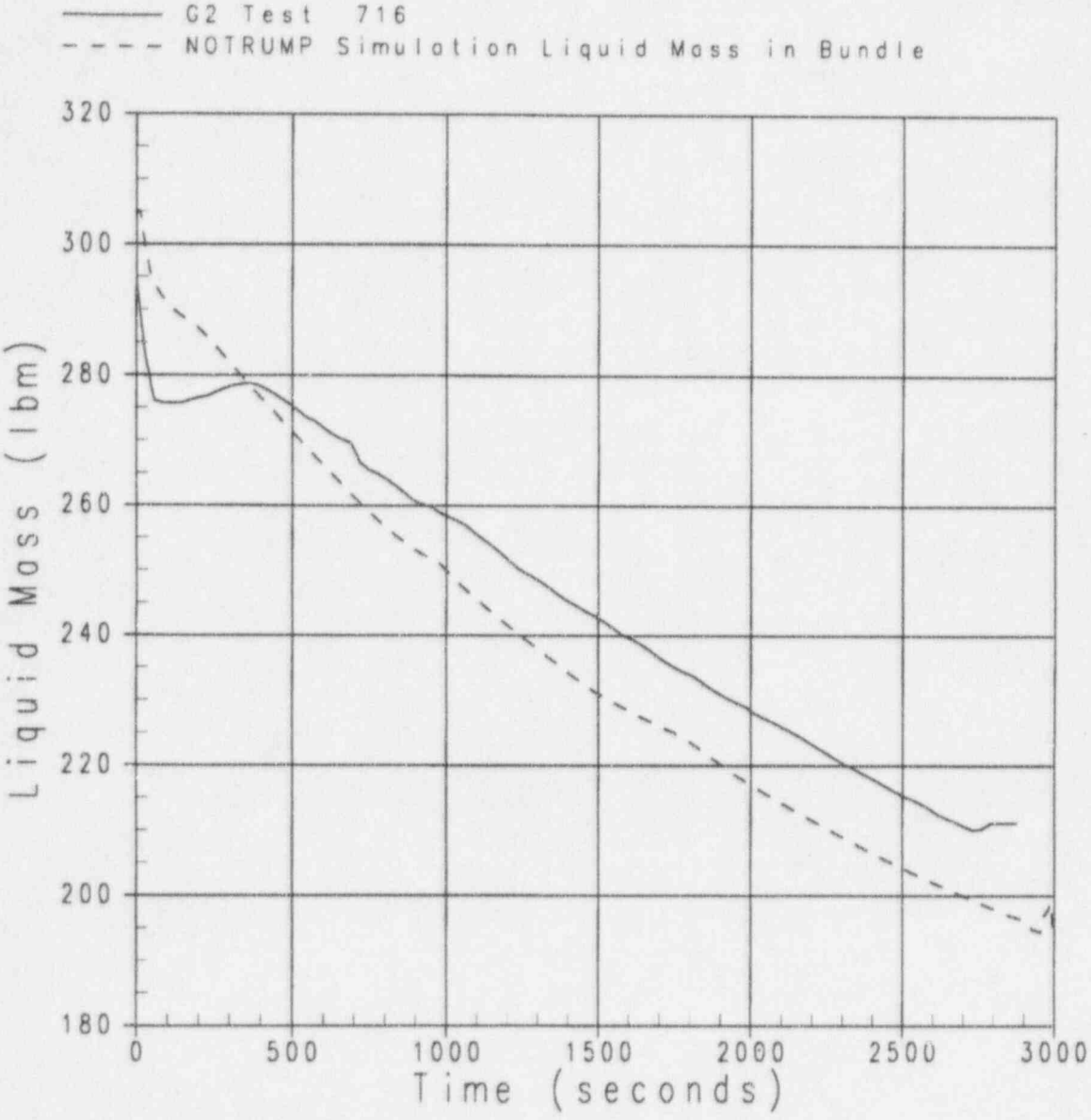

Figure 4.4-21 NOTRUMP Comparisons to Baffle Mass as Determined from the Pressure Drop for Test 716

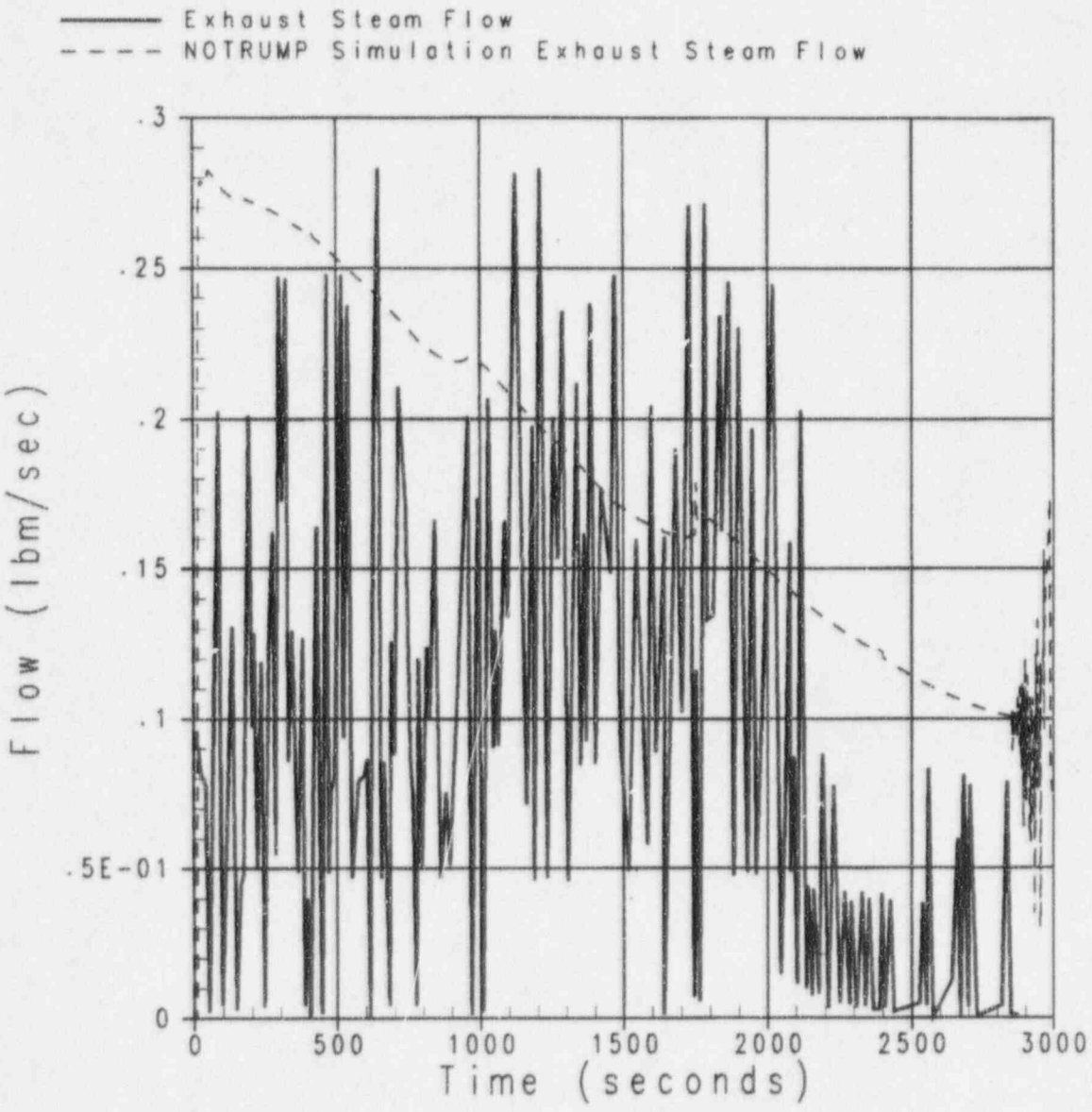

Figure 4.4-22 NOTRUMP Comparisons to Measured Steam Flow for Test 716

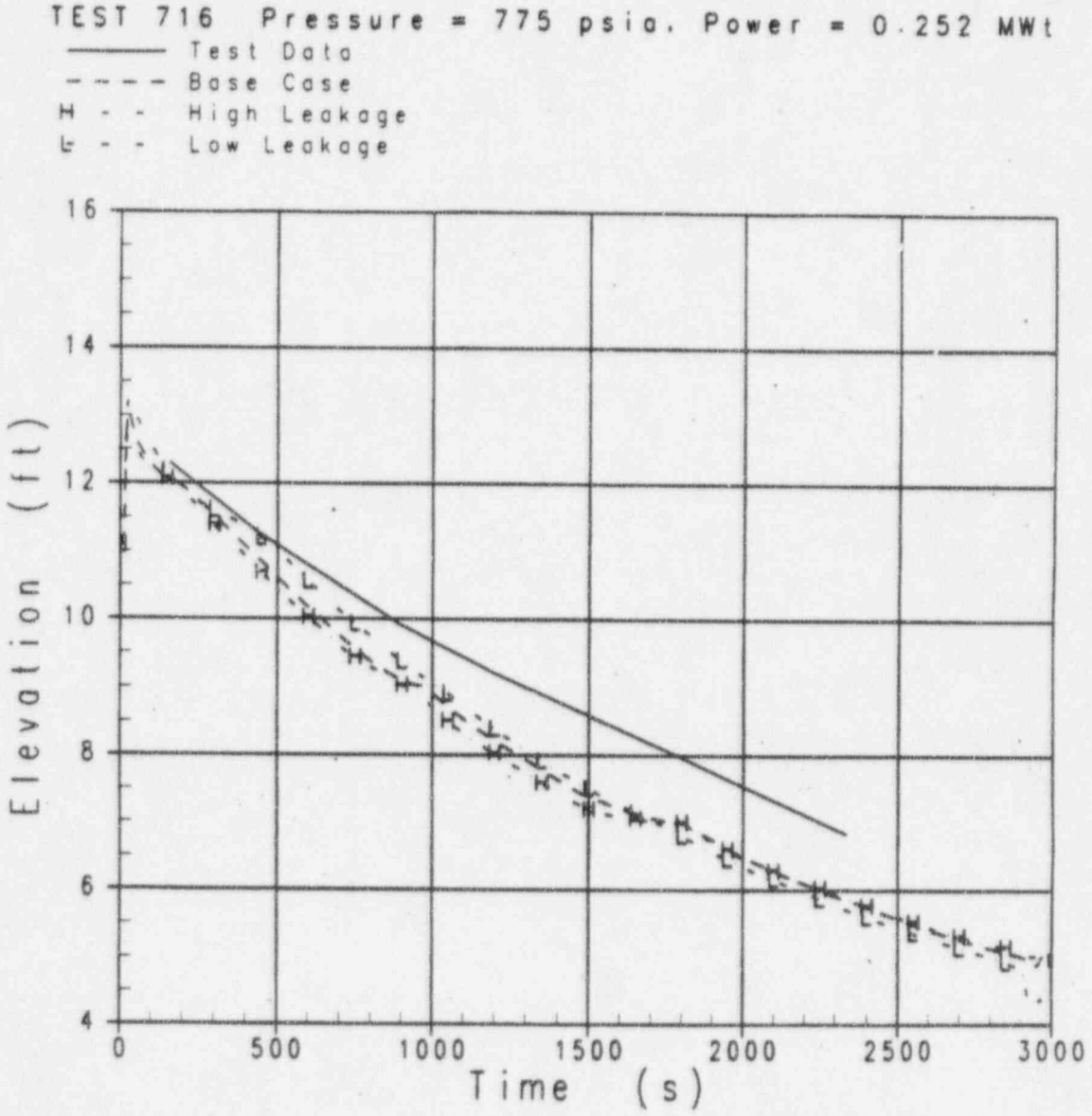

Figure 4.4-23 NOTRUMP Comparisons to G2 Test 716 Mixture Height with Uncertainties

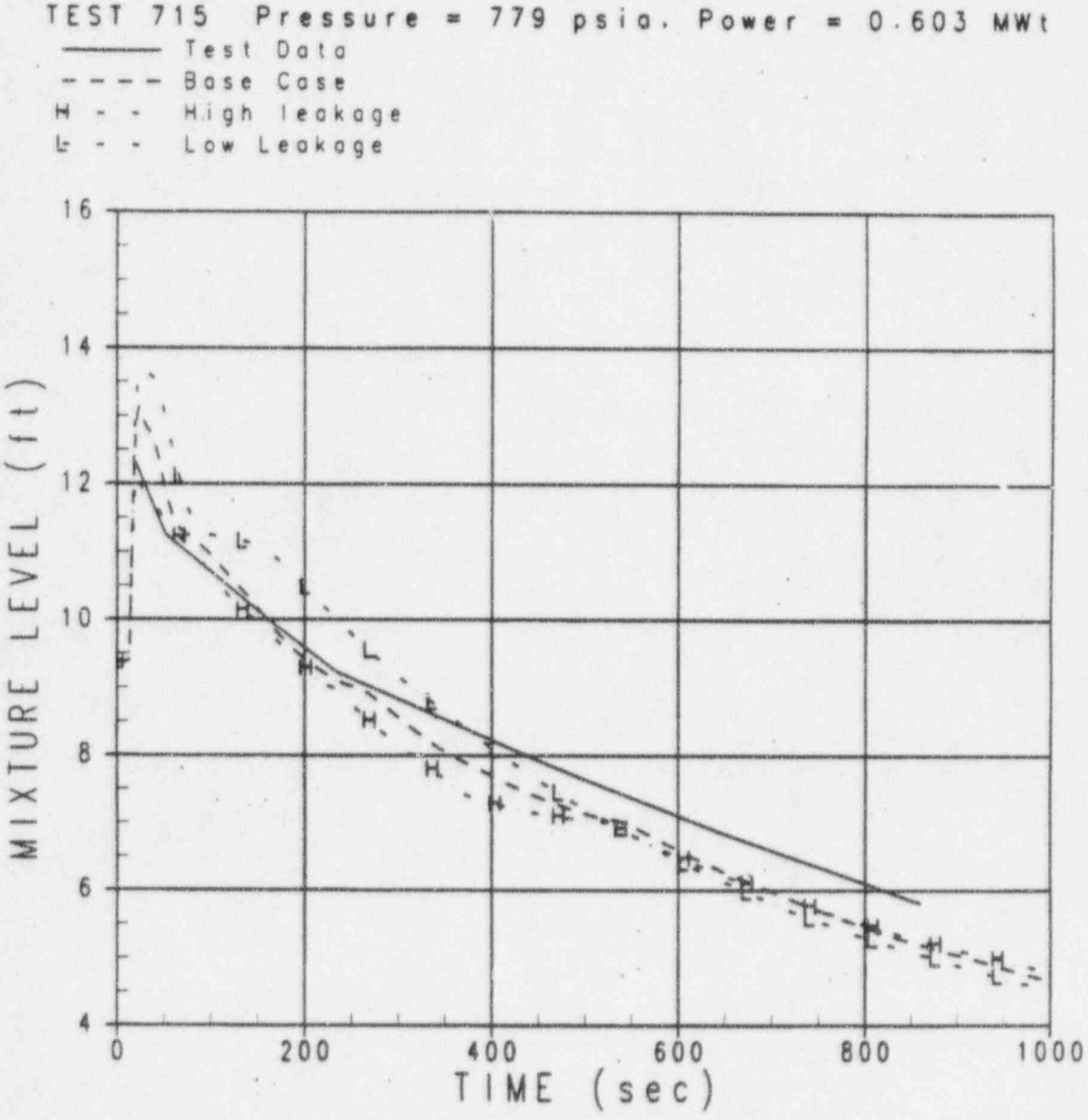

Figure 4.4-24 NOTRUMP Comparisons to G2 Test 715 Mixture Height with Uncertainties

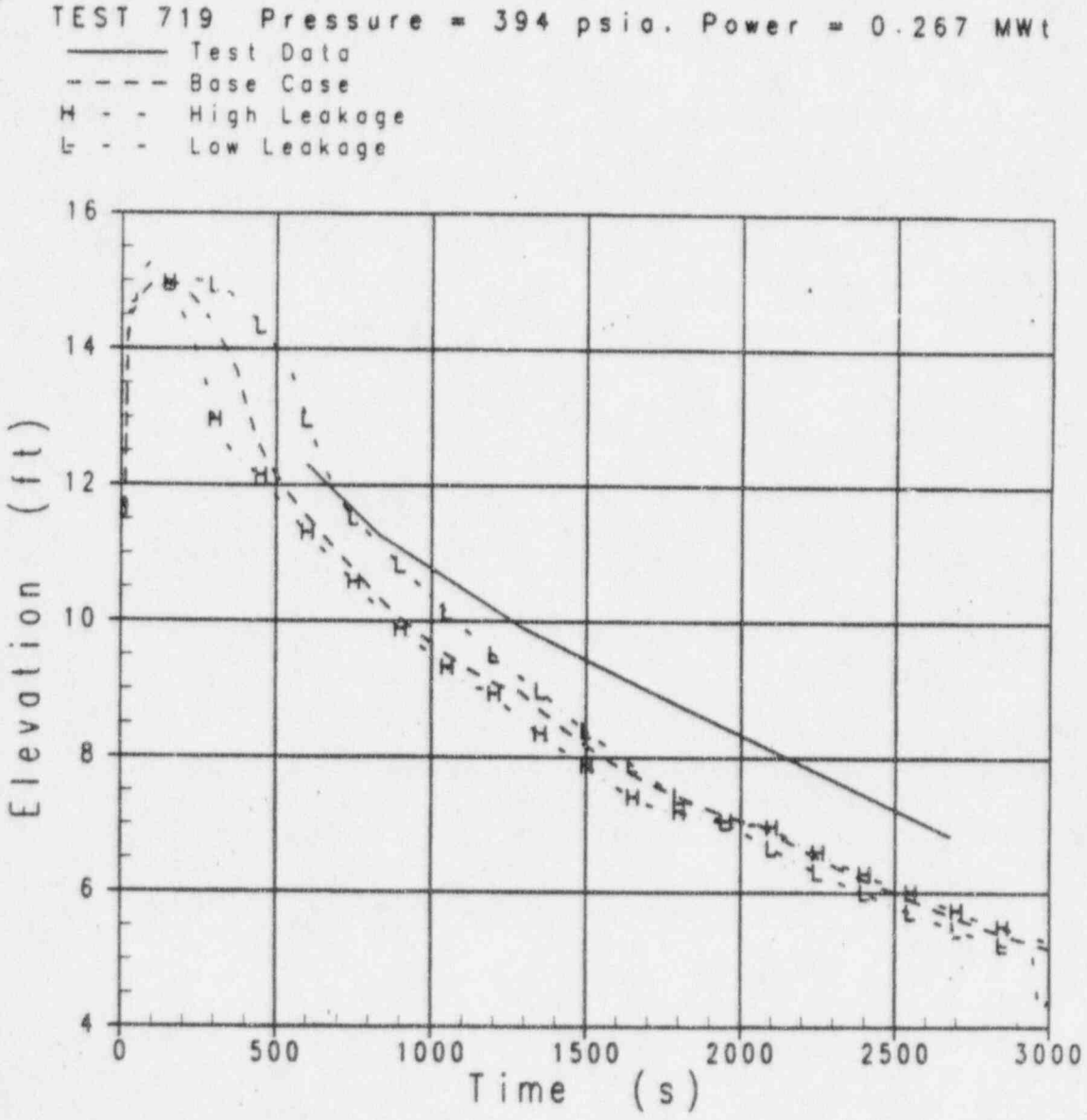

Figure 4.4-25 NOTRUMP Comparisons to G2 Test 719 Mixture Height with Uncertainties

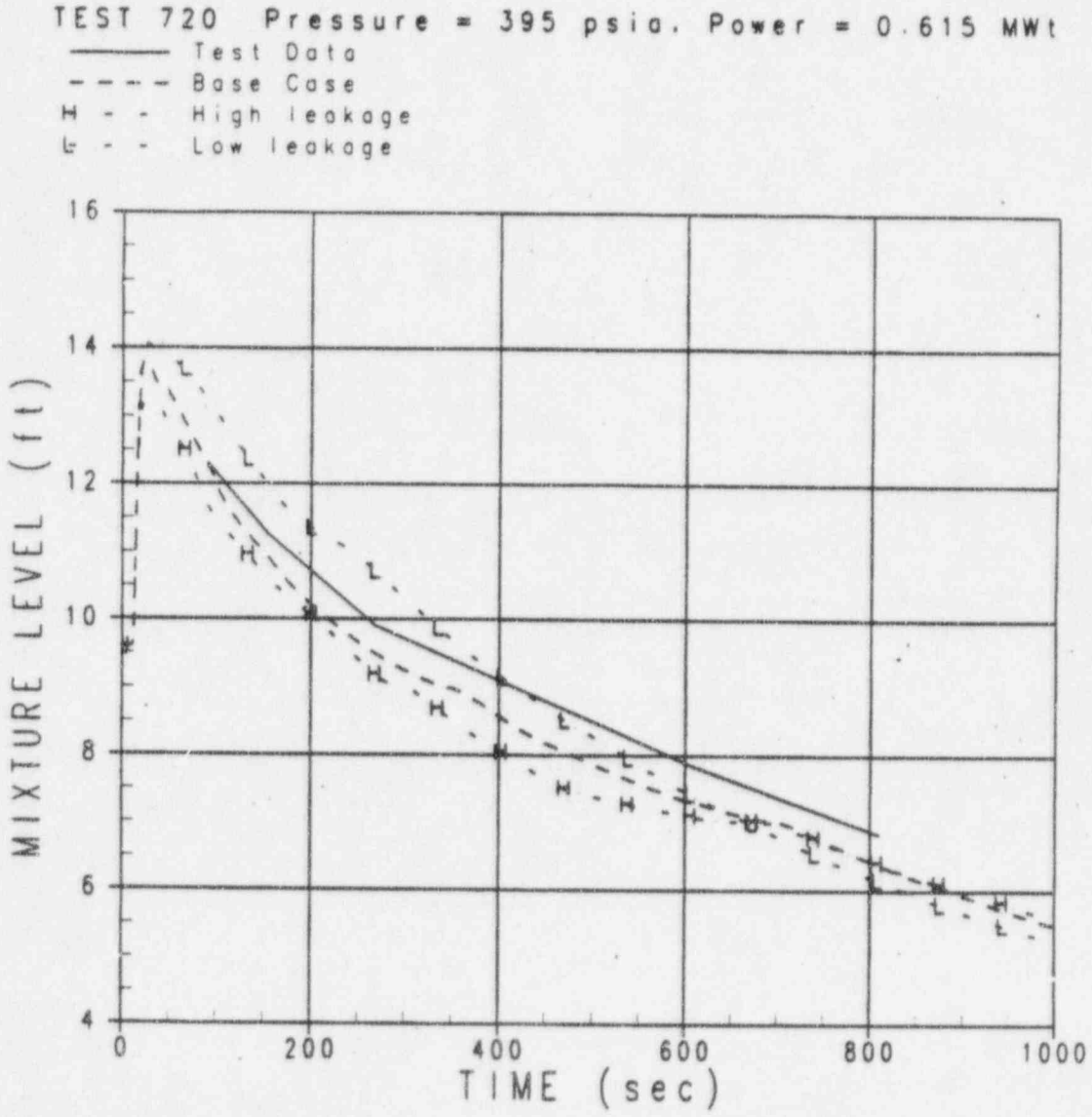

Figure 4.4-26 NOTRUMP Comparisons to G2 Test 720 Mixture Height with Uncertainties

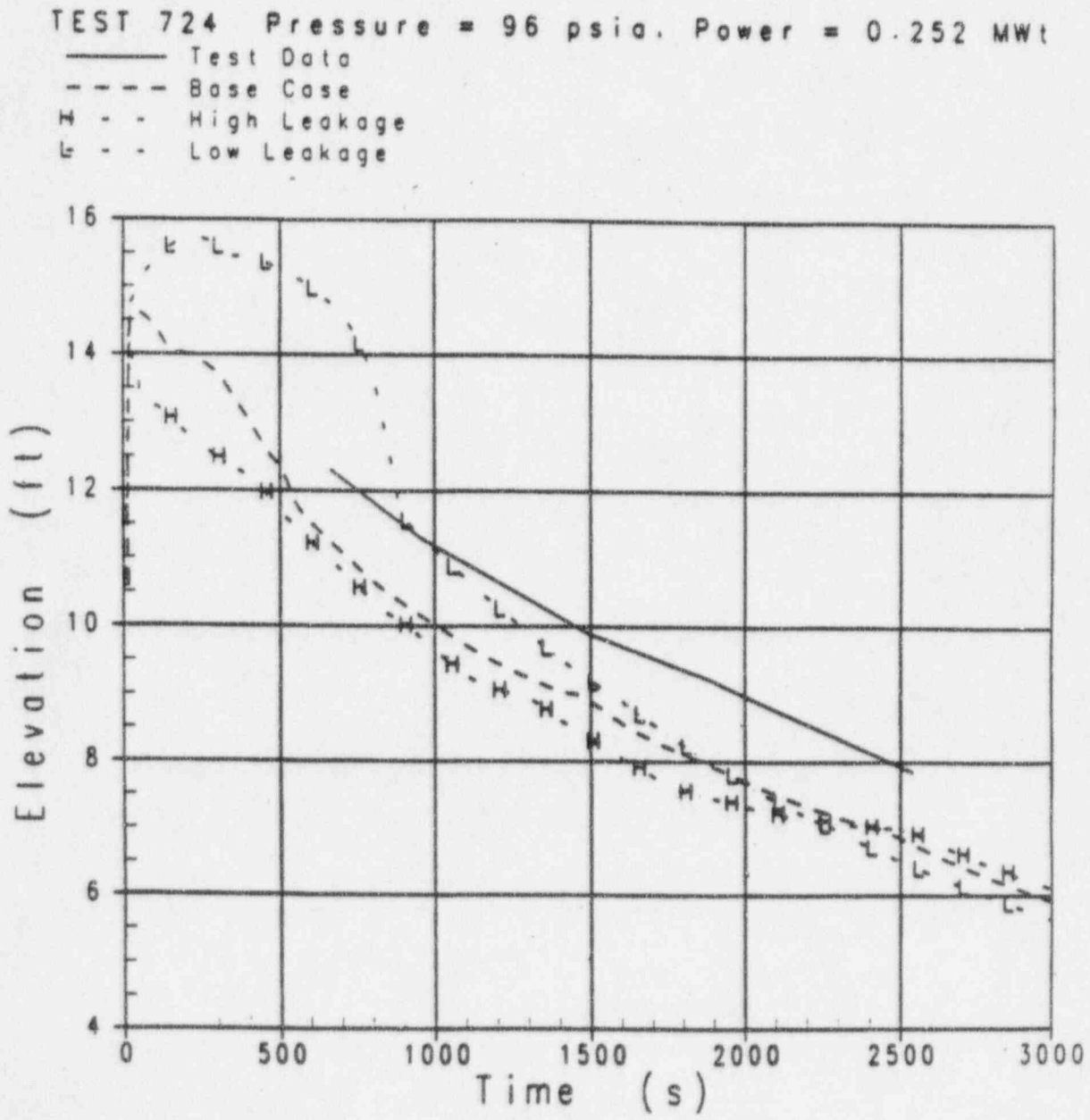

Figure 4.4-27 NOTRUMP Comparisons to G2 Test 724 Mixture Height with Uncertainties

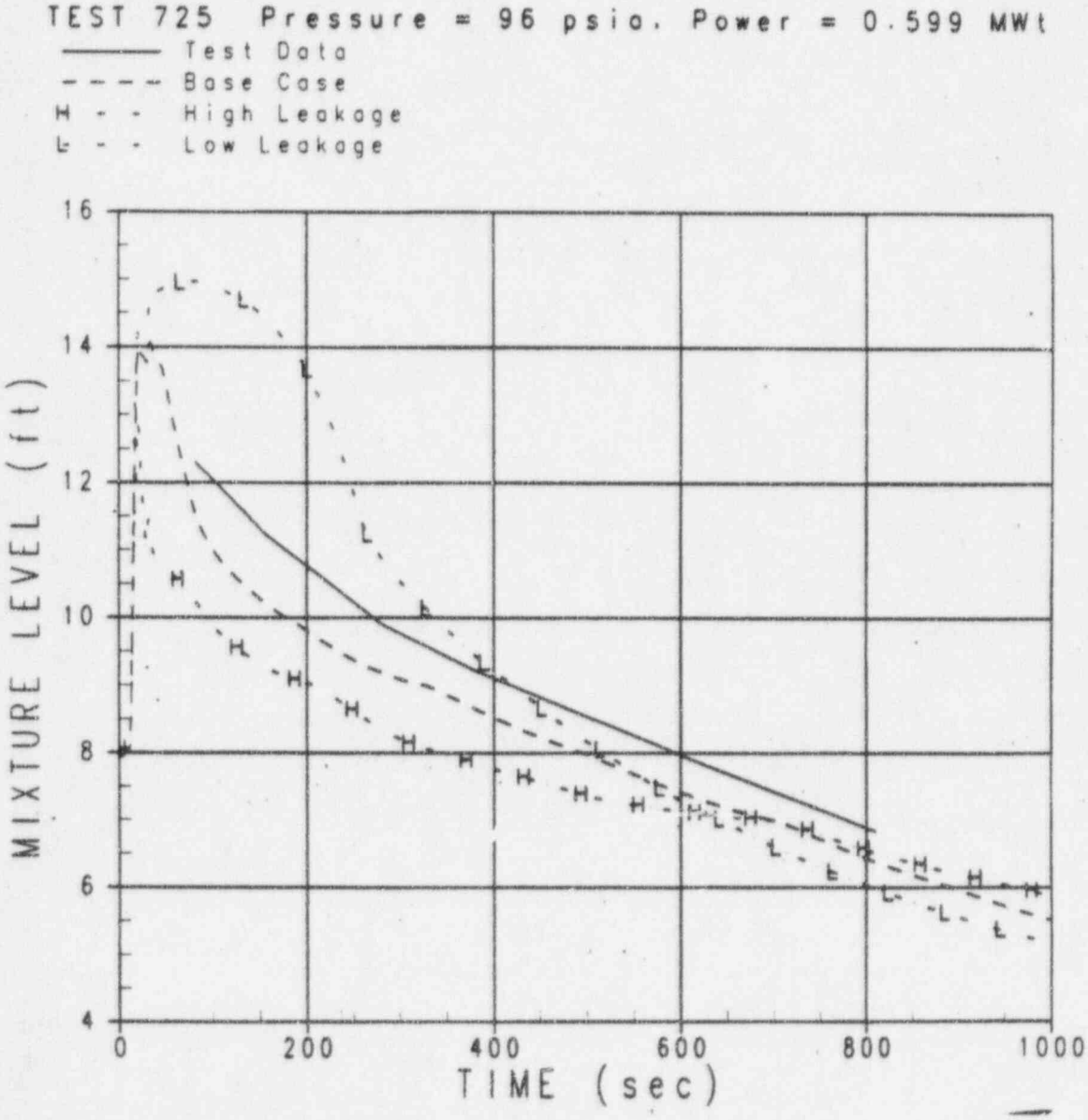

Figure 4.4-28 NOTRUMP Comparisons to G2 Test 725 Mixture Height with Uncertainties

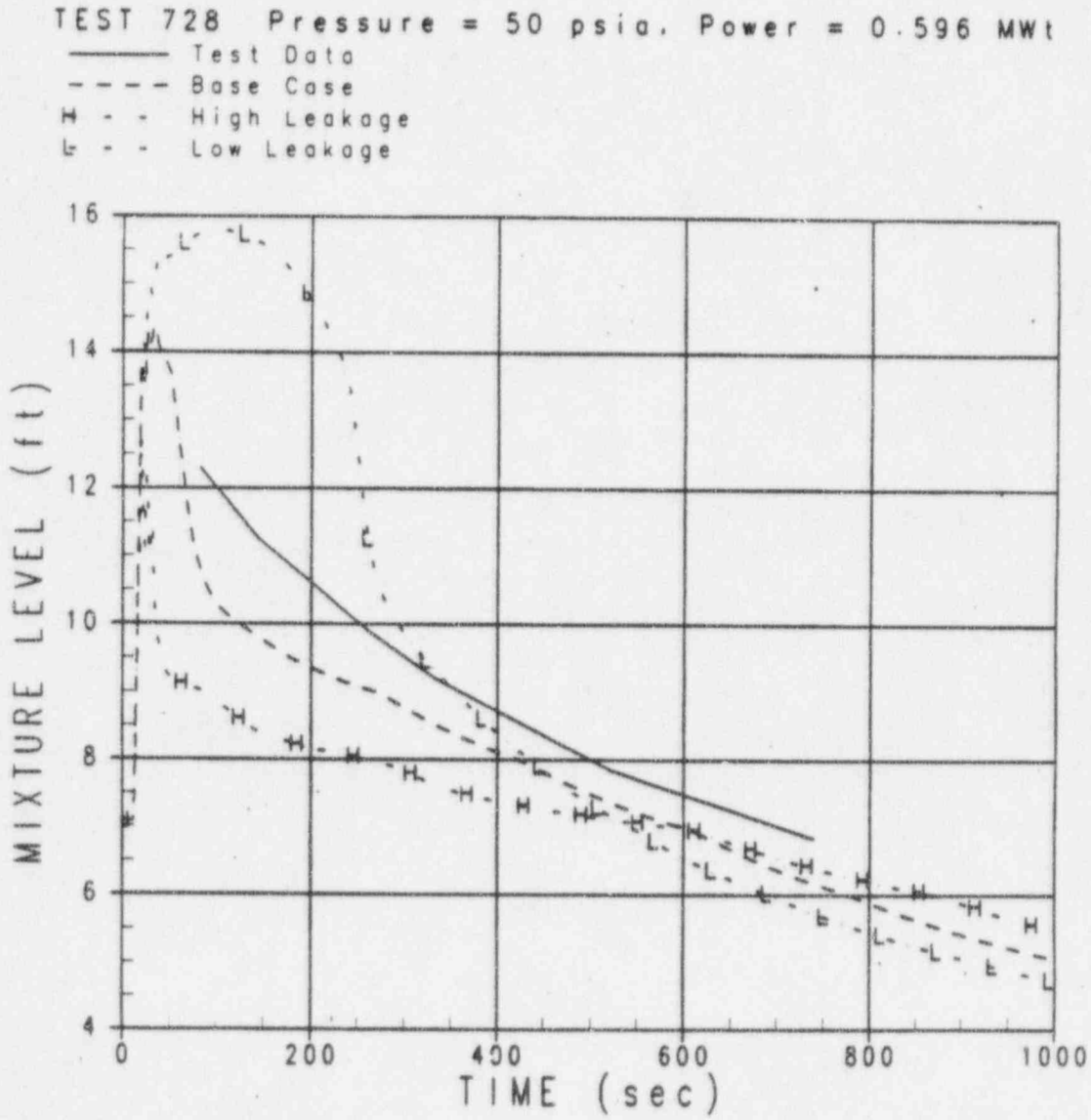

Figure 4.4-29 NOTRUMP Comparisons to G2 Test 728 Mixture Height with Uncertainties

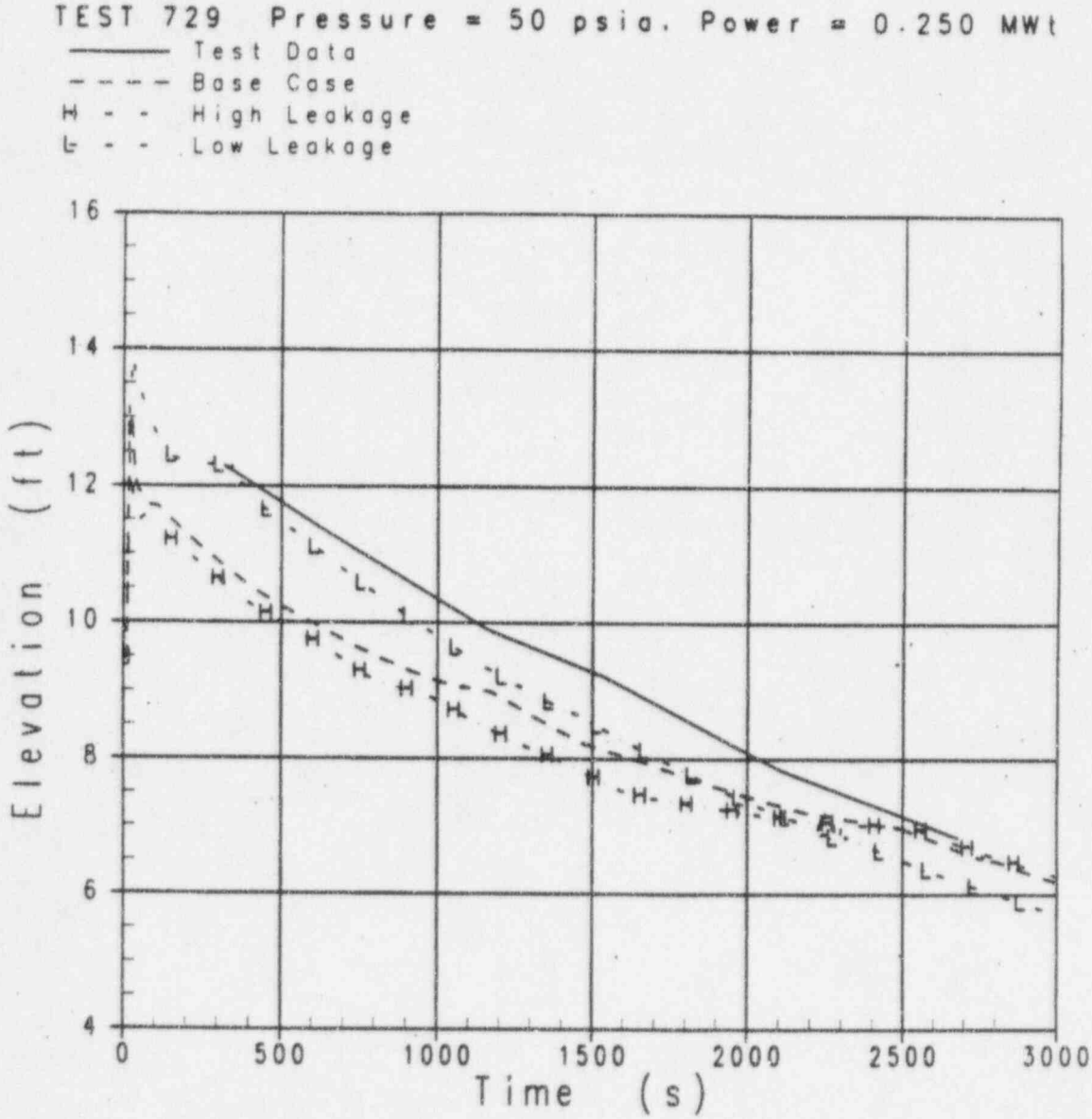

Figure 4.4-30 NOTRUMP Comparisons to G2 Test 729 Mixture Height with Uncertainties

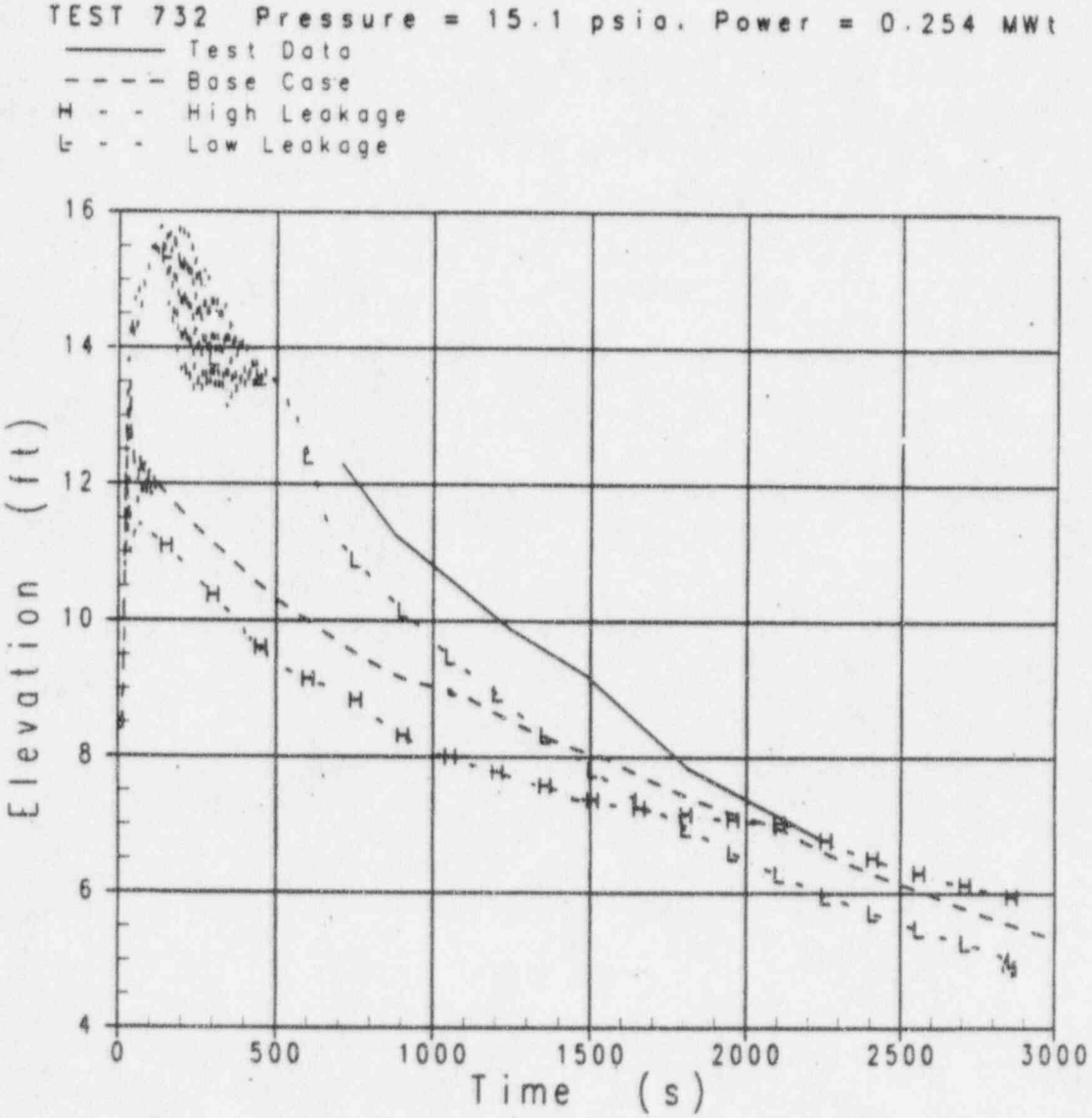

Figure 4.4-31 NOTRUMP Comparisons to G2 Test 732 Mixture Height with Uncertainties

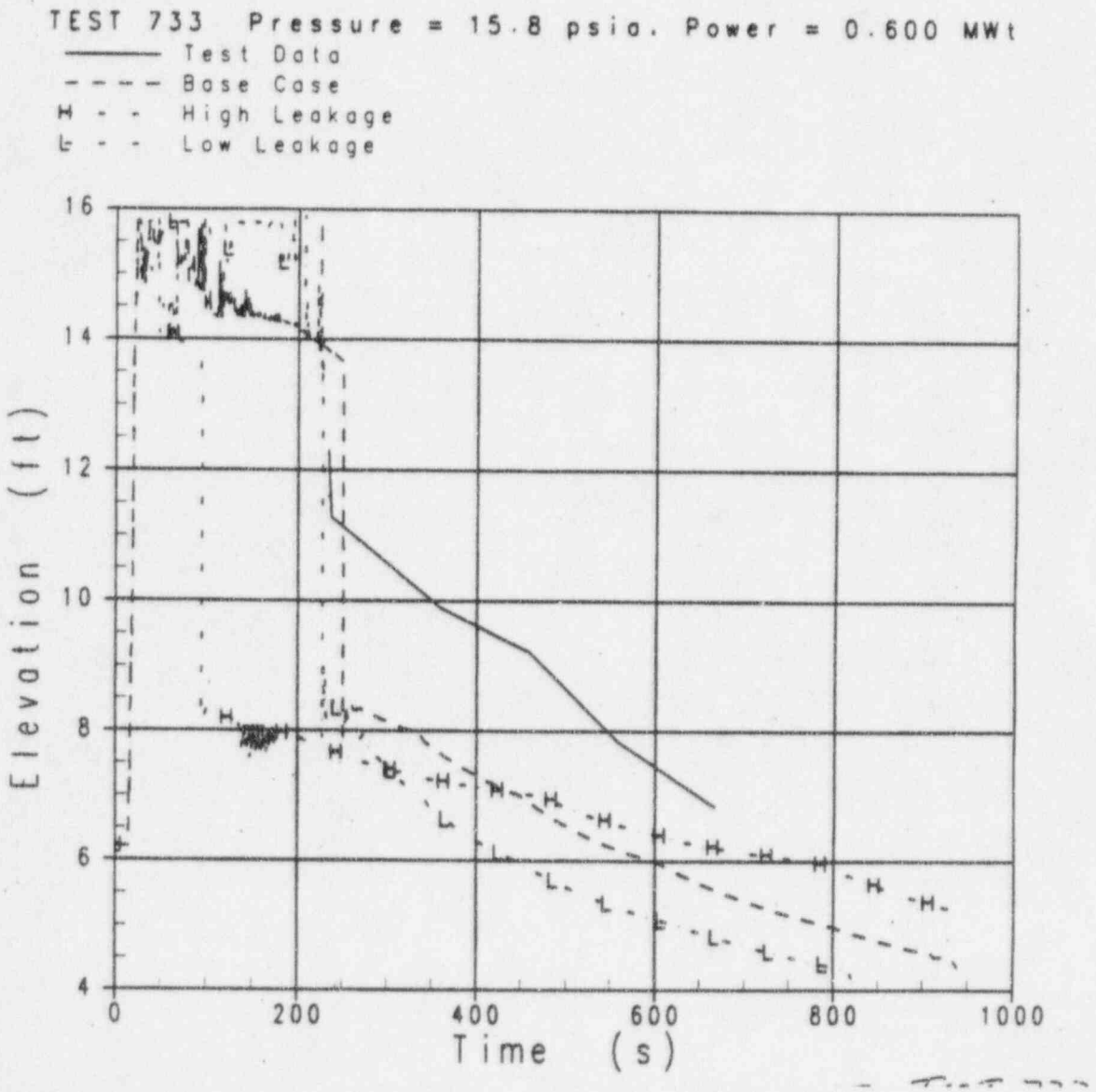

Figure 4.4-32 NOTRUMP Comparisons to G2 Test 733 Mixture Height with Uncertainties

4.5 Summary of Level Swell Comparisons

NOTRUMP has been compared to tests performed in three different test facilities to validate the drift flux models used to predict the two-phase level swell. The tests cover the range of expected conditions for the AP600 plant and include heated bundles in addition to depressurization effects. To compare the three different test series, the measured two-phase level is averaged over the time period of interest and compared to the averaged predicted level from the NOTRUMP calculations for a given test. The averaging process is shown in Figure 4.5-1 and indicates that the averaged value of the test two-phase level is higher than the averaged level obtained from the NOTRUMP calculation.

The averaging process was used on the Westinghouse G2, General Electric small blowdown vessel tests and the ACHILLES NOTRUMP comparisons. An average two-phase level was obtained from the tests and compared to the average two-phase level from the NOTRUMP calculation for the same time period. Figure 4.5-2 shows a scatter plot of the comparison of the average levels as obtained from the tests and the NOTRUMP calculations. Two of the General Electric tests were rerun matching the vessel mass as a function of time (tests 8-21-1 and 8-25-1). When the mass is better matched, the predicted two-phase level swell is in good agreement with the test data.

As the figure indicates, the NOTRUMP calculations of the average level swell are conservative for nearly all the tests. Therefore, the drift flux models used in the NOTRUMP code to predict the two-phase level are conservative for application to the AP600 plant.

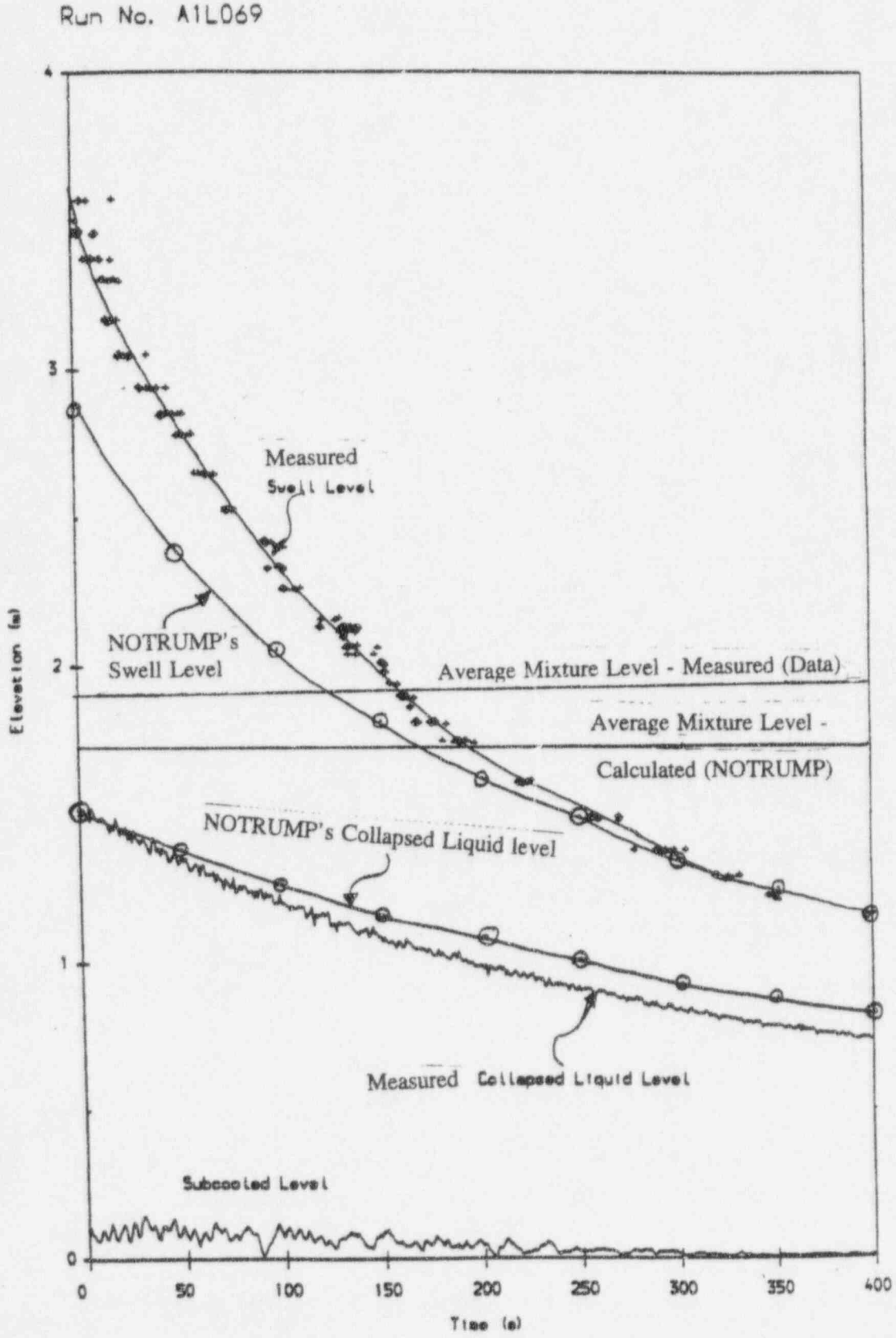

Figure 4.5-1 Level Swell Averaging Process

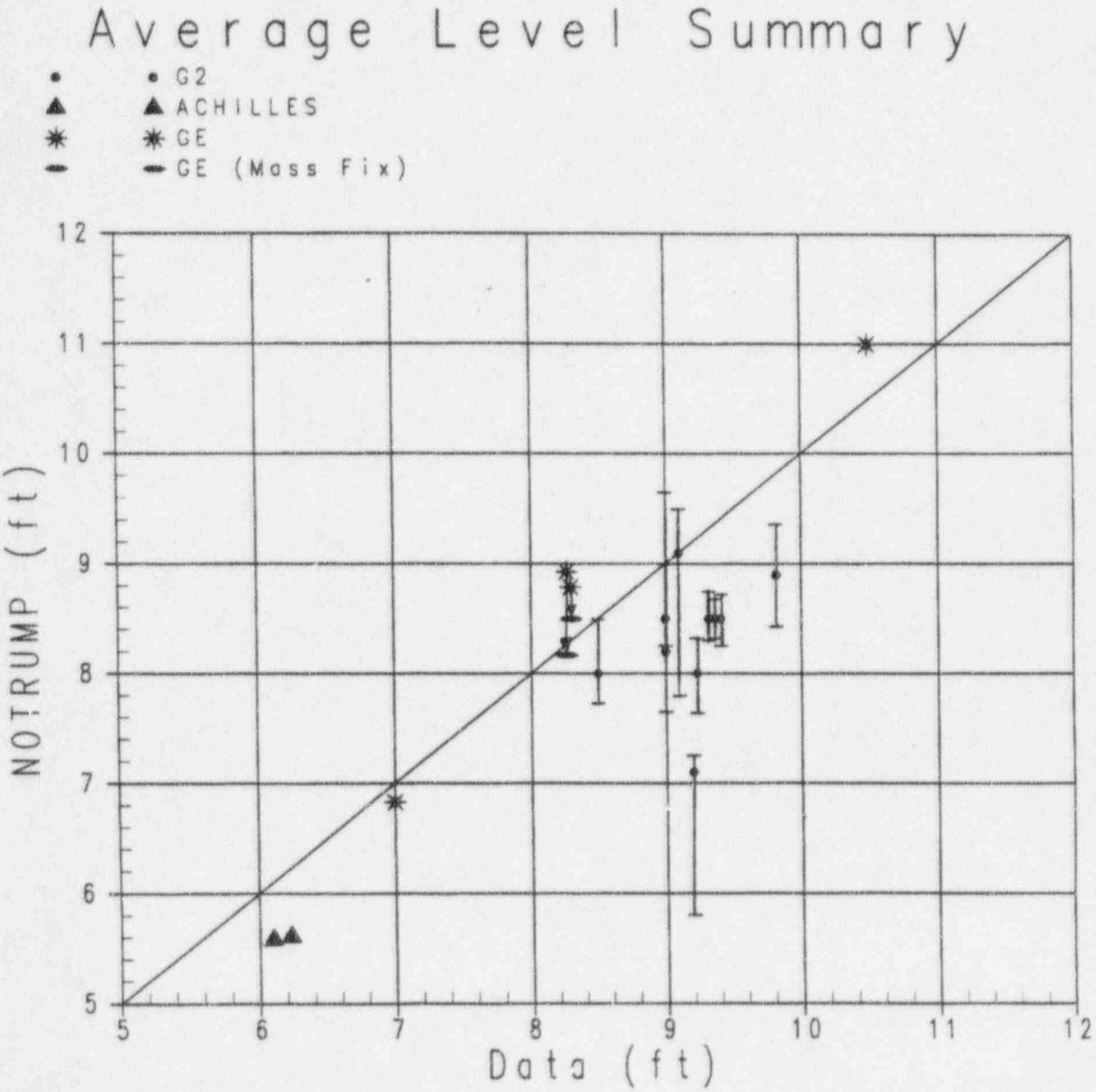

Figure 4.5-2 Data and NOTRUMP Average Level Swell Summary

4.6 Assessment Against the Small-Break Loss-of-Coolant Accident Phenomena Identification and Ranking Table

The small-break LOCA PIRT given in Section 1 identifies that the two-phase mixture level swell is a highly ranked phenomena for the reactor vessel, core, upper head, and upper plenum. The mixture level is most important in the core since it represents the interface between good cooling, when the fuel rods are in nucleate boiling, or poor cooling when the fuel rods are in steam cooling above the mixture level. Therefore, the prediction of the mixture level determines the calculated peak cladding temperature for the small-break transient. In the AP600 small-break LOCA analysis, core uncovery is not calculated and the predicted mixture level is above the core. Therefore, the concern is the accuracy of the NOTRUMP prediction of the two-phase mixture level so that there is confidence that the conclusion of no core uncovery is correct.

The comparisons of NOTRUMP to the two-phase level swell tests in this section of the report indicate that NOTRUMP underpredicts the mixture level over a wide range of thermal-hydraulic conditions typical of an AP600 small-break LOCA. Figure 4.5-2 indicates that the NOTRUMP mixture level predictions are conservative for nearly all the cases investigated. Therefore, NOTRUMP predicts a conservatively low core mixture level for a set of thermal-hydraulic conditions so that the conclusion of no core uncovery for the breaks investigated is valid for the AP600.

The assessment of the NOTRUMP two-phase level swell models performed in Section 4 confirms that they are applicable for the AP600 small-break LOCA transient. The assessment also confirms that NOTRUMP conservatively predicts the level swell phenomena, which is identified as a highly ranked PIRT item.

4.7 References

4-1 Westinghouse Electric Corporation, *Response to Request for Additional Information. 440.325* (December 1995).

4-2 Westinghouse Electric Corporation, *AP600 Standard Safety Analysis Report Update Document* (June 1995).

4-3 Meyer, P. E., et al., *NOTRUMP - A Nodal Transient Small-Break and General Network Code,* WCAP-10079-P-A (Proprietary) (August 1985).

4-4 Wright, R. F., et al., *AP600 SPES-2 Test Analysis Report*, WCAP-14254 (May 1995).

4-5 Andreychek, T. S., et al., *AP600 Low-Pressure Integral Systems Test at Oregon State University, Test Analysis Report*, WCAP-14292 - Revision 1 (September 1995).

4-6 Findlay, J. A. and G. L. Sozzi, *BWR Refill-Reflood Program - Model Qualification Task Plan*, NUREG-CR-1899 or GEAP-24898 (October 1981).

4-7 Slifer, B. C., *Loss of Coolant Accident and Er ergency Core Cooling Models for General Electric Boiling Water Reactors*, NEDO-1032y (April 1971).

4-8 Alamgir, M., *BWR Refill-Reflood Program-Model Qualification for BWR Safety Analysis*, NUREG-CR-2571 or GEAP-22049 (February 1984).

4-9 Pearson, K. G. and M. K. Denham, "ACHILLES Unballooned Cluster Experiments Part 4: Low Pressure Level Swell Experiments," AEEW-R2339 (July 1989).

4-10 Cunningham, J. P. and H. C. Yeh, "Experiments and Void Correlation for PWR Small-Break LOCA Conditions," Trans ANS, Vol 17, pp 363-370 (1973).

4-11 Holmes, B. J., "Analysis of an ACHILLES Low Pressure Level Swell Experiment Using RELAP 5/ Mod 3.1.2," AEA Technology, Presented at CAMP Meeting (October 1995).

4-12 Andreychek, T. S., "Heat Transfer above the Two-Phase Mixture Level under Core Uncovery Conditions in a 336 Rod Bundle," Volumes 1 and 2, EPRI Report NP-1692 (January 1981).